Investigating mechanisms that regulate ectopic lymphoid-like structures in inflammation

A Thesis submitted to Cardiff University in accordance to the requirements for the degree of Doctor of Philosophy in the School of Medicine

By

David G. Hill BSc (Hons)

March 2019

Summary

Lymph node-like follicles called ectopic lymphoid-like structures (ELS) often develop in inflamed tissues affected by autoimmunity and cancer. ELS range from co-localised T and B cell aggregates to highly segregated structures displaying germinal centre reactions. As such, ELS can prime local immune responses and influence chronic disease progression. To understand how interleukin (IL)-27 regulates ELS during inflammatory arthritis, studies established an RNA-sequencing and bioinformatic pipeline to characterise joint inflammation in IL-27 receptor (IL-27R)-deficient mice that develop synovial ELS. Molecular pathway analysis revealed that IL-27 shapes the inflammatory response through suppressing genes involved in leukocyte activation, effector T cell function and chemotaxis. Gene set enrichment analysis identified a prominent pathogenic T helper (Th)17 signature in ELS-rich synovitis, which was confirmed by increased infiltration of IL-17-producing T helper cells in the joints of IL-27R-deficient mice. The significance of the Th17/IL-17 axis on ELS development was also investigated in inflammation-associated gastric cancer. The spontaneous development of gastric tumours in *gp130*$^{Y757F:Y757F}$ mice coincided with the formation of extra-tumoural ELS in the gastric submucosa. Here, ELS displayed T and B cell segregation, reactive germinal centres, and their formation coincided with the temporal induction of homeostatic chemokines. Interestingly, genetic ablation of IL-17 in *gp130*$^{Y757F:Y757F}$ mice revealed that the early formation of lymphoid aggregates did not require IL-17. Rather, IL-17 was needed for the formation of mature ELS that comprised follicular dendritic cells and germinal centres. In clinical disease, while an ELS gene signature was associated with advanced gastric cancer, it did not indicate a favourable prognosis. The *gp130*$^{Y757F:Y757F}$ mice represent a new model for the study of ELS in cancer and an opportunity to test novel drugs that may target ELS. The cross-disease roles revealed for the Th17 programme in regulating ELS makes an attractive target for the immunomodulation of ELS-rich arthritis and cancer.

Acknowledgements

It has been quite a journey the past three and a half years, and whilst there have been many ups and downs it has been an incredibly enjoyable experience which is testament to the amazing group of people that I have had the pleasure of working with.

This journey has been made a thousand times easier through the guidance and support of Dr. Gareth Jones, who always made time for my project and remained patient with my stupid questions. I am thoroughly looking forward to our next chapter in Bristol.

I would also like to thank Prof. Simon Jones, for his sound advice and Prof. Anwen Williams for giving me that final push to get me across the line. A big thank you also goes to all the members of the group for their help, advice and support throughout the years. We started off as colleagues and end as friends. To Anna Cardus, for the hours spent gavaging mice together and evenings of FACS staining. Robert Jenkins, for saving me a fortune on outdoor gear and for making me feel like an amazing cyclist. Alicia Derrac, for times spent practicing presentations. Aisling Morrin, for her amazing rice crispy cakes. Jason Twohig, for making me think critically about my work and for feeding my sugar addiction. Ben Cossins, for help with all my bioinformatic problems and his good humour with all the vegetarian and Benji jokes. David Millrine, for making even my lunches look amazing. Robert Andrews, for all of his bioinformatic help. Barbara Szomolay, for help clustering the data. And finally, to Javier Uceda, for being the most positive person I have ever met. I will always have happy memories of our times spent together – watching Game of Thrones in the Tenovus cinema, playing squash, tennis and badminton and going swimming. He is a true inspiration and will be deeply missed.

I would like to thank my parents, though even for the past three and a half years they have had absolutely no idea what I have been doing, they have always supported and encouraged me to do what I enjoy.

And finally, to Katy for listening to all my problems and for knowing how to deal with my grumpy mood swings…chocolate!

List of publications and presentations

Publications

Lucchesi D, Pontarini E, **Hill DG**, Coleby R, Pitzalis C, Jones GW, Bombardieri M. Interleukin-27 regulates the magnitude of the ectopic germinal centre response in a virus-inducible model of sialadenitis. *Nat Communications.* In preparation.

Twohig JP, Cardus AF, Andrews R, Wiede F, Cossins BC, Liu X, Fernandez JU, **Hill DG**, Derrac Soria A, Szomolay B, Pepper CJ, Taylor PR, Tiganis T, Williams NM, Jones GW and Jones SA. Naïve T-cell activation re-tunes STAT1 signaling to deliver unique cytokine responses in memory CD4 T-cells. *Nat Immunol.* In press.

Hill DG, Yu L, Gao H, Balic J, West A, Oshima H, McLeod L, Oshima M, Gallimore A, D'Costa K, Bhathal PS, Sievert W, Ferrero RL, Jenkins BJ and Jones GW (**2018**) Hyperactive gp130/STAT3-driven gastric tumourigenesis promotes submucosal tertiary lymphoid structure development. *Int J Cancer.* 143(1)167-178

Jones GW, **Hill DG**, Cardus A, Jones SA **(2018)** IL-27 – a double agent in the IL-6 family. *Clin Exp Immunol.* 193(1):37-46

Jones GW, **Hill DG**, Sime K, Williams AS **(2018)** In vivo models for inflammatory arthritis. *Methods Mol Biol.* 1725:101-118

Jones GW, **Hill DG** and Jones SA **(2016)** Understanding Immune Cells in Tertiary Lymphoid Organ Development: It Is All Starting to Come Together. *Front Immunol.* 7:401

Presentations

Poster – "Common cytokine networks link the development, maintenance and activity of tertiary lymphoid structures across autoimmunity and cancer". **November 2018.** *Infection & Immunity Annual Meeting, Cardiff.*

Poster – "Common cytokine networks link the development, maintenance and activity of tertiary lymphoid structures across autoimmunity and cancer". **October 2018.** *International Cytokine and Interferon Society, Boston, USA.*

Oral – "Using cytokines to define biomarkers and therapeutic targets in Rheumatoid arthritis". **September 2018.** *Life Science Research Network Wales Congress, Cardiff, Wales*.

Oral – "Development and maintenance of tertiary lymphoid structures in inflammatory arthritis". **January 2018.** *School of Medicine Postgraduate Research Day, Cardiff*.

Oral – "Development and maintenance of tertiary lymphoid structures in inflammatory arthritis". **November 2017.** *Infection & Immunity Annual Meeting, Cardiff.*

Poster – "Global transcriptomic analysis identifies cytokine-regulated pathways that determine discrete synovial pathotypes in inflammatory arthritis". **October 2017.** *International Cytokine and Interferon Society, Kanazawa, Japan.*

Oral – "Identifying novel therapeutic targets and biomarkers in inflammatory arthritis". **May 2017.** *MRC GW4 Congress, Exeter*.

Poster – "Investigating the therapeutic potential of a novel Bcl-3 inhibitor in experimental inflammatory arthritis". **November 2016.** *Infection & Immunity Annual Meeting, Cardiff.*

Poster – "Investigating the therapeutic potential of a novel Bcl-3 inhibitor in experimental inflammatory arthritis". **October 2016.** *Life Science Research Network Wales Congress, Cardiff, Wales*.

Abbreviations

ACPA	Anti-citrullinated protein antibodies
ACR	American college of Rheumatology
ADAM	Adamlysin and disintegrin-associated metalloprotease
Ahr	Aryl hydrocarbon receptor
AIA	Antigen-induced arthritis
AID	Activation-induced cytidine deaminase
APC	Antigen presenting cell
BCR	B cell receptor
cDNA	Complimentary DNA
CFA	Complete Freund's Adjuvant
CRP	C-reactive protein
CTLA4	Cytotoxic T lymphocyte antigen-4
DAMP	Danger-associated molecular patterns
DAS	Disease activity score
DC	Dendritic cell
DEGs	Differentially expressed genes
DMARD	Disease modifying anti-rheumatic drug
DSS	Dextran sodium sulphate
EAE	Experimental autoimmune encephalomyelitis
EBI3	Epstein-Barr virus-induced gene 3
ELISA	Enzyme-linked immunosorbent assay
ELS	Ectopic lymphoid-like structure
ESR	Erythrocyte sedimentation rate
FCS	Fetal calf serum
FDC	Follicular dendritic cell
FF	*gp130*$^{F/F}$
FGF-2	Fibroblast growth factor-2
FoxP3	Forkhead box P3
FPKM	Fragments per kilobase of transcript per million mapped reads
FRC	Fibroblastic reticular cell
GM-CSF	Granulocyte-macrophage colony-stimulating factor
GSEA	Gene set enrichment analysis
HEV	High endothelial venule
HGF	Hepatocyte growth factor
iBALT	Inducible bronchus-associated lymphoid tissue
ICAM	Intracellular adhesion molecule
IFN	Interferon
IL	Interleukin
IL-27R	Interleukin-27 receptor
IL-6R	Interleukin-6 receptor
ILC	Innate lymphoid cell

IPA	Ingenuity Pathway Analysis
JAK	Janus-activated kinase
LFA-1	Lymphocyte function-associated antigen 1
log_2FC	Log_2 fold change
LPS	Lipopolysaccharide
LT	Lymphotoxin
LTβR	Lymphotoxin beta receptor
LTi	Lymphoid tissue inducer
LTo	Lymphoid tissue organiser
MAPK	Mitogen-activated protein kinase
mBSA	Methylated bovine serum albumin
MHC	Major histocompatibility complex
MMP	Matrix metalloproteinase
MRC	Marginal reticular cell
mRNA	Messenger RNA
NGS	Next generation sequencing
NK	Natural killer
NLR	Nucleotide-binding oligomerisation domain-like receptor
NMT	N-myristoyltransferase
NSCLC	Non-small cell lung cancer
OA	Osteoarthritis
PAMP	Pathogen-associated molecular pattern
PD-L1	Programmed death ligand 1
Pdpn	Podoplanin
PI3K	Phosphoinositide-3-kinase
PKB	Protein kinase B
PNAd	Peripheral node addressin
PRR	Pattern recognition receptor
qPCR	Quantitative polymerase chain reaction
RA	Rheumatoid arthritis
RANKL	Receptor activator of nuclear factor-kB ligand
RF	Rheumatoid factor
RIN	RNA integrity number
RNA-seq	RNA sequencing
RORγt	Retinoic acid receptor-related orphan receptor gamma-T
rRNA	Ribosomal RNA
SCID	Severe combined immunodeficient
SEM	Standard error of the mean
SHP2	SH2 domain containing tyrosine protein phosphatase
SLO	Secondary lymphoid organ
SOCS	Suppressor of cytokine signalling
STAT	Signal transducers and activators of transcription
TCGA	The Cancer Genome Atlas

TCR	T cell receptor
Tfh	T follicular helper
TGFβ	Transforming growth factor beta
Th	T helper
TLR	Toll like receptor
TNF	Tumour necrosis factor
Treg	Regulatory T
VCAM	Vascular adhesion molecule
VEGF-C	Vascular endothelial growth factor-C
VTP	Vascular targeting peptide
WT	Wild-type

Table of Contents

List of Figures

List of Tables

Chapter 1. General Introduction

1.1 The immune system

The immune system is a collective network of lymphoid organs and specialised leukocytes that is regulated by various proteins (e.g. cytokines, antibodies, complement factors), bioactive lipids (e.g. leukotrienes, prostaglandins) and carbohydrate moieties [1]. It provides defence against infectious agents (e.g. bacteria, viruses, fungi, parasites) and injury by distinguishing between 'self' and 'non-self'. However, dysregulation of this response can result in allergy and autoimmune disease [2]. The immune response is divided into two arms determined by the speed and specificity of the response, although there is much communication between them. These are termed innate and adaptive immunity.

1.1.1 Innate immunity

The inflammatory process is initiated through recognition of invading pathogens by pattern recognition receptors (PRRs) from the innate compartment. These recognise pathogen-associated molecular patterns (PAMPs) on invading pathogens and as such have co-evolved with microbes to protect against infection. PRRs also recognise danger-associated molecular patterns (DAMPs) induced in response to endogenous stress. The best known PRRs are Toll like receptors (TLRs) which can recognise a diverse range of PAMPs. Others include macrophage scavenger receptors, nucleotide-binding oligomerisation domain-like receptors (NLRs) that recognise intracellular pathogens, C-type lectin receptors (e.g. Dectin-1 and Clec-2) and AIM2-like receptors, as well as secreted PRRs such as C-reactive protein and mannose binding lectin [3]. Recognition of PAMPs and DAMPs by PRRs triggers cellular responses that promote anti-microbial and pro-inflammatory activities, such as phagocytosis, opsonisation, secretion of cytokines and chemokines and inflammasome activation. The inflammasome is a multimeric protein complex that assembles following recognition of PAMPs or DAMPs. The oligomerisation of pro-caspase-1 activates its protease activity that cleaves precursor cytokines (e.g. pro-IL-1β and pro-IL-18) to support host defence and inflammation [4]. Together, these activities alter the expression of adhesion molecules and recruitment of immune cells in order to progress the inflammatory response [3]. Importantly, innate cells such as dendritic cells can traffic to secondary lymphoid organs, such as the spleen and lymph node, and present antigens on MHC molecules to T cells in order to prime the adaptive response [5].

1.1.2 Adaptive immunity

Adaptive immunity generates responses against specific antigens and provides long term protection through the generation of immunological memory. The generation of unique receptors occurs early in development in the bone marrow and thymus for B and T cells respectively. For B cells, this is the B cell receptor (BCR) and T cells have the T cell receptor (TCR) [6]. The TCR is typically composed of an α- and β-chain, though some TCRs consist of a γ- and δ-chain and are expressed by $\gamma\delta$ T cells, which sit at the interface of innate and adaptive immunity. The BCR is a membrane bound IgM, hence is formed of heavy and light chains. The large repertoire of receptors is acquired through genetic recombination of variable, diverse and joining, V(D)J, gene clusters by enzymes encoded by the recombination activating genes, RAG-1 and RAG-2 [7, 8]. Since this is a random process, cells that recognise self-antigens are removed by negative selection before they enter the circulation [9].

1.1.3 Activation of adaptive responses

Antigens are presented to lymphocytes in secondary lymphoid organs by antigen presenting cells (APCs), such as dendritic cells. If a TCR or BCR recognises the antigen it is induced to proliferate and promote antigen-specific responses. T cells require both TCR activation and interaction of co-stimulatory molecules in order to differentiate into either effector or memory cells [10]. Co-receptors for T cell activation are CD80 (B7.1), CD86 (B7.2) and CD40, expressed on APCs, that bind CD28 and CD40 ligand (CD40L) on T cells respectively [11]. Co-receptors are upregulated on APCs following recognition of pathogens by PRRs [12].

The inflammatory environment and the nature of the pathogenic insult have a profound effect on the functional characteristics of lymphocytes. This can result in the activation and differentiation of naive T cells into effector T cell populations with defined cytokine signatures (*Figure 1.1*). For example, interleukin (IL)-12 promotes immunity against intracellular parasites by promoting the differentiation of naïve $CD4^+$ T cells into T helper (Th)1 cells that express T-bet and produce interferon (IFN)γ [13]. During helminth infection IL-4 predominates which induces the expression of GATA3 and drives the differentiation of naïve $CD4^+$ T cells into Th2 cells, which secrete IL-4, IL-5 and IL-13 [14]. Th17 cells are induced in response to TGFβ, IL-6, IL-21, IL-23 and IL-1β to provide immunity against extracellular bacteria and fungi [15]. TGFβ and IL-6 are required for

early Th17 differentiation, whereas IL-23 is required for full effector function and maintenance of a Th17 phenotype [15, 16]. The master transcriptional regulator of Th17 cells, retinoic acid receptor-related orphan receptor gamma-T (RORγt) is induced in response to STAT3 activation and leads to the expression of IL-17A, IL-17F and IL-22. Along with Th17 cells, γδ T cells, natural killer (NK) cells, group 3 innate lymphoid cells (ILC3s), neutrophils and eosinophils are also capable of producing IL-17 [17-20]. The cognate receptor for IL-17 comprises an IL-17RA and IL-17RC heterodimer, which is expressed ubiquitously with particularly high levels in haematopoietic cells [21, 22]. T follicular helper (Tfh) cells support the generation of high-affinity antibodies by B cells. Tfh cell differentiation is dependent on IL-6 and IL-21, which induce the expression of Bcl-6. Tfh cells upregulate the expression of CXCR5 which directs their recruitment to B cell zones within lymphoid organs [23]. Regulatory T (Treg) cells limit effector T cell responses and support immune tolerance and maintain homeostasis. Natural Treg (nTreg) cells are released from the thymus as a distinct lineage, but inducible Treg (iTreg) cells can also differentiate upon TCR activation in response to TGFβ [24].

Activation of B cells occurs in germinal centres and requires signals from Tfh cells. This results in expression of activation-induced cytidine deaminase (AID) which promotes class-switching and somatic hypermutation in order to increase the affinity and diversity of antibodies [25, 26]. Somatic hypermutation generates point mutations within the antigen-binding site in order to increase affinity. Class-switching involves the changing of the constant region of the heavy chain in order to generate antibodies with different effector functions. There are five antibody isotypes – IgM, IgD, IgG, IgA and IgE. IgG antibodies are further divided into IgG1, IgG2, IgG3 and IgG4. The effector functions of antibodies include, neutralisation, activation of complement and activation of phagocytes by binding of antibody constant regions to Fc receptors. Activated B cells differentiate into antibody-secreting plasma cells or memory B cells [27].

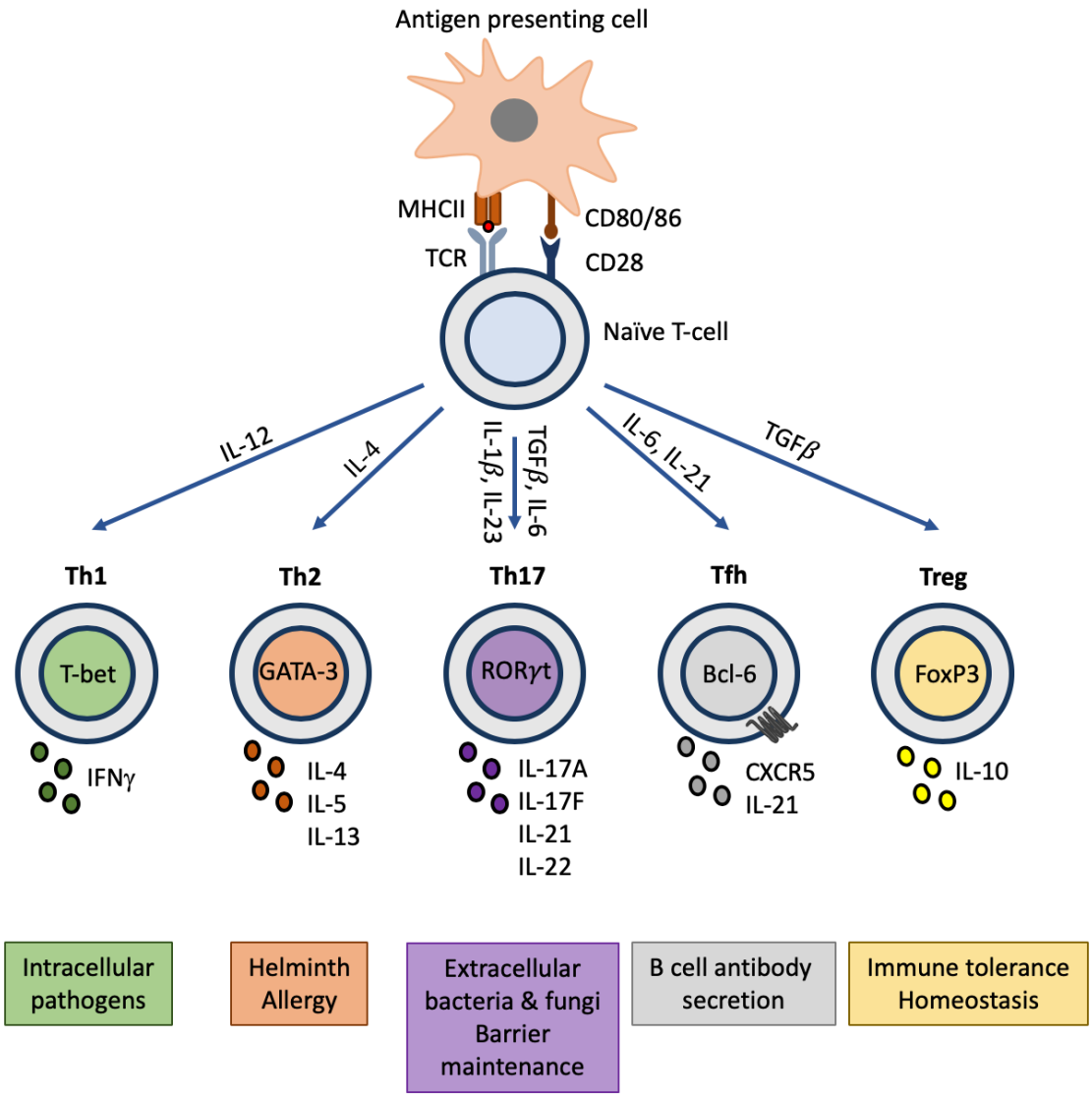

Figure 1.1 - T helper cell differentiation. Following activation of naïve CD4⁺ T cells by antigen presenting cells the local cytokine environment polarises them into different effector T cell subsets – T helper (Th)1, Th2, Th17, T follicular helper (Tfh) and regulatory T (Treg) cells. Each effector cell has a distinct master transcriptional regulator that determines its differentiation, expression of cell surface receptors and secretion of effector molecules. In response to different pathogens different effector T cell subsets are generated.

1.1.4 Inflammation

The symptoms of inflammation include heat (calor), redness (rubor), pain (dolor) and swelling (oedema) which arise from the accumulation of immune cells, secreted proteins and fluids at the site of infection or injury. Inflammation involves the organised recruitment of leukocytes and release of effector molecules in order to clear the infection. However aberrant regulation of this process can lead to chronic inflammation and tissue damage.

1.1.5 Resolution of Inflammation

Following clearance of the pathogen the inflammatory response has to cease in order to prevent tissue damage and injury. This is mediated through a balance of pro- and anti-inflammatory mediators that ensure appropriate regulation of leukocyte recruitment and apoptotic clearance, and the restoration of normal tissue architecture [28]. These mediators act to decrease vascular permeability, prevent the entry of neutrophils to sites of inflammation, and promote the infiltration of monocytes required for wound healing [29, 30]. They also stimulate macrophages to engulf apoptotic neutrophils, which reprograms them to adopt an anti-inflammatory phenotype resulting in the release of anti-inflammatory mediators and egress from inflamed tissue [31, 32]. Thus, these signals promote resolution of inflammation and tissue repair in order to restore tissue homeostasis.

1.1.6 Chronic Inflammation

Dysregulation of the inflammatory process through persistent, recurrent or unresolved inflammation can result in chronic inflammation [33]. For example, recognition of self-antigens leads to the development of chronic autoimmune diseases [34]. Additionally, it is now appreciated that chronic inflammation plays a role in many diseases including cancer, neurodegenerative disorders, type 2 diabetes and cardiovascular diseases. In these conditions, dysregulated and persistent inflammation leads to tissue damage and loss-of-function [33].

1.2 Cytokines and Chemokines

The inflammatory response is a complex process that must be tightly controlled by a host of extracellular protein and lipid mediators. These include, cytokines, chemokines, eicosanoids (e.g. prostaglandins) and leukotrienes. The following sections will briefly introduce cytokines and chemokines before focusing on the IL-6 family cytokines, IL-6 and IL-27.

1.2.1 Cytokines

Cytokines are small proteins released by both immune and stromal cells that participate in inflammatory processes by binding to specific receptors found on target cells. This can be on the cell that produced them (autocrine signalling), cells in close contact (juxtacrine signalling), adjacent cells (paracrine signalling), or act like hormones by entering the circulation to effect distant cells (endocrine signalling). The binding of cytokines to their cognate receptor activates diverse intracellular signalling cascades. For example, the binding of tumor necrosis factor-α (TNFα) to its receptor activates the NF-κB and mitogen activated protein kinase (MAPK) cascades [35], whereas IL-6 binding to its receptor predominantly activates the janus-activated kinase (JAK) and signal transducers and activator of transcription (STAT) pathway [36]. Through activation of these pathways, cytokines control cellular proliferation, differentiation and survival.

While their action can be highly disease and context specific, cytokines have been broadly classed as either pro- or anti-inflammatory. Typical pro-inflammatory cytokines include TNFα and IL-1β, that are produced early in the inflammatory response by cells such as macrophages to elicit numerous effects. For example, IL-1β induces the acute phase response, has a stimulatory effect on $CD4^+$ T cells and can support the differentiation of Th17 cells [37]. In contrast, cytokines such as IL-10 have potent anti-inflammatory effects. The suppressive effect of Treg cells on the inflammatory response is linked with their production of IL-10 [38]. Further to this, some cytokines are pleiotropic, thus can elicit both pro- and anti-inflammatory effects depending on the context in which they are acting. For example, IL-6 can inhibit the production of pro-inflammatory cytokines, chemokines and the microbicidal activities of macrophages to promote resolution of innate immune responses, yet IL-6 is also an important survival and commitment factor for T cells [36]. Hence, cytokines elicit diverse responses that regulate the inflammatory response.

1.2.2 Chemokines

Cytokines that act as chemoattractants are termed chemokines. Named from the Greek 'kinos' meaning movement, chemokines recruit leukocytes to the site of infection or injury along a concentration gradient. They are small (8-12 kDa) proteins that are typically characterised by the presence of four highly conserved cysteine residues that allow disulphide bridging important for their structural shape. The positioning of the N-terminal cysteine residues subdivides chemokines into four subfamilies. The CC chemokines have two adjacent N-terminal cysteines, while the cysteine residues in the CXC subfamily are separated by a single amino acid. These two subfamilies, comprising CCL1-28 and CXCL1-17 respectively, represent the majority of known chemokines. Additionally, there are the C subfamily (CL1 and CL2), which contain only a single N-terminal cysteine residue and the CX3C chemokine Fractalkine (CX3CL1), where the cysteines are separated by three amino acids. Nomenclature assigns chemokines to their subfamily based on positioning and number of cysteine residues followed by a number. An L or R is then added to designate either ligand or receptor respectively [39-41].

Chemokines signal by binding to seven transmembrane spanning G-protein coupled receptors on target cells. Binding induces changes in the cytoskeleton and lipid membrane resulting in movement along a chemokine gradient [42]. Chemokines can also interact with glycosaminoglycans present on the endothelial cell surface, which facilitates establishing a chemotactic gradient in injured or inflamed tissues. Whilst the chemotaxis of leukocytes to the site of infection or injury is the main role of chemokines they are also involved in processes that aid this. For example, chemokines increase the expression of lymphocyte function-associated antigen (LFA-1) an integrin involved in the tethering and diapedesis through the endothelium [43]. A subset of the CXC subfamily of chemokines that contain the motif, ELR (Glu-Leu-Arg), are neutrophil chemoattractants and are also found to be involved in angiogenesis [44, 45]. Importantly, homeostatic chemokines also play a role in the spatial organisation of lymphoid tissues. Here, the CCR7 ligands, CCL19 and CCL21, recruit and retain T cells in the T cell zone and CXCL13 binds its receptor CXCR5 on B cells to recruit them into the B cell follicle [46]. The development of lymphoid tissue will be discussed in detail in *section 1.4*.

1.3 The IL-6 family

The IL-6 family of cytokines all share a common 130 kDa signal transducing co-receptor called gp130. Members of this family include IL-6, IL-11, IL-27, oncostatin-M, ciliary neurotrophic factor, leukaemia inhibitory factor and cardiotrophin-1 [47]. The following sections will review the roles that IL-6 and IL-27 play in inflammation and disease.

1.3.1 IL-6 and the IL-6 receptor complex

IL-6 is a pleiotropic cytokine first identified for its ability to promote the activation of T cells, differentiation of B cells and regulate the acute phase response [48-53]. However, it is now appreciated that IL-6 has hormone-like roles beyond regulation of the immune response. For example, IL-6 is associated with mitochondrial activities, lipid metabolism, insulin resistance, the neuroendocrine system and neuropsychological behaviour [54-58]. Almost all immune cells and stromal cells are capable of producing IL-6 in response to various stimuli. Typically, IL-6 is secreted in response to IL-1β and TNFα, but expression is also induced by TLRs and other cytokines [36]. The receptor complex for IL-6 is composed of an IL-6 receptor-α subunit, that binds IL-6, in partnership with a signal-transducing co-receptor, gp130. Signalling through this method is termed 'classical signalling'. While gp130 is universally expressed, the IL-6 receptor is restricted to hepatocytes, leukocytes and megakaryocytes (*Figure 1.2*) [59, 60]. Whilst naïve, effector memory and central memory T cells all express IL-6 receptor, their response to IL-6 differs depending on whether they have previously experienced TCR activation [61]. A soluble form of the IL-6 receptor also exists through either the differential splicing of the *Il6ra* gene to produce a protein lacking the membrane anchor domain, or by proteolytic cleavage of membrane bound IL-6 receptor by adamylsin and disintegrin-associated metalloproteinases (ADAM)-17 and ADAM-10 [62]. Proteolytic cleavage of the IL-6 receptor therefore results in a reduction in cell surface levels of the receptor upon T cell activation [63]. Thus, this mode of signalling broadens the cell types that can respond to IL-6. This is termed IL-6 'trans-signalling' (*Figure 1.2*). It has been proposed that these distinct signalling mechanisms regulate different processes, with classical signalling predominantly involved in homeostasis and acute phase responses [36], while trans-signalling is associated with inflammatory activation of tissue, leukocyte recruitment and T cell function [64, 65].

Binding of IL-6 to the IL-6 receptor complex through either classical or trans-signalling promotes intracellular signalling cascades. Recruitment of SH2 domain containing tyrosine protein phosphatase (SHP2) activates the MAPK cascade and

phosphoinositide-3-kinase (PI3K)-protein kinase B (PKB; also known as AKT) pathway [66]. IL-6 can also activate SRC tyrosine kinases to promote the YAP-NOTCH pathway associated with tissue regeneration [67]. However, the activities of IL-6 in leukocytes is predominantly linked to the activation of the JAK-STAT pathway.

1.3.2 JAK-STAT signalling pathway

Binding of IL-6 to the IL-6 receptor complex promotes signalling by the JAK-STAT pathway. Binding results in association of JAKs (e.g. JAK1, JAK2, Tyk2) which phosphorylate tyrosine residues on the intracellular domain of gp130 [68]. This promotes the binding of STAT transcription factors to gp130 – namely STAT1 and STAT3, though IL-6 predominantly activates STAT3 (*Figure 1.2*). Subsequent phosphorylation of STAT proteins by receptor-associated JAKs promotes STAT dimerization, and their translocation to the nucleus where they initiate transcription. This process is tightly regulated by inhibitory mechanisms, for example, suppressors of cytokine signalling (SOCS)1 and SOCS3 which act through negative feedback to supress STAT1 and STAT3 activity respectively [68]. The importance of regulating STAT signalling downstream of IL-6 family cytokines is highlighted in mice that express a mutant form of gp130 that is unable to bind SOCS3. These mice develop exacerbated inflammation and cancer associated with hyperactivation of STAT3 [69-72].

1.3.3 IL-6 in inflammation

The pleiotropic properties of IL-6 are best illustrated by its contrasting roles in the resolution of inflammation and in the maintenance of chronic inflammation. For example, IL-6 regulation of neutrophil accumulation and apoptosis controls transition to a sustained population of mononuclear cells. Here, infiltrating neutrophils shed IL-6 receptor enabling IL-6 ‘trans-signalling’ in resident stromal cells, which alters chemokine expression profiles. This causes inhibition of neutrophil chemoattractants, CXCL1 and CXCL8 and expression of monocyte chemoattractants, CCL2 and CCL8, as well as regulating expression of adhesion molecules such as ICAM-1 and VCAM-1. Further to this, IL-6 also mediates neutrophil apoptosis [73]. It follows that *Il6*$^{-/-}$ mice develop heightened and prolonged neutrophil accumulation [74, 75]. IL-6 also has a role in wound healing. This is associated with its ability to inhibit pro-inflammatory cytokine release and microbial activities of macrophages [76, 77]. Hence these mechanisms of IL-6 action prevent tissue damage and drive the correct progression of the inflammatory response.

In contrast, IL-6 has a role in driving chronic inflammation, which may be best associated with its ability to shape adaptive immunity (*Figure 1.3*). The initial characterisation of IL-6 as B-cell stimulatory factor 2 highlights the role it plays in B cell differentiation and antibody production. This may be linked to the ability of IL-6 to induce Bcl-6 and IL-21, promoting the commitment to Tfh cells, which support B cell responses and class-switching [78-80]. While IL-6 has varying effects on the differentiation of T cell lineages, through the regulation of anti-apoptotic factors, Bcl-2 and Bcl-xL, it acts as an important survival factor for these cells [81]. However, IL-6 is required for the differentiation of Th17 cells. Here, IL-6 activation of STAT3 results in the expression of RORγt and expansion of Th17 cells that secrete IL-17A as their signature cytokine [15, 82-84]. Additionally, IL-6 inhibits the functions of Treg cells and at sites of inflammation can reprogramme them to adopt effector characteristics [85, 86]. For example, in collagen-induced arthritis, synovial fibroblast derived IL-6 converted FoxP3$^+$ T cells into Th17-like cells, that produced IL-17A and RANKL, and contributed to disease progression [87]. It follows that IL-6 is a hallmark of chronic inflammatory diseases. For example, *Il6*$^{-/-}$ mice show protection in experimental models of chronic inflammatory conditions, including inflammatory arthritis [88, 89] and experimental autoimmune encephalomyelitis (EAE) [90]. Thus, IL-6 has diverse pro- and anti-inflammatory roles as well as hormone-like properties.

1.3.4 IL-27 and the IL-27 receptor complex

IL-27 is a heterodimeric cytokine composed of an IL27p28 subunit and Epstein-Barr virus-induced gene 3 (EBI3) subunit. EBI3 also partners with the IL12p35 subunit to form IL-35 and low affinity interactions of IL27p28 with soluble IL-6R and cytokine-like factor 1 have been reported, however the physiological relevance of these remain to be fully determined [91]. Myeloid cells such as macrophages, monocytes and dendritic cells are the major sources of IL-27 [91]. However, during malaria infection IL-27 producing CD4$^+$ T cells were recently identified [92]. Activation of TLRs and signalling by type I and II interferons promotes the expression of IL-27. Like all IL-6 family cytokines, IL-27 signals through binding its cognate receptor, IL-27 receptor-α (IL-27R, also known as TCCR or WSX-1), in partnership with the signal-transducing co-receptor, gp130. The expression of IL-27R is largely restricted to lymphocytes, monocytes and osteoclasts (*Figure 1.2*). IL-27R is expressed on all CD4$^+$ T helper cell subsets, as IL-27 has broad roles in directing T cell effector characteristics (see *section 1.3.5*), and the activation of CD4$^+$ T cells leads to the upregulation of IL-27R surface expression [91]. Similar to IL-6, IL-27

predominantly signals through STAT1 and STAT3. However, IL-27 induces a group of immunoregulatory genes through activation of STAT1 (*Figure 1.2*) [93]. Thus, although IL-27 shares the same gp130 co-receptor it can often oppose the action of IL-6 (*Figure 1.3*).

1.3.5 IL-27 in inflammation

Using mouse models of infection, IL-27 was initially described as a pro-inflammatory cytokine due to its ability to promote IFNγ secretion by T helper cells. Here, IL-27 promoted the expression of STAT1, T-bet, IL12Rβ2 and IFNγ to support Th1 cells [94-98]. Early studies also showed that IL-27 promoted the growth and survival of T cells [94, 99]. However, this pro-inflammatory description for IL-27 was later challenged when infection of *Il27ra*$^{-/-}$ mice with *Toxoplasma gondii* led to a lethal CD4^{+} T cell response with elevated levels of IFNγ [100]. Further studies in models of infection, autoimmunity and inflammation revealed IL-27 to be a potent negative regulator of IL-2 and an inhibitor of adaptive immune responses [101-105]. For example, IL-27 promotes the production of IL-10 from T cells [103, 106, 107], and supports the development of immunosuppressive CXCR3^{+} Treg populations [102]. IL-27 also suppresses effector T helper responses. In this context, it often antagonises the actions of IL-6. For example, IL-6 supports the development of Th17 cells [15, 82-84], however IL-27 inhibits Th17 cell function by supressing expression of RORγt, the master transcriptional regulator for Th17 development [105, 108]. IL-27 also inhibits Th2 responses by antagonising expression of GATA3, the master transcriptional regulator of Th2 responses [98, 109-111]. In this regard, *Il27ra*$^{-/-}$ mice showed enhanced resistance to helminth infection associated with increased production of Th2 cytokines, IL-4, IL-5 and IL-13 [111]. Similarly, exaggerated T helper responses in *Il27ra*$^{-/-}$ mice have been linked with enhanced viral and fungal clearance [112, 113]. The expression of co-inhibitory receptors, PD-L1 and CTLA-4, on T cells is also upregulated by IL-27, further restricting T cell responses [114, 115]. Thus, in chronic inflammatory conditions, IL-27 mainly has anti-inflammatory effects that often oppose the actions of IL-6 (*Figure 1.3*).

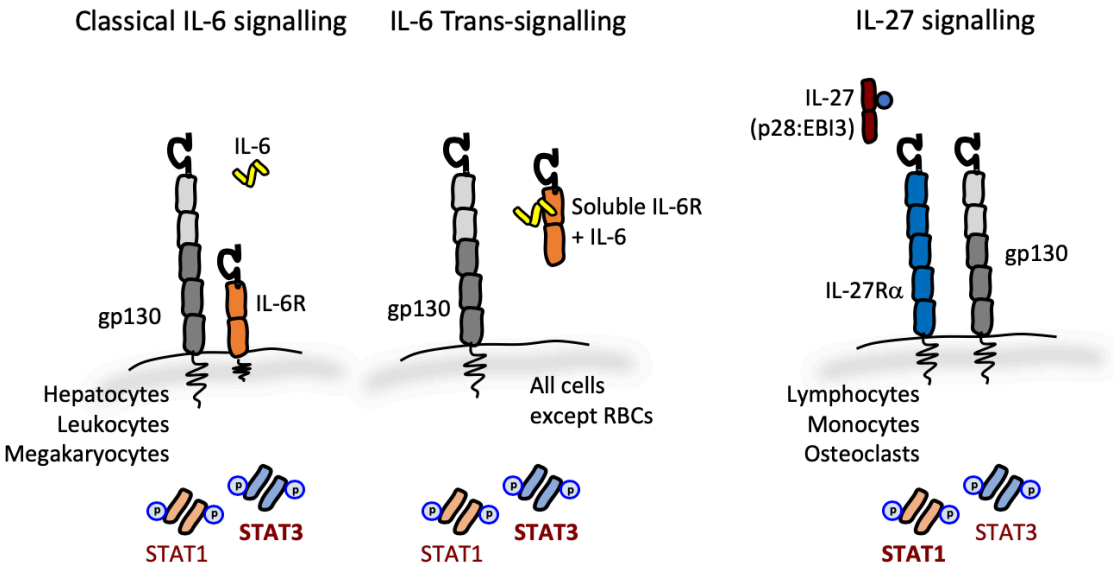

Figure 1.2 - The IL-6 and IL-27 receptor complexes. The composition of the IL-6 and IL-27 receptor complexes, the cell types expressing the receptors and the STAT transcription factors are shown. The preferential activation of STATs by IL-6 and IL-27 is indicated in bold. RBCs, red blood cells. Adapted from Jones *et al*. 2018.

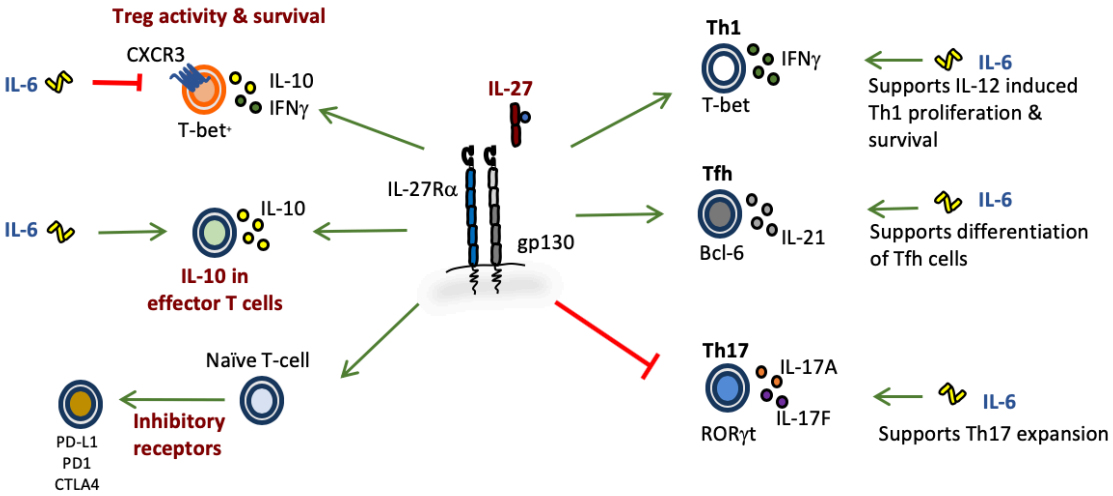

Figure 1.3 - The immunomodulatory actions of IL-6 and IL-27 in adaptive immunity. IL-6 and IL-27 often have opposing actions on adaptive immunity. IL-27 supports the expression of co-inhibitory receptors programmed death ligand 1 (PD-L1), programmed death 1 (PD-1) and cytotoxic T lymphocyte antigen-4 (CTLA4) on T cells. IL-27 also supports the development of IL-10 producing T-bet^{+}CXCR3^{+} Treg cells, whereas IL-6 inhibits Treg cells. IL-27 also inhibits IL-6 driven Th17 differentiation. However, IL-6 and IL-27 can both promote IL-21 production in Tfh cells, support IFNγ producing Th1 cells and induce IL-10 expression in effector T cells. Adapted from Jones *et al.* 2018 and Yoshida and Hunter 2015.

1.4 Ectopic Lymphoid-like Structures

Secondary lymphoid organs (SLOs), such as the spleen and lymph nodes, have a highly organised structure that allows communication and interaction of immune cells for the generation of antigen specific responses, an essential component of the adaptive immune response [116]. However, antigen specific responses may also be generated at sites distinct from SLOs. The first evidence of this comes from studies of the immune response in organisms that lack lymph nodes [117]. It is now becoming evident that in tissues affected by non-resolving inflammation, for example in cancer, infection and autoimmunity, infiltrating leukocytes can often form organised lymphoid aggregates within the inflamed tissue that promote adaptive immune responses [118]. These structures can exist as simple aggregates of T and B cells or more organised structures that resemble SLOs. Therefore, they are referred to as ectopic lymphoid-like structures (ELS; also called tertiary lymphoid structures, TLS). How and why these structures develop at these sites is currently unknown. To understand the mechanisms responsible for the development of ELS, researchers have relied on information derived from the development of SLO. In the sections below the development of SLOs is outlined and differences between the development of SLOs and ELS are highlighted.

1.4.1 Secondary Lymphoid Organogenesis

SLO development is initiated during embryogenesis through the interaction of haematopoietic derived lymphoid tissue inducer (LTi) cells with stromal lymphoid tissue organiser (LTo) cells [119]. LTi cells are characterised as $CD45^+CD4^+CD3^-$ cells with the transcription factors RORγt and Id2 required for their development. LTi cells also express CXCR5 and IL-7R, and accumulate at pre-determined sites of lymph node development due to local production of IL-7 and CXCL13, the ligand for CXCR5, by stromal cells in response to retinoic acid signals released by neurons and ILC3s [120, 121]. IL-7 and RANKL expressed by LTo cells support the differentiation and survival of LTi cells and upregulate lymphotoxin (LT) αβ on the surface of LTi cells [122-124]. The interaction of LTαβ with LTβ receptor (LTβR) found on LTo cells activates the canonical and non-canonical NF-κB pathways leading to expression of CXCL13, CCL19 and CCL21 as well as survival factors such as BAFF and adhesion molecules such as ICAM-1, VCAM-1 and MAdCAM-1 [125]. This leads to the recruitment of more LTi cells, which initiates a positive feedback loop through binding of homeostatic chemokines to their receptors which leads to upregulation of LTαβ and enlargement of the developing LN [126]. LTi cells enter the developing LN as they express the integrin $\alpha_4\beta_7$, the ligand for

MAdCAM-1 expressed on all embryonic blood vessels [127]. After birth, there is a switch in vascular addressin expression by HEVs; MAdCAM-1 is downregulated and PNAd is upregulated [128]. PNAd acts as a ligand for L-selectin to allow the recruitment of naïve T and B cells and expansion of the LN [129]. To further support SLO development, LTo cells can also differentiate into follicular dendritic cells (FDCs) found in B cell follicles and germinal centres, fibroblastic reticular cells (FRCs) found in the T cell zones and marginal reticular cells (MRCs) found at the edge of follicles. FRCs express CCL19 and CCL21 to attract $CCR7^+$ T cells and produce podoplanin and extracellular matrix components which form a scaffold for the organisation of T cells [130, 131]. FRCs have recently been shown to support interactions between APCs and T cells, promote antigen-specific immune tolerance and restrict the expansion of newly generated naïve T cells [132]. FDCs express CXCL13 and CD21 to recruit and organise $CXCR5^+$ B cells and BAFF, a B cell survival and proliferation factor [133, 134]. A new stromal cell subset called versatile stromal cells that reside in the T cell zone has also been identified [135]. Indeed, the complexity of stromal cell subsets within LNs has recently been elucidated through the use of single-cell RNA sequencing which identified nine distinct clusters [136]. Hence SLOs display a highly organised structure comprising of segregated T cell and B cell zones, germinal centres, HEVs and stromal cell networks (*Figure 1.4A*).

Therefore, according to the characteristics of SLO, it has been proposed that the minimal requirements to form ELS include: (i) organised T and B cell zones; (ii) $PNAd^+$ HEVs for the extravasation of L-$selectin^+$ immune cells; (iii) expression of homeostatic chemokines (CCL19, CCL21 and CXCL13) required for lymphoid organ organisation; and (iv) stromal cell networks such as FDC networks for germinal centres reactions. Where the requirements for ELS are not met they are better described as lymphoid aggregates [137].

1.4.2 Mediators of ELS development

While ELS share many of the features of SLOs, it is emerging that there are key differences. Firstly, in terms of structure, ELS are not encapsulated. They are also inducible structures that form in response to inflammatory stimuli at sites of inflammation rather than at pre-determined locations based on developmental signals [138]. However, ELS can only form in permissive tissues and an association has been made with mucosal epithelium. For example, overexpression of CCL21 induces the formation of ELS in the pancreas but not in the skin [139]. Interestingly, despite the lack of epithelium, ELS can form in synovium of patients with RA [118]. Thus, certain tissues are more permissive to

ELS formation than others. It is also emerging that the initiation cues required for ELS development differ from secondary lymphoid organogenesis. Whilst LTi cells are central to the initiation of SLO development, ELS can form in the absence of LTi cells. Here, ELS can still form in mice deficient in RORγt and the transcriptional repressor Id2, despite the lack of LTi cells [140-142]. This has led to the notion that resident stromal tissue cells or infiltrating inflammatory cells can initiate the development of ELS at sites of disease (*Figure 1.4B*).

Th17 cells, including cytokines linked with Th17 effector responses, have recently been associated with tissue inflammation featuring ELS. In this regard, a direct role in promoting ELS formation was demonstrated through the adoptive transfer of *in vitro* generated Th17 cells into mice with EAE [143]. Additionally, the Th17 cell effector cytokines, IL-17A and IL-22, have been linked to the development of inducible bronchus-associated lymphoid tissue (iBALT) [142, 144] and the development of ELS in salivary glands following local challenge with adenovirus [145]. Interestingly, γδ T cells are also capable of producing IL-17A and IL-22. During the development of iBALT in response to *Pseudomonas aeruginosa* infection the main source of IL-17 was from γδ T cells [144]. Following adenovirus delivery, IL-22 regulation of ELS development in the salivary gland was initially associated with IL-22 expression in γδ T cells. However, this was replaced by a prominent αβ T cell response [145]. Interleukin-21, derived from either Th17 or Tfh cells, has also been implicated with ELS development. Here, elevated levels were observed in synovial tissue in a murine model of inflammatory arthritis and in inflamed salivary glands that featured ELS [146, 147]. Furthermore, expression of Tfh markers, including Bcl-6 and CXCR5, have been linked with ELS development in an experimental uveitis model [148].

Innate cells have also been linked with ELS development. For example, LPS-induced iBALT was associated with increased levels of neutrophils within the lung. Interestingly, neutrophil depletion, using an anti-Ly6G antibody, reduced iBALT formation [149]. Mirroring the central role played by LTi cells in SLO development during ontogeny, adult LTi cells have also been implicated in ELS development. In this regard, adult LTi cells are classed as group 3 innate lymphoid cells (ILC3s) and share many effector characteristics with Th17 cells, including RORγt expression, the chemokine receptor CCR6, secretion of IL-17, IL-22, and granulocyte-macrophage colony-stimulating factor (GM-CSF), and responsiveness to IL-23 and aryl hydrocarbon receptor (Ahr) ligands. Using *Cxcr5*$^{-/-}$ mice that lack Peyer's patches (lymphoid follicles found within the small

intestine), adoptive transfer of adult $CD4^{+}CD3^{-}$ LTi cells led to the development of intestinal lymphoid aggregates [150]. Additionally, overexpression of IL-7 led to an increase in intestinal lymphoid aggregates that was associated with an increase in the number of LTi cells [151]. Thus, multiple immune cells have been linked with the development of ELS during inflammation and their contribution to this process is likely to be complex and context dependent.

While potential propagators of ELS are being identified in numerous disease settings, less is known about mediators that inhibit ELS development. Recently however, our group identified IL-27 as an inhibitor of ELS development in a model of inflammatory arthritis [146]. Here, *Il27ra*$^{-/-}$ mice developed exacerbated inflammatory arthritis characterised by an increase in leukocyte infiltration and synovial exudate. Additionally, in the absence of IL-27 receptor, mice developed synovial ELS that was associated with an increase in homeostatic chemokine expression [146]. In addition, in a mouse model of primary Sjögren's syndrome, IL-27 gene therapy using a recombinant adeno-associated virus vector reduced the size of lymphocyte aggregates in salivary glands [152]. Hence, IL-27 has emerged as a novel inhibitor of ELS development.

A common feature in the development of SLOs and ELS is the production of homeostatic chemokines. However, during ELS development additional cell types, other than LTo cells, may acquire the ability to produce these chemokines. Here, stromal cells may play a role in shaping ELS development. For example, infection with *Pseudomonas aeruginosa* results in iBALT development associated with IL-17 driven CXCL12 production from pulmonary stromal cells [144]. Similarly, IL-17 stimulation of synovial fibroblasts from patients with RA induces the expression of CXCL12 [153]. Other studies using an influenza infection model identified that stromal cells and peripheral node addressin (PNAd)-positive HEVs produced CXCL13, CCL19 and CCL21 required for iBALT formation [154]. Interestingly, iBALT still developed in *Cxcl13*$^{-/-}$ mice suggesting that other chemokines can direct the recruitment of B cells in this model [154]. Following adenovirus challenge in the salivary gland IL-22 induced the expression of CXCL13 from stromal cells and CXCL12 from epithelial cells that contributed to ELS development [145]. Hence, stromal cells contribute to ELS development through secreting homeostatic chemokines including CXCL13, CXCL12, CCL19 and CCL21, which may influence the composition and activity of ELS.

Thus, immune cells and stromal cells can adopt features of LTi cells and LTo cells respectively, in order to initiate the development of ELS in chronically inflamed tissue (*Figure 1.4*).

1.4.3 The Function of ELS in disease

For ELS to support B cell responses and antibody production they must recapitulate the function of SLOs. The expression of AID, which promotes somatic hypermutation and class-switch recombination, identifies the presence of active germinal centres. AID is expressed in lymphoid aggregates from the synovium of RA patients [155]. In trans-well co-culture studies, synovial fibroblasts from RA patients increased the expression of AID in B cells [156]. Class-switch recombination can also be detected using PCR directed against circular transcripts (e.g., Iγ-Cμ for IgM-IgG class-switching) that are generated by the looping out of DNA during genomic recombination. These circular transcripts have been identified in ELS following cytomegalovirus challenge in the salivary gland and in a murine model of lupus [157, 158]. Furthermore, transfer of AID-positive lymphoid aggregates into severe combined immunodeficient (SCID) mice resulted in the release of human anti-citrullinated protein antibodies (ACPAs) into the circulation [155]. Similarly, the transfer of salivary gland biopsies featuring ELS from patients with Sjögren's syndrome into SCID mice resulted in the release of human antibodies against ribonucleoproteins Ro (Sjögren's syndrome antigen A; SSA) and La (Sjögren's syndrome antigen B; SSB) [159]. Hence, ELS are sites of active class-switching and autoantibody production within inflamed tissues.

In addition, a number of studies demonstrate that ELS can display functional anti-pathogen responses. For example, following influenza virus infection in mice, ELS formed in the lung that generated plasma cells specific for influenza virus nucleoprotein [160]. In this model, ELS were maintained through chemokine secretion by dendritic cells. Importantly, depletion of dendritic cells resulted in decreased levels of class-switch dependent IgA [160], indicating that ELS can generate antigen-specific responses and class-switching. Indeed, anti-pathogen responses have also been observed at ELS independently of SLO involvement. In spleen, lymph node and Peyer's patches (SLP) mice, reconstitution with wild type bone marrow prior to influenza infection resulted in the development of ELS within the lung (iBALT) that were effective in clearing the virus [161].

Thus, it is proposed that the development of ELS in autoimmunity is detrimental, due to the perpetuation of the immune response, whereas ELS development in infection may be beneficial through the establishment of local anti-pathogen responses.

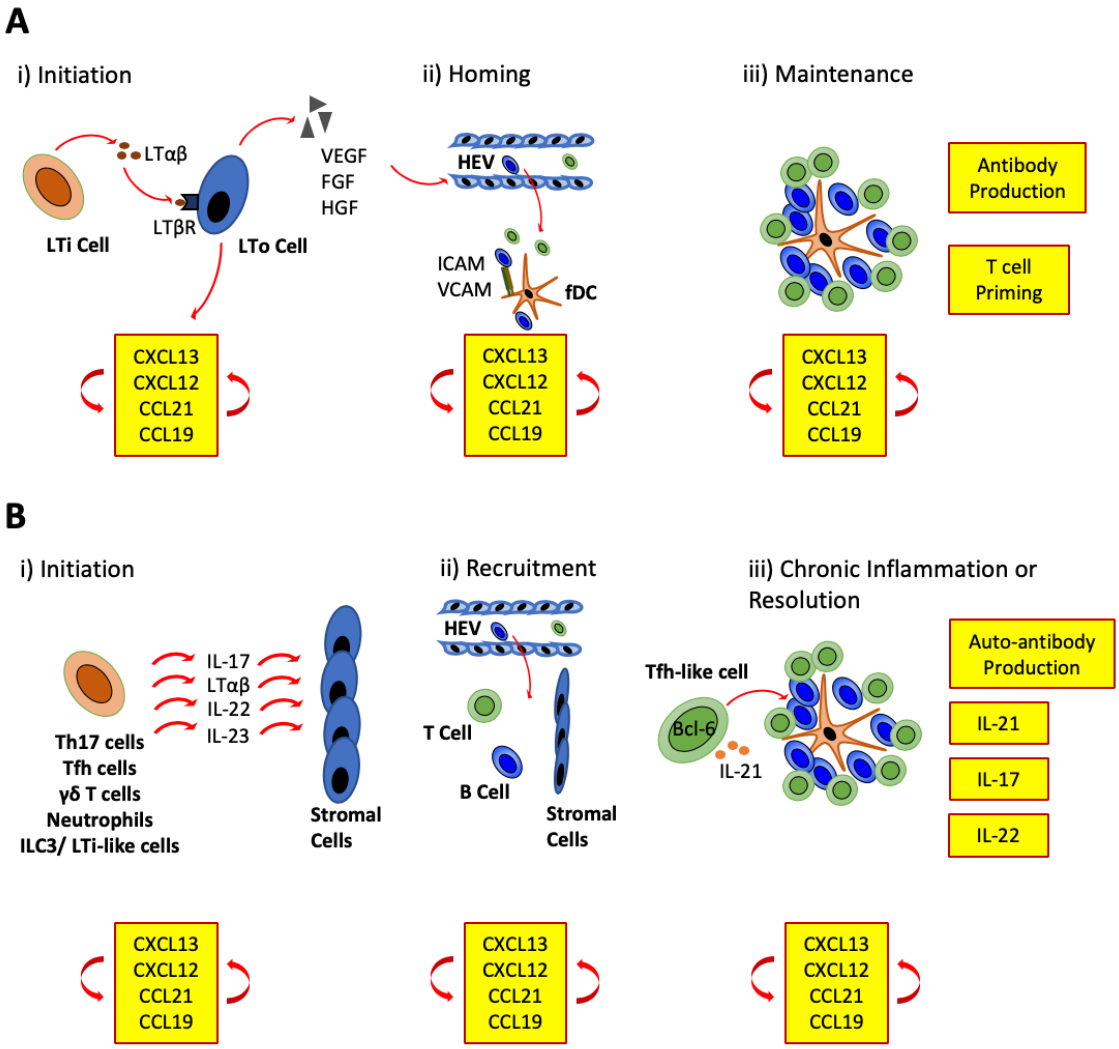

Figure 1.4 - Secondary lymphoid organogenesis and ectopic lymphoid-like structure development. (A) The development of secondary lymphoid organs (SLOs) occurs at pre-programmed sites during embryogenesis. It is mediated through the interaction of LTi cells, which secrete LTαβ, with LTo cells, that express the LTβ receptor. This interaction stimulates LTo cells to secrete homeostatic chemokines (CXCL13, CXCL12, CCL19 and CCL21) that recruit and spatially organise cells into lymphoid organs. The recruitment of cells is supported by the release of VEGF, FGF and HGF from LTo cells that promotes the formation of high endothelial venules (HEVs). LTo cells are also capable of differentiating into follicular dendritic cells (fDCs) that upregulate expression of adhesion molecules to further support leukocyte recruitment. SLOs are sites of T cell priming and antibody production. (B) At sites of chronic inflammation ectopic lymphoid-like structures (ELS) can form. Immune cells can substitute the role of LTi cells and the release of effector molecules can induce stromal cells to produce homeostatic chemokines involved in the recruitment and spatial organisation of cells into ELS. ELS are sites of T cell priming and plasticity of T cells may support the activities of B cells and antibody production. LTi, lymphoid tissue inducer; LTo, lymphoid tissue organiser; LT, lymphotoxin; VEGF, vascular endothelial growth factor; FGF, fibroblast growth factor; HGF, hepatocyte growth factor; ICAM, intracellular adhesion molecule; VCAM, vascular cell adhesion molecule.

1.5 Rheumatoid arthritis

Rheumatoid arthritis (RA) affects approximately 0.5% to 1% of the global adult population making it the most common rheumatic autoimmune disease [162]. It is characterised by chronic inflammation of the joints, resulting in synovial inflammation and hyperplasia, autoantibody production and cartilage and bone erosion. As a consequence, RA is associated with musculoskeletal defects resulting in a decline in physical ability. It is also linked with an increased risk in developing comorbidities. The inflammatory environment in RA causes muscle and adipose tissue to become insulin resistant, effects cognitive function, alters cholesterol levels, and is associated with an increased risk of cardiovascular disease leading to premature death [34, 163, 164].

1.5.1 Risk factors associated with RA

The mechanisms that lead to a breach of tolerance in RA are poorly understood. However, there are numerous genetic and environmental risk factors associated with its development. For example, smoking, which promotes the citrullination of proteins, is an environmental risk factor for the development of RA. Many of the genetic risk alleles identified overlap with immune regulatory genes. For example, alleles that contain the shared epitope (QKRAA) in the *HLA-DRB1* locus are particularly susceptible to developing RA. These residues form part of the antigen presenting binding site, and it is thought that they allow the presentation of arthritogenic peptides [165]. Additionally, risk alleles have been found in *PTPN22*, a protein tyrosine phosphatase that downregulates T cell receptor responses [166], *PADI4*, a peptidylarginine deaminase able to citrullinate proteins and *CTLA4*, an immune checkpoint receptor expressed on activated T cells [165]. Interestingly, genetic variations in *IL6ST* (encoding gp130) and *IL6R* are common to patients with RA [167, 168] and a single nucleotide polymorphism in *IL27* was linked to more advanced disease [169]. Hence, while the cause of RA remains unknown, it is generally thought that environmental and genetic predisposition contributes to the breach of immunological tolerance and autoantibody generation.

1.5.2 Disease pathogenesis

A hallmark of RA is the presence of autoantibodies such as rheumatoid factor (RF), directed against Fc fragments of IgG, and autoantibodies against citrullinated peptides (ACPAs) [162]. Whilst not all patients have circulating autoantibodies, their presence is associated with more severe joint damage and increased mortality [170-172]. Additionally, circulating ACPAs can be detected up to 10 years before diagnosis [173],

and over time their concentration and epitope diversity increases [162]. It is proposed that a subsequent trigger then promotes articular localisation and the onset of clinical disease.

Joint swelling in RA is characterised by infiltration of leukocytes, synovial hyperplasia, thickening of the synovial lining and pannus formation. Inflammatory cells found within the synovium include, T and B cells, macrophages, dendritic cells, neutrophils, natural killer (NK) cells and monocytes [174]. The inflamed synovium invades cartilage and promotes bone destruction, which is facilitated by soluble mediators such as cytokines [54]. For example, RANKL (receptor activator of nuclear factor-κB ligand) is secreted by synovial fibroblasts and activated T cells in response to IL-1β, TNFα, IL-6 and IL-17, and is essential for the differentiation of osteoclasts and subsequent bone resorption. Additionally, pro-inflammatory cytokines induce chondrocytes to secrete matrix metalloproteases (MMPs) that cleave proteoglycans and collagens that form cartilage [54]. Furthermore, inflammatory cytokines can enter the circulation resulting in systemic inflammation, fatigue, depression and other associated comorbidities.

1.5.3 Assessment of disease activity

Assessment of a patient's disease activity enables identification of the stage of disease and response to therapy. One such measure is the Disease Activity Score (DAS)28 index which provides a continuous measure of disease activity [175]. It considers the number of swollen and tender joints out of 28 examined, serum markers of inflammation (e.g. CRP) and personal assessment of health, in order to calculate an overall disease activity score. A DAS28 score greater than 5.1 indicates active disease, less than 3.2 low disease activity and a score below 2.6 indicates remission [176].

Other measures include the American College of Rheumatology (ACR) score which allows judgment of improvement but not a measure of disease activity. An ACR20 score means that a patient has 20% fewer swollen or tender joints, a reduction in overall assessment of RA and reduction in serum markers of inflammation. An ACR50 and ACR70 response indicates a 50% and 70% improvement respectively [177]. Whilst the DAS28 is routinely used in the clinic, ACR scores are a standardised measure of response to therapy in clinical trials.

1.5.4 Treatment of RA

The treatment of RA aims to reduce systemic and local inflammation and prevent irreversible joint damage [178]. This is achieved through the use of disease modifying

anti-rheumatic drugs (DMARDs) and various biologic drugs and small molecule inhibitors directed against signalling pathways or inflammatory cytokines that contribute to the pathogenesis of RA (*Figure 1.5*). Early diagnosis and intervention, during a "therapeutic window of opportunity" increases the likelihood of therapy being effective and achieving disease remission [179]. In this context, a recent study showed that a single infusion of rituximab in patients with autoantibodies but no clinical symptoms delayed the onset of RA [180].

Upon diagnosis DMARD therapy is recommended, and treatment generally begins with the use of methotrexate [175]. If disease activity does not reduce (determined using the DAS28 score) TNF inhibitors (e.g., etanercept, infliximab) can be used in conjunction with methotrexate. For patients with high disease activity, methotrexate combined with TNF inhibitors is typically used from diagnosis [181, 182]. In this context, studies have shown that the combination of methotrexate with TNF inhibitors has a synergistic effect [183]. However, not all patients respond equally well to any individual drug. For example, approximately 40% of patients show poor responses to anti-TNF therapy [184-186]. In a treat-to-target approach, other biologic agents can be used until disease activity is reduced. In this regard, patients display marked improvement in disease activity when switched to either a different TNF inhibitor [187] or to a different biologic [188-190]. These commonly include anti-IL6R (e.g. tocilizumab), anti-CD20 (e.g. rituximab), CTLA4-IgG (e.g. abatacept) and JAK inhibitors (e.g. tofacitinib). While the mode of action for these drugs differs quite considerably, they all combat inflammation through actions on target cells, cytokines and signalling cascades that drive disease progression (*Figure 1.5*).

Tocilizumab – a human monoclonal antibody that acts as an IL-6 receptor antagonist. In this regard it recognises both membrane bound and soluble IL-6 receptor, as such it inhibits both classical and trans-signalling [191].

Rituximab – a B cell targeting antibody that binds CD20 to deplete B cells. The mechanism by which rituximab depletes B cells is debated but could be due to cytotoxicity and inducing apoptosis [192].

Abatacept – a CTLA4-IgG that blocks the co-stimulatory interaction between CD28 and CD80 or CD86 expressed on APCs that is required for T cell activation [178]. Thus, abatacept functions to suppress T cell activation and release of effector molecules.

Tofacitinib – a small molecule inhibitor that inhibits the JAK-STAT pathway. It primarily targets JAK1 and JAK3 [178].

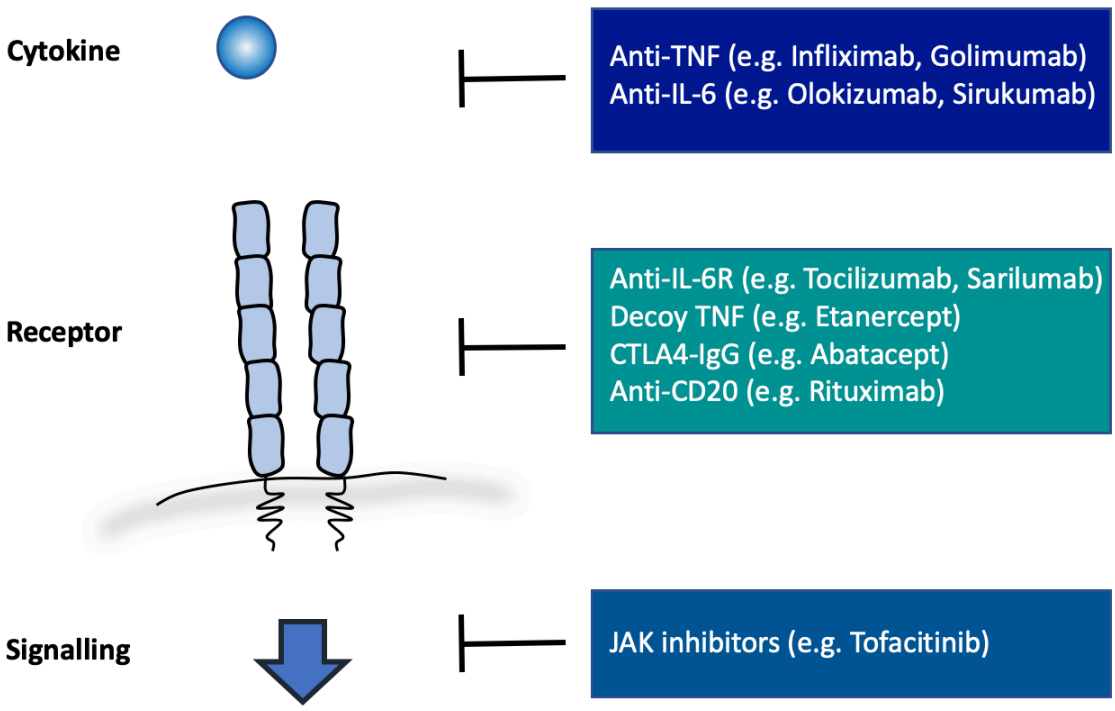

Figure 1.5 - Biologic agents for the treatment of Rheumatoid arthritis. Current biologics for the treatment of Rheumatoid arthritis reduce inflammation by targeting inflammatory cytokines and the activities of T and B cells. They target either (i) the cytokine (ii) the receptor or (iii) the intracellular signalling pathway. Different biologic targets are shown in the boxes and drug names indicated in brackets.

1.6 Ectopic lymphoid-like structures in Rheumatoid arthritis

The development of minimally invasive ultrasound-guided synovial biopsy sampling has advanced our understanding of disease pathogenesis in RA [174]. It is now appreciated that RA is a highly heterogenous disease. Infiltrating immune cells can either be found randomly distributed throughout the synovial cavity or spatially organised into ELS. These patterns of synovial pathology have been termed 'diffuse' and 'follicular' synovitis respectively. While RA is typically characterised by the infiltration of immune cells a third pattern of synovial pathology termed 'pauci-immune', comprises few immune cells yet is still found in active disease (*Figure 1.6*) [155, 193-195]. These different forms of synovitis impact disease progression and severity, and the clinical response to mainstream therapies, including anti-TNF and anti-CD20 specific antibodies [195-197].

1.6.1 The role of IL-6 and IL-27 in RA

The cytokines IL-6 and IL-27 play key roles in shaping synovial pathology. Despite signalling through the same co-receptor, gp130, IL-6 and IL-27 levels in RA correspond with differences in disease activity [47]. For example, IL-6 is highly expressed in the synovial fluid of RA patients [198] and blockade of IL-6 signalling is clinically beneficial highlighted by the use of tocilizumab. Equally, in animal models of inflammatory arthritis *Il6*$^{-/-}$ mice display a protected phenotype with reduced synovial leukocyte infiltration and erosive joint damage [69, 88, 89, 199].

In contrast, in collagen-induced arthritis systemic administration of IL-27 resulted in reduced incidence of disease and histological paw score. This was associated with reduced collagen-specific antibody titres and decreased serum levels of IL-6 and IL-17 [200]. Furthermore, the local injection of adenovirus expressing IL-27 into the ankles of mice following the induction of collagen-induced arthritis resulted in reduced joint inflammation and bone erosion, which was also associated with decreased expression of IL-6 and IL-17 in inflamed joints [201]. Thus, IL-27 can act both systemically and locally to improve synovitis and joint damage in inflammatory arthritis. Elevated levels of synovial and serum IL-27 observed in clinical RA may therefore reflect an effort to counteract persistent local and systemic inflammation.

Consistent with the anti-inflammatory properties of IL-27 when administered during experimental inflammatory arthritis, recent studies using the antigen-induced arthritis (AIA) model in *Il27ra*$^{-/-}$ mice resulted in exacerbated disease. Here, synovitis was associated with elevated adaptive immune responses in *Il27ra*$^{-/-}$ mice, highlighted by

increased T cell infiltrate and mBSA-specific antibody titres. Moreover, *Il27ra*$^{-/-}$ mice developed synovial ELS with 100% penetrance, characterised by the presence of CD21^{+} follicular dendritic cells, Bcl-6, a marker of germinal centre B cells, and increased expression of homeostatic chemokines [146]. Crucially, this is reflected in synovial biopsies from RA patients. Here, patients with follicular disease, characterised by the presence of synovial ELS, displayed decreased expression of *IL27* compared to patients with diffuse synovitis [146]. Thus, IL-6 and IL-27 have opposing roles in shaping synovial pathology.

1.6.2 ELS and disease severity

ELS within the synovium of RA patients have been shown to express AID and generate autoantibodies [155] (*see section 1.4.3*). Subsequently the presence of ELS within the synovium of RA patients has been shown to correlate with disease severity and degree of inflammation. For example, levels of CXCL13 and CD20, that mark the presence of ELS, correlate with the degree of erosive bone damage [202, 203]. Additionally, the presence of lymphoid aggregates within the joints of RA patients correlated with elevated synovial autoantibodies, RF and ACPAs [204]. However, in other studies despite the presence of lymphoid aggregates correlating with an increase in serum levels of inflammatory markers, ESR and CRP, there was no difference in clinical measures, such as DAS28 scores, or autoantibody levels [205]. Thus, the effect of synovial ELS on disease severity in RA is debated.

1.6.3 ELS and response to therapeutics

Anti-TNF therapy is the frontline biologic used in RA [178]. However not all patients respond to treatment. In one study, the improvement in DAS28 scores was found to be significantly lower in patients with synovial lymphoid aggregates following the use of anti-TNF therapies [197]. Here, the presence of lymphoid aggregates within the synovium of RA patients was a negative predictor of the response to anti-TNF therapy, despite the elevated levels of TNFα within the synovium of patients with 'follicular' pathology [194, 206]. Comparable findings were also reported by Dennis *et al.,* where CXCL13 serum levels were used as a predictive marker of lymphoid-rich synovitis [195]. Here, CXCL13^{high}/sICAM^{low} patients displayed better clinical responses (ACR50) to anti-IL-6R (tocilizumab) as compared to anti-TNF (adalimumab) inhibitors. However, the relationship between the presence of synovial ELS and response to biological drugs remains a controversial topic, and synovial lymphoid aggregates have also been linked with improved clinical responses to anti-TNF treatment [207].

Studies have also investigated the link between clinical response to rituximab, an anti-CD20 antibody, and the presence of lymphoid aggregates. Here, it is also evident that not all patients respond equally to treatment [196]. Following rituximab treatment, patients with lymphoid aggregates showed no reduction in autoantibody levels [204]. This may represent the lack of expression of CD20 by antibody secreting plasma cells [208]. Interestingly, while rituximab treatment has been shown to effectively deplete circulating B cells, little effect was observed in B cells residing within ELS with no difference in the number or area of lymphoid aggregates within the synovium [209]. Thus, ELS may provide an environment that supports B cell survival during anti-CD20 treatment. Notably, 6 months after rituximab treatment, patients with higher circulating levels of CXCL13 displayed a significant increase in the number of circulating B cells compared to patients with low CXCL13 levels [210]. Hence, CXCL13 levels may indicate the extent of B cell replenishment following treatment and could potentially be used to inform of treatment strategies.

Taken together, these studies suggest that ELS can affect the response to biologic therapy, however a greater understanding is needed in this area.

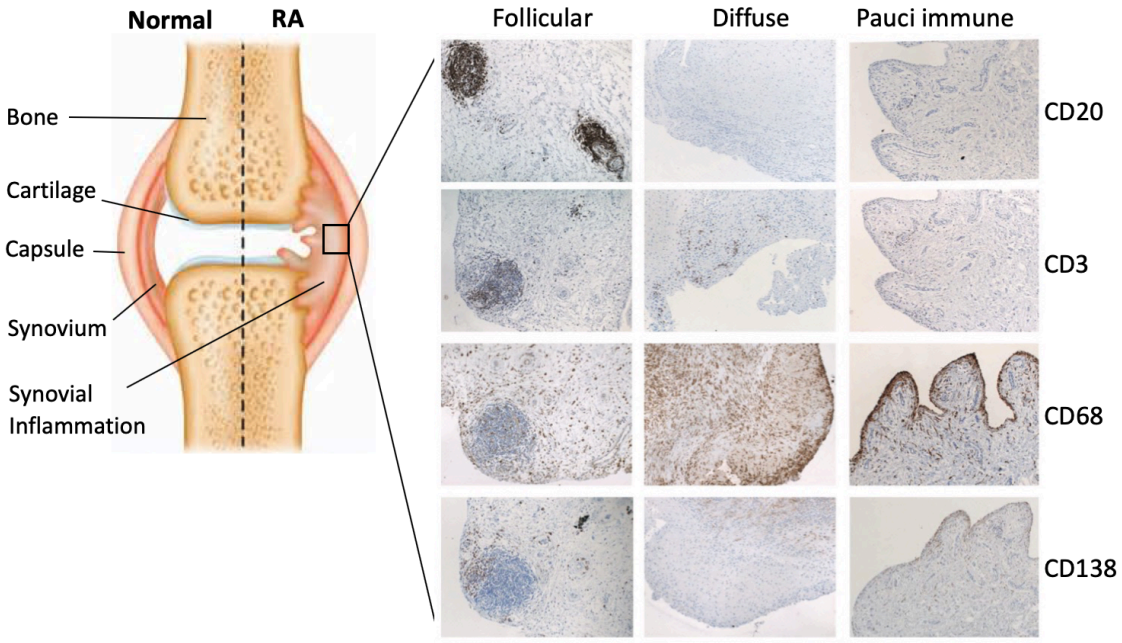

Figure 1.6 - Joint pathology in Rheumatoid Arthritis. Normal (left of joint) and inflammation-associated erosion in rheumatoid arthritis (right of joint). Immunohistochemical staining for CD20 (B cells), CD3 (T cells), CD68 (monocyte/macrophage) and CD138 (plasma cells) highlights differences in synovial pathology. Synovial inflammation can comprise diffuse leukocyte infiltrates (diffuse) also associated with being myeloid-rich, contain follicular aggregates of lymphocytes (follicular) or have low infiltration of immune cells (pauci immune). Adapted from Pitzalis *et al.* 2013.

1.7 Gastric cancer

Gastric cancer is the second largest cause of cancer related deaths worldwide [211]. Most gastric cancers arise from gastric epithelium (adenocarcinomas), with other malignancies arising from connective tissue (sarcoma) and lymphatics (lymphoma) being less common. However, all are highly heterogenous with regards to growth, architecture and pathogenesis [212]. Gastric cancers can be further classified based on their histological appearance. Two subtypes exist - intestinal and diffuse carcinomas. Diffuse carcinomas are poorly differentiated and composed of solitary tumour cells. Intestinal-type carcinomas are well differentiated and form glandular structures reminiscent of colorectal carcinomas, hence the name [213]. Gastric cancer develops as a result of an inflammatory process that progresses from chronic gastritis to intestinal metaplasia. Factors associated with an increased risk of gastric cancer include diet, smoking, genetic predisposition (e.g. mutations in E-cadherin) and infection [211]. For the latter, chronic gastritis caused by infection with *Helicobacter pylori* is a major risk factor for gastric cancer. In this context, it is now estimated that over 20% of all human cancer cases are associated with chronic inflammation [214].

However, a question that remains unanswered is how chronic inflammation triggers tumourigenesis in the gastric epithelium. In this regard, it is thought that an inflammatory microenvironment consisting of inflammatory cells, cytokines, chemokines and growth factors act on epithelial cells to trigger intracellular signalling pathways and activation of transcription factors [215]. A key transcription factor associated with gastric tumourigenesis is STAT3. Activation of STAT3 induces the transcription of genes involved in cell progression and survival and angiogenesis [216]. In clinical gastric cancer, patients display increased STAT3 activation in response to heightened levels of the IL-6 family cytokine, IL-11 [217, 218]. Similarly, mice that have constitutive activation of STAT3 downstream of the IL-6 family signalling receptor, gp130, spontaneously develop gastric tumours. These mice, termed *gp130*$^{Y757F:Y757F}$ (*gp130*$^{F/F}$) (*Figure 1.7*), have a 'knock-in' substitution of tyrosine 757 for a phenylalanine in the cytoplasmic domain of gp130, which disrupts the binding of SOCS3. Hence the negative feedback inhibition mediated by SOCS3 on gp130 signalling is inhibited, which leads to prolonged and hyperactivation of STAT3 and subsequent gastric tumourigenesis. This phenotype is driven by the IL-6 family cytokine, IL-11 (*Figure 1.7*) [219-221].

Another transcription factor implemented in gastric tumourigenesis is NF-κB. Here, pro-inflammatory cytokines (e.g. IL-1β, TNFα) and PRRs, that detect microbial

pathogens (e.g. TLR2), can activate the NF-κB pathway. This can lead to cell proliferation, survival, migration and angiogenesis as well as increasing transcription of pro-inflammatory cytokines that further perpetuates the inflammatory environment [215]. Importantly, there is also cross-regulation between these two pathways. For example, hyperactivation of STAT3 in *gp130*$^{F/F}$ mice resulted in the transcriptional induction of TLR2 on gastric epithelial cells and resultant activation of NF-κB [222].

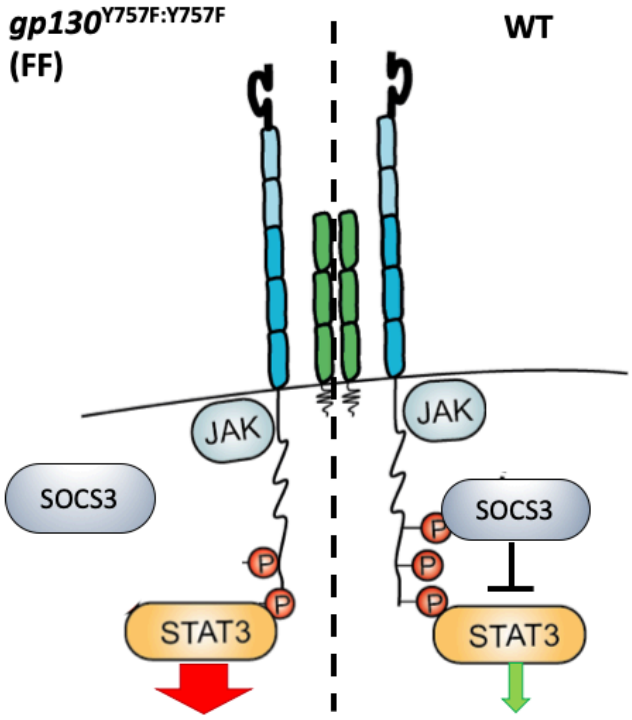

Figure 1.7 - Hyperactive STAT3 signalling in gp130$^{Y757F:Y757F}$ mice causes gastric tumourigenesis. The IL-6 family of cytokines signal through a co-receptor called gp130 to activate STATs. Gastric tumourigenesis in *gp130*$^{Y757F:Y757F}$ (*gp130*$^{F/F}$) mice is driven by IL-11 binding to the IL-11 receptor. Binding results in association of JAKs which phosphorylate tyrosine residues on the intracellular domain of gp130. This promotes the binding of STAT3. Subsequent phosphorylation of STAT3 by receptor-associated JAKs promotes STAT dimerization, and their translocation to the nucleus where they initiate transcription. In WT mice, this process is tightly regulated by suppressors of cytokine signalling 3 (SOCS3) which binds to phosphorylated tyrosine 757 and acts through negative feedback to supress STAT3 activity. In *gp130*$^{F/F}$ mice, there is a substitution of tyrosine 757 for a phenylalanine in the intracellular domain of gp130. This disrupts the binding of SOCS3 and therefore leads to a loss of the negative feedback inhibition mediated by SOCS3 on STAT3 activity. Thus, *gp130*$^{F/F}$ mice have hyperactivation of STAT3 (indicated by the size of the arrow) leading to gastric tumourigenesis.

1.8 Ectopic lymphoid-like structures in cancer

Chronic inflammation is a feature of many tumours and as such provides an environment for the development of ELS. However, one would assume that the highly immunosuppressive tumour environment might prevent the formation of ELS. Nonetheless, ELS have now been described in many cancers including colorectal [223-225], breast [226, 227], melanoma [226, 228-230], ovarian [226, 231] and non-small cell lung cancer (NSCLC) [226, 232-234]. These range from simple lymphoid aggregates to highly organised structures more reminiscent of SLOs. Akin to the development of ELS in autoimmunity, tumour-associated ELS also share the same set of molecules as SLOs (*see section 1.4*). However, it is important to note that the permissiveness of the tumour microenvironment is likely to have an effect on tumour-associated ELS development. For example, metastases from melanoma, lung and colorectal cancers induce a higher density of lymphoid aggregates than metastases from breast cancer [235]. Thus, tumour-associated ELS are likely to differ between different types of cancer, depending on the permissiveness of the tissue to ELS formation, as well as between patients.

Since ELS are typically seen as sites of T cell priming and antibody generation, it raises the question whether tumour-associated ELS are capable of inducing anti-tumour responses. The first example of this came from using tumour-specific antibody-LTα fusion proteins in mouse tumour models. Here, administration of antibody-LTα fusion protein resulted in a decrease in pulmonary metastases and increased survival. This was attributed to an increased T cell response and the development of lymphoid aggregates at the tumour site [236]. In addition, by using LT$\alpha^{-/-}$ mice that lack lymph nodes it was found that the generation of tumour-specific T cells occurred in lymphoid aggregates at the tumour site, rather than being primed at SLOs [237]. In ELS that developed in melanoma, sequencing of immunoglobulin heavy chains revealed that B cells had undergone somatic hypermutation, class-switching and affinity maturation [228]. However, it was not determined whether the antibodies generated were directed against tumour antigens. In this context, studies of ELS in NSCLC identified the presence of germinal centre B cells, characterised by the expression of AID, Bcl-6 and Ki-67, as well as the presence of plasma cells that secreted antibodies against tumour antigens (e.g. NY-ESO-1, TP53, LAGE-1) [233]. The density of germinal centre B cells correlated with the density of plasma cells suggesting that these responses were generated at tumour-associated ELS, rather than in the periphery [233]. Furthermore, in patients with NSCLC, the immune cell populations found within ELS were identified using flow cytometry and

differential expression of cell surface markers. Whilst the main populations present were memory cells, naïve T and B cells were also detected [233, 234]. Hence the activation and differentiation of naïve T and B cells could occur in tumour-associated ELS, promoting anti-tumour immunity.

In this regard, there are examples where the development of tumour-associated ELS is associated with a favourable clinical outcome. For example, the targeting of LIGHT, an alternative LTβR ligand produced by activated T cells, to tumours using a vascular targeting peptide (VTP) resulted in the formation of intratumoural ELS, characterised by segregated T and B cell zones and $PNAd^+$ HEVs [238]. Here, the development of ELS resulted in increased tumour infiltration of $CD4^+$ and $CD8^+$ T cells, loss of tumour cells and increased survival [238]. In colorectal cancer a high density of ELS correlated with improved patient survival [239, 240]. In NSCLC, a higher number of cytotoxic IFNγ-generating $CD8^+$ T cells were observed in patients that developed ELS and were associated with the presence of mature dendritic cells. Whilst patients with high levels of $CD8^+$ T cells had improved survival, a further increase in survival was seen when combining high levels of $CD8^+$ T cells with the presence of ELS [241]. Hence, tumour-associated ELS may provide a microenvironment that allows $CD8^+$ T cells to develop enhanced effector functions to support anti-tumour immunity.

However, the presence of ELS is not always associated with favourable outcomes. In line with a role for Tregs in suppressing self-reactive T cells in SLOs, the presence of Tregs in ELS also has immunosuppressive effects. In primary breast tumours, high numbers of $FoxP3^+$ Treg cells within ELS was associated with an increased risk of death [242]. In a mouse model of lung adenocarcinoma, the presence of Tregs in ELS suppressed anti-tumour responses. Importantly, Treg depletion led to T cell proliferation within ELS and generation of anti-tumour responses leading to tumour regression [243]. The presence of ELS also correlated with a poor prognosis in hepatocellular carcinoma. Here, the development of ELS was linked with NF-κB activation. Mice overexpressing IKKβ in hepatocytes developed ELS and aggressive hepatocellular carcinomas. It was shown that ELS functioned as microniches providing survival and growth factors to support tumour progenitor cells until they egressed to form tumours [244].

Thus, ELS characterised in cancer often show similarities with those seen in autoimmune conditions. However, their contribution to disease processes often differs. Therefore, there is a need to understand how these structures arise and whether the inflammatory context has a bearing on their involvement.

1.9 Aims

The development of ELS is characteristic of chronic inflammatory diseases. They can develop at sites of tumourigenesis and in the synovium of patients with RA. In this regard, previous studies in our group have demonstrated the opposing role that IL-6 and IL-27 have on synovial pathology. Here, *Il27ra*$^{-/-}$ mice develop exacerbated disease and the presence of synovial ELS. The work presented in this thesis aims to-

1. **Establish RNA sequencing of the inflamed synovium**

In order to identify transcriptomic changes associated with the development of ELS in inflammatory arthritis, RNA extraction from the synovium and cDNA library preparation must be optimised for RNA sequencing.

2. **Identify gene changes associated with the development of ELS during inflammatory arthritis**

Adopting a transcriptomic approach, experiments will explore the major inflammatory pathways and gene expression changes associated with the development of synovial ELS in *Il27ra*$^{-/-}$ mice.

3. **Investigate cross-disease mechanisms that govern ELS in inflammation**

Studies will characterise the development of ELS in a mouse model of gastric cancer and identify whether there are common mechanisms governing ELS development and activity across inflammatory arthritis and inflammation-associated cancer.

4. **Target pathways associated with ELS development**

Mediators of ELS development identified through RNA sequencing will be targeted using a genetic and therapeutic approach to determine the effect on ELS development in inflamed tissues.

Chapter 2. Materials and Methods

2.1 Reagents

All chemicals were purchased from Sigma-Aldrich unless stated otherwise. Cell culture media and supplements were sourced from Gibco (ThermoFisher Scientific). Cells were routinely cultured in RPMI 1640 supplemented with 10% (v/v) fetal calf serum (FCS), 2 mM L-glutamine, 100 U/ml penicillin, 100 μg/ml streptomycin, 1 mM sodium pyruvate and 50 μM 2-mercaptoethanol unless indicated otherwise.

2.1.1 Antibodies for immunohistochemistry

Primary and secondary antibodies for immunohistochemistry are listed in *Table 2.1*.

2.1.2 Antibodies for flow cytometry

Fluorochrome-conjugated antibodies for use in flow cytometry are listed in *Table 2.2*. Matched isotype control antibodies were purchased from BD Biosciences.

Table 2.1 – Antibodies for immunohistochemistry

Target	Primary Antibody	Clone	Company	Secondary Antibody	Company
CD3	Rabbit anti-human	Polyclonal	Dako	Biotinylated swine anti-rabbit	Dako
B220	Rat anti-mouse	RA3-6B2	BD Biosciences	Biotinylated rabbit anti-rat	Dako
CD21	Goat anti-mouse	D-19	Santa Cruz	Biotinylated donkey anti-goat	Santa Cruz
Bcl-6	Rabbit anti-mouse	N-3	Santa Cruz	Biotinylated swine anti-rabbit	Dako
pY-STAT3	Rabbit anti-mouse	D3A7	Cell Signalling	Biotinylated goat anti-rabbit	Vector Laboratories
CXCL13	Goat anti-mouse	Polyclonal	R&D Systems	Biotinylated rabbit anti-goat	Dako
HEVs	Rat anti-mouse	MECA-79	In house	Biotinylated rabbit anti-rat	Dako
Ki67	Rabbit anti-mouse	Polyclonal	Abcam	Biotinylated goat anti-rabbit	Vector Laboratories
Podoplanin	Biotinylated Hamster anti-mouse	8.1.1	BioLegend	NA	NA

Table 2.2 – Antibodies for flow cytometry

Target	Species	Conjugate	Clone	Isotype	Company
CD3	Hamster anti-mouse	PE Cy7	145-2C11	IgG	BioLegend
CD4	Rat anti-mouse	eFluor 450 PerCP Cy 5.5	RM4-5	IgG2a	eBioscience
CD25	Rat anti-mouse	PE	PC61.5	IgG1	eBioscience
CD44	Rat anti-human/ mouse	APC	IM7	IgG2b	eBioscience
CD62L	Rat anti-mouse	FITC	MEL-14	IgG2a	eBioscience
CD8a	Rat anti-mouse	PerCP Cy 5.5	53-6.7	IgG2a	eBioscience
CD11b	Rat anti-human/ mouse	APC	M1/70	IgG2b	BioLegend
δγTCR	Hamster anti-mouse	APC	eBioGL3	IgG	eBioscience
RORγT	Rat anti-human/ mouse	APC PE	AFKJS-9	IgG2a	eBioscience
NK1.1	Mouse anti-mouse	FITC	PK136	IgG2a	eBioscience
IL17A	Rat anti-mouse	PE	TC11-18H10.1	IgG1	BD Biosciences
IL17A	Rat anti-mouse	Alexa Fluor 647 Alexa Fluor 488	TC11-18H10.1	IgG1	BioLegend

2.2 *In vivo* studies of inflammatory arthritis

2.2.1 Mice

Experiments were performed using C57BL/6 wild-type, *Il27ra*$^{-/-}$ and *Il6ra*$^{-/-}$ mice. Wild-type mice were purchased from Charles River. *Il27ra*$^{-/-}$ mice have been described previously and were originally sourced from The Jackson Laboratory (line B6N.129P2-*Il27ra*^{tm1Mak}/J) [96]. In brief, a targeting vector was used to replace an exon encoding part of the extracellular fibronectin type III domain of the IL-27 receptor with a neomycin resistance (neo) cassette. *Il6ra*$^{-/-}$ mice were generated at GlaxoSmithKline (Stevenage, UK) using a traditional replacement vector to disrupt IL-6 recognition of the receptor by deleting exons 4, 5 and 6 [63]. Mice were bred and housed under specific-pathogen-free (SPF) conditions at Cardiff University. All experiments were carried out in accordance with Home Office approved project licences 30/2928 (2015-2017) and PB3E4EE13 (2017-2019), with consideration of the 3 R's (Replace, Reduce, Refine) [245].

2.2.2 Murine antigen-induced arthritis

Antigen-induced arthritis (AIA) was established in 8-12 week-old male mice as described previously (*Figure 2.1*) [246, 247]. A methylated-BSA (mBSA)-specific immune response was generated by subcutaneous injection of an emulsion of mBSA in Complete Freund's Adjuvant (mBSA/CFA) into the right flank (100 µl using a 1 ml syringe and 25G needle). The mBSA/CFA emulsion was prepared by mixing equal volumes of 2 mg/ml mBSA and CFA, before repeatedly passing through an 18G needle to form a white, stable emulsion (*Figure 2.1B*). At the same time, mice were also administered *Bordetella pertussis* toxin (160 ng in 100 µl) by intraperitoneal injection (1 ml syringe, 25G needle). Seven days later, mice received an identical subcutaneous booster immunisation of mBSA/CFA into the left flank.

Inflammatory arthritis was triggered 21 days after initial immune priming by an intraarticular injection of mBSA (10 µl of 10 mg/ml) into the knee using a 29G insulin syringe (*Figure 2.1A and C*). Local joint swelling was measured using a POCO 2T micrometer (Kroeplin) to temporally monitor clinical signs of inflammatory arthritis. At defined time points, mice were killed under terminal anaesthesia or using a schedule 1 method (CO_2 followed by cervical dislocation).

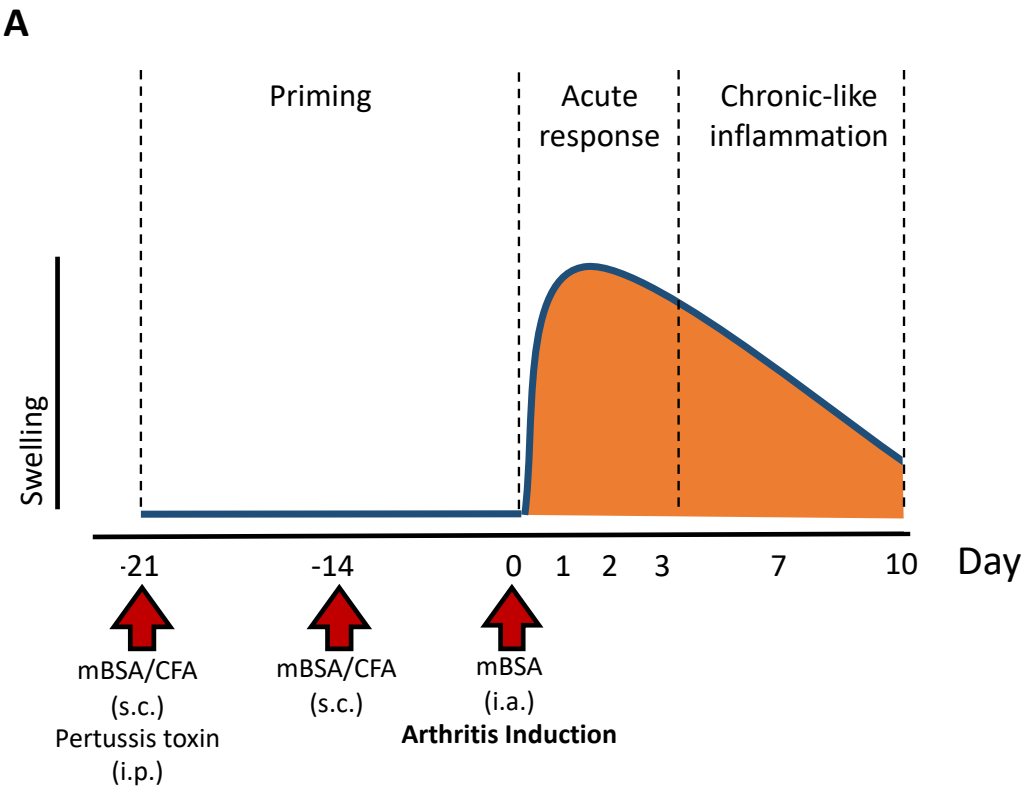

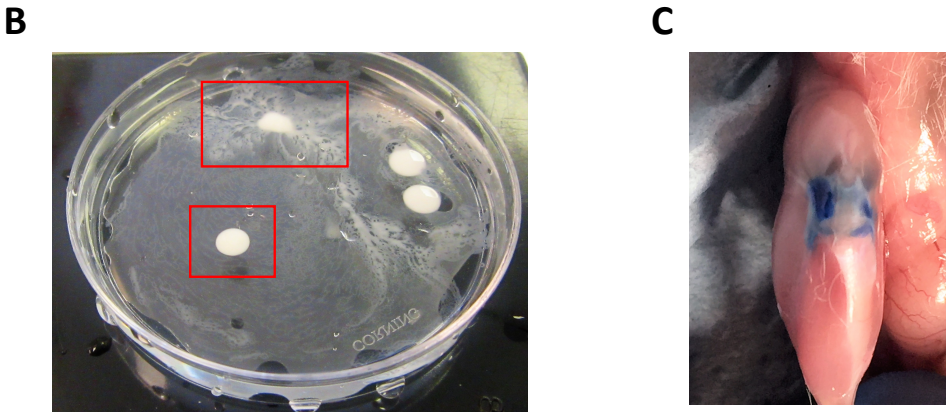

Figure 2.1 - Antigen-induced arthritis. (A) Timeline of joint swelling and disease stages of antigen-induced arthritis. The priming phase establishes an antigen-specific T cell and antibody response to mBSA in the absence of synovitis. The acute response is marked by an early T cell response and the infiltration of innate leukocyte populations including neutrophils and inflammatory macrophages. The chronic-like phase of AIA features a prominent effector T cell response within the joint and regions of B cell infiltration. Arrows mark the time and routes of mBSA/CFA and Bordetella pertussis toxin administrations to induce AIA. Joint swelling is measured on days 0, 1, 2, 3, 7 and 10 post arthritis induction. (B) A stable mBSA/CFA emulsion suitable for immunisations will remain intact when dropped onto water (bottom box) and does not disperse (top box). (C) Intraarticular injections can be practiced using a dye. A successful injection can be visualised as a symmetrical distribution of ink around the patellar ligament. Adapted from Jones et al., 2018. s.c., subcutaneous; i.p., intraperitoneal; i.a., intraarticular.

2.2.3 Collection of blood serum

Whole blood was collected by cardiac puncture (1 ml syringe, 25 G needle). To recover serum, blood was incubated at room temperature for 30 min to allow coagulation. Samples were centrifuged (2,000 xg, 10 min, 4°C) and the serum carefully transferred to a sterile tube before being stored at -80°C.

2.2.4 Preparation of knee joints for histology

Whole knee joints were recovered by cutting through the bones proximal (femur) and distal (tibia and fibula) to the knee. Following the removal of skin, knees were placed into histology cassettes and fixed in 10% (v/v) neutral buffered formal saline, pH 7.4 at 4˚C. After 3 days, joints were transferred into 0.5 M EDTA, pH 8, for decalcification and the solution changed twice a week. Complete decalcification was confirmed by X-ray using a Kodak FX-Pro imaging system (*Figure 2.2*). Fixed and decalcified joints were processed and embedded in paraffin using the HistoCore PEARL and Arcadia H instruments from Leica Biosystems. Parasagittal serial sections of 7 μm were prepared using a Leica RM2235 rotary microtome.

2.2.5 Haematoxylin, fast green and safranin O staining of tissue

Tissue sections were de-waxed in three changes of xylene and rehydrated in decreasing concentrations of absolute ethanol – 100%, 90% and 70% (3 min each) before placing in distilled water. Synovitis and bone and cartilage erosion were evaluated after staining in haematoxylin, fast green and safranin O. Briefly, sections were first placed in Harris Haematoxylin (VWR International Ltd) for 5 minutes. Excess stain was removed under running tap water, and the sections transferred to 0.01% (w/v) fast green for 5 minutes. Samples were dipped briefly in 1% (v/v) acetic acid and incubated in 0.2% (w/v) safranin O for 5 minutes. After staining, sections were dehydrated through 70%, 90% and 100% absolute ethanol and cleared by three changes of xylene. Coverslips were placed onto stained slides using DPX mountant.

2.2.6 Histological assessment of joint pathology

Histological sections were scored for joint damage and inflammation by two independent observers blinded to the experimental design [69, 146, 246]. Haematoxylin staining was used to identify regions of synovial cellular infiltration, while proteoglycan staining by safranin O was used to detect erosion of the articular cartilage (*Figure 2.3*). The arthritic

index is the aggregate score for the inflammatory infiltrate, synovial exudate, synovial hyperplasia and cartilage/bone erosion, as outlined in *Table 2.3*.

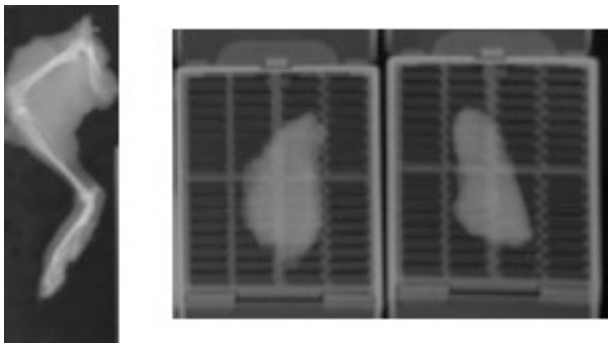

Figure 2.2 - Decalcification of knee joints. X-ray images of formalin-fixed mouse knees from an AIA experiment. A whole leg showing the presence of calcified bone can be seen on the left. Images on the right show knees (in histology cassettes) following EDTA decalcification. Images captured using a Kodak FX-Pro imaging system (Settings: Exposure, 30s; f-stop, 4.96; FOV, 200; focal plane, platen.

Table 2.3 – Scoring criteria for histological assessment of joint pathology

Synovial Infiltrate	
0	Normal
1	Focal inflammatory infiltrates, adposity hardly affected
2	Focal inflammatroy infiltrate equals adiposity
3	Inflammatory infiltrate dominates cellular histology
4	Substantial inflammatory infiltrate with severe loss of adiposity
5	Ablation of adiposity due to inflammatory infiltrate
Synovial Exudate	
0	Normal
1	Evidence of inflammatory cells in space
2	Moderate numbers of inflammatroy cells in space, with evidence of fibrin deposits
3	Substantial number of inflammatory cells with large fibrin deposits
Synovial Hyperplasia & Pannus Formation	
0	Normal (1-3 layers thick)
1	Over three layer thick synovial lining and evidence of thickening and/ or invasion of joint space
2	Over three layer thick synovial lining 'creeping' over cartilage surfaces and/or finger-like processes into joint space
3	Over three layer thick synovial lining showng substantial covering of cartialge surfaces with evident cartilage loss
Cartilage & Bone Erosion	
0	Normal
1	Detectable loss of cartilage detected by Safranin O staining
2	Detectable erosion of underlying bone by pannus activity
3	Pannus has destroyed a significant part of the bone

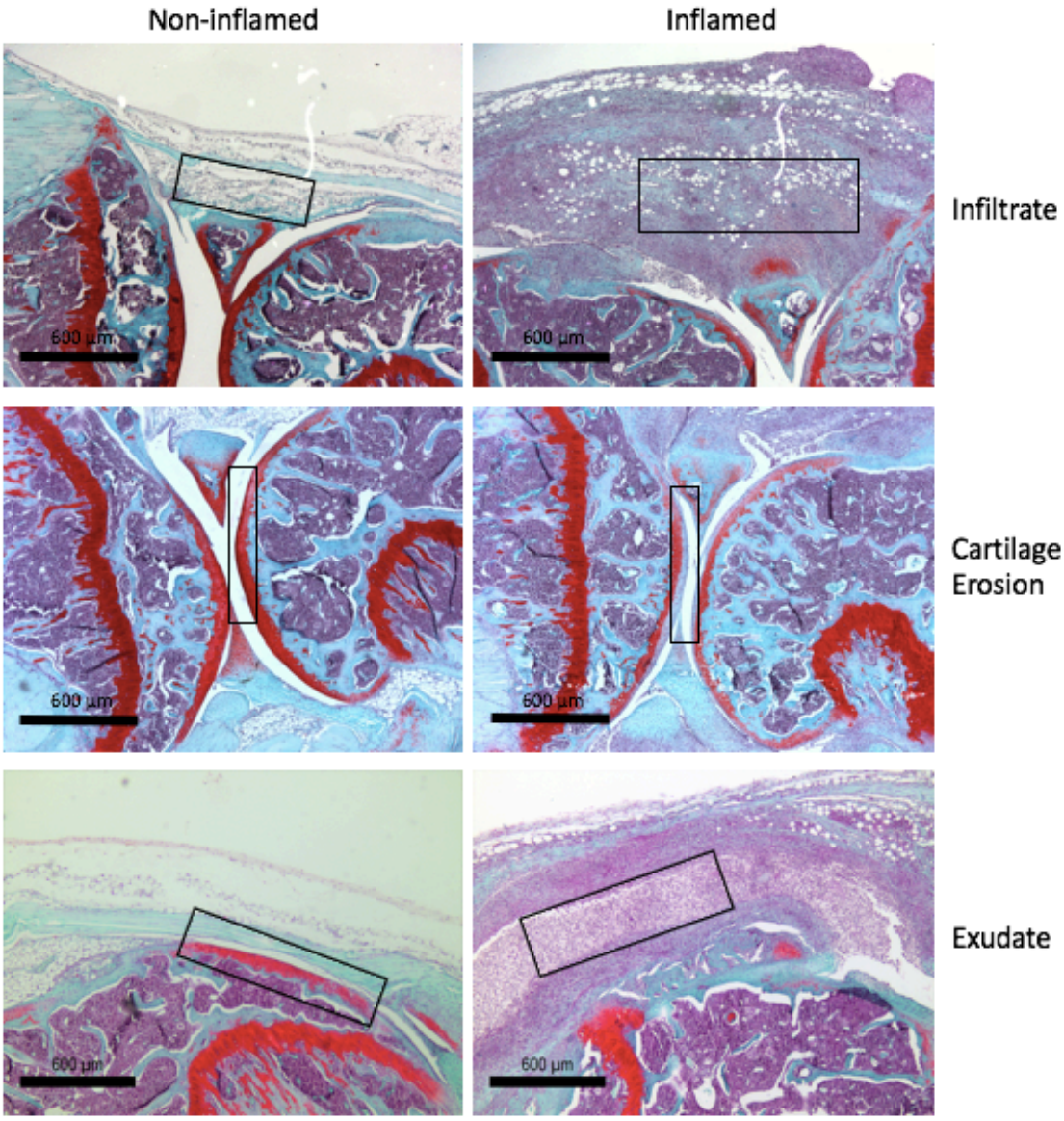

Figure 2.3 - Histological assessment of AIA. Haematoxylin, fast green and safranin O staining of knee joints at day 10. Boxes highlight areas of inflammatory infiltrate (top), cartilage erosion (seen by loss of red safranin O staining; middle) and exudate (bottom). Scale bars: 600 μm.

2.2.7 Extraction of synovial RNA

Inflamed synovial tissue was recovered by dissection under a microscope and was adapted from a protocol designed for the isolation of rat synovial tissue [248]. Synovial tissue was immediately placed into RNA*later* (Ambion) and stored at -80°C. For recovery of RNA, synovium was removed from RNA*later* and weighed. Total RNA was extracted by homogenising in 600 μl of RLT buffer (Qiagen) supplemented with 1% (v/v) β-mercaptoethanol, per 20 mg of tissue using a D1000 handheld homogeniser (Benchmark scientific). High-quality RNA was purified using a RNeasy Mini kit with on-column DNaseI digestion (Qiagen) according to the manufacturer's instructions. The quality and quantity of eluted RNA was determined using a Nanodrop 2000 spectrophotometer (ThermoFisher scientific) by measuring A260/280 and A260/230 ratios, using absorbance measurements at 230 nm, 260 nm and 280 nm, to detect contaminating proteins and phenols respectively.

2.2.8 Analysis of mBSA-specific immune responses

Antigen-specific responses to mBSA were determined by measuring mBSA-specific IgG titres in serum (see *section 2.8.1*) and cellular cytokine responses following *ex vivo* mBSA restimulation. For the latter, inguinal lymph nodes were recovered and gently homogenised through sterile 40 μm cell strainers (Greiner Bio-one) to obtain single cell suspensions. Cells were resuspended in supplemented RPMI 1640 media and seeded in 96-well flat bottom plates at $5x10^5$ cells/well. Cells were re-stimulated with 20 μg/ml of mBSA and incubated at 37°C for 72 hours. Culture supernatants were collected for analysis of cytokine secretion by ELISA as outlined in *section 2.8.2*.

2.2.9 Isolation of joint-infiltrating leukocytes

The inflamed synovium was dissected as described previously [248] and placed into supplemented RPMI 1640 media on ice. An enzymatic digest was performed to recover synovial leukocytes, using 1 mg/ml Collagenase type 4 (Worthington Biochemicals) in supplemented RPMI 1640 media. Digestion was performed at 37°C for 1-2 hours, with a gentle vortex every 15 min. Cells were passed through a 40 μm cell strainer to remove tissue debris, centrifuged (350 xg, 5 min), and resuspended in supplemented RPMI 1640 media before proceeding with flow cytometric analysis (*section 2.5*).

2.3 Inflammation-associated gastric cancer

2.3.1 Animals

Experiments were performed using age-matched 4-week, 3-month and 6-month old wild-type control mice and *gp130*$^{Y757F:Y757F}$ (*gp130*$^{F/F}$) mice that spontaneously develop inflammation-associated gastric antrum adenomas [219]. At the molecular level, these mice have a knock-in phenylalanine mutation that replaces tyrosine residue 757 in the cytoplasmic domain of gp130. This disrupts the negative feedback imposed on gp130 by SOCS3. Six-month old *gp130*$^{F/F}$ mutant derivatives, heterozygous for *Stat3* (*gp130*$^{F/F}$:*Stat3*$^{+/-}$) or *Il17a* deficient (*gp130*$^{F/F}$:*Il17a*$^{-/-}$) were also used to investigate the role of STAT3 and IL-17A in tumour-associated ELS development. Mice were generated as previously described [219, 221, 249], were on a mixed C57BL/6 X 129/Sv background and were maintained under SPF conditions at the Hudson Institute of Medical Research (Australia). Experiments were performed in accordance with, and approved by, the Monash Medical Centre 'A' Monash University Animal Ethics Committee.

2.3.2 Haematoxylin and eosin staining of stomach tissue

Stomachs were dissected and fixed in 10% (v/v) neutral buffered formalin, pH 7.4, and embedded in paraffin at the histology facility at the Hudson Institute of Medical Research, before being shipped to Cardiff University. For initial histological assessment of tumour-associated ELS, slides were stained with haematoxylin and eosin (H&E). Briefly, sections were de-waxed in three changes of xylene and rehydrated in decreasing concentrations of absolute ethanol before placing in distilled water (see *section 2.2.5*). Sections were placed in Harris Haematoxylin (VWR International Ltd) for 5 minutes and excess stain was removed under running tap water. Sections were blued by placing in 1% (w/v) sodium bicarbonate for 30 seconds before placing in eosin for 5 minutes. After staining, sections were dehydrated through increasing concentrations of absolute ethanol and cleared by three changes of xylene (see *section 2.2.5*). Coverslips were placed onto stained slides using DPX mountant. For a comprehensive characterisation of the composition, cellular organisation and activity of tumour-associated ELS, immunohistochemistry was performed as outlined in *section 2.7*.

2.4 *In Vitro* T cell cultures

Spleens were recovered by dissection and a single cell suspension generated by gently homogenising through a sterile 40 μm cell strainer (Greiner Bio-one) in supplemented RPMI 1640. Recovered cells were collected by centrifugation (350 xg, 5 min) and contaminating red blood cells were lysed by resuspension in RBC lysis buffer (BioLegend). To enrich for $CD4^+$ T cells (typically >90% purity), cells were again collected by centrifugation (350 xg, 5 min) and $CD4^+$ T cells were recovered by negative selection using a MACS $CD4^+$ T cell Isolation Kit (Miltenyi Biotec) according to manufacturer's instructions. This kit uses a cocktail of biotinylated antibodies to select non-$CD4^+$ T cells. These cells are magnetically labelled using Anti-Biotin MicroBeads and separated from target $CD4^+$ T cells using a magnetic column.

Enriched populations of naïve $CD4^+CD25^-CD44^{lo}CD62L^{hi}$ T cells were obtained by flow cytometry cell sorting. Briefly, $CD4^+$ T cells (2 x 10^7 cells/ml) were treated with Fc Block (4 μg/ml; BD Biosciences), before incubation with fluorochrome-conjugated antibodies to CD4, CD25, CD44, and CD62L used at a final dilution of 1/200 (*Table 2.2*). Cell sorting was performed using a BD FACS Aria III (BD Biosciences) using the gating strategy presented in *Figure 2.4*.

$CD4^+$ T cells (1 x 10^5 cells/well) were cultured in Nunclon delta surface 96-well U-shape bottom plates (ThermoFisher scientific) in supplemented RPMI 1640 [63, 146]. For activation, cells were co-stimulated with plate bound anti-CD3 (1 μg/ml anti-CD3; clone 145-2C11, R&D systems) and soluble anti-CD28 (5 μg/ml; clone 37.51, eBioscience). Cytokines were included at the following concentrations to promote differentiation of naïve $CD4^+$ T cells into defined T helper lineages: For Th1 differentiation, IL-12 (20 ng/ml); for Th2 cells, IL-4 (40 ng/ml); for Treg cells, TGFβ (5 ng/ml); for Th17 cells, TGFβ (1 ng/ml) and IL-6 (20 ng/ml), as indicated in the relevant sections. Where indicated anti-IL-2 was added at 10 μg/ml. Cells were incubated for 4 days at 37°C before staining by flow cytometry (*section 2.5*). Alternatively, cells were resuspended in 250 μl RLT buffer before purifying RNA using a RNeasy Mini kit (Qiagen) according to the manufacturer's instructions. Gene expression was determined as outlined in *section 2.6*.

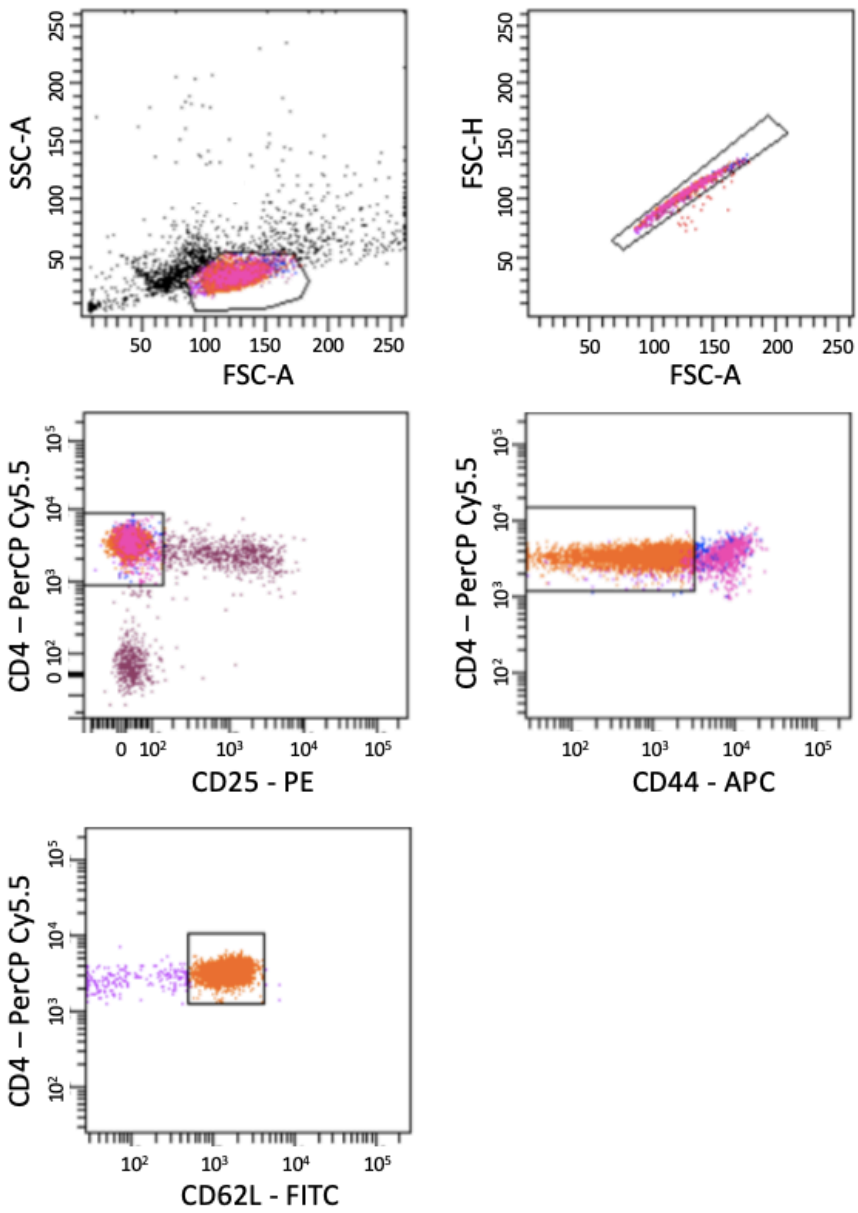

Figure 2.4 - Gating strategy for sorting of naïve cells. Lymphocytes were first identified based on their forward scatter and side scatter profiles. Single events were then selected based on the forward scatter area and height profiles. A disproportionate ratio between the area and height indicates multiple cells being acquired at the same time. Naïve T cells were then identified as $CD4^{+}CD25^{-}CD44^{lo}CD62L^{hi}$.

2.5 Flow Cytometry

Flow cytometry was performed on cells recovered from inflamed joint tissue (*section 2.2.9*) and draining lymph nodes (*section 2.2.8*) during AIA, and from $CD4^+$ T cells cultured *in vitro* (*section 2.4).* To quantify the number of cells recovered from inflamed joint tissues and draining lymph nodes, cell counting beads (Life Technologies) were used as instructed by the manufacturer.

2.5.1 Cell surface staining

Cells were centrifuged (520 xg, 3 min) and resuspended in Zombie Aqua live/dead stain (BioLegend) in PBS for 5 minutes in the dark. Cells were washed twice in FACS buffer (0.5 % BSA, 5 mM EDTA, 7.5 mM Sodium Azide in PBS) and non-specific staining was prevented by incubating cells in 4 μg/ml rat anti-mouse CD16/CD32 (Fc block; clone 2.4G2, BD biosciences) for 15 minutes. Cells were incubated in FACS buffer containing fluorochrome-conjugated antibodies specific to cell surface receptors (*Table 2.2*) at a working dilution of 1/200. Cells were washed twice (520 xg, 3 min) before resuspending in CellFix (BD Biosciences) and acquiring on a BD FACS Canto II (BD Biosciences). Data was analysed using FlowJo Version 10.

2.5.2 Intracellular flow cytometry

Before intracellular cytokine staining, cells were first stimulated (4 hours at 37°C) with 50 ng/ml PMA and 500 ng/ml ionomycin in the presence of the Golgi protein transport inhibitor, monensin (3 μM). Live/dead staining, Fc block and labelling of cell surface receptors was performed as described in *section 2.5.1*, before proceeding with intracellular cytokine or transcription factor staining.

Cells were fixed and permeabilised using Cytofix/Cytoperm (BD Biosciences) and washed twice with permeabilization wash buffer (BD Biosciences) according to manufacturer's recommendations. Intracellular IL-21 staining was carried out as previously described [250]. In brief, IL-21 was detected using a soluble IL-21 receptor Fc followed by a goat anti-human f(ab)'-PE. Cells were then washed twice with permeabilization wash buffer and all other cytokines and transcription factors were labelled using fluorochrome-conjugated antibodies (*Table 2.2*) at a working dilution of 1/100 for 30 minutes. Cells were again washed twice as above and resuspended in CellFix (BD Biosciences). Cells were acquired on a BD FACS Canto II (BD Biosciences) and data analysis performed using FlowJo version 10.

2.6 RNA expression analysis

Analysis of gene expression was performed on RNA recovered from synovial tissue (*section 2.2.7*), T cells cultured *in vitro (section 2.4*), and stomach antrum and tumour tissue (*section 2.3*). For the latter, RNA was isolated from snap-frozen antrum and tumour tissue using TRIzol reagent (ThermoFisher scientific) and performed at the Hudson Institute of Medical Research.

2.6.1 cDNA synthesis

Reverse transcription of total RNA to cDNA was performed using a nanoScript 2 Reverse Transcription kit (Primerdesign) using random oligonucleotide primers. For all reactions, 1 μg of RNA was used. Resulting cDNA was diluted by adding an equal volume of RNase-free water to obtain a final cDNA concentration of 25 ng/μl. For stomach antrum and tumour tissue a Transcriptor High Fidelity cDNA Synthesis kit was used (Roche).

2.6.2 Quantitative real-time PCR

Gene expression was quantified using TaqMan Gene Expression Assays (Applied Biosystems) in a MicroAmp Optical 384-well reaction plate (Applied Biosystems). The reaction was performed using 5 μl TaqMan Fast Advance Master Mix, 0.5 μl TaqMan Primers and Probes with the FAM-MGB reporter, 3.5 μl nuclease-free water and 1 μl of cDNA (generated as outlined in *section 2.6.1*) and amplified and acquired using the QuantStudio 12K Flex Real-Time PCR system (Applied Biosystems). Data was analysed using a comparative threshold cycle (Ct) method. This is the PCR cycle number at which the signal of the reporter crosses a set threshold in the exponential phase of amplification. Ct values for genes of interest are then standardised against an internal housekeeping control, whose expression is known to remain unchanged in different conditions. For all experiments genes were normalised against *Actb*.

For stomach antrum and tumour tissue, SYBR Green chemistry (Applied Biosystems) was used to quantify gene expression. Detection of gene expression was performed using the 7900 HT Fast RT-PCR system (Applied Biosystems) and analysed using the Sequence Detection system version 2.3 software (Applied Biosystems) using a comparative threshold cycle method as described above.

2.7 Immunohistochemistry

Immunohistochemical staining was performed on parasagittal serial sections of formalin fixed paraffin embedded knee joints (*section 2.2.4*) and formalin fixed paraffin embedded mouse stomachs (*section 2.3.2*). Sections were de-waxed in three changes of xylene and rehydrated in decreasing concentrations of absolute ethanol – 100%, 90% and 70% (3 min each) before placing in distilled water. Antigen retrieval was performed by heating sections at 95°C for 40 minutes in 10mM sodium citrate buffer containing 0.05% (v/v) Tween 20. Slides were allowed to cool to room temperature for 20 minutes before endogenous peroxidase activity was blocked using 3% (v/v) H_2O_2. Non-specific antibody binding was blocked by incubating sections with 10% (v/v) serum (*Table 2.4*) of the same species from which the secondary antibody was raised. For CD21 detection, a serum free universal protein block (CAS block; Invitrogen) was used. Primary antibodies (*Table 2.4*) were incubated overnight at 4°C, in TBS (0.05 M Tris Base, 0.9% (w/v) NaCl, 0.05% (v/v) Tween 20), unless stated otherwise. Antibody labelling was detected using biotinylated secondary antibodies (*Table 2.4*) specific to the primary antibody. Visualisation of antibody labelling was performed using the Vectastain ABC kit and the 3,3'-diaminobenzidine (DAB) staining kit (both from Vector Laboratories) according to manufacturer's protocols. This system combines an avidin-conjugated horseradish peroxidase with DAB chromagen that precipitates at the site of antibody binding to yield a localised brown colour. Slides were counterstained in Harris Haematoxylin (1 min; VWR International Ltd) before coverslipping in DPX mountant. Sections were visualised using a Leica DM 2000 microscope and Leica Application Suite v4.9 software. Positive staining was quantified using the Leica QWin microscope imaging software, which quantifies the area of staining based on the number of brown DAB-positive pixels.

Table 2.4 – Working concentration of antibodies for immunohistochemistry

Target	Primary Antibody	Working Concentration	Secondary Antibody	Working Dilution	Serum Block
CD3	Rabbit anti-human	3 µg/ml	Biotinylated swine anti-rabbit	1/200	Swine
B220	Rat anti-mouse	0.31 µg/ml	Biotinylated rabbit anti-rat	1/200	Rabbit
CD21	Goat anti-mouse	1 µg/ml	Biotinylated donkey anti-goat	1/200	CAS block
Bcl-6	Rabbit anti-mouse	4 µg/ml	Biotinylated swine anti-rabbit	1/200	Swine
pY-STAT3	Rabbit anti-mouse	0.8 µg/ml	Biotinylated goat anti-rabbit	1/200	Goat
CXCL13	Goat anti-mouse	15 µg/ml	Biotinylated rabbit anti-goat	1/200	Rabbit
HEVs	Rat anti-mouse	5 µg/ml	Biotinylated rabbit anti-rat	1/200	Goat
Ki67	Rabbit anti-mouse	1 µg/ml	Biotinylated goat anti-rabbit	1/200	Goat

2.8 ELISA

2.8.1 Direct ELISA to measure mBSA-specific antibody titres

Antibodies specific to mBSA in serum were measured as described previously [69, 146]. Costar half-well 96-well plates (Corning Inc.) were coated overnight with 5 μg/ml mBSA in PBS at room temperature. After washing in PBS containing 0.05% (v/v) Tween 20, nonspecific binding was blocked using 5% (w/v) milk extract in PBS containing 0.05% (v/v) Tween 20 for 1 hour. Multi-well plates were washed as above. Serum was diluted 1/100 - 1/10000 in 5% (w/v) milk extract in PBS and added to the microplates for 2 hours at room temperature. After washing, mBSA-specific antibodies were detected using a horseradish peroxidase conjugated goat anti-mouse IgG (0.5 mg/ml, 2 hours, Dako). The chromogenic peroxidase substrate 3,3',5,5'-tetramethylbenzidine blue (TMB; KPL Inc.) was used to quantify serum IgG binding to mBSA, before measuring absorbance at 450 nm using a FLUOstar Omega plate reader (BMG Labtech).

2.8.2 Detection of inflammatory cytokines by ELISA

Inflammatory cytokine secretion into cell culture supernatants were quantified using commercially available ELISA kits from R&D Systems. All ELISAs were carried out following the manufacturer's instructions and utilised a sandwich ELISA approach combining capture antibodies, detection antibodies and a range of protein standards at specified concentrations.

2.9 Transcriptomic profiling of synovium

For RNA sequencing of mouse synovium, RNA was extracted as outlined in *section 2.2.7* and quality determined on a Nanodrop 2000 spectrophotometer (ThermoFisher scientific) as well as an Agilent bioanalyser using an RNA Nano kit (Agilent Technologies). Libraries were prepared with 0.5 – 1 μg of total RNA. A poly (A) capture method using a Dynabead mRNA Direct Kit (Ambion) was used to isolate mRNA. Libraries were then prepared using the TruSeq Stranded Total RNA Library Prep Kit (Illumina) following the manufacturer's instructions before sequencing on a HiSeq 4000 (Illumina). A detailed description of the optimisation and establishing the methodology of RNA sequencing for analysis of inflamed synovial tissue is provided in *Chapter 3*, *section 3.2*.

2.10 Statistics

Where pilot data was available, the appropriate sample size for experimental groups was determined by statistical power analysis using G*Power (http://www.gpower.hhu.de/) [251]. For *in vivo* studies where no preliminary data was available, pilot experiments were performed using small group sizes calculated in accordance with the resource equation [252]:

$$E = N - T$$

Where N = total number of animals, T = number of treatments/groups and E must be between 10 and 20.

Statistical analysis was performed using GraphPad Prism software. Where studies comprised two experimental groups and the data was normally distributed, a Student's t-test was used to determine statistical significance. For data that was not normally distributed a Mann-Whitney U-test was performed. To identify statistical significance between multiple groups for normally distributed data a one-way ANOVA with Tukey's multiple comparison test was used. Where experimental groups were compared across multiple time points, a two-way ANOVA was used with a Bonferroni post-test. A $p < 0.05$ was considered statistically significant. Graphs are presented as mean ± standard error of the mean (SEM) unless indicated otherwise.

Chapter 3. Development and optimisation of RNA sequencing of mouse synovium

3.1 Introduction

The transcriptome is the complete set of RNA transcripts found within a cell or population of cells. For example, the transcriptome can be investigated at a single cell, tissue or whole organism level. Understanding how the expression of transcripts change during disease can provide insight into the mechanisms that underpin disease progression and has the potential to identify novel biomarkers and therapeutic targets that improve patient stratification and treatment.

The development of next generation sequencing (NGS) technologies such as RNA sequencing (RNA-seq) are now replacing 'first-generation' Sanger sequencing and hybridisation approaches, such as microarray methods, for genome analysis [253]. RNA-seq provides cheaper, faster and more accurate transcript quantification than previous approaches [254]. As an active area of development, RNA-seq can now be used to identify small RNAs, splice variants, low expressed transcripts and map transcription start sites, all from a small amount of starting material [255]. In this regard, the limitations of RNA-seq are ever changing with single-cell RNA-seq analysis now becoming mainstream. Furthermore, since RNA-seq directly determines the sequence of cDNA it can be used to identify novel transcripts, thus overcoming a limitation of microarray approaches [255]. These advantages of RNA-seq make it an ideal tool for interpretation of gene regulation in a disease setting.

RA patients present with distinct synovial pathotypes that may influence the course of disease and the clinical response to frontline biological therapy [193]. Understanding how RNA transcript expression changes between these pathotypes could aid in the identification of therapeutic targets and novel biomarkers for patient stratification. Importantly, the use of RNA-seq to investigate mechanisms that regulate synovial ELS may also provide insight into how ELS are regulated in other inflammatory settings.

This chapter describes the optimisation of RNA-seq methodologies for the evaluation of inflamed synovial tissue from a mouse model of inflammatory arthritis. In this regard, genetically modified IL-27R-deficient mice that develop lymphoid-rich synovitis featuring ELS will be compared to control wild type mice that display a diffuse pattern of leukocyte infiltration [146]. Mice deficient in IL-6 are protected from developing chronic joint inflammation [69, 88, 199, 256]. Previously uncharacterised IL-6R-deficient mice, that I hypothesise will similarly display a 'low inflammatory' phenotype, will also be investigated.

3.2 Materials and Methods

3.2.1 Optimisation of extraction of high-quality RNA from the synovium

Since RNA-seq required high-quality RNA, a comparison of different extraction methods was performed. For TRIzol extraction, synovium was removed from RNA*later* (Ambion) and placed in 1 mL of TRIzol (Ambion) before being passed through a 19-gauge followed by a 21-gauge needle to disrupt the tissue. Once homogenised, 200 *µ*l of chloroform was added per 1 mL of TRIzol before centrifuging (12,000 xg, 15 min). Following centrifugation, the mixture separates into an organic phase, containing DNA and proteins, and an aqueous phase, containing RNA. The aqueous phase was carefully removed and an equal volume of 70% ethanol was added. RNA was purified using a RNeasy Mini kit with on-column DNaseI digestion (Qiagen) according to the manufacturer's instructions. Extraction of synovial RNA by homogenisation in a commercial lysis buffer was performed as outlined in *section 2.2.7*.

3.2.2 Input RNA quality control

Synovial RNA was extracted as outlined in *section 3.2.1*. The quantity and integrity of the purified total RNA was assessed using a NanoDrop 2000 spectrophotometer (ThermoFisher Scientific) and an Agilent 2100 Bioanalyser using an RNA Nano kit (Agilent technologies) following the manufacturer's instructions. Samples with an RNA Integrity Number (RIN) greater than 8 were required for library preparation. The RIN value is a ratio of the 18S and 28S ribosomal RNA (rRNA) and therefore serves as a measure of the quality of the RNA. For library preparation 0.5 – 1 *µ*g of total RNA was used as input.

3.2.3 Removal of ribosomal RNA

Ribosomal RNA (rRNA) was removed from samples by poly (A) capture using a Dynabead mRNA Direct Kit (Ambion). This method uses an oligo d(T) probe to bind the polyadenylated tail of mRNA. The probes are bound to magnetic beads in order to positively select the mRNA from RNA species that are not polyadenylated such as rRNA. Efficient removal of rRNA was confirmed on an Agilent 2100 Bioanalyser using an RNA Pico kit (Agilent technologies) following the manufacturer's instructions.

3.2.4 Library Preparation

Libraries were prepared using the TruSeq Stranded Total RNA Library Prep Kit (Illumina) following the manufacturer's instructions. This contained all reagents required for the

multiple steps involved in library preparation as outlined in *figure 3.1*. Libraries were prepared for three biological replicates for each genotype and time point in line with ENCODE guidelines [257].

Fragmentation. Purified mRNA was fragmented by heating to 94°C for a given amount of time as stated in the relevant passage of text.

Reverse transcription and adapter ligation. A reverse transcription reaction was utilised to generate cDNA using a SuperScript II reverse transcriptase (Invitrogen). This was followed by a purification step using Agencourt AMPure beads (Beckman Coulter). These are magnetic beads coated with carboxyl groups, that in the presence of salt, bind to DNA. Sequencing adapters were then annealed to the purified cDNA. These serve as barcodes to identify samples when pooled, as well as primers for amplification on the flow cell prior to sequencing (*Figure 3.2*). A further magnetic bead purification using AMPure beads was utilised to remove adapter dimers and smaller artefacts. Here, the volumetric ratio of salt to DNA was critical. Since larger DNA fragments have a higher charge, they will bind to the beads at lower salt concentrations. Hence a low bead to DNA ratio results in binding of larger fragments, allowing adapter dimers and smaller fragments to be separated. This ratio was optimised for binding the correct sized fragments for sequencing.

PCR amplification and library quantification. Ligated cDNA libraries were then PCR amplified and purified with a final magnetic AMPure bead clean. Libraries were assessed on an Agilent 2100 Bioanalyser using a high sensitivity DNA kit (Agilent technologies) following the manufacturer's instructions. Final cDNA libraries were quantified by qPCR using DNA of known concentrations as directed in the KAPA Library Quantification Kit (KAPA Biosystems). Libraries were diluted to a final concentration of 10 pM and combined into a single pool. The pooled libraries were sequenced across multiple lanes, in order to remove bias derived from sequencing on different lanes, using a HiSeq 4000 (Illumina) and pair-end sequencing (*Figure 3.2*). To conform to ENCODE guidelines libraries were sequenced to have greater than 30 million mapped reads [257].

3.2.5 Read mapping strategy

A workflow for the mapping strategy of RNA-seq data is outlined in *figure 3.3*. Firstly, raw sequencing files (fastq files) were trimmed in order to remove adapter sequences and low-quality reads, since these would affect mapping to the genome. A quality control was then performed using the fastQC software (Babraham Institute) in order to determine the

quality of the sequencing. The sequencing files were then mapped to a reference genome (mm10/ gb38.90) using STAR software. STAR is splice aware, hence reads are able to map over splice junctions. Duplicate reads were identified and marked using Picard (Broad Institute) and further analysis performed to assess the quality of the libraries (e.g. number of reads, percentage duplication). Reads per gene were determined using the featureCounts software.

3.2.6 Differential gene expression analysis

To identify differentially expressed genes between two samples, a differential gene expression analysis was performed using the DESeq2 package (Bioconductor). Firstly, normalised read counts were calculated, which accounts for different depth of sequencing of individual samples. The fragments per kilobase of transcript per million mapped reads (FPKM) was then calculated from the normalised counts, which considers the length of the gene. Since analysis was focused on identifying changes in the same gene in different conditions the normalised counts were used to calculate fold expression changes and statistical analysis.

3.2.7 Evaluation of duplicated reads

To determine whether duplicate reads could potentially bias gene expression analysis within the data set the dupRadar package (Bioconductor) was used [258]. This package plots the number of duplicates per gene, identified using Picard (*see section 3.2.5*) against its fold change, calculated using the DESeq2 package as described in *section 3.2.5*.

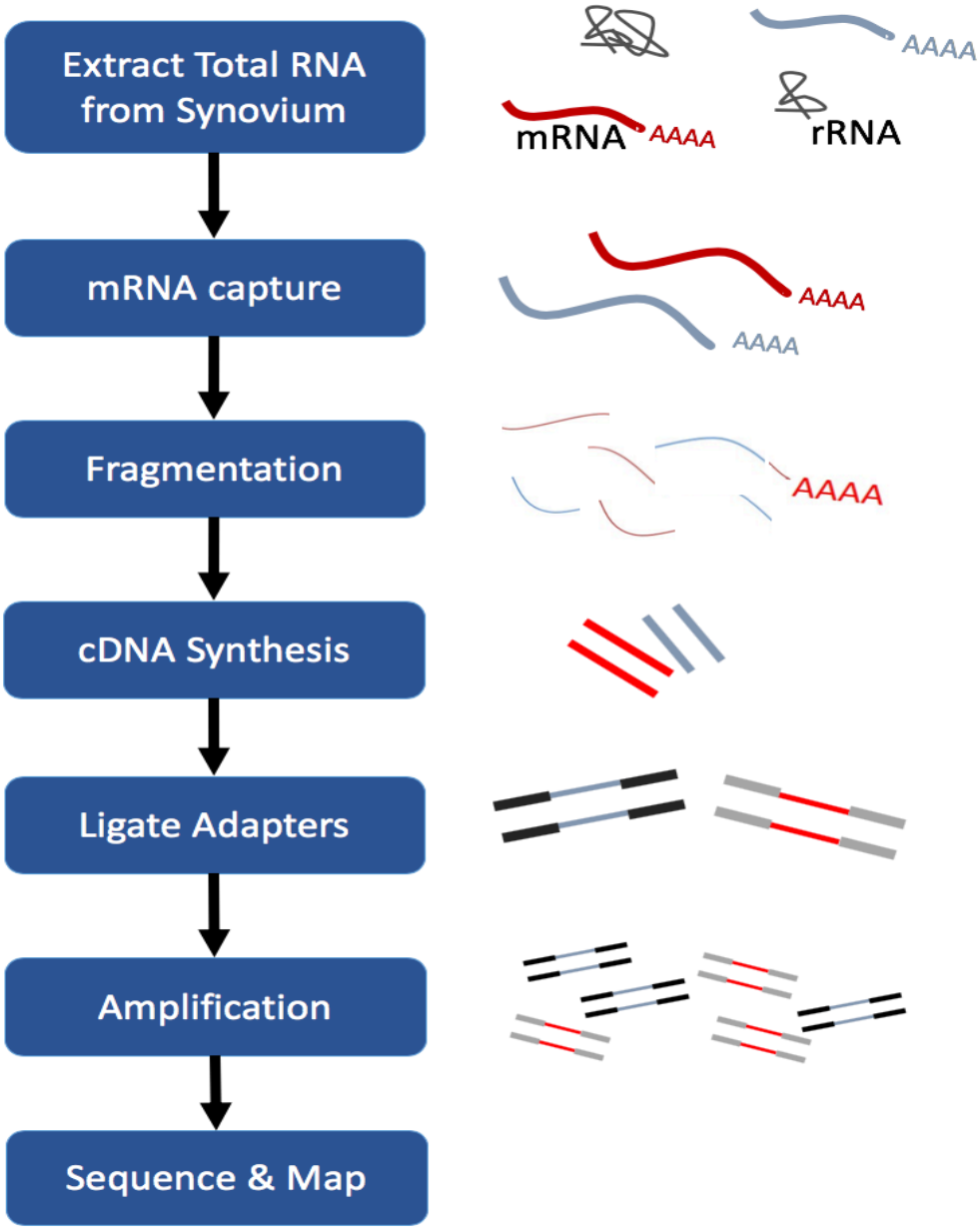

Figure 3.1 - Workflow of RNA-seq library preparation. Total RNA is extracted from the synovium. A poly(A) capture method isolates mRNA from rRNA. RNA is fragmented into suitable sizes for sequencing before a reverse transcription reaction is utilised to form cDNA. Unique adapters are then added which served as barcodes to enable multiplexing of samples, as well as primers for amplification on the flow cell. Finally, cDNA libraries are amplified, before being quantified and sequenced.

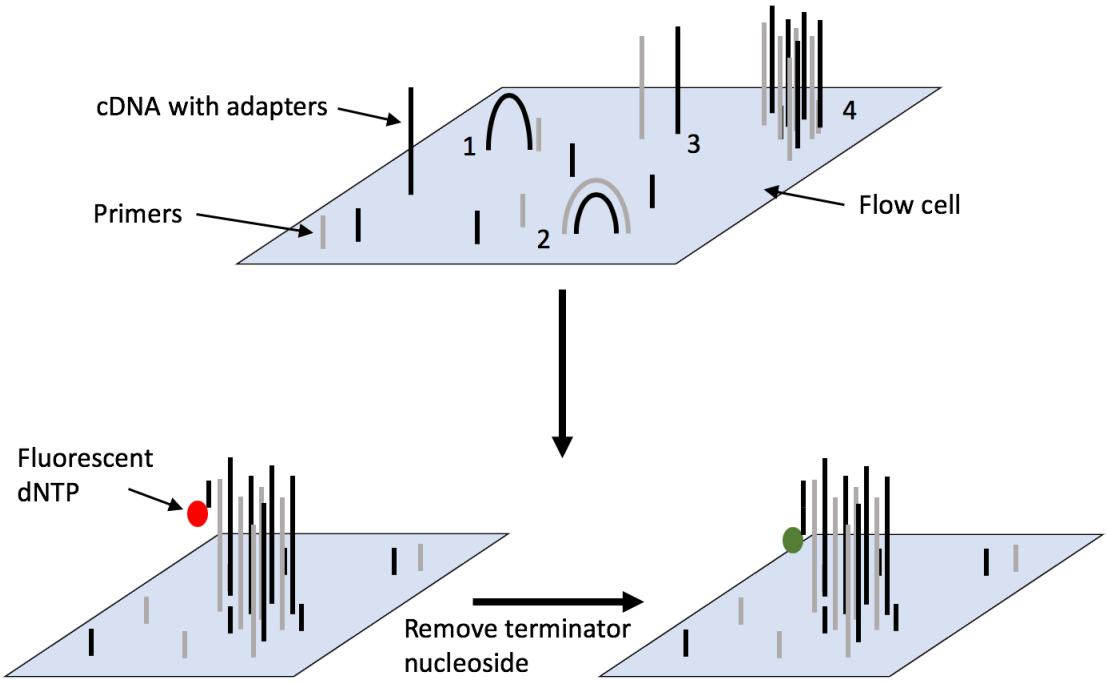

Figure 3.2 - Illumina HiSeq 4000 sequencing chemistry. The cDNA sequence is determined by a strategy termed 'reversible terminator sequencing'. The flow cell contains primers that are complimentary to the adapters ligated on the cDNA library (1). Each fragment is then copied by bridge amplification (2). Clusters formed of thousands of copies of each fragment are made by rounds of amplification (4). Fluorescently labelled 'terminator' dNTPs are added to determine the sequence. The 3' end of the dNTPs is blocked to prevent extension, to allow imaging of the fluorescence. The sequencing proceeds by removing the blocked 3' end and fluorescent label. The next dNTP can then be incorporated, and the cycle continues to obtain the full sequence.

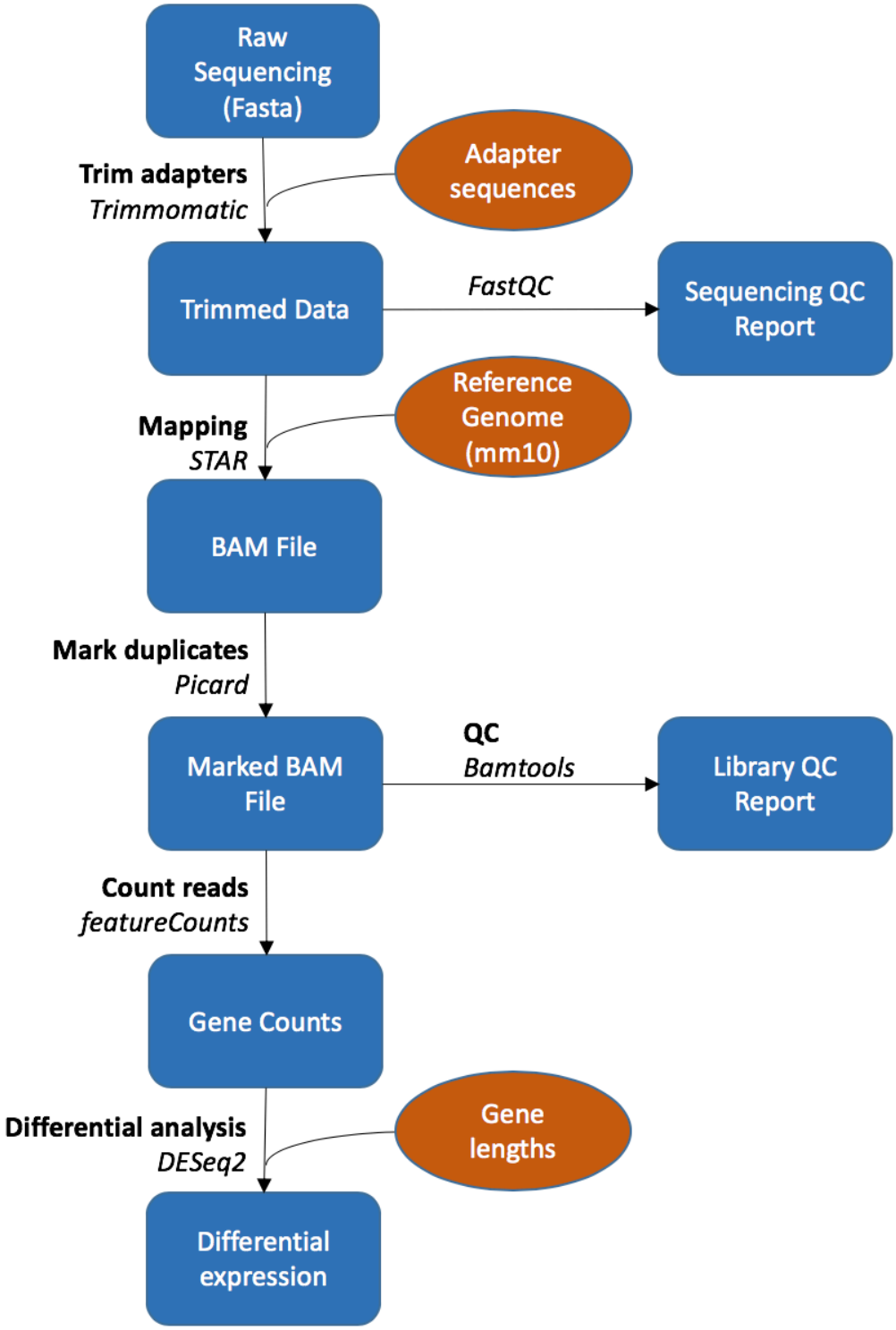

Figure 3.3 - Workflow of RNA-Seq data mapping. The process begins with raw sequencing files from Illumina sequencing. The resulting file format from each process is shown in a blue box. Reference files used to trim, map and assign gene lengths are shown as orange circles. The processes carried out are shown at each stage in bold, and the software used is shown underneath in italics.

3.3 Results

3.3.1 Investigating control of synovial pathology by IL-27 and IL-6

The IL-6 family cytokines, IL-6 and IL-27 are key cytokines that shape innate and adaptive immune responses within the inflamed synovium, albeit often with opposing actions [47]. Whilst the induction of inflammatory arthritis in *Il6*$^{-/-}$ mice results in reduced synovial leukocyte infiltration and joint damage compared to control WT mice [69, 88, 199, 256], *Il27ra*$^{-/-}$ mice display exacerbated disease and the presence of ELS within the synovium [146].

Before proceeding with RNA-seq evaluation of synovial inflammation in WT, *Il27ra*$^{-/-}$ and *Il6ra*$^{-/-}$ mice, I first determined whether my technical proficiency in establishing AIA resulted in joint pathology that was consistent with my laboratory's previous observations. This was also an opportunity to determine whether previously uncharacterised *Il6ra*$^{-/-}$ mice, first described by our group [63], were protected from developing AIA thus being consistent with the amelioration of inflammatory arthritis observed in *Il6*$^{-/-}$ mice [69, 199, 256].

Indeed, histological analysis of joint pathology at day 10 post arthritis induction revealed the presence of infiltrating leukocytes in WT and *Il27ra*$^{-/-}$ mice that were notably reduced in *Il6ra*$^{-/-}$ mice (*Figure 3.4A*). Evaluation of disease severity based on joint histopathology (arthritic index; *Figure 3.4B*) confirmed that *Il6ra*$^{-/-}$ mice were protected from developing chronic joint inflammation, displaying a reduction in inflammatory infiltrate, exudate and cartilage and bone erosion (*Figure 3.4A and B*). Consistent with the development of synovial ELS in *Il27ra*$^{-/-}$ mice, dense accumulations of CD3^{+} T cells were observed in the inflamed synovium of these mice (*Figure 3.5A and B*). Synovial ELS were characterised by the induction of homeostatic chemokines (*Figure 3.5C*) the presence of CD21^{+} follicular dendritic cells and Bcl-6, a marker of germinal centre B cells (*Figure 3.5D*) [146]. Evaluation of knee joint swelling during the course of AIA correlated with disease severity. Here, *Il27ra*$^{-/-}$ mice displayed increased joint swelling and *Il6ra*$^{-/-}$ mice had decreased swelling compared to WT mice (*Figure 3.5E*). Interestingly, *Il6ra*$^{-/-}$ mice had decreased mBSA specific serum IgG titres (*Figure 3.5F*), suggesting an impaired adaptive immune response in these mice. Thus, induction of AIA in my studies was consistent with previously described roles for IL-27 and IL-6 in regulating synovial histopathology and provided rationale for a transcriptomic evaluation of the discrete synovial pathologies seen in these mice.

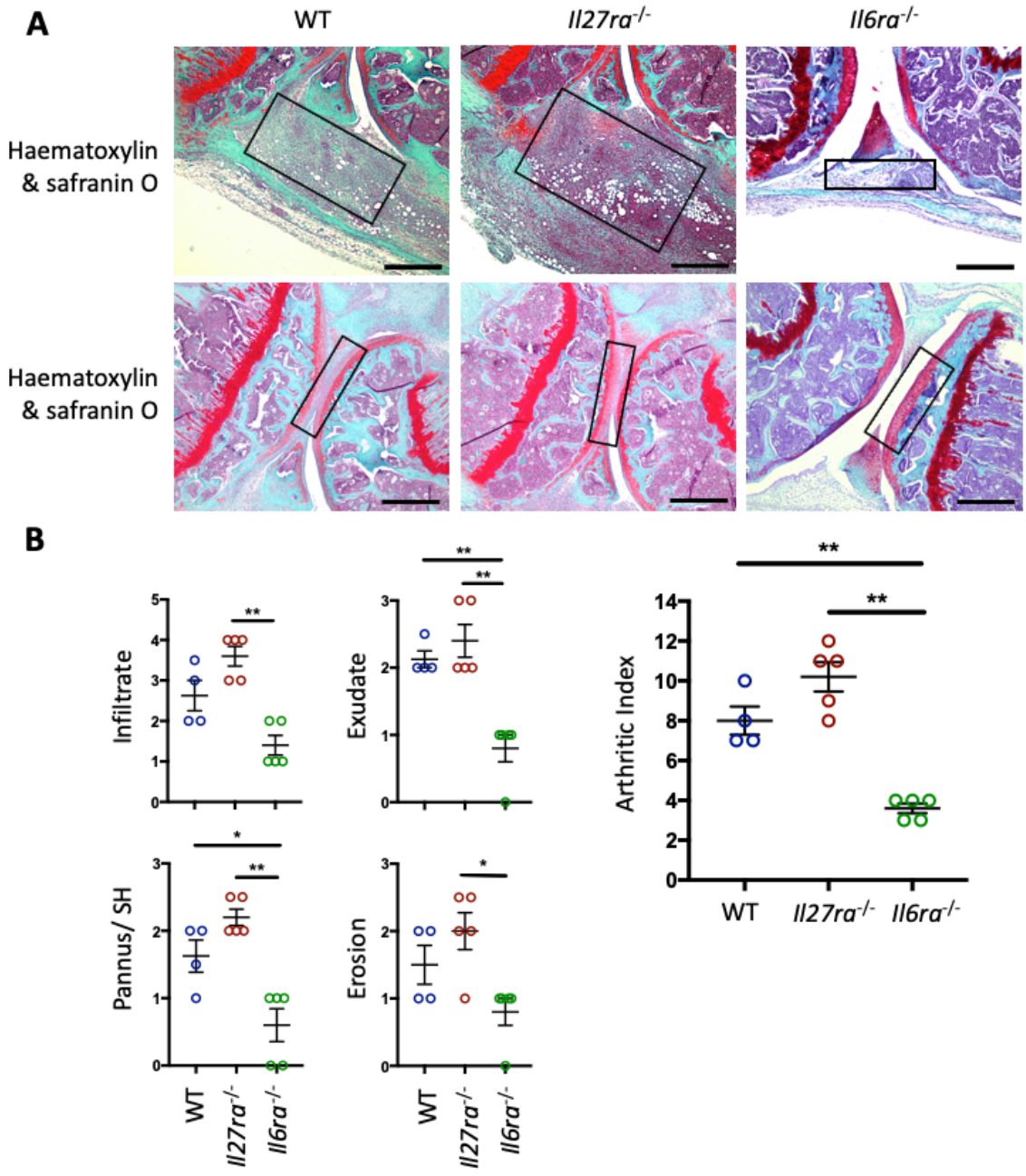

Figure 3.4 - Induction of AIA in WT, *Il27ra*$^{-/-}$ and *Il6ra*$^{-/-}$ mice. (A) Representative images of Haematoxylin and safranin O staining at day 10 of AIA. Boxed areas highlight regions of inflammatory infiltrate (top) and cartilage erosion (bottom), identified by loss of safranin O staining. (B) Histopathology scoring of AIA at day 10. (A, B) WT, $n = 4$; Il27ra$^{-/-}$ and *Il6ra*$^{-/-}$, $n = 5$. Scale bars: (A) 500 µm. Graphs represent mean ± SEM. * $p < 0.05$; ** $p < 0.01$.

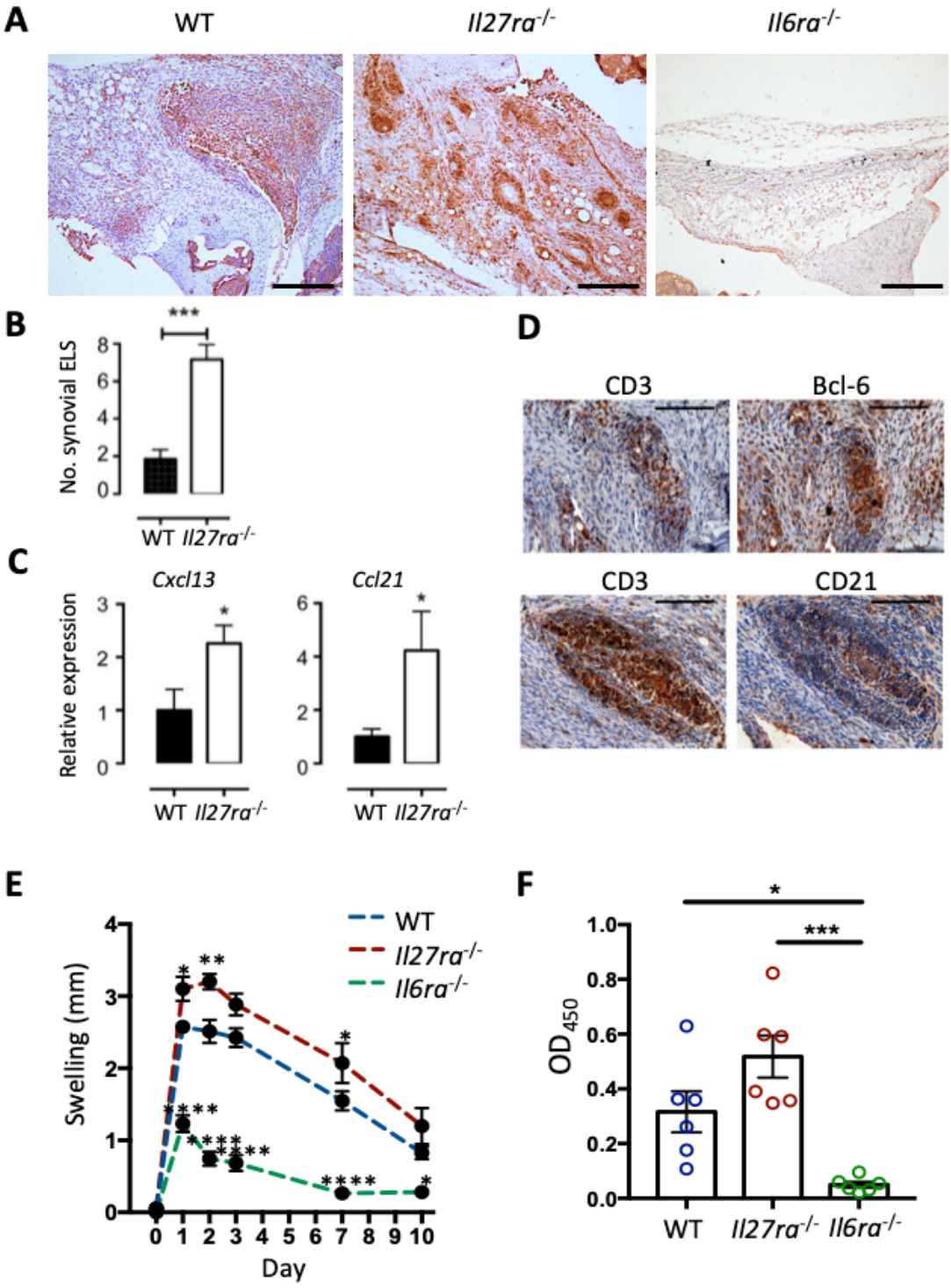

Figure 3.5 - Assessment of AIA in WT, *Il27ra*$^{-/-}$ and *Il6ra*$^{-/-}$ mice. (A) Representative images of immunohistochemistry for CD3 at day 10 of AIA. (B) The number of synovial ELS were quantified in synovial sections. (C) qPCR of indicated genes in WT and *Il27ra*$^{-/-}$ mouse synovium at day 3 of AIA. (D) Serial sections from *Il27ra*$^{-/-}$ mice stained for CD3 and Bcl-6 (top) and CD3 and CD21 (bottom). (E) Swelling of knee joints following intra-articular injection of mBSA. (C) mBSA specific antibody titres at day 10 post arthritis induction. (A) WT, $n = 4$; *Il27ra*$^{-/-}$ and *Il6ra*$^{-/-}$, $n = 5$. (B) $n = 8$ / group. (C) $n = 6$ / group. Scale bars: (A) 250 µm. Graphs represent mean ± SEM. * $p < 0.05$; ** $p < 0.01$; *** $p < 0.001$; **** $p < 0.0001$.

Panels B-D adapted from previously published work (Jones et al. 2015).

3.3.2 Optimising the extraction of high-quality RNA for sequencing

To evaluate gene signatures associated with the different synovial pathologies observed in WT, *Il27ra*$^{-/-}$ and *Il6ra*$^{-/-}$ mice, whole tissue RNA-seq was employed. For RNA-seq, extracting high-quality RNA is paramount as it influences the ability to map reads to the genome; low quality RNA leads to poor mapping [259]. Therefore, RIN values greater than 8 are required. As such, optimisation of RNA extraction from the synovium was required. Trizol extraction (*see section 3.2.1*) yielded low quality RNA with RIN values of approximately 6 (*Figure 3.6A*), whilst homogenisation of synovium in a commercial lysis buffer (*see section 2.2.7*) yielded high quality RNA with RIN values between 8 and 9 (*Figure 3.6B*). Therefore, homogenisation of synovium was used to extract total RNA for library preparation and sequencing.

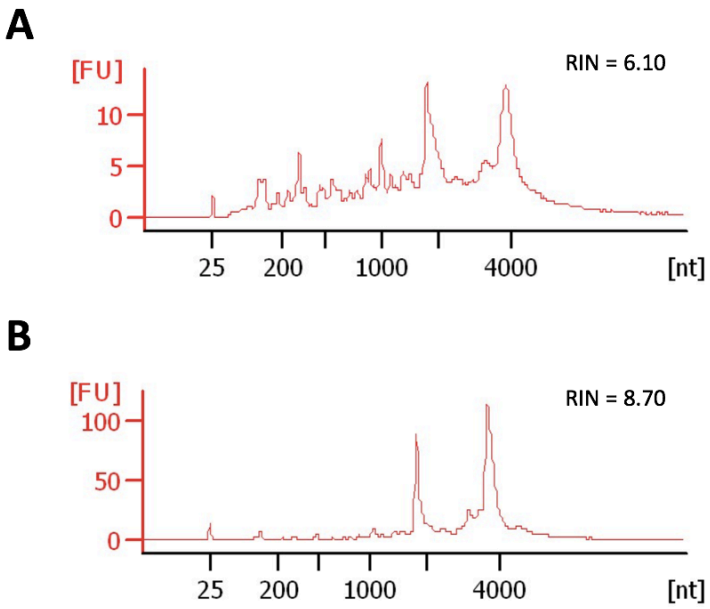

Figure 3.6 - Optimisation of RNA extraction from mouse synovium. (A-B) Representative bioanalyser traces comparing total RNA extraction from mouse synovium. Total cellular RNA was extracted using Trizol (A) or after homogenisation using a benchtop homogeniser (B) before further purification using a Qiagen RNeasy Mini Kit with an on-column DNaseI digestion. (A) Trizol extraction; RIN = 6.10. (B) Homogenisation; RIN = 8.70.

3.3.3 Optimisation of RNA-seq of mouse synovium

An initial step in RNA-seq is the fragmenting of RNA into suitable sizes for sequencing. For the HiSeq 4000 platform, fragment sizes of approximately 260 bp to 280 bp are recommended. Thus, fragmentation of RNA into suitable sizes was optimised by incubating the recovered RNA for between 2 and 8 minutes at 94°C (*Figure 3.7*). Bioanalyser traces confirmed that an optimal peak size was obtained when fragmenting synovial RNA for 6 minutes.

Libraries were then prepared as outlined in *section 3.2*. Initially rRNA was removed using magnetically labelled oligos specific to rRNA sequences. When placed in a magnetic field this removes rRNA and leaves all other RNAs (e.g. mRNAs, microRNAs, lncRNAs etc.) for downstream sequencing steps. A TruSeq Stranded Total RNA Library Prep Kit was used to generate cDNA libraries of optimal size (*Figure 3.8A*). Reads were mapped to the reference genome as outlined in *section 3.2.5* and assigned an RNA classification. *Figure 3.8B* shows that a high proportion of reads mapped to rRNA genes suggesting an ineffective removal of rRNA during depletion steps. Consequently, this resulted in a high number of duplicated reads as there were highly abundant and repetitive sequences (*Figure 3.8C*).

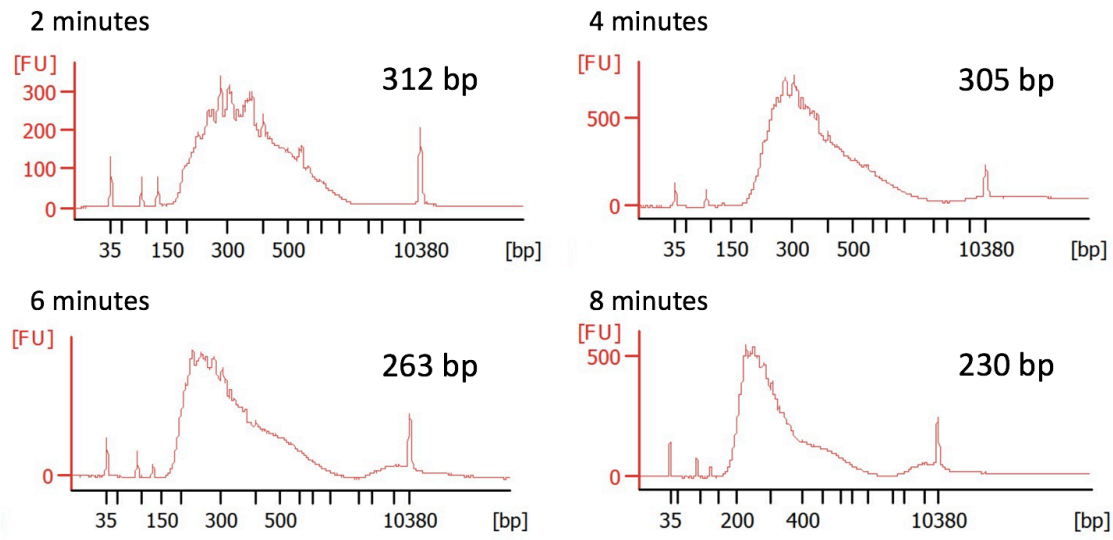

Figure 3.7 - Optimisation of fragmentation time for synovial RNA. Total RNA was fragmented for the indicated amount of time. Libraries were made with resulting fragmented RNA and the peak size determined by running on a bioanalyser. Peak size for each product is indicated in base pairs. Optimal peak size for library preparation for the Illumina platform is approximately 260 - 280 bp.

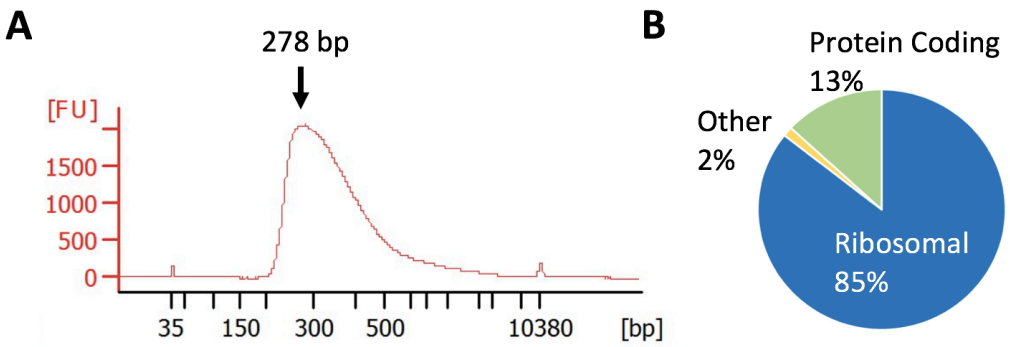

C

Total Read Pairs (x10^6)	**69**
Mapped Read Pairs (x10^6; % of total)	**57 ; 83**
Duplicate Read Pairs (x10^6; % of total)	**47 ; 82**

Figure 3.8 - Ribosomal RNA contamination of libraries resulted in poor coverage. (A) Representative bioanalyser trace of cDNA product after library preparation. Arrow shows the peak fragmentation size. (B) Proportions of protein coding genes (green), ribosomal genes (blue) and other genes (composed of lncRNA, microRNA; yellow) as assigned by Ensembl. (C) Summary statistics from RNA sequencing showing the number of read pairs and the percentage of the total number of reads. A high number of duplicated read pairs is highlighted in red.

3.3.4 Contamination of cDNA libraries by ribosomal species

Given the high proportion of contaminating rRNA reads observed following sequencing, samples were visualised using a bioanalyser to determine the efficiency of the rRNA depletion step. A comparison of two rRNA depletion kits from different manufacturers, and a poly(A) capture kit for isolation of mRNA was also investigated. Whilst both rRNA depletion kits left peaks that correlated with 18S and 28S peaks in the resulting total RNA (*Figure 3.9A*), the poly(A) capture kit was efficient in removing these peaks (*Figure 3.9A*), with significantly reduced (4%) contaminating rRNA (*Figure 3.9B*). Therefore, based on these optimisation studies, a poly(A) capture method to positively select mRNA species was chosen as the most appropriate method of library preparation for RNA-seq.

3.3.5 cDNA library preparation using poly(A) capture of mRNA

Library preparation was performed as outlined in *section 3.2* using a poly(A) capture method to purify mRNA, followed by a TruSeq Stranded Total RNA Library Prep Kit. Resulting libraries were visualised on a bioanalyser trace and had an optimal peak size of 280bp (*Figure 3.10A*). Reads were mapped to the reference genome as outlined in *figure 3.3* and assigned an RNA classification as in *figure 3.8B*. After changing to a poly(A) capture method, resulting in a more efficient removal of rRNA, approximately 80-90% of reads mapped to protein-coding genes and less than 5% mapped to rRNA (*Figure 3.10B*). The decrease in rRNA content was further highlighted by a reduction in the duplication of reads (*Figure 3.10C*). A high percentage (98%) of reads were mapped to the reference genome indicating the high quality of input RNA.

Further to this, quality controls performed during the analysis pipeline also showed a high quality of sequencing with a high accuracy of base calling (*Figure 3.11A*). For high complexity random libraries, an equal proportion of each base is expected (*Figure 3.11B-C*). The initial 10 base pairs of sequencing are disproportionate due to sequencing of primers and adapters which are synthetic and not random (*Figure 3.11B*).

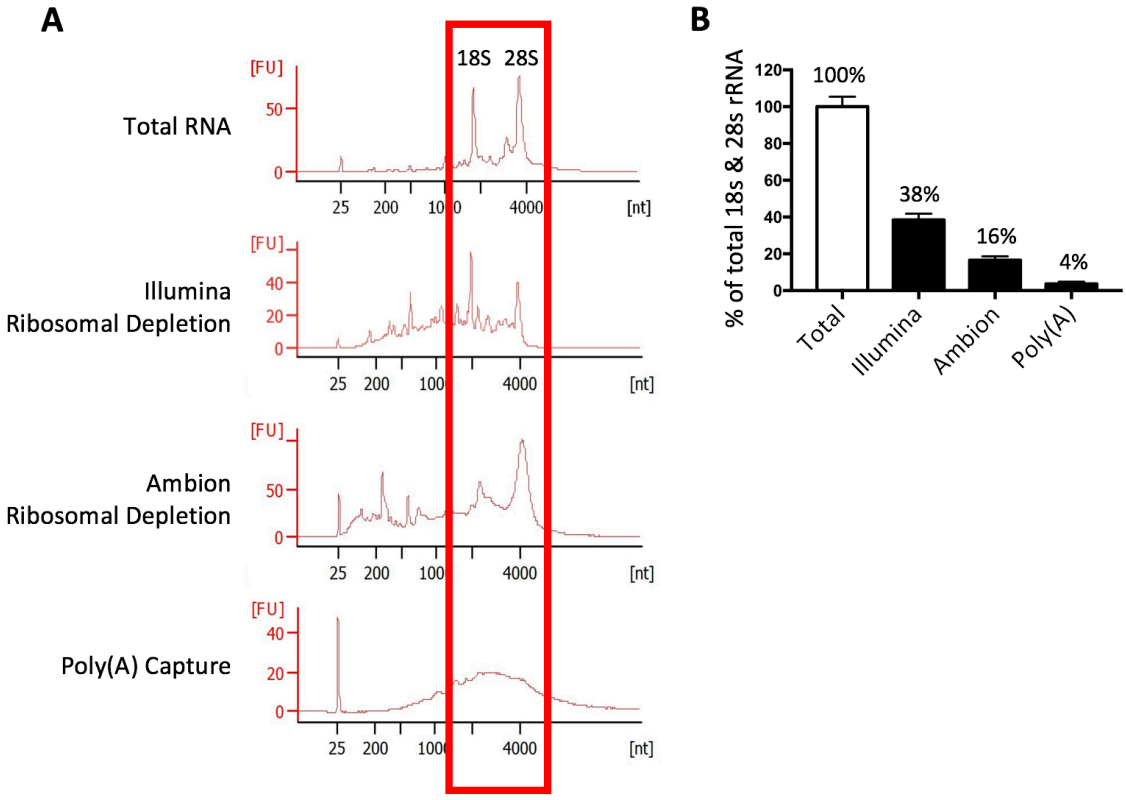

Figure 3.9 - Comparison of methods to remove ribosomal species from mouse synovium. (A) Representative bioanalyser traces of total RNA (top), after ribosomal depletion using two different commercially available kits (middle) and following poly(A) capture of mRNA species (bottom). The red boxed area highlights the 18s and 28s ribosomal RNA peaks. (B) Quantification of the remaining ribosomal RNA as a percentage of total RNA.

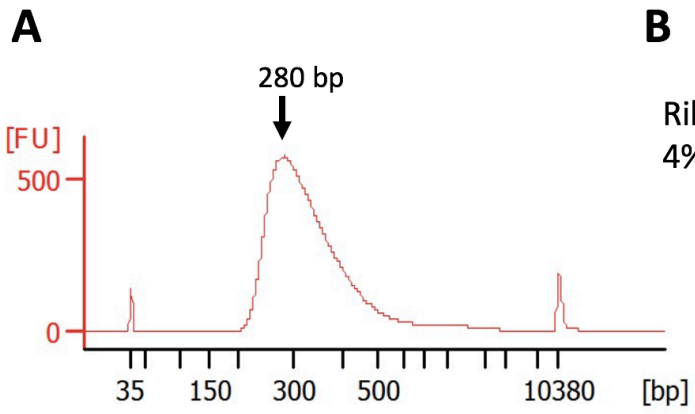

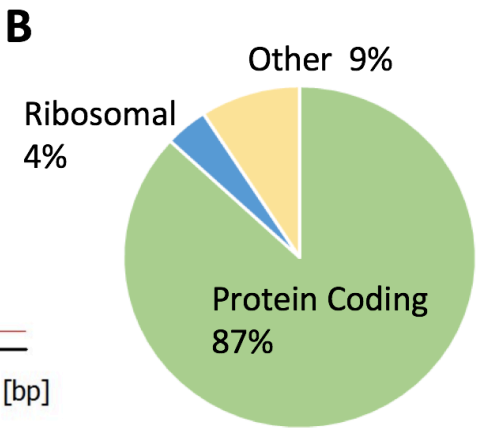

C

Total Read Pairs (x10^6)	**63**
Mapped Read Pairs (x10^6 ; % of total)	**62 ; 98**
Duplicate Read Pairs (x10^6 ; % of total)	**30 ; 48**

Figure 3.10 - Complete removal of ribosomal RNA by polyadenylation capture. (A) Representative bioanalyser trace of cDNA product after library preparation. Arrow shows the peak fragmentation size. (B) Proportions of protein coding genes (green), ribosomal genes (blue) and other genes (composed of lncRNA, microRNA; yellow) as assigned by Ensembl. (C) Summary statistics from RNA sequencing showing the number of read pairs and the percentage of the total number of reads.

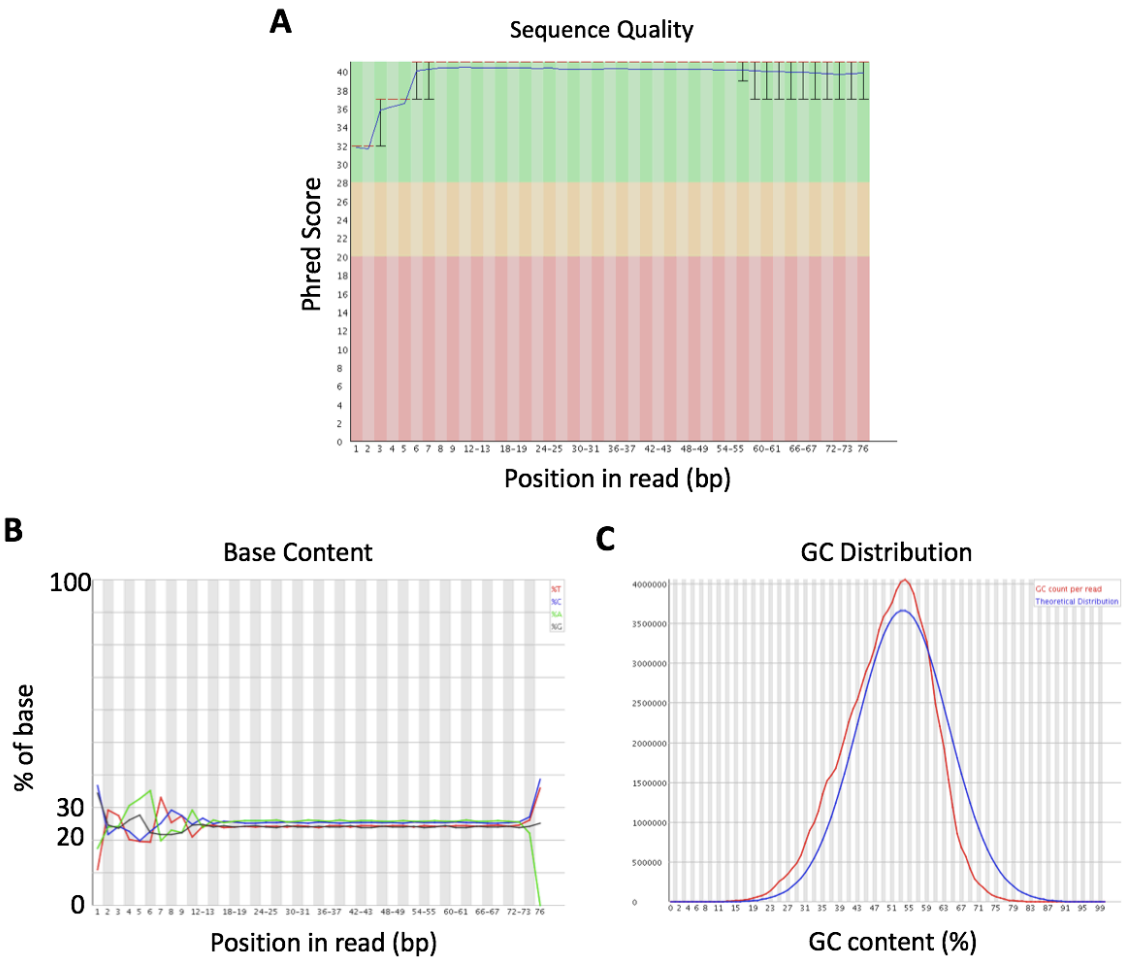

Figure 3.11 - Quality of Sequencing determined by FastQC report. (A-C) Representative traces from a FastQC report showing the quality of the sequencing. (A) Box and whisker plot of phred quality scores of each base called at each position within a read. The red line represents the median value and upper and lower lines represent the 90% and 10% values. The blue line is the mean quality score. A phred score of 30 means there is 99.9% accuracy in the base called. A phred score of 40 gives 99.99% accuracy. (B) Trace showing the percentage of each base at a position in the read that has been called. For a random library an equal proportion of each base is expected. (C) Comparison of the GC content of a library (red), compared to a normal GC distribution (blue).

3.3.6 Gene expression is not affected by duplication

Duplicated reads can arise from two sources. PCR duplicates (i.e. the read originates from the same cDNA molecule) or from biological replicates (i.e. reads with identical sequences but from different cDNA molecules). Convention in RNA-seq is to include duplicated reads in the analysis as it does not typically skew data [260]. Consistent with this, dupRadar analysis within the Bioconductor package confirmed that duplicated reads within the data set did not bias differential gene expression. Here, the number of duplicates per gene showed no correlation with fold change of the gene (*Figure 3.12*). Duplicated reads were consequently included in the bioinformatic analysis reported in *Chapter 4.*

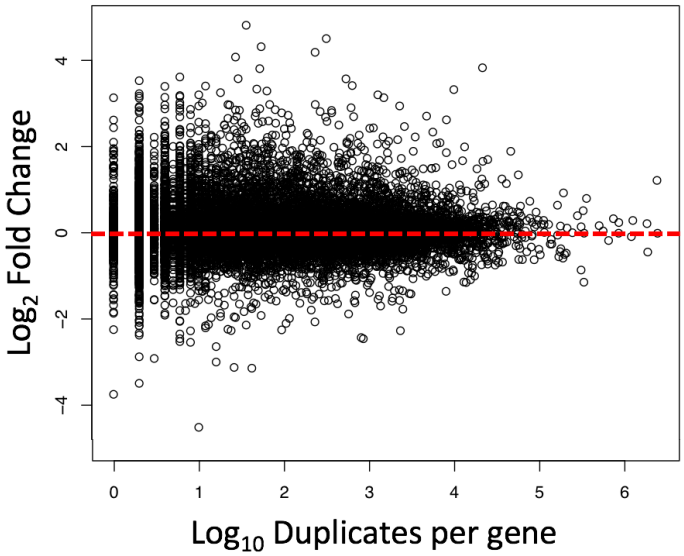

Figure 3.12 - Gene duplication does not affect the gene expression. Representative plot showing how duplication of a gene effects the fold change of the gene. Plots were generated using the dupRadar analysis, within the Bioconductor package. The red dotted line indicates a $\log_2$ fold change of 0.

3.4 Discussion

This chapter outlines, for the first time, the establishment of RNA-seq methodologies for the evaluation of synovial inflammation in an experimental model of inflammatory arthritis. The extraction of high-quality synovial RNA, fragmentation of the purified RNA, removal of rRNA and the preparation of cDNA libraries were key steps that required significant optimisation to generate high quality sequencing reads.

Before proceeding with RNA-seq of the synovium I showed that my induction of the AIA model was consistent with previous studies in these mice. The *Il6ra*$^{-/-}$ mice had not been characterised in this model previously. Consistent with the reduced development of AIA in *Il6*$^{-/-}$ mice, and with the use of the anti-IL-6R monoclonal antibody, tocilizumab, for the treatment of clinical RA, *Il6ra*$^{-/-}$ mice displayed ameliorated inflammatory arthritis. Similarly, in agreement with a role for IL-6 in directing the transition from an innate to an adaptive immune response [64], *Il6ra*$^{-/-}$ mice showed reduced mBSA-specific antibody titres reflecting that observed in AIA-challenged *Il6*$^{-/-}$ mice [199]. However, while I hypothesised that *Il6ra*$^{-/-}$ mice would display a similar phenotype to *Il6*$^{-/-}$ mice, there are examples of where the IL-6R-deficient mice display different phenotypes to IL-6 knockout mice. In this regard, *Il6*$^{-/-}$ and *Il6ra*$^{-/-}$ mice show a difference in skin wound healing [261] and recovery from dextran sodium sulphate (DSS)-induced colitis [262]. This may relate to the description of p28, p28:CLF and ciliary neurotrophic factor as low affinity ligands for the IL-6R that may allow the receptor to have distinct biological activities to IL-6 [263-265]. Therefore, the initial evaluation of inflammatory arthritis that I have undertaken in *Il6ra*$^{-/-}$ mice suggests a similar protected phenotype to that observed in *Il6*$^{-/-}$ mice. Further comparative investigations throughout the full time course of AIA would provide additional insight into how the IL-6R and IL-6 influence inflammatory arthritis progression.

During the early optimisation of library preparations for RNA-seq, an interesting finding that required significant optimisation to overcome was the persistent presence of rRNA following depletion steps, despite testing a number of commercial rRNA depletion kits. This may suggest an enrichment of rRNA in the synovium, where the commercial kits may have been saturated with rRNA during depletion resulting in a failure to efficiently remove all rRNA from samples. However, additional experiments using decreasing levels of input RNA showed no improvement in the ability to efficiently deplete rRNA content (data not shown). Similarly, technical support from an Illumina representative encountered the same difficulty, suggesting that this was a tissue specific problem rather

than an error in methodology. Hence positive selection using poly(A) capture was used to isolate mRNA for sequencing. While this resulted in a loss of RNA species that lack a poly(A) tail (e.g., microRNA, linc RNA etc), identification of protein-coding genes associated with the development of synovial ELS was deemed the priority.

An advantage of RNA-seq over hybridisation techniques is that depth of sequencing can be varied. As samples are sequenced to a greater depth more transcripts are identified and quantification is more precise [266]. In order to identify genes that have low expression levels, as well as highly expressed genes, samples were sequenced to a high depth (> 60 million paired-end reads). However, increasing the depth of sequencing can also result in increased background and duplication levels [267]. Duplicated reads can arise from two sources: PCR duplicates (i.e. the read originates from the same cDNA molecule) or from biologically relevant replicates (i.e. reads with identical sequences but from different cDNA molecules). The question remains whether removing duplicates results in improved accuracy by reducing background noise from PCR duplicates, or whether it reduces accuracy by removing biologically relevant replicates. In line with previous studies [260, 268, 269], the levels of duplication had no effect on differential gene expression. Consequently, read duplicates were retained in the analysis.

In summary, this chapter describes the optimisation of RNA-seq methodologies to study gene expression changes in the synovium during inflammatory arthritis. This approach has the potential to reveal new mechanisms that govern the development and progression of joint inflammation, including ELS-rich synovitis, and identify new therapeutic targets and biomarkers that may improve the treatment of patients with inflammatory arthritis.

Chapter 4. Transcriptomic analysis of joint inflammation featuring synovial ELS

4.1 Introduction

The synovitis associated with RA is highly heterogenous. Histological assessment of joint pathology identifies 3 broad classifications of synovitis termed 'pauci-immune', 'diffuse' and 'follicular', where the latter is characterised by lymphoid-rich aggregates called ectopic lymphoid-like structures (ELS) [155, 193-195]. Importantly, synovial ELS act as sites of T cell priming and autoantibody generation (e.g. RF, ACPA). While this remains a controversial topic, the presence of synovial ELS in RA has been linked with an inferior response to biological drug therapies (e.g. anti-TNF inhibitors) and are associated with severe local and systemic inflammation [195-197]. At present, biomarkers for RA are lacking. While disease-specific autoantibodies such as RF and ACPA correlate with disease severity, they unreliably predict underlying joint pathology [193]. Identifying cytokine-regulated mechanisms that determine the development of distinct synovial pathotypes has the potential to define biomarkers for patient stratification and to identify novel therapeutic targets for the treatment of RA patients with ELS-rich disease.

Transcriptomic approaches are now being used to investigate differences in gene expression between RA patients with defined forms of pathology in an attempt to improve patient stratification and treatment decisions [195]. For example, microarray analysis has identified 4 synovial phenotypes termed 'myeloid', 'lymphoid', 'fibroid' and 'low inflammatory' that display differential responses to biological drugs [195]. These phenotypes are comparable to those identified through histological approaches used to assess joint pathology [146, 155, 193-195]. However, the synovitis associated with RA does not always fall neatly into these broad classifications, and patients often display pathologies that lie between these definitions. Therefore, the use of genetically modified mice that display defined patterns of synovial histopathology may offer advantages in identifying the cytokine-driven mechanisms that promote these discrete forms of joint inflammation.

The experiments outlined in this chapter will use optimised RNA-seq methodologies (*see Chapter 3*) to investigate joint inflammation in AIA-challenged WT, *Il27ra*$^{-/-}$ and *Il6ra*$^{-/-}$ mice that display histological features of synovitis that resemble those seen in RA [146]. Studies aimed to identify IL-27-regulated genes and pathways associated with the development of lymphoid-rich synovitis featuring ELS.

4.2 Methods

4.2.1 Heatmaps

Heatmaps were generated using Morpheus software available from the Broad Institute (https://software.broadinstitute.org/morpheus/). Heatmap visualisations used $\log_2$ fold change ($\log_2$FC) compared to a healthy WT control joint or a WT inflamed joint at an equivalent time point, as indicated in the text and figure legend. Data sets were hierarchically clustered using one minus Pearson correlation coefficient.

4.2.2 Ingenuity Pathway Analysis

Ingenuity Pathway Analysis (IPA; Qiagen) was used to identify canonical pathways associated with differentially regulated genes identified between genotypes and across the time course of AIA. Relevant pathways were determined by their p-value.

4.2.3 K-means clustering

Genesis software was used to perform K-means clustering. The optimal number of clusters was determined using statistical tests (Silhouette statistic and Gap method) and was performed in collaboration with Dr. Barbara Szomolay. The Silhouette and gap method provide a statistical measure of how individual genes behave in response to inflammatory activation. A high value indicates that genes displaying a similar profile of expression are appropriately grouped into clusters that share common patterns of regulation [270, 271].

4.2.4 Gene Set Enrichment Analysis

Gene Set Enrichment Analysis (GSEA) was performed using software from the Broad Institute (http://www.broad.mit.edu/gsea). Gene sets for effector T helper cell subsets (Th1, Th2, Th17 and Treg cells) and pathogenic Th17 cells are publicly available (GEO, GSE45975 and GSE39820 respectively) [272, 273]. Data sets were pre-ranked using the $\log_2$FC prior to GSEA.

4.3 Results

4.3.1 Transcriptomic profiles reflect synovial pathology

IL-6 and IL-27 are key cytokines that shape the inflammatory environment within the synovium during AIA. Using histopathological approaches, *Il6*$^{-/-}$ mice have previously been reported to be protected from developing inflammatory arthritis, with mice having reduced synovial infiltration and joint damage [69, 199, 256]. In *Chapter 3*, histological evaluation of synovitis in *Il6ra*$^{-/-}$ mice with AIA showed a similarly reduced profile of disease. In contrast, *Il27ra*$^{-/-}$ mice displayed exacerbated disease and the presence of ELS within the synovium at day 10 [146]. RNA-seq of synovium from WT, *Il27ra*$^{-/-}$ and *Il6ra*$^{-/-}$ mice was performed to identify transcriptomic changes associated with differences in synovial pathology. Here, samples clustered into two distinct groups: (i) genes expressed in naïve synovium across all genotypes and (ii) genes expressed post arthritis induction (*Figure 4.1A*). An interesting exception to this was synovial RNA-seq data from *Il6ra*$^{-/-}$ mice at day 10 of AIA, which clustered with the naïve samples and was therefore consistent with the reduced synovial inflammation observed in *Il6ra*$^{-/-}$ mice (see *Figure 3.4*).

While the aim of this study was to understand the cytokine-regulated mechanisms that control joint inflammation in each of these genotypes, we first determined whether differences were observed from the synovium of non-challenged WT, *Il27ra*$^{-/-}$ and *Il6ra*$^{-/-}$ mice. Very few differences were observed between tissues derived from WT and *Il6ra*$^{-/-}$ mice (50 differentially expressed genes; DEGs). However, there were 1198 DEGs observed when comparing naïve synovium from *Il27ra*$^{-/-}$ with WT mice (*Figure 4.1B*). Since genes expressed in naïve synovium clustered separately from inflamed synovium (*Figure 4.1A*) it was hypothesised that differences in baseline were not associated with inflammatory pathways. To confirm this, IPA was performed on DEGs, and the top 5 pathways were associated with bone remodelling (e.g. *Spp1*, *Col2a1*, *Mmp9*), cell cycle regulation (e.g. *Cdc25b*, *Wee1*) and synthesis of amino acids and ribonucleotides (e.g. *Pak3*, *Map3k9*) (*Figure 4.1C*). Importantly, whilst some of these pathways included inflammatory mediators, these were not predominantly differentially regulated. Interestingly however, expression of the homeostatic chemokine, *Cxcl13*, was significantly increased in naïve synovium from *Il27ra*$^{-/-}$ mice (*Figure 4.1D*). Thus, whilst there were differences between naïve synovium from WT, *Il27ra*$^{-/-}$ and *Il6ra*$^{-/-}$ mice, these were not principally linked with the control of inflammation.

Transcriptomic analysis of the inflamed synovium from AIA challenged WT, *Il27ra*$^{-/-}$ and *Il6ra*$^{-/-}$ mice hierarchically clustered genes into those differentially regulated early in disease (day 3) and once synovial pathology was established (day 10) (*Figure 4.2*). Whilst there were gene expression differences between all three genotypes at day 3, more prominent differences were observed at day 10. Here, clusters of IL-27 regulated genes that may be uniquely expressed during the development of synovial ELS were observed (*Figure 4.2*). Additionally, *Il6ra*$^{-/-}$ mice displayed lower expression of a large number of genes prominently expressed at day 10 in WT and *Il27ra*$^{-/-}$ mice. This is consistent with the protected phenotype observed in *Il6ra*$^{-/-}$ mice, where histopathology revealed a reduced local adaptive immune response in inflamed joints and lower mBSA-specific antibody titres (*see Chapter 3*). Interestingly a cluster of genes highly upregulated in *Il6ra*$^{-/-}$ mice at day 10 was identified (*Figure 4.2*). Since IL-6 controls the switch from an innate to adaptive immune response [64], I asked whether genes upregulated in *Il6ra*$^{-/-}$ mice at day 10 (*Figure 4.3A*) were associated with an impairment in this transition. Indeed, IPA analysis revealed the top 5 pathways were associated with innate signalling, cell adhesion and bone and matrix remodelling (*Figure 4.3B and C*). Genes identified within these pathways included *Dkk1*, an IL-6 regulated inhibitor of new bone formation [274], and *Mmp12*, a macrophage-expressed matrix metalloproteinase associated with synovial thickening and cartilage destruction [275]. Thus, the heightened expression of genes associated with innate immunity in *Il6ra*$^{-/-}$ mice, combined with a diminished adaptive immune response, suggests that the transition from innate to adaptive immunity in IL6R-deficiency is dysregulated. Together, these data show that the distinct patterns of synovial histopathology observed in WT, *Il27ra*$^{-/-}$ and *Il6ra*$^{-/-}$ mice are also associated with different transcriptomic profiles.

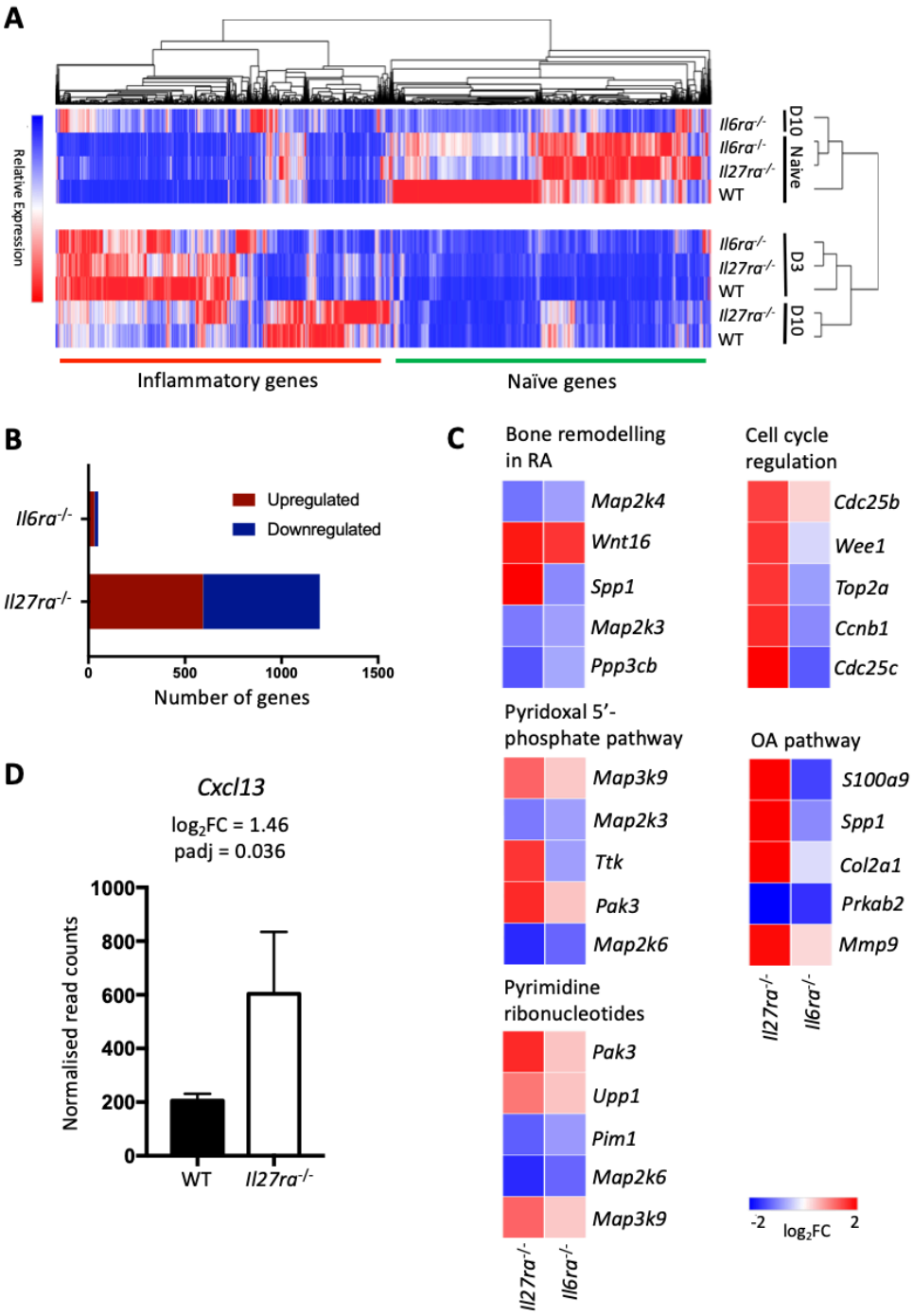

Figure 4.1 - Naïve synovium from WT, *Il27ra*$^{-/-}$ and *Il6ra*$^{-/-}$ mice have different transcriptomic profiles. (A) Relative expression of differentially expressed protein-coding genes in WT, *Il27ra*$^{-/-}$ and *Il6ra*$^{-/-}$ mice in naïve synovium and at day 3 and day 10 post induction of AIA ($p < 0.05$, $\log_2FC > 1.5$). Coloured bars highlight clusters of genes expressed during inflammatory arthritis (red) and those expressed in naïve synovium (green). Heatmap was clustered using one minus Pearson correlation. (B) The number of differentially expressed genes in naïve synovium of *Il27ra*$^{-/-}$ and *Il6ra*$^{-/-}$ mice when compared to a healthy WT control joint ($p < 0.05$, $\log_2FC > 1$). (C) The top 5 canonical pathways associated with the differentially expressed genes from panel B as determined by IPA. Representative genes comprising the pathways are also shown with expression determined by comparing to a healthy WT control joint. (D) Expression of *Cxcl13*, depicted as normalised read counts, in naïve synovium from WT and *Il27ra*$^{-/-}$ mice. OA, osteoarthritis.

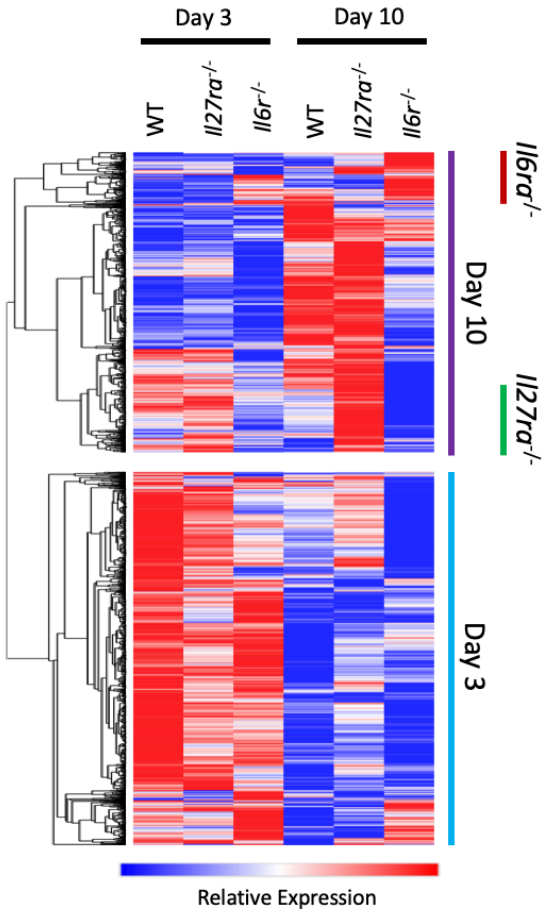

Figure 4.2 - Different transcriptional profiles are observed in the inflamed synovium of WT, *Il27ra*$^{-/-}$ and *Il6ra*$^{-/-}$ mice. Relative expression of differentially expressed protein coding genes ($p < 0.05$, $\log_2$FC > 1.5) between genotypes at day 3 and day 10 of AIA when compared to a healthy WT control joint. Coloured bars highlight clusters of genes regulated at day 3 (blue), day 10 (purple), in *Il6ra*$^{-/-}$ mice (red) and in *Il27ra*$^{-/-}$ mice (green). Heatmap was clustered using one minus Pearson correlation.

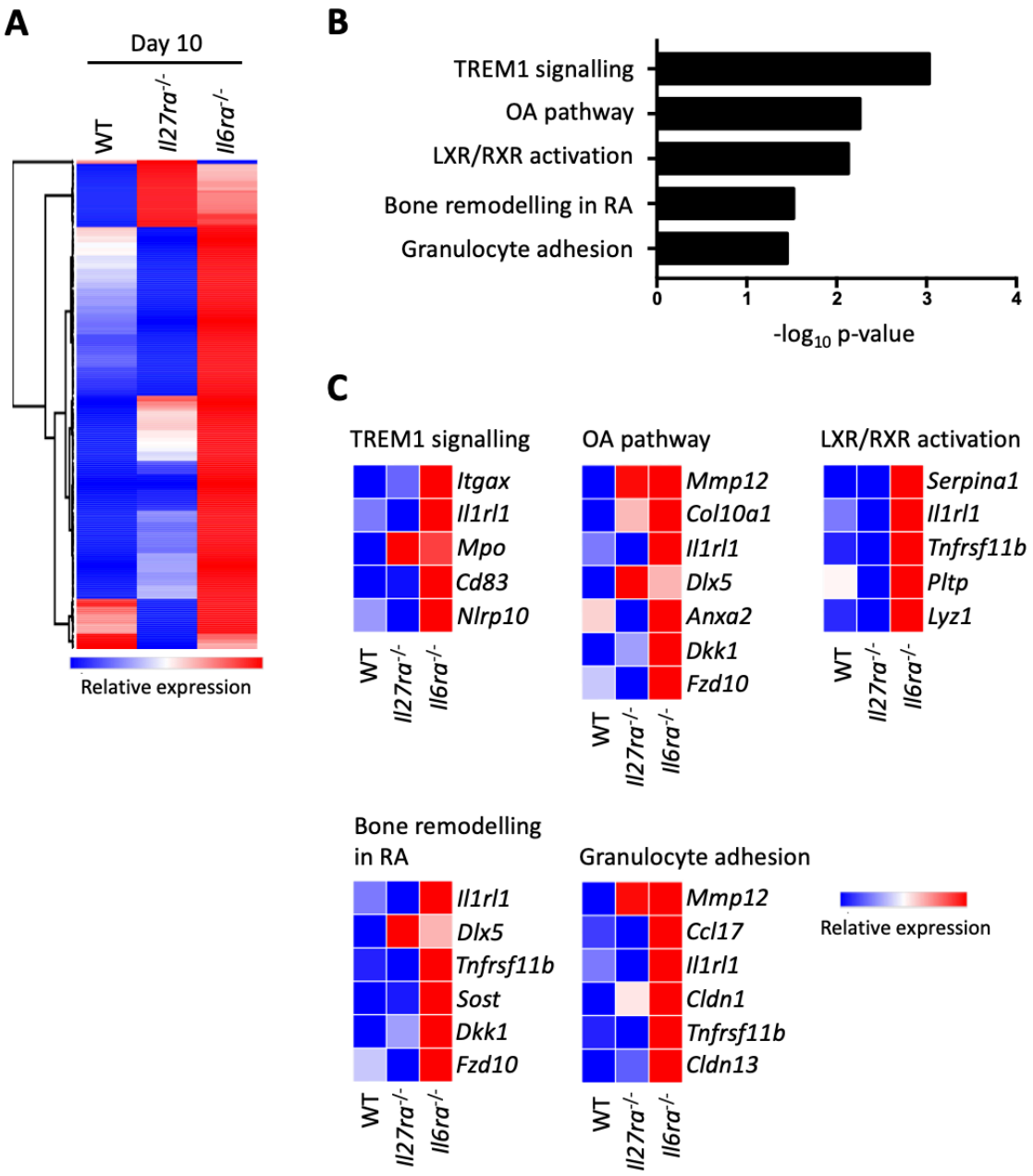

Figure 4.3 - A cluster of highly expressed genes in *Il6ra*$^{-/-}$ mice are associated with innate immune responses. (A) Relative expression of the cluster of genes highly expressed in *Il6ra*$^{-/-}$ mice at day 10 of AIA ($p < 0.05$, $\log_2$FC > 1.5) when compared to a healthy WT control joint. Heatmap was clustered using one minus Pearson correlation. (B) The top 5 canonical pathways associated with the differentially expressed genes from panel A as determined by IPA. (C) Relative expression of genes comprising the pathways shown in panel B as determined by IPA. OA, osteoarthritis.

4.3.2 ELS-rich synovitis is associated with an increase in DEGs

At day 3 of AIA, which precedes the development of synovial ELS [146], there were 111 DEGs (50 upregulated, 61 downregulated) between *Il27ra*$^{-/-}$ and WT. In line with the previously described exacerbation of inflammatory arthritis observed in *Il27ra*$^{-/-}$ mice [146], 363 genes were differentially regulated at day 10. Whilst the number of downregulated genes was comparable to day 3 (64 genes), there was a large increase in the number of upregulated genes (299 genes) (*Figure 4.4A and B*). Surprisingly, *Il6ra*$^{-/-}$ mice had a large number of DEGs at both day 3 and day 10 compared to WT (*Figure 4.4A and B*). Interestingly however, inflammatory genes prominently expressed in *Il27ra*$^{-/-}$ mice (e.g., *Il17a, Il17f*, *Il21*) were often downregulated in *Il6ra*$^{-/-}$ mice (*Figure 4.4A*), which may reflect the often opposing outcomes that IL-6 and IL-27 have in adaptive immunity [47, 93, 105]. Therefore, exacerbated synovitis featuring ELS in *Il27ra*$^{-/-}$ mice was associated with an increase in transcriptomic output.

We next used IPA to identify canonical pathways associated with the DEGs in *Il27ra*$^{-/-}$ and *Il6ra*$^{-/-}$ mice. At day 3, the relatively small number of DEGs identified in *Il27ra*$^{-/-}$ mice (*see Figure 4.4*) were linked with few pathways, that were primarily associated with innate immune involvement (*Figure 4.5A*). In contrast, at day 10 *Il27ra*$^{-/-}$ mice were enriched for pathways involved in T cell activation, effector responses, signalling and differentiation. Mice deficient in IL-6R were strongly enriched for pathways associated with fibrosis, macrophage and fibroblast responses, and osteoblast and osteoclast responses (*Figure 4.5B*). Thus, our transcriptomic analysis of the inflamed synovium reflects key features of synovial inflammation in these mice [69, 146] and is identifying key pathways consistent with previously defined roles for IL-6 and IL-27 in regulating fibrosis, osteoclastogenesis, innate immune regulation, T cell differentiation and effector characteristics [47].

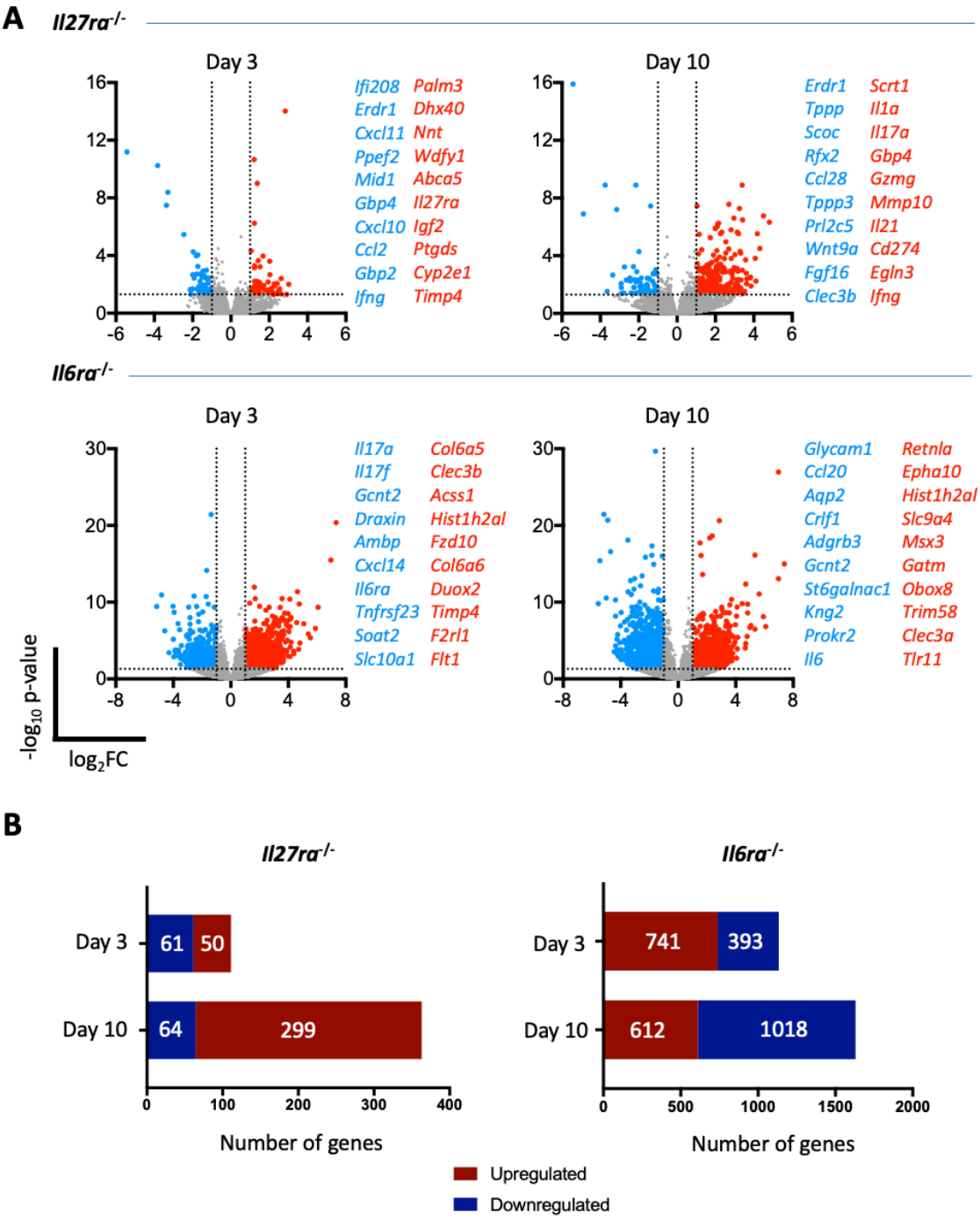

Figure 4.4 - Synovitis featuring ELS in *Il27ra*$^{-/-}$ mice is associated with an increase in gene expression. (A) Volcano plots of gene expression profiles in *Il27ra*$^{-/-}$ and *Il6ra*$^{-/-}$ mice compared to WT mice at day 3 and day 10 of AIA. Dotted lines identify significant genes ($log_2FC > 1$, $p < 0.05$). At each time point the 10 most upregulated (red) and downregulated (blue) protein-coding genes are shown. (B) The number of differentially expressed genes ($log_2FC > 1$, $p < 0.05$) either upregulated (red) or downregulated (blue) in *Il27ra*$^{-/-}$ and *Il6ra*$^{-/-}$ compared to WT at day 3 and day 10 of AIA.

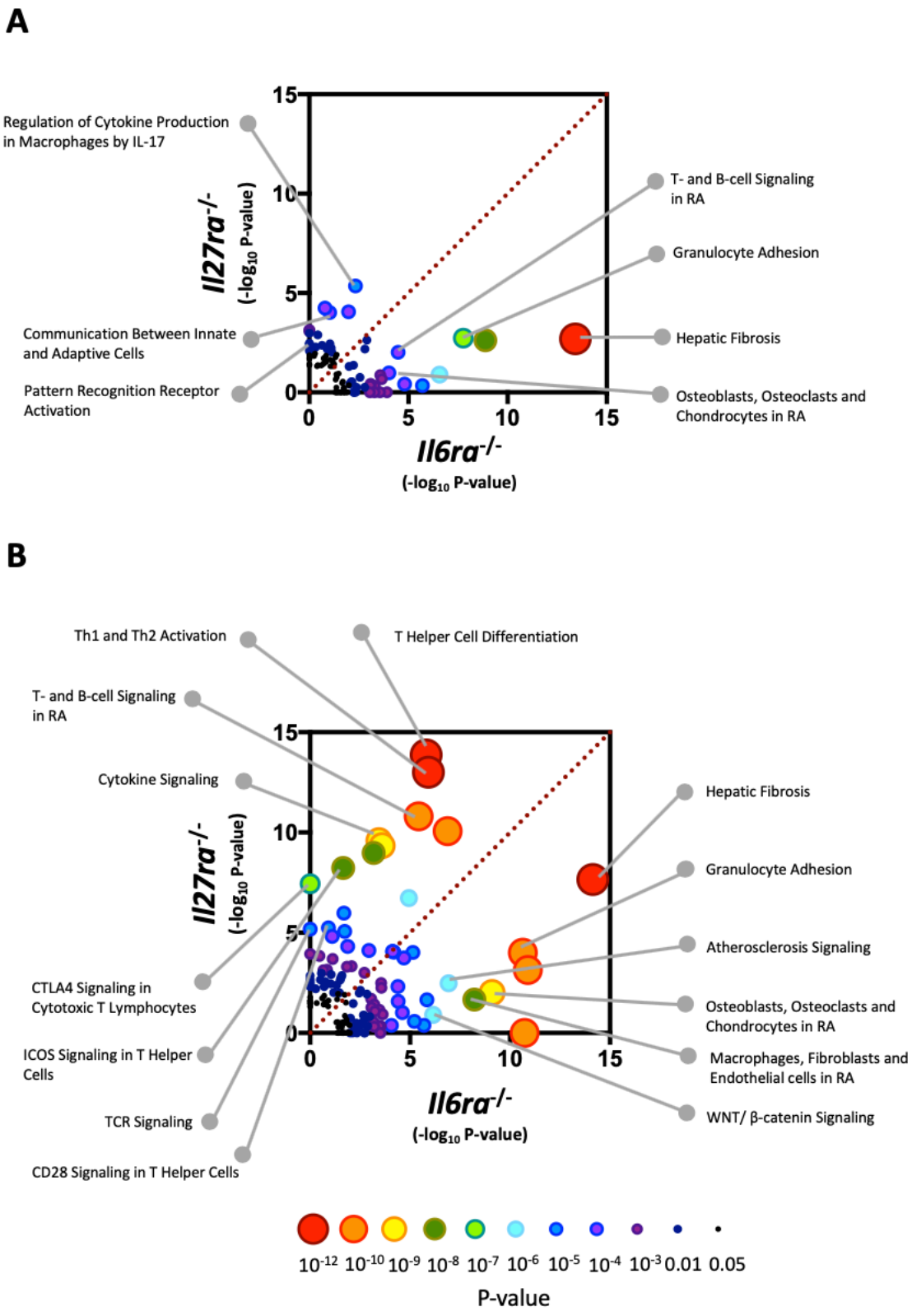

Figure 4.5 - IPA identifies IL-6 and IL-27 regulated pathways associated with synovial inflammation. (A-B) Dot plot of canonical pathways identified by IPA when comparing *Il27ra*$^{-/-}$ and *Il6ra*$^{-/-}$ synovium to WT synovium at day 3 (A) and day 10 (B) of AIA. The statistical significance of the pathway is represented by the size and colour of the dot. The diagonal red dotted line represents an equal significance of the pathway in both genotypes.

4.3.3 K-means clustering to identify patterns of gene behaviour

While the IPA analysis of RNA-seq datasets described in the previous sections provide some insight into the regulation of AIA in WT, *Il27ra*$^{-/-}$ and *Il6ra*$^{-/-}$ mice, the large number of DEGs observed made interpretation of the data very challenging. To resolve this, K-means clustering was used to identify groups of genes that displayed similar patterns of expression across the time course of AIA. To first gain insight into how genes behaved in WT mice, the optimal number of clusters was determined using statistical tests. The silhouette method identified 2 or 3 gene clusters as optimal, whereas the gap statistic method identified 4 or 5 clusters as optimal (*Figure 4.6A*). Using these values as a guide, 5 gene clusters were selected as these separated broadly into genes that were (i) upregulated to different extents (clusters 2 and 5), (ii) downregulated to a different degree (clusters 1 and 3), and (iii) appeared to selectively increase at day 10 (cluster 4) (*Figure 4.6B*).

Canonical pathways associated with each gene cluster were determined using IPA. Cluster 1, comprised of genes associated with metabolic pathways such as the TCA cycle (e.g. *Idhg3, Sdh*) and oxidative phosphorylation (e.g. *Atp5c1, Sdha*) (*Figure 4.7*). Clusters 2 and 5 comprised genes that were upregulated in AIA and were highly enriched for genes involved in T cell activation, differentiation and signalling. These genes included effector cytokines (e.g. *Ifng*, *Il17a*, *Il21*, *Il22*, *Tgfb*), transcriptional regulators (e.g. *Stat1*, *Tbx21*), cell surface receptors (e.g. *Cd40l*, *Cd274*, which encodes the immune checkpoint PD-L1) and mediators of cell trafficking (e.g. *Cxcl3*, *Icam1*, *Glycam1*) (*Figure 4.7*). Cluster 4 transcripts, that were predominantly increased at day 10 of AIA, were enriched for fibrosis, bone remodelling and matrix remodelling pathways, highlighted by an increase in the expression of collagens (e.g. *Col1a1*, *Col1a2*, *Col6a4*, *Col23a1*), bone morphogenic proteins (e.g. *Bmp1*, *Bmp15*) and matrix metalloproteinases (e.g. *Mmp2*, *Mmp11*, *Mmp23b*) (*Figure 4.7*). Thus K-means clustering has allowed the identification of gene expression behaviours associated with the development of synovitis during AIA.

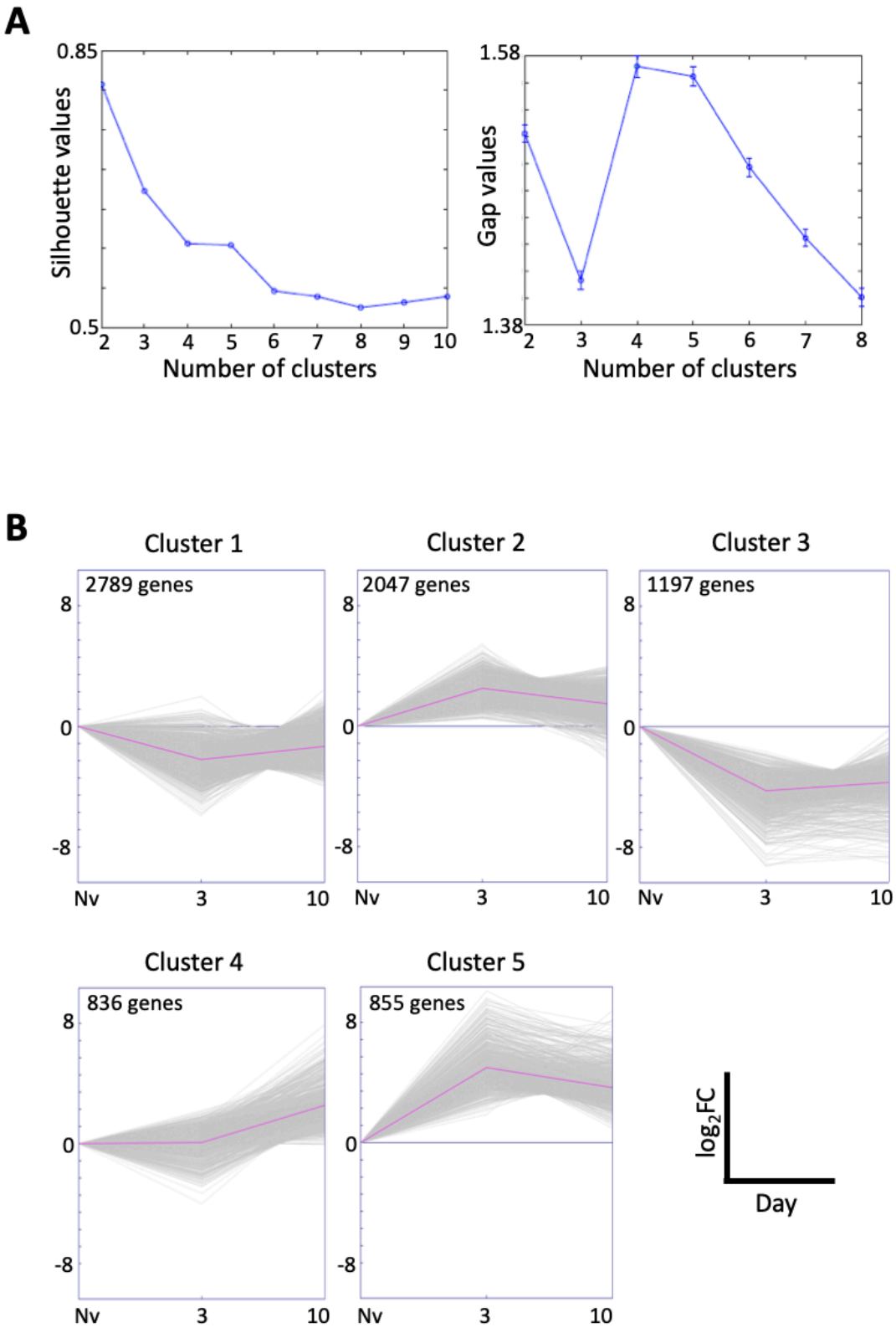

Figure 4.6 - K-means clustering of the synovial transcriptome during the time course of AIA. (A) Mathematical determination of the optimal number of clusters to use for K-means clustering using the silhouette and gap statistic methods. (B) K-means clustering of differentially expressed genes ($log_2FC > 1.5$, $p < 0.05$) in WT mice across the time course of AIA when compared to a healthy control joint. The number of genes in each cluster is identified in the top left corner.

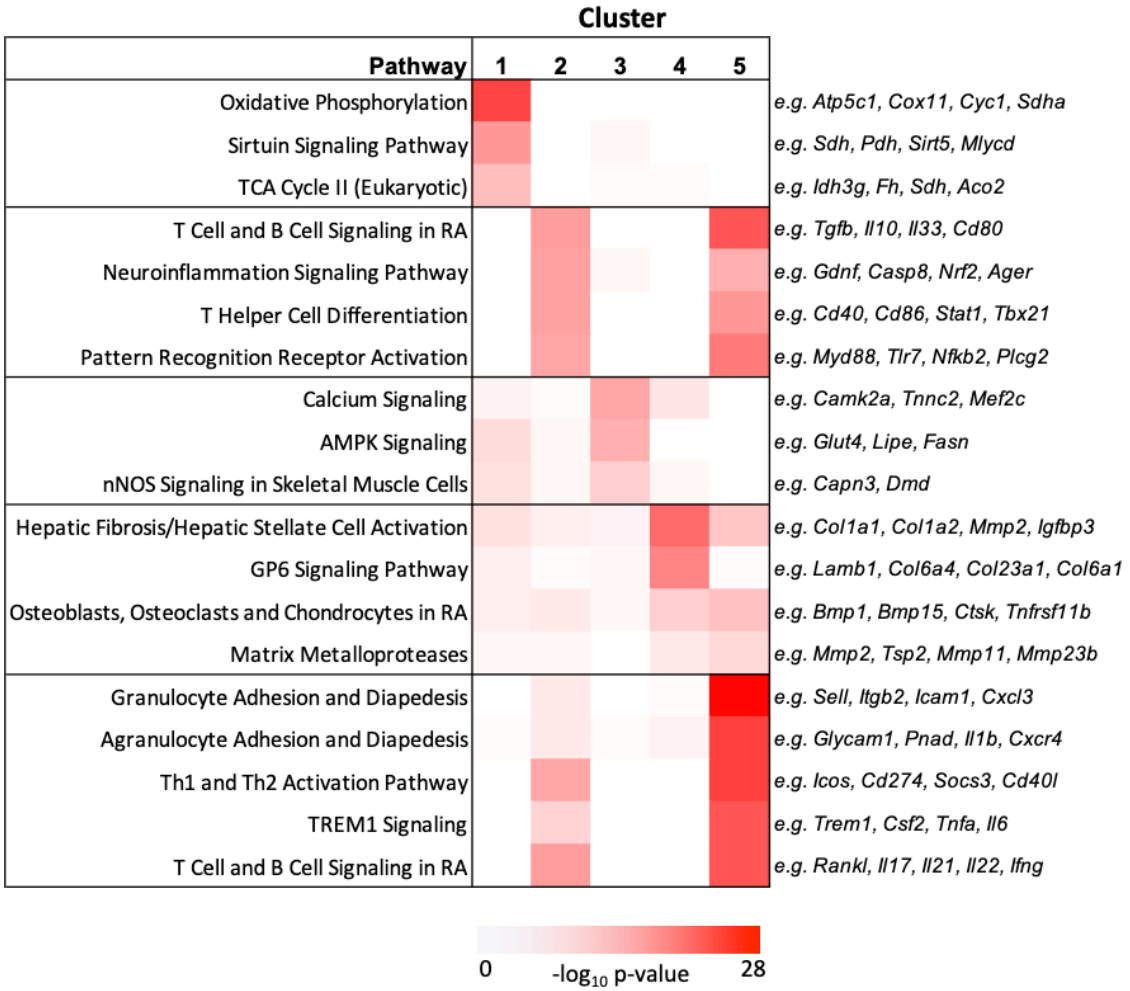

Figure 4.7 - Individual gene clusters in WT mice are linked with different canonical pathways. The top canonical pathways, as determined by IPA, associated with each cluster of differentially expressed genes ($\log_2$FC > 1.5, $p < 0.05$) in WT mice across the time course of AIA when compared to a healthy control joint. Examples of differentially regulated genes from each pathway are shown on the right.

4.3.4 ELS-rich synovitis is prominently associated with T cell pathways

Having identified patterns of gene behaviour in WT mice with AIA, we next wanted to uncover genes associated with the development of synovial ELS. For this, the number of DEGs in *Il27ra*$^{-/-}$ mice relative to WT control mice over the time course of AIA were identified for each cluster (*Figure 4.8A*). Cluster 2 and cluster 5, which were associated with inflammatory pathways and T cell signalling in WT mice (*see Figure 4.7*), had the largest number of DEGs, accounting for 63% of the total number (*Figure 4.8A*). DEGs from these clusters were mostly upregulated at day 10 when ELS-rich synovitis is established in *Il27ra*$^{-/-}$ mice (*Figure 4.8A*). Pathway analysis of cluster 2 and cluster 5 DEGs revealed an upregulation of T helper cell activation and cytokine signalling (*Figure 4.8B*). These genes included effector cytokines (e.g. *Il17a*, *Ifng*, *Il17f*), cell surface receptors (e.g. *Cd3e*, *Icos*, *Cd274*, *Il27ra*) and transcriptional regulators (e.g. *Stat1*, *Gata3*, *Tbx21*). Notably, cytokine signalling associated with IL-17 regulation was greatly enriched in DEGs from cluster 5 (*Figure 4.8B*). For other clusters, a smaller number of DEGs were observed. Therefore, pathway analysis with fewer genes may have contributed to the lower significance observed (*Figure 4.8B*). Hence, synovial ELS development is associated with local upregulation of T helper cell activation and cytokine signalling.

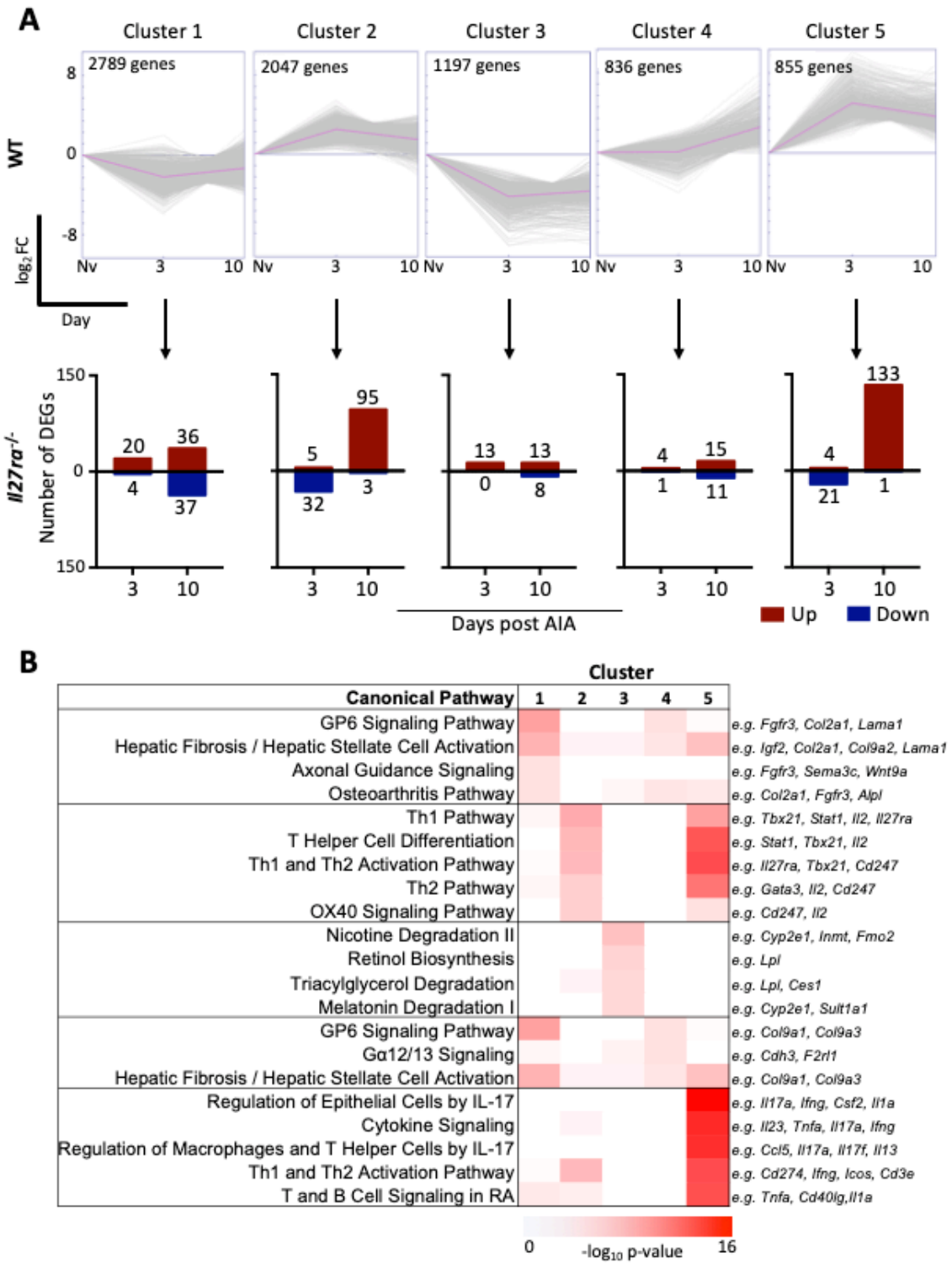

Figure 4.8 - Canonical pathways associated with differentially expressed genes in *Il27ra*$^{-/-}$ mice. (A) The number of differentially expressed genes ($\log_2$FC > 1, $p < 0.05$) for each cluster in *Il27ra*$^{-/-}$ mice compared to WT mice at the same time point of AIA. Upregulated genes are shown in red and downregulated genes in blue. The number of differentially regulated genes is indicated above each bar. (B) Canonical pathways associated with each cluster of differentially expressed genes in *Il27ra*$^{-/-}$ mice, as determined by IPA. Examples of differentially regulated genes from individual pathways are shown on the right.

4.3.5 Adhesion and matrix remodelling pathways are linked with synovial ELS

Whilst autoantibodies such as RF and ACPA correlate with disease severity they unreliably predict underlying joint pathology [193]. As such, biomarkers that can inform of underlying synovial pathology are lacking. Such biomarkers would have the potential to stratify patients according to synovial pathotype and inform of treatment decisions. Since genes in cluster 4 were uniquely upregulated in established disease, when ELS were present (*see Figure 4.6B*), we questioned whether DEGs in *Il27ra*$^{-/-}$ mice from this cluster may identify pathways and gene signatures characteristic of ELS. The highest number of DEGs were identified at day 10, with some genes being highly expressed compared to WT mice and others downregulated (*Figure 4.9A and B*). Prominently downregulated genes in *Il27ra*$^{-/-}$ mice included *Erdr1*, a negative regulator of cell migration and proliferation, whose overexpression in inflammatory arthritis has been shown to have a therapeutic effect [276, 277]. Interestingly another downregulated gene, *Cd5l*, has recently been implicated in regulating Th17 cell pathogenicity [278]. This may reflect the important role IL-27 plays in suppressing Th17-type responses. In contrast, genes that were upregulated were associated with cell adhesion (e.g. *Madcam1*, *Msln*, *Cdh3*) and matrix remodelling (e.g. *Col9a3*, *Ibsp*, *Matn3*). Hence these genes link canonical pathways with ELS-rich synovitis and may provide gene signatures with the potential to support the stratification of RA patients with this form of inflammatory arthritis.

4.3.6 T cell pathways are enriched in ELS-associated disease

T helper cell activation and cytokine signalling pathways were upregulated in DEGs from cluster 5 in *Il27ra*$^{-/-}$ mice (*see Figure 4.8B*). *Figure 4.10A* shows the genes within pathways and their expression compared to WT mice. Whilst genes show comparable expression between WT and *Il27ra*$^{-/-}$ mice at day 3, they are highly upregulated in *Il27ra*$^{-/-}$ mice at day 10. Given the opposing roles often played by IL-27 and IL-6 in the control of T cell responses, pathway analysis also included data from *Il6ra*$^{-/-}$ mice. As expected, the majority of these genes were downregulated in *Il6ra*$^{-/-}$ mice that develop a low inflammatory phenotype (*Figure 4.10A*). Of particular interest are the Th17-associated genes, *Il17a*, *Il17f*, *Il21* and *Il22* as well as the Th1 signature cytokine *Ifng* (*Figure 4.10B*) which are all highly expressed in *Il27ra*$^{-/-}$ mice at day 10. In contrast, in *Il6ra*$^{-/-}$ mice that fail to mount Th17 responses [63], expression of Th2-assocaited genes, such as *Il5* and *Il13*, were more prominent. Interestingly, genes encoding key mediators of lymphoid organogenesis (e.g., *Lta* and *Cxcl13*), were also increased in *Il27ra*$^{-/-}$ mice (*Figure 4.10A and B*).

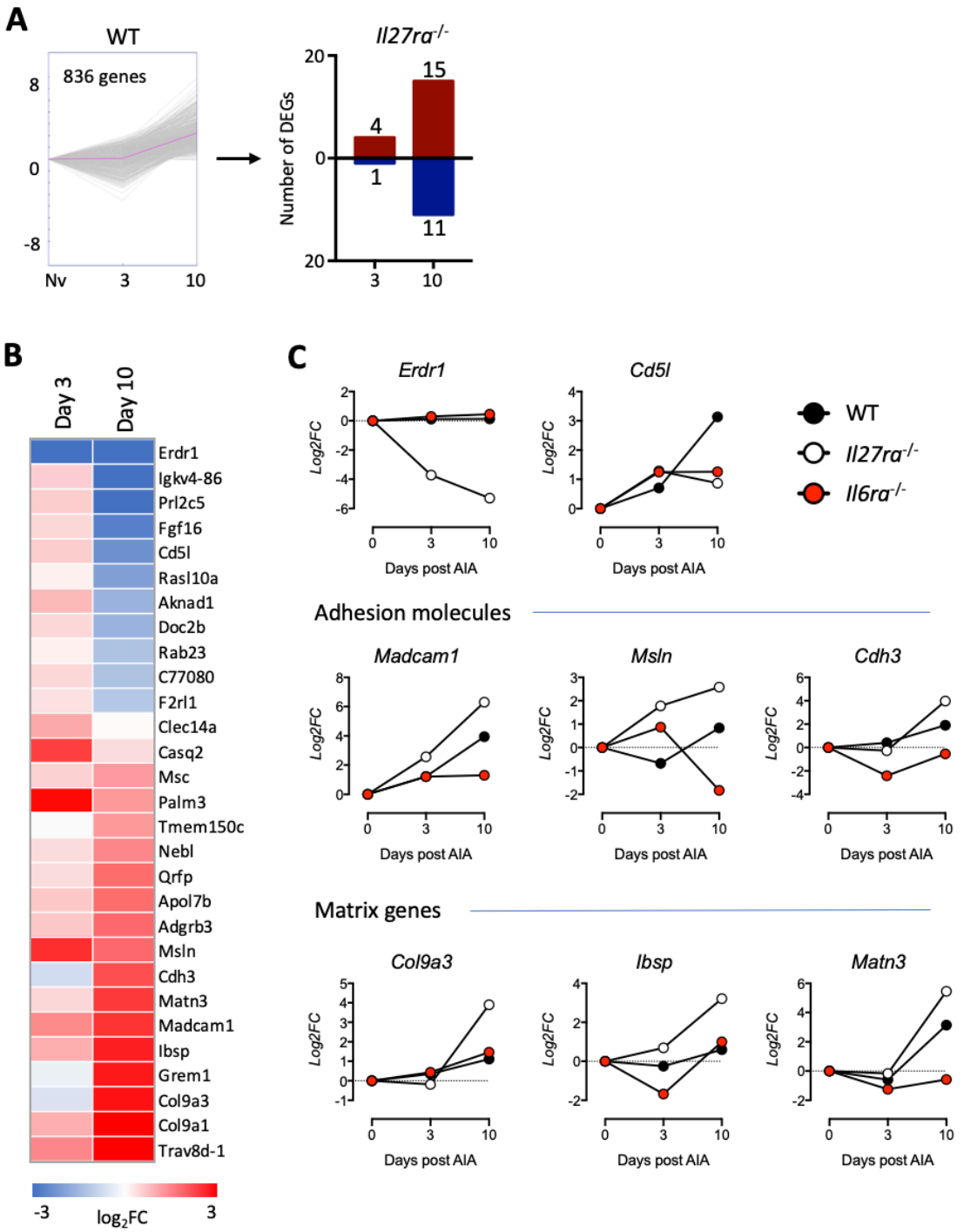

Figure 4.9 - Increased expression of adhesion molecules and matrix remodelling genes in *Il27ra*$^{-/-}$ mice. (A) The number of differentially expressed genes ($log_2FC > 1$, $p < 0.05$) for cluster 4 in *Il27ra*$^{-/-}$ mice compared to WT mice at the same time point of AIA. (B) Heatmap of differentially expressed genes in *Il27ra*$^{-/-}$ mice from cluster 4 compared to WT mice at the same time point. (C) Selected genes associated with adhesion molecules and matrix remodelling are plotted for WT, *Il27ra*$^{-/-}$ and *Il6ra*$^{-/-}$ mice when compared to a healthy WT control joint.

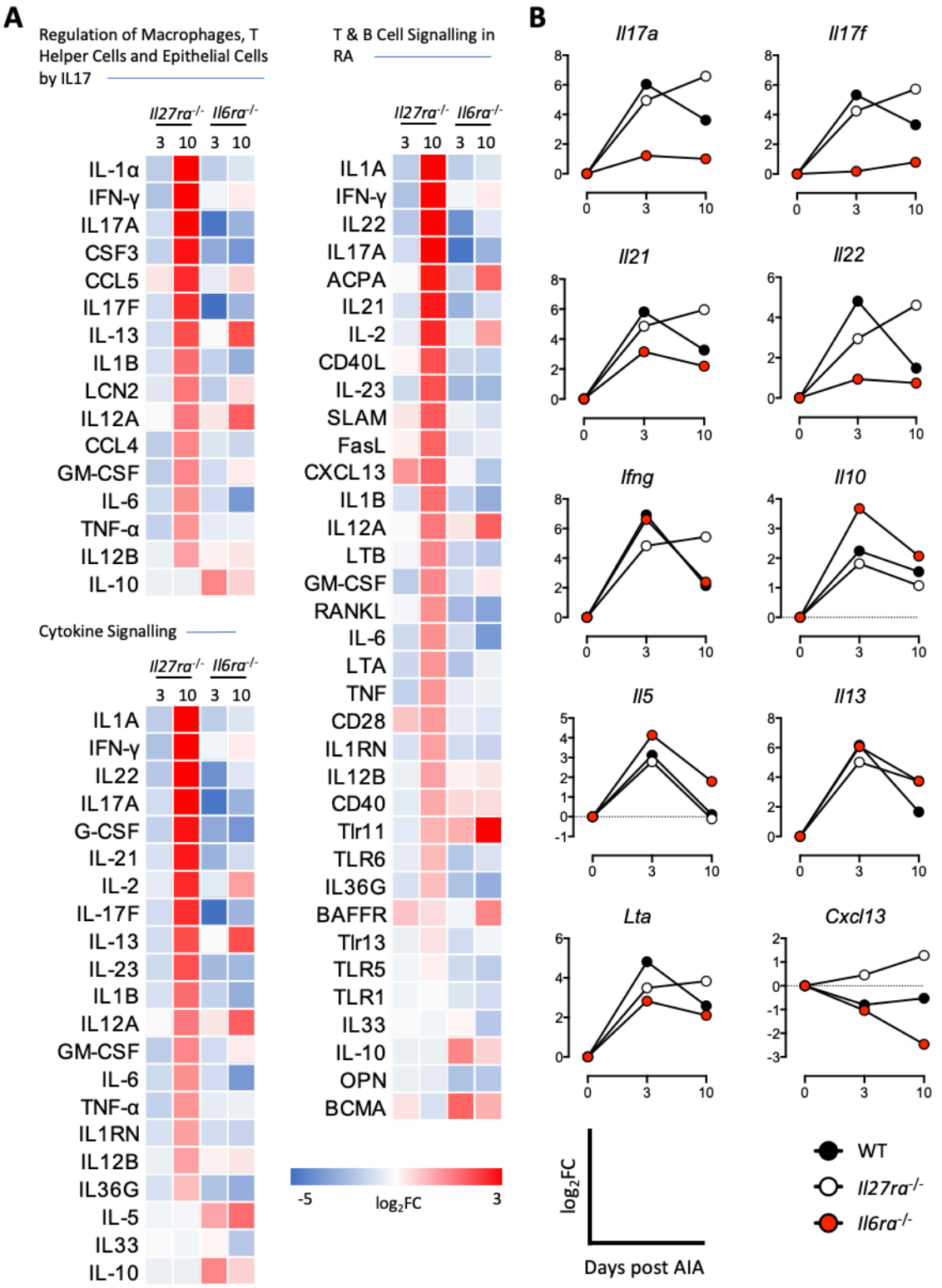

Figure 4.10 - T cell pathways are increased in ELS-associated synovitis. (A) Heatmap of genes that comprise differentially regulated canonical pathways from cluster 5, as determined by IPA. Gene expression is shown relative to a healthy WT control joint at the same time point. (B) Selected genes are plotted for WT, *Il27ra*$^{-/-}$ and *Il6ra*$^{-/-}$ mice when compared to a healthy control joint.

4.3.7 Synovial ELS development is associated with increased Th17 gene profiles

The anti-inflammatory effects of IL-27 in adaptive immunity include its ability to inhibit IL-2 production and certain T cell responses [47, 91], whilst supporting the development of CXCR3^{+} Treg populations [102]. For example, IL-27 has been shown to inhibit Th17 [279] and Th2 [98] responses and promote IL-10 secretion from T cells [103]. In inflammatory arthritis, DEGs from cluster 5 in *Il27ra*$^{-/-}$ mice were associated with the regulation of T helper cell cytokine expression, particularly IL-17 (*see Figure 4.8B and Figure 4.10*). Since IL-27 has complex roles in regulating CD4^{+} T cell responses, GSEA was used to determine enrichment for particular T helper cell subsets in these DEGs, using previously reported gene sets for Th1, Th17, Th2 and Treg cells (GSE45975) [273]. Here, DEGs were enriched for markers of Th17 cells when compared to Th2 and Treg cells (*Figure 4.11*). However, an equal proportion of genes were associated with a Th17 and a Th1 phenotype (*Figure 4.11*).

To further evaluate the role of T helper cells in ELS development, the total number of DEGs were mapped onto gene expression profiles of canonical T helper cell subsets from GSE45975 (*Figure 4.12A*) [273]. Genes were only included if differentially expressed in the dataset. Hence, in line with *figure 4.11*, Th1 and Th17 genes had a greater number of DEGs in inflammatory arthritis (*Figure 4.12A*). Expression of Th1 gene profiles were similar between WT and *Il27ra*$^{-/-}$ across AIA. (*Figure 4.12A*). These genes were mostly increased at day 3 and reduced to lower levels by day 10 (*Figure 4.12B*). However, expression of the Th1 signature cytokine, *Ifng*, was decreased in *Il27ra*$^{-/-}$ mice at day 3 compared to WT, consistent with the original observation that IL-27 promotes the production of IFNγ [94, 95, 97, 98, 280]. In contrast, *Ifng* expression was increased at day 10 in *Il27ra*$^{-/-}$ mice compared to WT (*Figure 4.12B and see Figure 4.4A*). Similarly, expression of *Tbx21* (T-bet), the master transcriptional regulator of Th1 cells, was also elevated at day 10. At day 3, Th17 profiles were increased in both WT and *Il27ra*$^{-/-}$ mice. Consistent with the role of IL-27 as an inhibitor of the Th17 programme, whilst Th17-associated genes returned to lower levels by day 10 in WT, their expression was maintained and increased in *Il27ra*$^{-/-}$ mice (*Figure 4.12A and B*). In contrast, Th2 signature cytokines, such as *Il4* and *Il5*, were increased in *Il6ra*$^{-/-}$ mice (*Figure 4.12B*), in line with previous findings (*see Figure 4.10*) [281]. Hence these data highlight an increased and maintained Th17-type gene signature is associated with ELS development in *Il27ra*$^{-/-}$ mice.

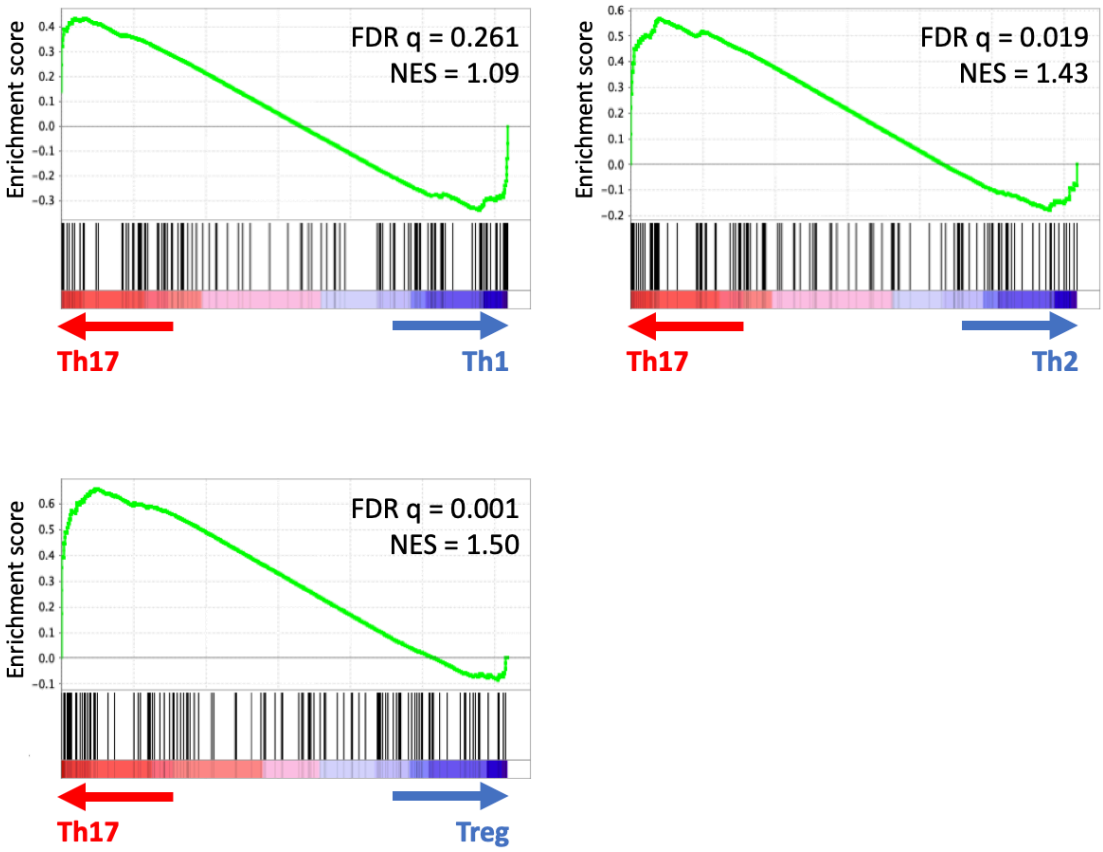

Figure 4.11 - Enrichment of Th17 and Th1 genes in ELS-associated synovitis. (A) Gene set enrichment of differentially expressed genes from cluster 5 in *Il27ra*$^{-/-}$ mice analysed against previously reported gene sets for Th17, Th1, Th2 and Treg cells (data from GEO, GSE45975). The area under the curve highlights how enriched the data set is for a particular phenotype. NES; Normalised Enrichment Score. FDR q; False Discovery Rate q-value.

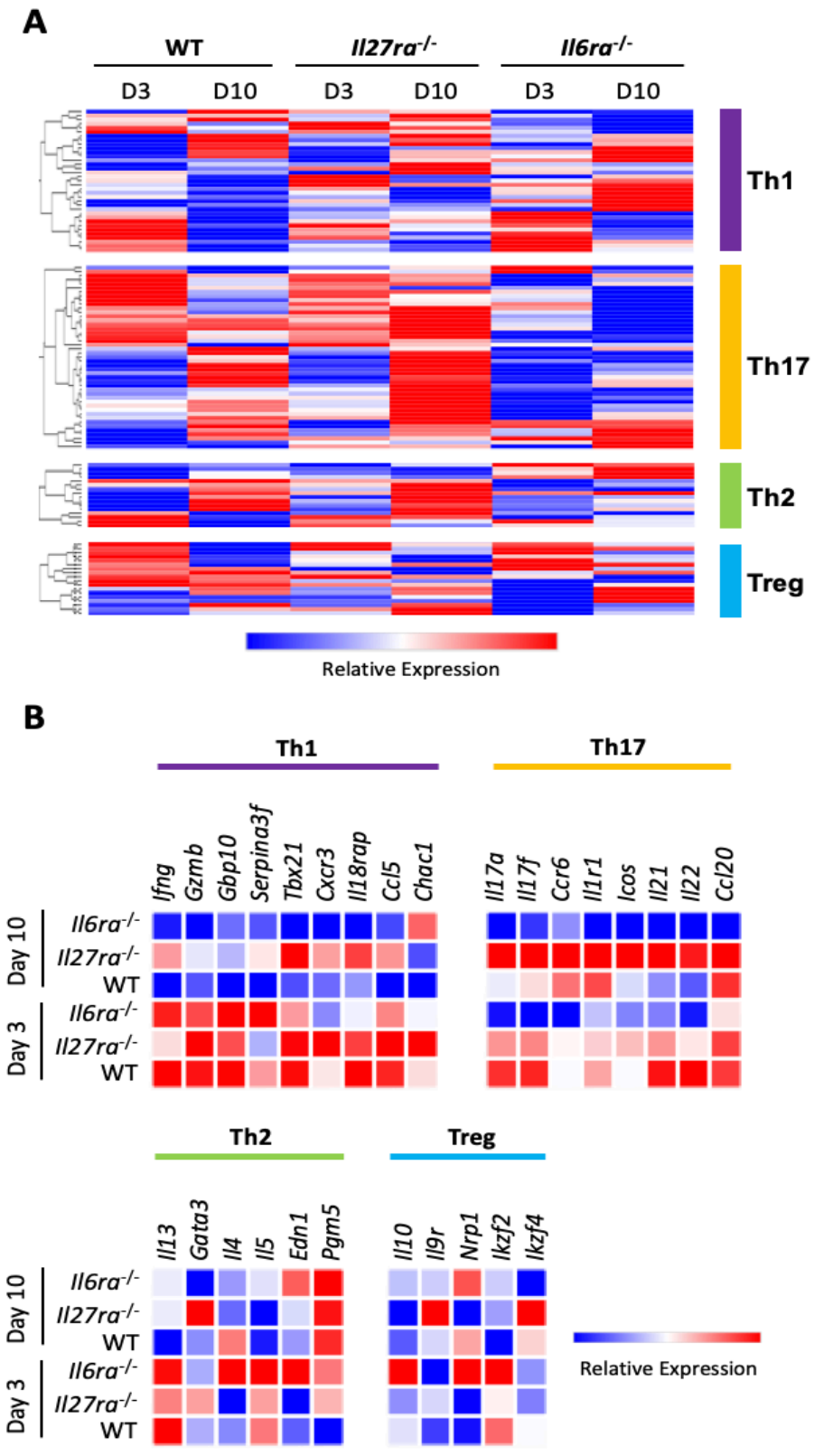

Figure 4.12 - Th17 cells are maintained in ELS-associated synovitis. (A) Heatmap of differentially expressed genes ($log_2FC > 1.5$, $p < 0.05$) when compared to a healthy control joint mapped to the top 200 genes of each T helper cell subset. Genes for T helper cell subsets are only included if they were also differentially regulated in AIA (data from GEO, GSE45975). (B) Expression across the time course of AIA in example genes from each T helper cell subset from panel A for WT, *Il27ra*$^{-/-}$ and *Il6ra*$^{-/-}$ mice.

4.3.8 STAT3 transcriptional regulation correlates with ELS development

STAT3 is a key transcriptional regulator of Th17 cell development [20]. Similarly, STAT3 control of leukocyte infiltration is key to determining disease severity in inflammatory arthritis [69]. Hence, the association of STAT3 in ELS development within the inflamed synovium was evaluated using GSEA and previously identified STAT3 regulated genes from GSE40918 [282]. In this context, if STAT3 promotes the development of ELS-rich synovitis it was predicted that STAT3-induced genes would be increased in *Il27ra*$^{-/-}$ mice while STAT3-repressed genes would be decreased. At day 3, prior to the development of synovial ELS, genes identified as being induced by STAT3 were expressed in both *Il27ra*$^{-/-}$ mice and WT mice. Notably, STAT3-repressed genes were significantly decreased in *Il27ra*$^{-/-}$ mice compared to WT mice (*Figure 4.13A*). In line with a role for IL-27 in inducing IFNγ expression [94, 95, 97, 98, 280], the repressed genes contained many IFNγ-inducible genes such as *Gbp4*, *Ccl4*, *Ccl3* and *Igtp* (*Figure 4.13B*). At day 10, once ELS were established, genes identified as being induced by STAT3 were highly enriched in *Il27ra*$^{-/-}$ mice. However, in contrast to day 3, genes identified as being repressed by STAT3 were also enriched in *Il27ra*$^{-/-}$ mice at day 10 (*Figure 4.13C*). Consequently, DEGs at day 10 did not appear to correlate with STAT3 activity. Importantly, induced genes comprised Th17 cytokines including, *Il22*, *Il17a*, *Il17f, Il23r* and *Rorc* (*Figure 4.13D*).

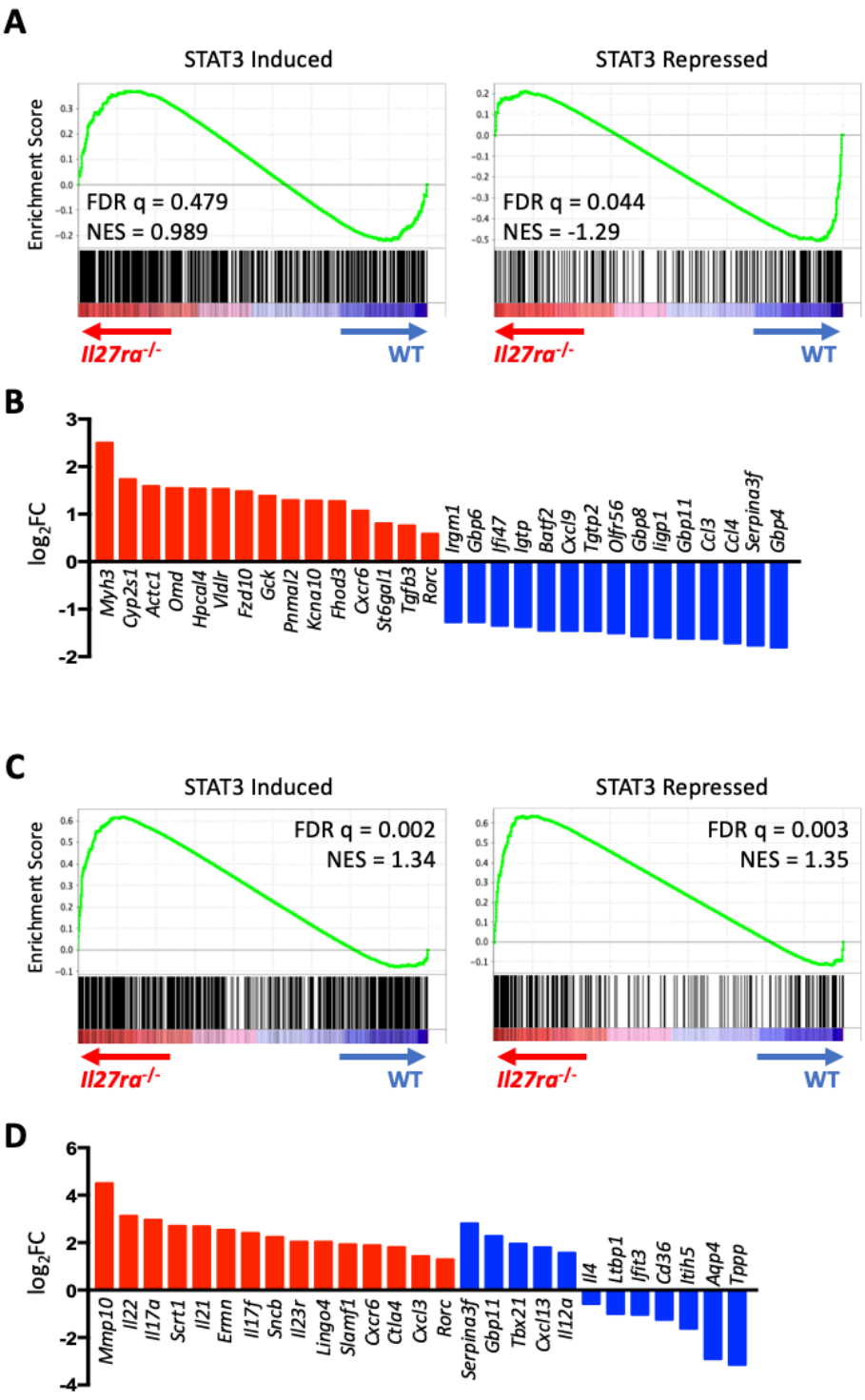

Figure 4.13 - A STAT3 signature precedes ELS development. (A-D) GSEA using a set of genes previously reported to be STAT3 regulated (either induced or repressed; data from GEO, GSE40918). (A) GSEA plots for STAT3 induced or repressed genes at day 3 of AIA. (B) The expression (log_2FC) of representative STAT3 regulated genes identified in panel A between *Il27ra*$^{-/-}$ and WT mice at day 3 of AIA. (C) GSEA plots for STAT3 induced or repressed genes at day 10 of AIA. (D) The expression (log_2FC) of representative STAT3 regulated genes identified in panel C between *Il27ra*$^{-/-}$ and WT mice at day 10 of AIA. The area under the curve highlights how enriched the data set is in a particular phenotype. NES; Normalised Enrichment Score. FDR q; False Discovery Rate q-value.

4.3.9 Joint-infiltrating CD3$^+$ CD4$^+$ Th17 cells are the main source of IL-17A

Since synovial ELS were associated with a maintained Th17-type response (*see Figure 4.11 and Figure 4.12*), I characterised the IL-17A secreting cells within the inflamed synovium of mice with AIA. For this, the isolation of joint infiltrating cells was optimised. Use of a collagenase digestion isolated a clear and viable CD3$^+$CD4$^+$ population that was lost when using mechanical disruption of the tissue (*Figure 4.14A*). Hence enzymatic digestion of synovial tissue was the preferred method for isolating joint-infiltrating cells.

Using the pan T cell marker, CD3, and a myeloid cell marker, CD11b, the majority of IL-17A producing cells were found to be CD3$^+$ (*Figure 4.14B*). To determine the CD3$^+$ population that was producing IL-17A within the joint, antibodies for CD4, NK1.1, CD8 and $\gamma\delta$TCR were used to discriminate T helper, natural killer, cytotoxic and $\gamma\delta$ T cells respectively. Whilst all CD3$^+$ populations produced varying levels of IL-17A, the largest population (approximately 90% of CD3$^+$ IL-17A-producing cells) were CD4$^+$ cells (*Figure 4.14C*). Interestingly, the proportion and cellular distribution of IL-17A producing cells were comparable for all populations between WT and *Il27ra*$^{-/-}$ mice (*Figure 4.14D and E*). However, *Il27ra*$^{-/-}$ mice develop increased synovitis and heightened synovial T cell infiltration [146]. Consequently, there was a significant increase observed in the number of CD3$^+$CD4$^+$ IL-17A-producing cells within the joint (*Figure 4.14F*). Although only accounting for approximately 5% of IL-17-producing cells within the joint, a comparable increase was also suggested for $\gamma\delta$ T cells, albeit not statistically significant at the group sizes investigated. This data highlights CD3$^+$CD4$^+$ T helper cells as the main source of IL-17A within the inflamed joint during AIA, the number of which are increased in the synovium of *Il27ra*$^{-/-}$ mice.

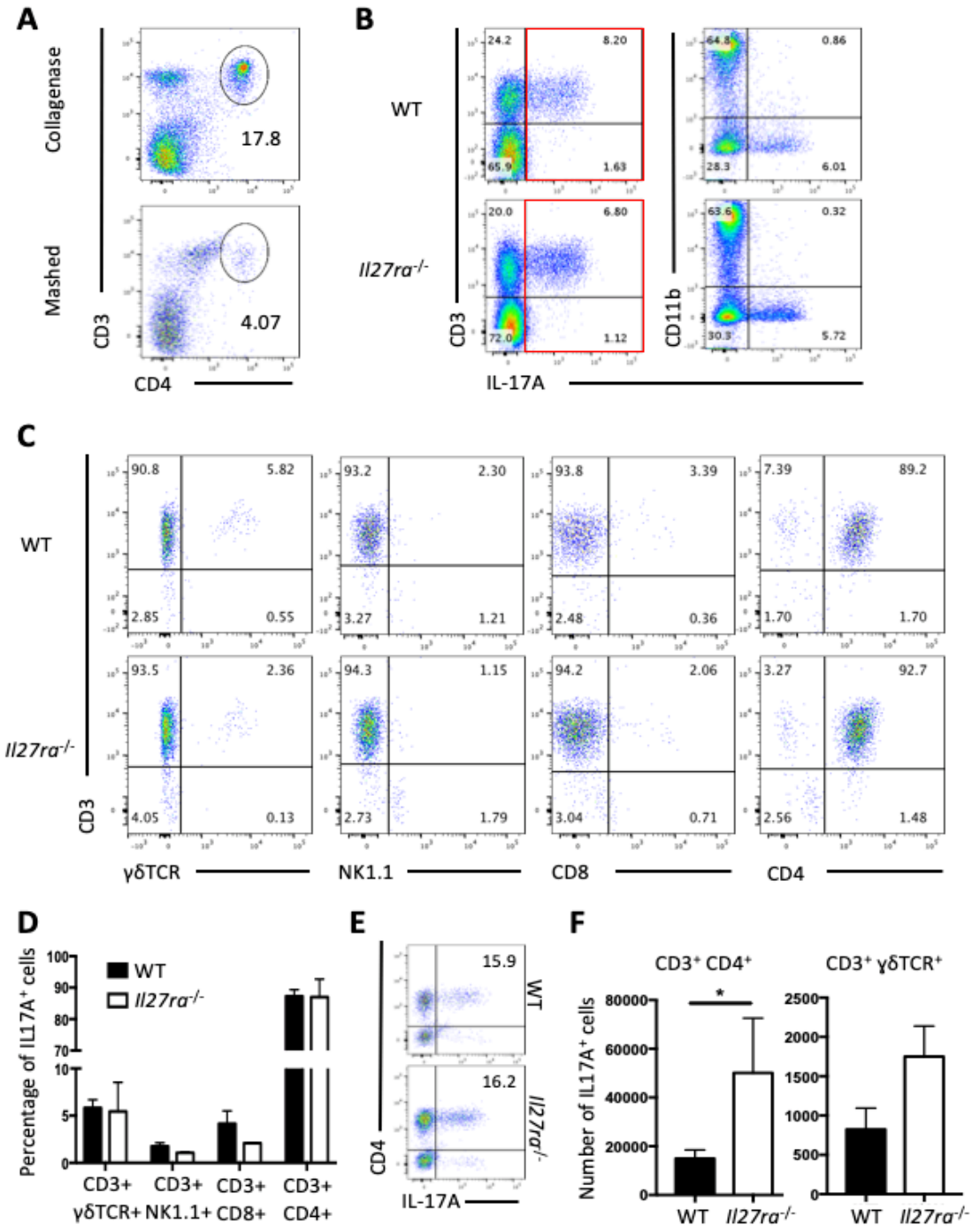

Figure 4.14 - Joint-infiltrating CD3⁺CD4⁺ cells are the main producers of synovial IL-17A. (A-E) Flow cytometry analysis of joint infiltrating cells at day 10 of AIA. (A) Inflamed synovium was either digested in 1 mg/mL collagenase IV or mechanically disrupted to isolate joint-infiltrating cells. Successful isolation was determined by flow cytometric analysis of CD3⁺CD4⁺ T cells. (B-C) Flow cytometric analysis of joint infiltrating cells at day 10 of AIA isolated by enzymatic digestion of the inflamed synovium in 1 mg/mL collagenase IV. (C) Representative flow cytometry plots gated on IL-17A⁺ cells shown in red box in panel B. (D) Cellular distribution of IL-17-producing cells within the inflamed joints of WT and *Il27ra*$^{-/-}$ mice shown as a percentage of total. (E) The percentage of IL-17A-producing T helper cells in WT and *Il27ra*$^{-/-}$ mice. (F) The total number of IL-17A-producing T helper cells and γδ T cells in WT and *Il27ra*$^{-/-}$ mice. (D-E) WT, $n = 4$; *Il27ra*$^{-/-}$, $n = 3$. * $p < 0.05$.

4.3.10 A pathogenic Th17 cell signature is linked with ELS development

Th17 cells display functional plasticity. For example, intestinal Th17 cells have a homeostatic role and adopt regulatory characteristics including the secretion of IL-10 [283]. Conversely, Th17 cells drive the pathogenesis of experimental autoimmune encephalomyelitis (EAE), a model of multiple sclerosis, through secretion of pro-inflammatory mediators [284]. This has led to the notion of pathogenic and non-pathogenic Th17 cells. To identify whether ELS-rich synovitis was enriched for pathogenic Th17 cells, which have been linked with the initiation of inflammatory diseases, GSEA was performed using gene sets for pathogenic and non-pathogenic Th17 cells [272]. In this context, Th17 cells, expanded *in vitro* in different conditions, were deemed pathogenic if they caused the onset of EAE when adoptively transferred into mice [272]. Genes upregulated in *Il27ra*$^{-/-}$ mice at day 10 were highly enriched in a pathogenic Th17 signature (*Figure 4.15A*). The pathogenic signature comprised genes such as *Cxcl3*, *Il22* and *Icos*, which were all upregulated in *Il27ra*$^{-/-}$ mice (*Figure 4.15B*). Similarly, T-bet (*Tbx21*), the master transcriptional regulator of Th1 cells, was associated with a pathogenic Th17 signature and was highly upregulated in *Il27ra*$^{-/-}$ mice (*Figure 4.15B*) potentially highlighting the plastic nature of Th17 cells through their ability to acquire Th1 effector characteristics. Hence, these data revealed a pathogenic Th17 phenotype that was associated with ELS-rich synovitis in IL-27R-deficiency.

4.3.11 Regulation of ELS-associated chemokine expression by Th17 cells

The homeostatic chemokine, CXCL13, is associated with ELS development in a number of inflammatory diseases [138]. Importantly, expression of *Cxcl13* was upregulated in *Il27ra*$^{-/-}$ mice that develop synovial ELS [146] (*see Figure 4.10B*). Interestingly, expression of the signature Th17 cytokines *Il17a*, *Il21* and *Il22* all positively correlated with the expression of *Cxcl13* in AIA (*Figure 4.16A*). Since the development of ELS was associated with an upregulation of IL-17-producing cells (*see Figure 4.12 and Figure 4.14*), we determined whether these cells directly produced CXCL13. Interestingly, naïve CD4^{+} T cells expanded *in vitro* under polarising conditions for Th1, Treg and Th17 cells revealed Th1 cells as the most prominent CXCL13-producing subset (*Figure 4.16B*). In contrast to *in vivo* correlations, cultures that produced high levels of *Il17a* had decreased expression of *Cxcl13* (*Figure 4.16A and B*). Thus, under these culture conditions, Th17 cells do not secrete the lymphoid chemokine CXCL13.

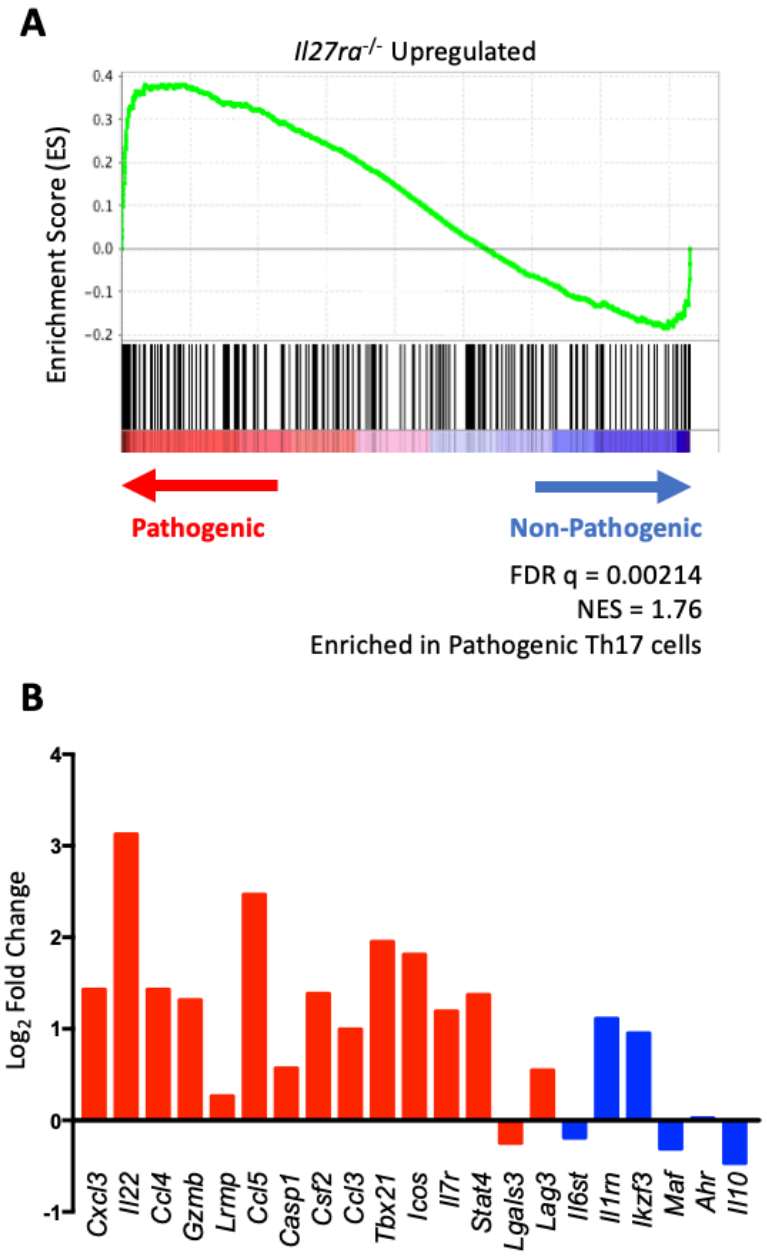

Figure 4.15 - A pathogenic Th17 signature is associated with ELS development. (A) GSEA plots using genes upregulated in *Il27ra*$^{-/-}$ mice at day 10 of AIA compared to WT ($log_2FC > 1$, $p < 0.05$). Upregulated genes were mapped to data sets previously reported to be differentially expressed between pathogenic and non-pathogenic Th17 cells (data from GEO, GSE39820). (B) The expression in *Il27ra*$^{-/-}$ mice of representative pathogenic (red) and non-pathogenic (blue) genes presented relative to WT at day 10 of AIA.

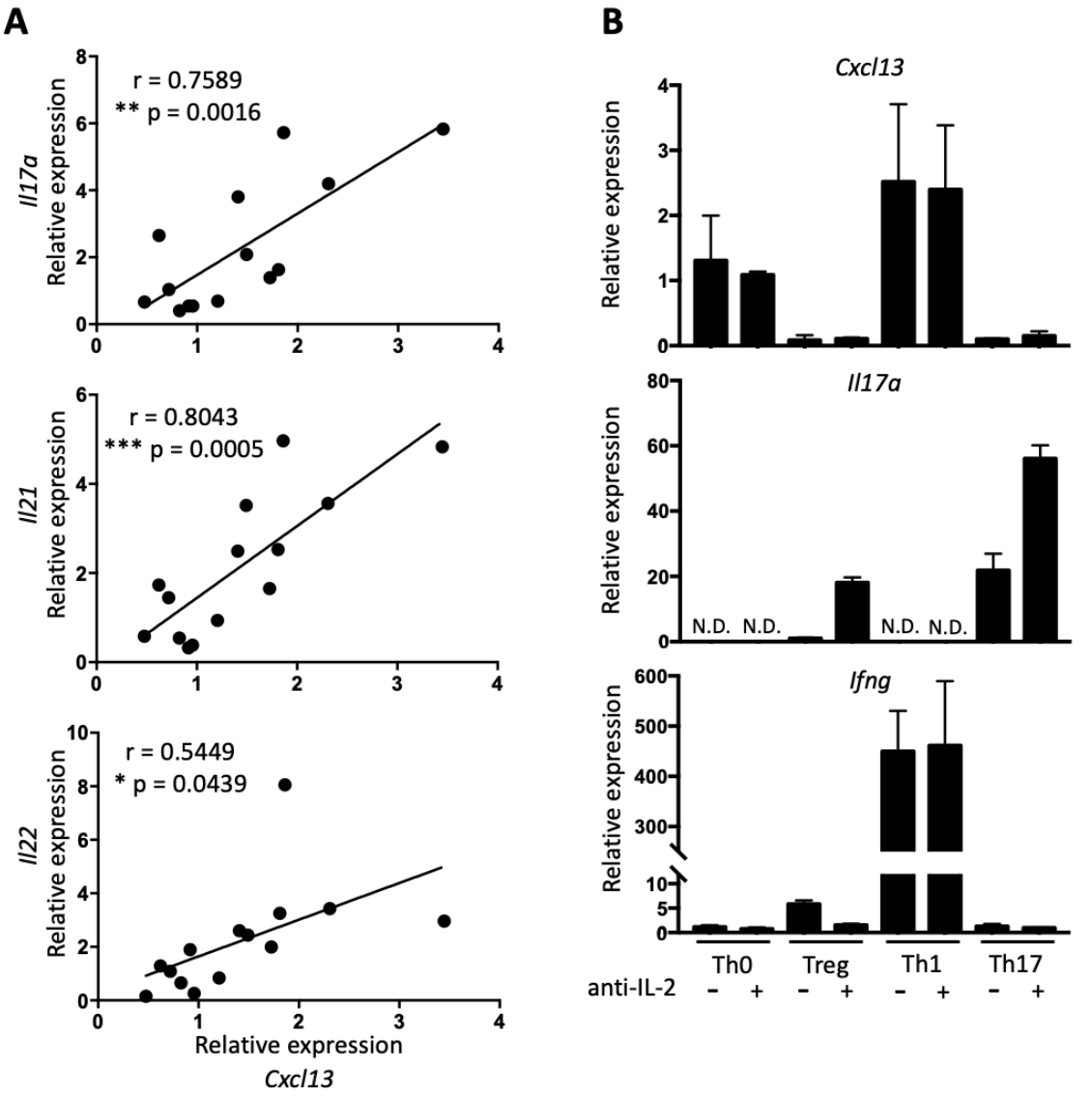

Figure 4.16 - In vitro generated Th17 cells do not secrete CXCL13. (A) Correlation analysis in WT and *Il27ra*$^{-/-}$ mice of the expression of Th17 signature cytokines (*Il17a*, *Il21* and *Il22*) and *Cxcl13* as determined by qPCR. (B) Relative expression of *Cxcl13*, *Il17a* and *Ifng*, determined by qPCR, following the activation of naïve T cells in the presence of the indicated T-cell polarising cytokines for 48 hours. Th1 (IL-12, 20 ng/ml), Treg (TGFβ, 2 ng/ml), Th17 (TGFβ, 1 ng/ml and IL-6, 20 ng/ml). Where indicated anti-IL-2 was added at 10 μg/ml to support a more robust differentiation of Th17 cells. The expression of all genes has been made relative to an internal housekeeping gene, *Actb*.

4.4 Discussion

The activities associated with ELS contribute to local T cell priming and antibody generation within inflamed tissues. The presence of synovial ELS in RA has therefore been linked with severe local and systemic inflammation, as well as inferior responses to frontline biological drug therapies such as anti-TNF inhibitors [195-197]. Hence, understanding the mechanisms underlying ELS development and maintenance within the inflamed synovium could aid in identifying improved therapeutic targets for the treatment of patients with ELS-rich synovitis. In this chapter, a transcriptomic approach was used to identify synovial gene expression changes in a novel model of inflammatory arthritis featuring synovial ELS. Here, ELS-rich synovitis was associated with a heightened T cell response within the inflamed joints of *Il27ra*$^{-/-}$ mice. Using GSEA and previously published gene signatures for defined T helper cell subsets, analysis identified a central involvement of pathogenic Th17 cell response in synovitis displaying ELS. Based on observations presented in *Chapter 3*, I also hypothesised that a transcriptomic evaluation of synovitis in *Il6ra*$^{-/-}$ mice would support my histopathological analysis that showed that these mice are protected from developing chronic joint inflammation during AIA.

The success of the IL-6 receptor targeted monoclonal antibody tocilizumab for the treatment of RA has highlighted the important role IL-6 plays in RA progression [36]. Although *Il6*$^{-/-}$ mice have been shown to be protected from developing inflammatory arthritis [69, 199, 256], the development of AIA in *Il6ra*$^{-/-}$ mice has not previously been investigated. Whilst histological analysis performed in *Chapter 3* revealed reduced disease severity and synovial T cell infiltration in *Il6ra*$^{-/-}$ mice, this chapter characterised gene expression changes associated with establishing AIA in these mice. Differences in the transcriptomic output between *Il6ra*$^{-/-}$ and WT mice were observed throughout the time course of AIA. However, hierarchical clustering revealed the most apparent changes to be observed at day 10. Here, *Il6ra*$^{-/-}$ mice showed a significant reduction in gene expression, reflecting the amelioration of chronic joint inflammation seen in these mice. Whilst I expected the *Il6ra*$^{-/-}$ mice to show a downregulation of genes compared to WT, to reflect the protected phenotype seen in these mice, there were also a lot of upregulated genes. This may suggest a different form of pathology in these mice, where hyperactivity of stromal and tissue-resident cells feature following the resolution of leukocyte infiltration. Interestingly, pathway analysis found that a cluster of genes highly expressed at day 10 in *Il6ra*$^{-/-}$ mice was primarily associated with innate signalling

pathways, consistent with the known role for IL-6 in promoting resolution of innate immune responses and the transition towards adaptive immunity [64]. Consistent with a role for IL-6 in promoting adaptive immune responses and the progression of arthritis, the expression of pro-inflammatory cytokines linked with effector T cell responses (e.g. *Il17a*, *Ifng*, *Il17f*, *Il21*) were also decreased in *Il6ra*$^{-/-}$ mice. However, the expression of the Th2 signature cytokines *Il4* and *Il5* were elevated in *Il6ra*$^{-/-}$ mice. While IL-6 has long been implicated in directing Th1 and Th2 responses [81], this observation supports previous data from our group that showed enhanced Th2 cell differentiation in *Il6ra*$^{-/-}$ T cells. Here, conditioned media recovered from peritoneal leukocytes stimulated with a cell-free bacterial supernatant supported Th2 cell differentiation in *Il6ra*$^{-/-}$ CD4^{+} T cells, while WT cells developed into Th1 effector cells [281]. Similarly, IL-6 derived from antigen presenting cells has been shown to inhibit Th2 differentiation. Here, CD4^{+} T cells co-cultured with IL-6-deficient bone marrow derived dendritic cells produced increased levels of IL-4 compared to cultures with WT bone marrow derived dendritic cells [285]. Together, this transcriptomic analysis of synovial pathology in *Il6ra*$^{-/-}$ mice supports an important role for IL-6 in promoting and maintaining adaptive immune responses and regulating the recruitment and effector characteristics of joint-infiltrating T helper cells.

Transcriptomic analysis of synovial inflammation has allowed the identification of pathways associated with the induction of AIA. While many of the highly upregulated pathways were associated with inflammatory pathways, such as adhesion and chemotaxis, innate signalling and activation, T and B cell signalling and differentiation (discussed below), other pathways such as bone remodelling and metabolism were also altered. Interestingly there is evidence for a role of metabolic dysfunction in RA. Glycolytic enzymes such as glucose-6-phosphate isomerase, enolase and aldolase have been identified as potential triggers for loss of self-tolerance. These factors induced pro-inflammatory cytokines and autoantibodies leading to the development of autoimmunity [286]. Additionally, analysis of serum samples from RA patients by mass spectrometry identified decreased levels of amino acids and glucose and increased levels of fatty acids and cholesterol [287]. Furthermore, lactate, produced by immune cells in high energy demands, has been shown to be increased in RA patients, increases IL-17 expression by CD4^{+} T cells and has been linked with the development of ELS [288]. Here, expression of *SLC5A12*, a co-transporter for lactate expressed on CD4^{+} T cells, correlated with synovial tissue T cell score and the presence of ELS [288]. However, metabolic pathways identified through IPA and associated with the induction of AIA in WT mice were not prominently changed in *Il27ra*$^{-/-}$ mice. However, expression of *Cd5l*, a

novel regulator of Th17 pathogenicity [278], was differentially regulated in *Il27ra*$^{-/-}$ mice. Loss of CD5L in pathogenic Th17 cells leads to alterations in fatty acid and cholesterol metabolism resulting in altered RORγt activity [278]. This is consistent with the recent identification of cholesterol metabolites (e.g., oxysterols) as putative ligands for RORγt [289, 290].

By using pathway analysis tools and mapping DEGs to markers of T helper cell subsets, this study identified an increased Th17 response during ELS-associated inflammatory arthritis in *Il27ra*$^{-/-}$ mice. Th17-associated genes upregulated during ELS-rich synovitis included *Il17a, Il17f, Il21* and *Il22*. Interestingly, Th17 cells have been linked to initiation of ELS development in other inflammatory diseases. For example, the development of ELS in the lungs (called inducible bronchus-associated lymphoid tissue; iBALT) was dependent on IL-17 production by CD4^{+} T cells in response to challenge with lipopolysaccharide (LPS) and *Pseudomonas aeruginosa* [142, 144]. However, ELS development can also be IL-17 independent. In this regard, following challenge with a replication deficient modified vaccinia virus Ankara, iBALT development was independent of IL-17A and IL-17F [144]. Whilst IL-17A is the signature cytokine for the Th17 cell subset, these cells also produce IL-21 and IL-22, which have been linked with ELS development in a model of salivary gland inflammation with Sjögren's syndrome-like characteristics [145, 147]. In this model, despite the production of IL-17A within inflamed salivary glands, IL-22 was the key determinant of ELS development within inflamed salivary glands. Here, IL-22 was produced locally in the salivary gland, firstly by γδ T cells and then later by T helper cells. In the absence of IL-22, lymphoid aggregates were significantly smaller and had decreased expression of the homeostatic chemokines CXCL13 and CXCL12 [145]. Thus, Th17 cells have been implicated as propagators of ELS development, and while IL-17A is the signature cytokine of these cells, other cytokines linked with the Th17 programme are also emerging as regulators of ELS.

STAT3 activation in inflammatory arthritis drives leukocyte infiltration and influences disease severity [69]. Using GSEA and publicly available datasets that define STAT3-reulgated genes, a robust STAT3 signature was associated with ELS-rich joint inflammation in *Il27ra*$^{-/-}$ mice. In this regard, *gp130*$^{Y757F:Y757F}$ mice, that display hyperactive STAT3 signalling, developed increased synovitis that was associated with an elevation in the number of IL-17A-secreting cells within the joint [69]. This is consistent with a previous study that links the presence of synovial ELS with enhanced STAT3

activity [291]. In previous studies from my laboratory, significant phosphorylated-STAT3 staining detected by immunohistochemistry was found within the joint, but not exclusively restricted to synovial ELS [146]. Thus, while STAT3 activity is strongly linked with joint inflammation during inflammatory arthritis, STAT3 remains a poor marker for ELS activity, likely due to its broad roles in orchestrating inflammation.

Although most predominantly described as anti-inflammatory, IL-27 was first identified as an inducer of an IFNγ secretion in T helper cells [94, 95, 97, 98, 280]. Transcriptomic analysis of joint inflammation in *Il27ra*$^{-/-}$ mice revealed decreased expression of *Ifng*, as well as IFNγ-regulated target genes at day 3 post arthritis induction. Thus, these data were in line with the original description of IL-27 as a Th1-supporting cytokine. However, interestingly, *Ifng* was increased in *Il27ra*$^{-/-}$ mice at day 10 post arthritis induction. This latter observation is more consistent with the more recent understanding of IL-27 as a potent suppressor of effector T cell responses, through its negative regulation of IL-2 signalling [100-105]. Therefore, this study suggests temporal differences in how IL-27 regulates Th1 responses. Therefore, IL-27 may support 'early' Th1 cell commitment, but then later act to inhibit effector Th1 responses and support resolution of inflammation.

Another factor contributing to the elevated expression of *Ifng* at day 10 of AIA may be the highly plastic nature of Th17 cells (*Figure 4.17*). Through GSEA we identified a robust pathogenic Th17 phenotype in *Il27ra*$^{-/-}$ mice, consistent with the known role of IL-27 as a potent inhibitor of Th17-type responses [105]. In addition, we identified differential expression of a novel regulator of Th17 cell pathogenicity, *Cd5l* [278]. Whilst pathogenic Th17 cells maintain characteristics of Th17 cells, such as *Il22* expression, they can also express *Tbx21* (T-bet), the master transcriptional regulator of Th1 cells [272]. In this regard, the acquisition of Th1 effector characteristics by Th17 cells can be required for pathogenicity. For example, adoptive transfer of pathogenic Th17 cells into mice during EAE causes high disease incidence and disease severity [272]. Using *Il17a* fate-reporter mice, plasticity of Th17 cells can be tracked. In a model of EAE, Th17 cells were found to gain expression of IFNγ that contributed to disease progression [292]. Here, the pro-inflammatory cytokines produced in the CNS were derived through plasticity of Th17 cells, with only a limited contribution from classic Th1 cells [292]. Similarly, IL-23 driven induction of IFNγ in Th1-like cells that were derived from Th17 precursors was required for the development of colitis [293]. In addition, Th17 cells can also acquire the effector characteristics of other T helper subsets. In lymphoid aggregates in the small intestines (called Peyer's patches) migrating Th17 cells adopt a Tfh-like phenotype by inducing

expression of Bcl-6, IL-21 and CXCR5 [294]. These plastic 'Tfh-like' ex-Th17 cells induced the expression of AID, required for class-switching and somatic hypermutation, and supported the development of IgA producing germinal centre B cells [294]. However, plasticity towards a Tfh-like phenotype was not observed in EAE, suggesting that the local environment is an important mediator of plasticity [294]. Importantly, ex-Th17 cells that a adopt a Th1-like phenotype have been isolated from joints of RA patients. Here, polyfunctional and pro-inflammatory ex-Th17 cells secreted increased levels of IFNγ, GM-CSF and TNF [295]. Taken together, this demonstrates that the plasticity of Th17 cells could contribute to the pro-inflammatory environment that supports ELS development and may account for the increase in *Ifng* expression observed during the later time point of AIA.

Homeostatic chemokines are required for SLO development and are also associated with ELS development in numerous diseases [138]. Given the prominent Th17 response within the joint, I hypothesised that these cells produce CXCL13. Whilst levels of *Cxcl13* correlated with the expression of Th17-associated cytokines within the inflamed joint, *in vitro* T cell cultures revealed that expression of *Il17a* in Th17-polarised cells was not linked with *Cxcl13* expression. Here, IFNγ-producing Th1 cells expressed the highest level of *Cxcl13*. This is in contrast to *in vitro* cultures with human $CD4^+$ T cells where TGFβ, a cytokine required for the differentiation of Th17 cells, was required for CXCL13 secretion [296, 297]. In these studies, T helper cells cultured in the presence of TGFβ and IL-6 produced high levels of CXCL13, whereas those differentiated in response to IL-12 saw minimal induction. Also, addition of anti-IL-2 increased expression of CXCL13 [297]. Thus, the studies using mouse T cell cultures herein are in contrast to previous experiments that suggest human IL-17-producing T helper cells directly produce CXCL13. However, Th17-associated cytokines may regulate the release of homeostatic chemokines from stromal cells. In mucosal tissues, IL-17 and IL-22 have been shown to induce homeostatic chemokines in stromal cells to support ELS development [144, 145]. Interestingly, transcriptomic analysis comparing synovium taken from naïve healthy mice revealed that expression of *Cxcl13* was increased in *Il27ra*$^{-/-}$ mice compared to WT mice. Notably, genes linked with inflammatory pathways were not a prominent feature at baseline. This suggests that IL-27 may inhibit CXCL13 production within the joint, potentially predisposing *Il27ra*$^{-/-}$ mice to developing synovial ELS once leukocyte infiltration is initiated. However, the molecular basis underlying the elevated expression of *Cxcl13* in *Il27ra*$^{-/-}$ synovium at baseline requires further investigation.

Through the use of transcriptomic approaches, the data presented in this chapter has identified canonical pathways and gene signatures linked with ELS-associated joint pathology in experimental inflammatory arthritis. Based on these transcriptomic studies and growing evidence of a role for T helper cells in promoting ELS development, analysis of joint-infiltrating leukocyte populations confirmed the presence of a prominent Th17 cell response in *Il27ra*$^{-/-}$ mice with ELS-rich synovitis. Thus, our cellular analysis of the biology associated with synovial ELS mirrors prominent inflammatory pathways identified through transcriptomic analysis of joint inflammation. Thus, immunomodulation of the Th17/IL-17 axis may provide a novel therapeutic opportunity for the treatment of diseases featuring ELS. In this context, the following two chapters will identify the significance of targeting the Th17/IL-17 axis on ELS development by (i) using genetic ablation of IL-17A in a novel model of ELS development in gastric cancer (*Chapter 5*) and (ii) drug targeting of the Th17 axis in a model of inflammatory arthritis featuring synovial ELS (*Chapter 6*).

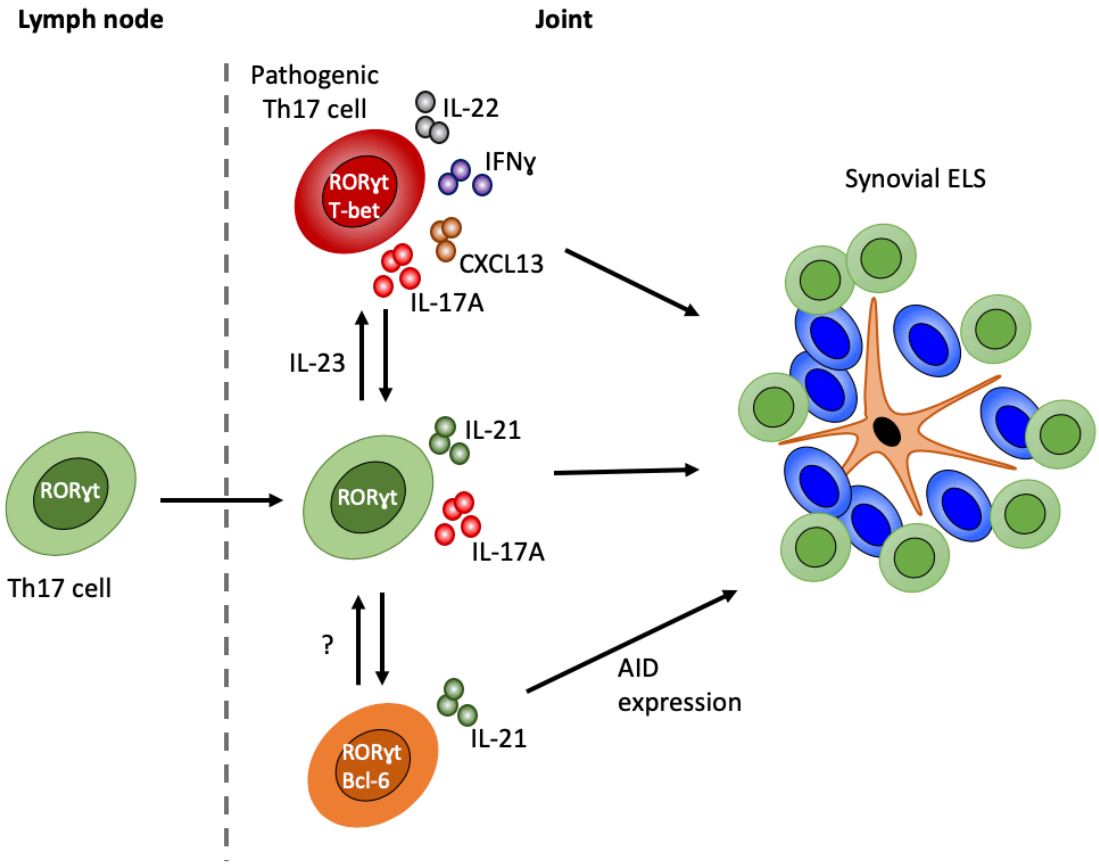

Figure 4.17 - Potential role for Th17 cells and T helper cell plasticity in supporting synovial ELS development. Upon induction of inflammatory arthritis Th17 cells are recruited from the lymph node and enter the joint. Upon inflammatory cues, such as exposure to IL-23, Th17 cells form 'pathogenic' Th17 cells that may contribute to joint pathology. Th17 cells can exhibit a high degree of plasticity and can take on effector characteristics typically associated with Th1 cells, leading to the secretion of a milieu of cytokines including IFNγ and the homeostatic chemokine CXCL13. Unknown inflammatory mediators may also direct the plasticity of Th17 cells to a Tfh-like phenotype that supports antibody responses. The secretion of IL-21 and induction of AID in B cells, required for class-switching and somatic hypermutation, may support the development, maintenance and activity of ELS. AID; activation induced cytidine deaminase.

Chapter 5. IL-17 control of tumour-associated ectopic lymphoid-like structures

5.1 Introduction

ELS can potentially develop in any tissue where persistent inflammation is present. Consequently, ELS have been observed in inflamed tissues affected by infection, autoimmunity, cancer and transplant rejection [118]. The diversity of tissues and clinical conditions where ELS have been described suggest that common, cross-disease mechanisms may be involved in regulating the development, maintenance and function of these inducible lymphoid organ-like compartments. The presence of tumour-associated ELS in certain cancers have been linked with improved patient survival and positive prognosis; possibly through the ability to promote local anti-tumour immune responses at ELS [137]. Hence, immunomodulation of ELS to support anti-tumour immunity may represent an attractive approach to cancer treatment [238, 298, 299].

In clinical gastric cancer, patients display heightened levels of the IL-6 family cytokine, IL-11, and increased STAT3 activation [217, 218]. Genetically modified *gp130*$^{F/F}$ mice have previously been generated as a clinically relevant model of gastric cancer [219-221]. Hyperactivation of STAT3 in response to IL-11 in these mice leads to the spontaneous development of gastric antrum adenomas. Previous studies in the *gp130*$^{F/F}$ mouse model of gastric cancer revealed accumulations of uncharacterised cellular aggregates within the gastric submucosa [219-221, 249]. Whilst the presence of tumour-associated ELS have been identified in numerous cancers, their role and development in gastric cancer is yet to be determined.

In this chapter, I discover that gastric tumourigenesis in *gp130*$^{F/F}$ mice is associated with the development of highly organised ELS. The transcriptomic approaches outlined in *Chapter 4* identified a pathogenic Th17 signature linked with synovial ELS in experimental inflammatory arthritis. This chapter aims to investigate whether a Th17-type response is similarly associated with the formation of tumour-associated ELS in *gp130*$^{F/F}$ mice. Through genetic ablation of the Th17 signature cytokine IL-17A, studies will investigate the importance of the Th17 axis in the development, maintenance and function of tumour-associated ELS.

5.2 Materials and Methods

5.2.1 Dual Immunohistochemistry

Two-step immunohistochemistry was used for the detection of segregated T and B cell zones at ELS within the same tissue section. Antigen retrieval, endogenous peroxidase blocking, and serum blocking was performed as described in *section 2.7*. The first antigen, CD3, was detected by incubating with the primary anti-CD3 antibody (Dako; see *Table 2.1*) overnight at 4°C. Antigen labelling was detected using a biotinylated secondary antibody (see *Table 2.1*), the Vectastain ABC kit and DAB chromagen as outlined in *section 2.7*. The tissue was then blocked with appropriate serum before detection of the second antigen, B220, by incubating with an anti-B220 antibody (BD Biosciences; see *Table 2.1*) for 2 hours at room temperature. Antigen labelling was detected as above except using VIP chromagen (Vector Laboratories) for visualisation. Slides were counterstained and mounted as detailed in *section 2.7*.

5.2.2 Peanut agglutinin staining of germinal centres

For detection of germinal centre reactions, sections were prepared as in *section 2.7*. Following incubation in CAS block, slides were treated with biotinylated peanut agglutinin (Vector Laboratories) for 1 hour at room temperature. Peanut agglutinin is a plant lectin that recognises a galactosyl (β-1,3) *N*-acetylgalactosamine structure present on the surface of germinal centre B cells. Staining was visualised using the Vectastain ABC kit and DAB chromagen (both from Vector Laboratories) as detailed in *section 2.7*.

5.2.3 The Cancer Genome Atlas

Clinical information and sequencing data for patients with stomach adenocarcinomas were downloaded from The Cancer Genome Atlas (TCGA) data portal (TCGA-STAD) using the data transfer tool. This cohort comprised of 398 patient tumour cases, of which 173 were histologically classified as having intestinal-type gastric cancer. Sequencing data from matched tumour and non-tumour tissue was available for 33 gastric cancer patients. Expression levels are represented by fragments per kilobase of exon per million mapped reads (FPKM).

5.3 Results

5.3.1 Submucosal cellular aggregates are ectopic lymphoid-like structures

Hyperactive STAT3 signalling in *gp130*$^{F/F}$ mice leads to the spontaneous development of gastric antrum adenomas characterised by elongated pits and enlarged glandular structures that are absent in WT mice (*Figure 5.1A and B*) [219-221, 249, 300]. These previous studies also identified the presence of cellular aggregates within the inflamed gastric submucosa. Consistent with these observations, our histological evaluation of stomach sections revealed the presence of cellular aggregates in the gastric submucosa of *gp130*$^{F/F}$ mice, which were absent in age-matched WT mice (*Figure 5.1C and D*). Immunohistochemistry was employed to determine whether these cellular aggregates display characteristics consistent with the appearance of ELS. Indeed, the cellular aggregates comprised a rich co-localisation of CD3^{+} T cells and B220^{+} B cells, a pattern typical of lymphoid organisation (*Figure 5.2A*). Whilst B cells were largely restricted to ELS, T cells were also found as diffuse infiltrates throughout the gastric submucosa (*Figure 5.2A*). Further immunohistochemistry revealed that the lymphocytic aggregates also contained CD21^{+} follicular dendritic cell networks and podoplanin (pdpn)-expressing cells, suggesting the presence of stromal cells required for lymphoid organ development, structural organisation and antigen presentation (*Figure 5.2B*) [143, 301]. Also present were CXCL13-expressing cells, marking the presence of a homeostatic chemokine required for spatial cellular organisation within lymphoid organs. Further to this, peripheral node addressin (PNAd)-positive cells were present (*Figure 5.2B*). PNAd is a sulphated and fucosylated glycoprotein found on high endothelial venules (HEVs) and acts as the receptor for CD62L (L-selectin) to allow the tethering and rolling of naïve and central memory T cells into lymphoid tissues. Thus, tumour-associated cellular aggregates that develop in *gp130*$^{F/F}$ mice are lymphoid-rich and display a composition consistent with ELS.

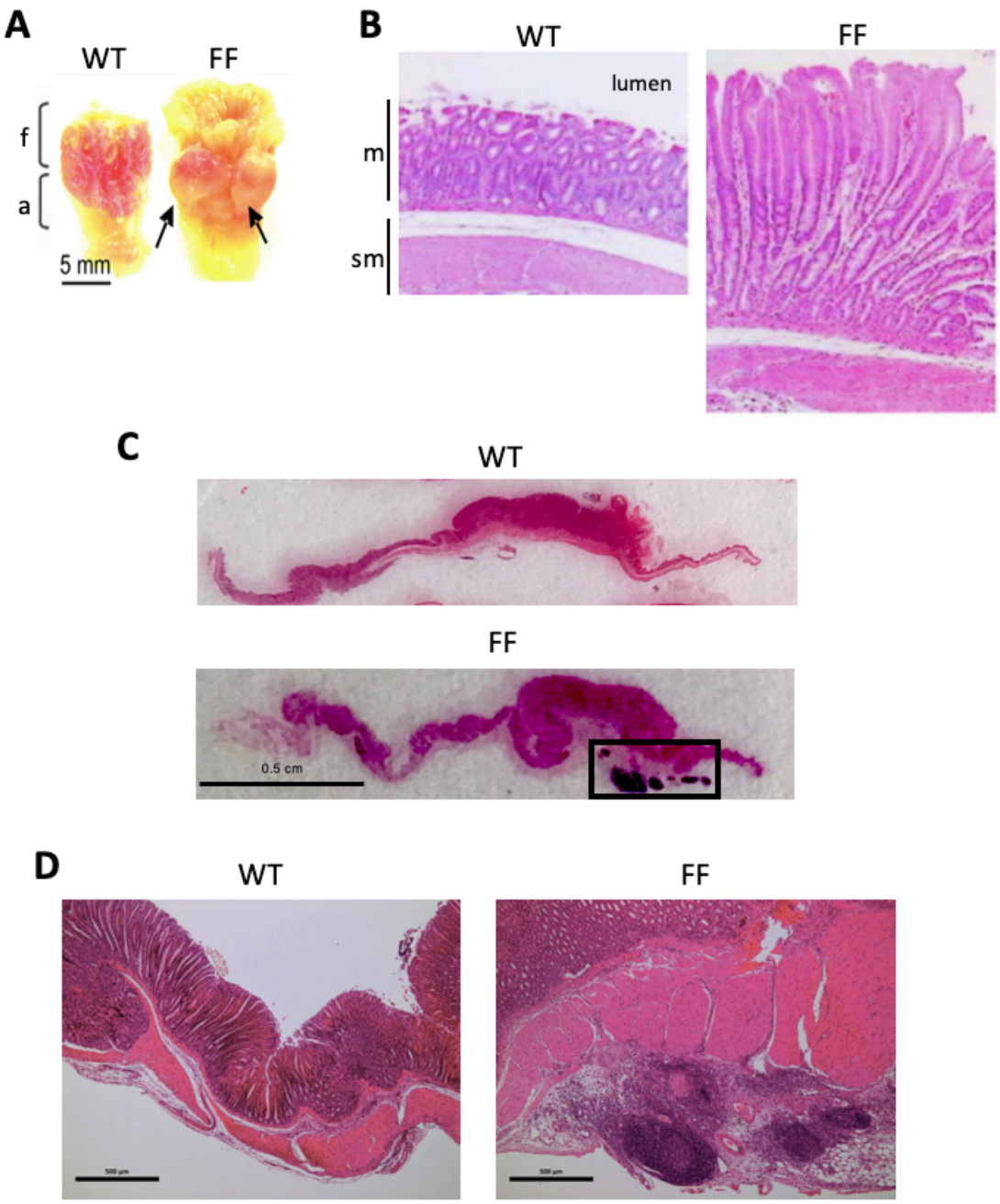

Figure 5.1 – *gp130*$^{F/F}$ mice develop submucosal cellular aggregates. (A) Representative appearance of stomachs from 3 month old mice. Stomachs were opened and pinned with the lumen facing the viewer. Arrows indicate tumours. Fundic (f) and antral (a) regions are labelled. (B) Representative haematoxylin and eosin (H&E) staining of stomach sections from 6 week old mice showing elongated pits and enlarged glandular structures. The mucosa (m) and submucosa (sm) are labelled. (C-D) Representative H&E staining of cross sections through the gastric antral tissue of wild-type (WT; *gp130*$^{+/+}$) and *gp130*$^{F/F}$ (FF) mice at 6 months of age (n = 4 / group). Boxed area in (A) shows submucosal cellular aggregates in *gp130*$^{F/F}$ mice. Scale bars: (A) 0.5 cm, (B) 500 μm.

Panels A and B adapted from previously published work (Judd et al. 2004 and Ernst et al. 2008).

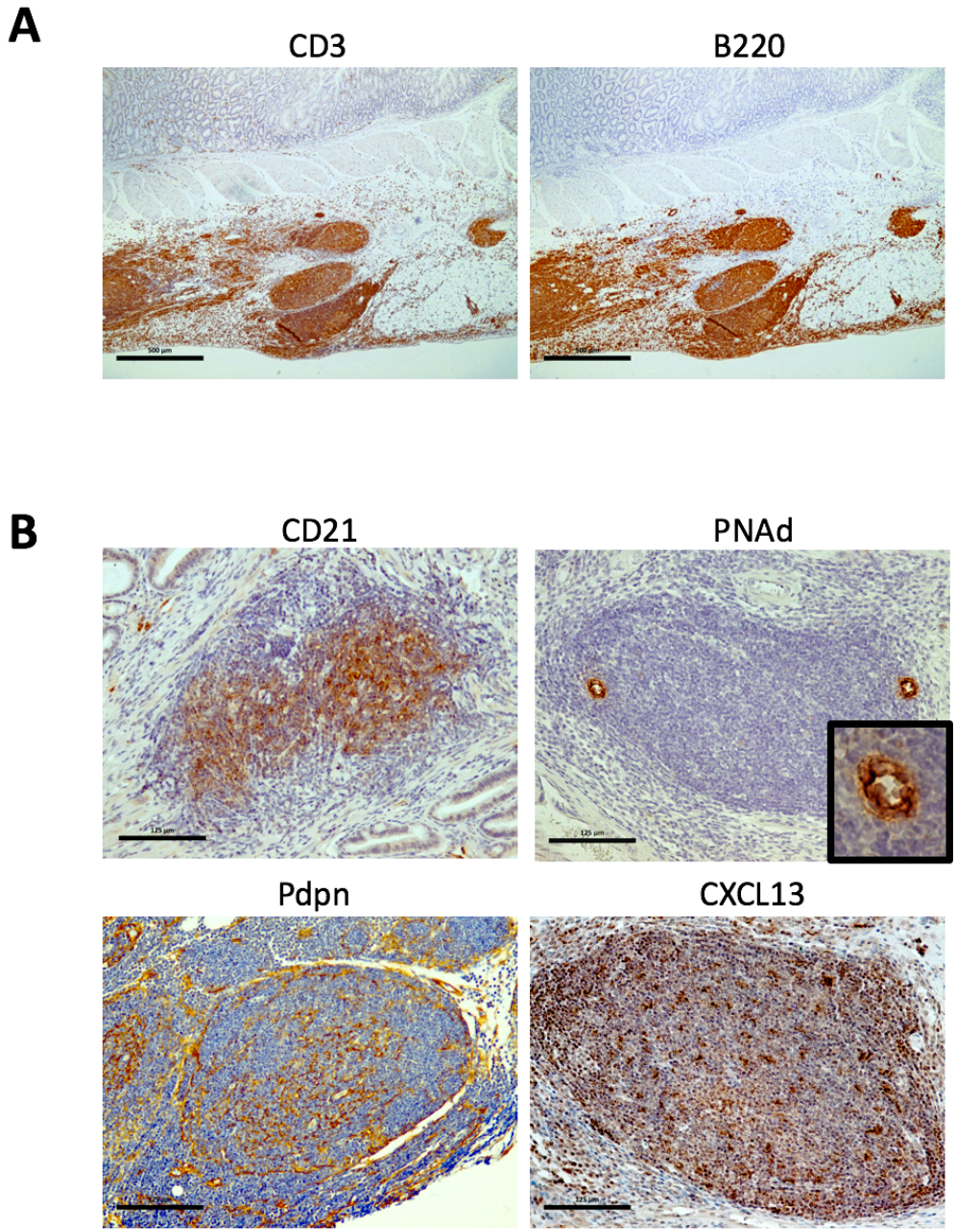

Figure 5.2 – Submucosal cellular aggregates in *gp130*$^{F/F}$ mice are ELS. (A) Representative immunohistochemistry of CD3 and B220 in sequential sections showing co-localisation in *gp130*$^{F/F}$ mice at 6 months of age (n = 4). (B) Representative immunohistochemistry of CD21, podoplanin (Pdpn), PNAd^{+} HEVs (boxed area shows high power image) and CXCL13 in 6-month-old *gp130*$^{F/F}$ mice (n = 3). Scale bars: (A) 500 μm; (B) 125 μm.

5.3.2 Tumour-associated ELS display functional germinal centres

Next, studies were performed to identify whether the submucosal ELS observed in *gp130*$^{F/F}$ mice displayed markers of functional germinal centres. Consistent with the presence of CD21^{+} follicular dendritic cell networks (see *Figure 5.2B*), ELS displayed reactive germinal centres as determined by the co-localisation of peanut agglutinin staining with Bcl-6-positive cells (*Figure 5.3A*). Peanut agglutinin binds to glycosylated proteins found on germinal centre B cells, and Bcl-6 is the master transcriptional regulator of Tfh cells and germinal centre B cells. Consistent with the appearance of functional germinal centres, staining for the cell cycle antigen Ki-67 also suggested the presence of proliferating germinal centre B cells (*Figure 5.3B*). As shown in *figure 5.2A*, ELS were comprised of dense accumulations of T and B cells. Interestingly, dual immunohistochemistry for CD3 and B220 revealed the presence of compartmentalised ELS featuring T and B cell segregation (*Figure 5.3C*). Here, the B cell zone co-localised with peanut agglutinin staining at germinal centres (*Figure 5.3C*). However, ELS lacking compartmentalised T and B cell zones also showed reactive germinal centres, suggesting that ELS displaying less cellular organisation were also functional.

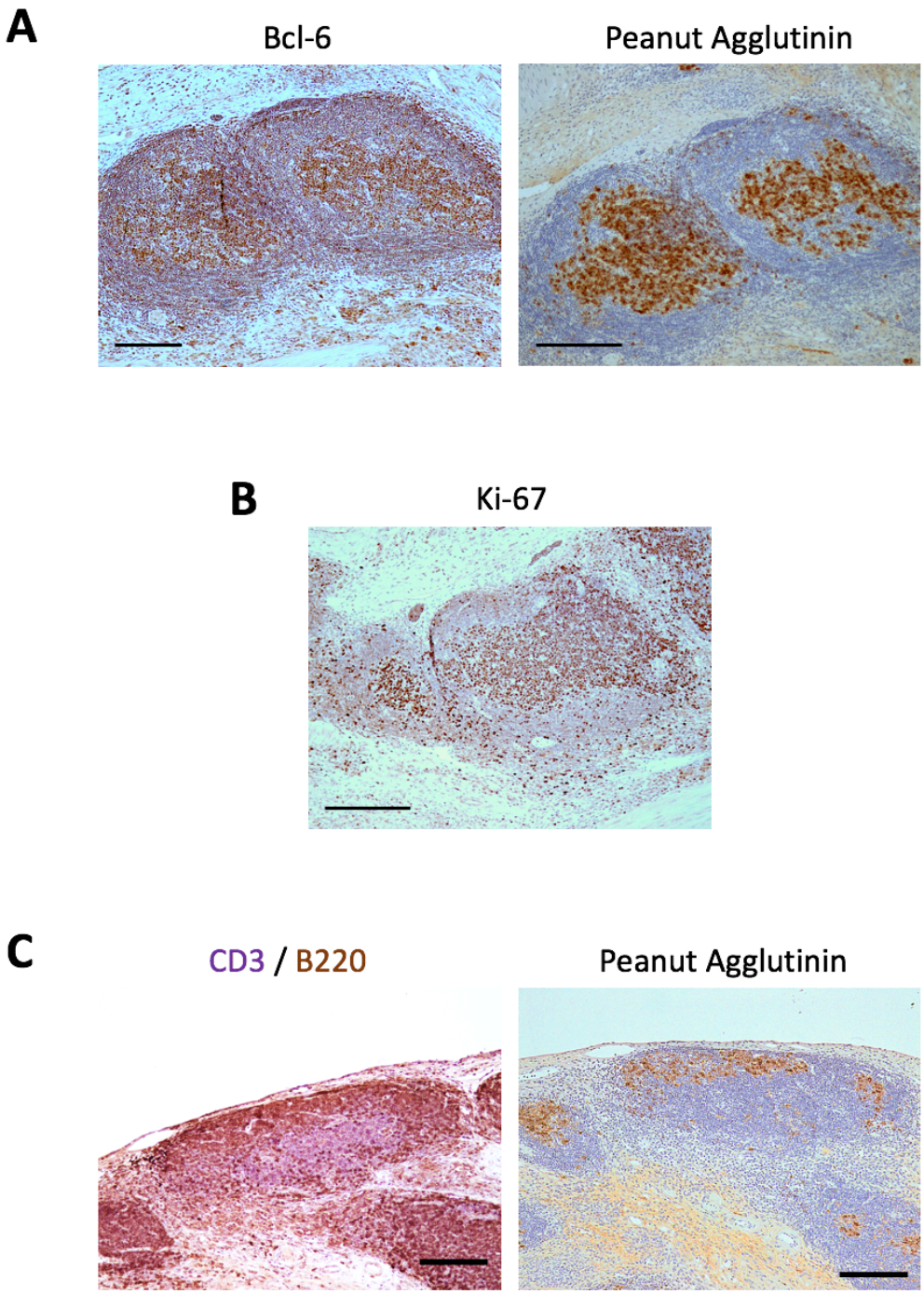

Figure 5.3 – Submucosal tumour-associated ELS in *gp130*$^{F/F}$ mice have functional germinal centres and display cellular segregation. (A) Representative immunohistochemistry of Bcl-6 and peanut agglutinin in serial sections. (B) Representative immunohistochemistry of Ki-67^{+} cells. (C) Representative dual immunohistochemistry for CD3 (purple) and B220 (brown) showing segregation into distinct compartments and co-localisation of B cell zones with peanut agglutinin staining. (n = 3 A-B, n = 2 C). Scale bars: (A) 500 μm; (B) 125 μm; (C-D) 250 μm.

5.3.3 Gastric tumourigenesis and ELS development are tightly coupled

Since hyperactive STAT3 signalling in *gp130*$^{F/F}$ mice leads to the spontaneous development of gastric adenomas and submucosal ELS, experiments aimed to identify whether ELS developed prior to, or as a result of gastric tumourigenesis. Gastric adenomas spontaneously develop in *gp130*$^{F/F}$ mice by 6 weeks of age and develop into advanced tumours by 6 months of age [219, 249]. Therefore, we monitored the development of ELS by immunohistochemistry in 4-week, 3-month and 6-month-old mice. Indeed, immunohistochemistry for CD3 and B220 in 4-week-old mice revealed that ELS were absent. In 3-month and 6-month-old mice, ELS were identified as dense accumulations of T cells and B cells (*Figure 5.4A*). Lymphoid aggregates were quantified based on B220 staining, since B cells were mostly restricted to ELS (*see Figure 5.2A*). The number, total area and average area of aggregates were all increased in 3-month and 6-month-old *gp130*$^{F/F}$ mice compared to WT control mice (*Figure 5.4B-D*).

Homeostatic chemokines play a key role in the development of secondary lymphoid organs and ELS [138]. To determine whether the temporal development of ELS was also reflected in the pattern of homeostatic chemokine expression, qPCR was performed on gastric antrum tissue from WT and *gp130*$^{F/F}$ mice (FF^{A}). At the later time points of 3 and 6 months, tumours from *gp130*$^{F/F}$ mice (FF^{T}) were also examined. At 4 weeks of age, which precedes the development of gastric adenomas and ELS in *gp130*$^{F/F}$ mice, the expression of *Cxcl13*, *Ccl21* and *Cxcl12* in the gastric antrum was comparable to control WT mice, while *Ccl19* was not detected (*Figure 5.5A*). Similarly, no difference was observed in the expression of *Bcl6*, the master transcriptional regulator of T follicular helper cells and germinal centre B cells. In 3-month and 6-month-old *gp130*$^{F/F}$ mice, the development of ELS was associated with heightened expression of *Cxcl13*, *Ccl19* and *Ccl21* in gastric antrum tissue (FF^{A}) when compared to WT mice or tumours from *gp130*$^{F/F}$ mice (*Figure 5.5B and C*). Consistent with the detection of Bcl-6 at tumour-associated ELS (*see Figure 5.3A*), *Bcl6* transcripts were also increased in gastric antrum and tumour tissue from *gp130*$^{F/F}$ mice (*Figure 5.5B and C*).

In inflammatory arthritis, IL-27 has an inhibitory effect on the development of synovial ELS [146]. To determine whether IL-27 may similarly control the development of tumour-associated ELS, *Il27* expression (which encodes for the IL-27p28 subunit) was examined in 6-month-old WT and *gp130*$^{F/F}$ mice. Levels of the *Il27* transcript were comparable between WT and *gp130*$^{F/F}$ gastric antrum as well as in tumour tissue, suggesting that

ELS development in the gastric submucosa of *gp130*$^{F/F}$ mice was not due to a loss of an inhibitory IL-27 signal (*Figure 5.5D*).

Together, these data suggest that temporal induction of homeostatic chemokines, required for the recruitment of hematopoietic cells and the spatial organisation of lymphoid organs and ELS, coincides with the development of gastric adenomas.

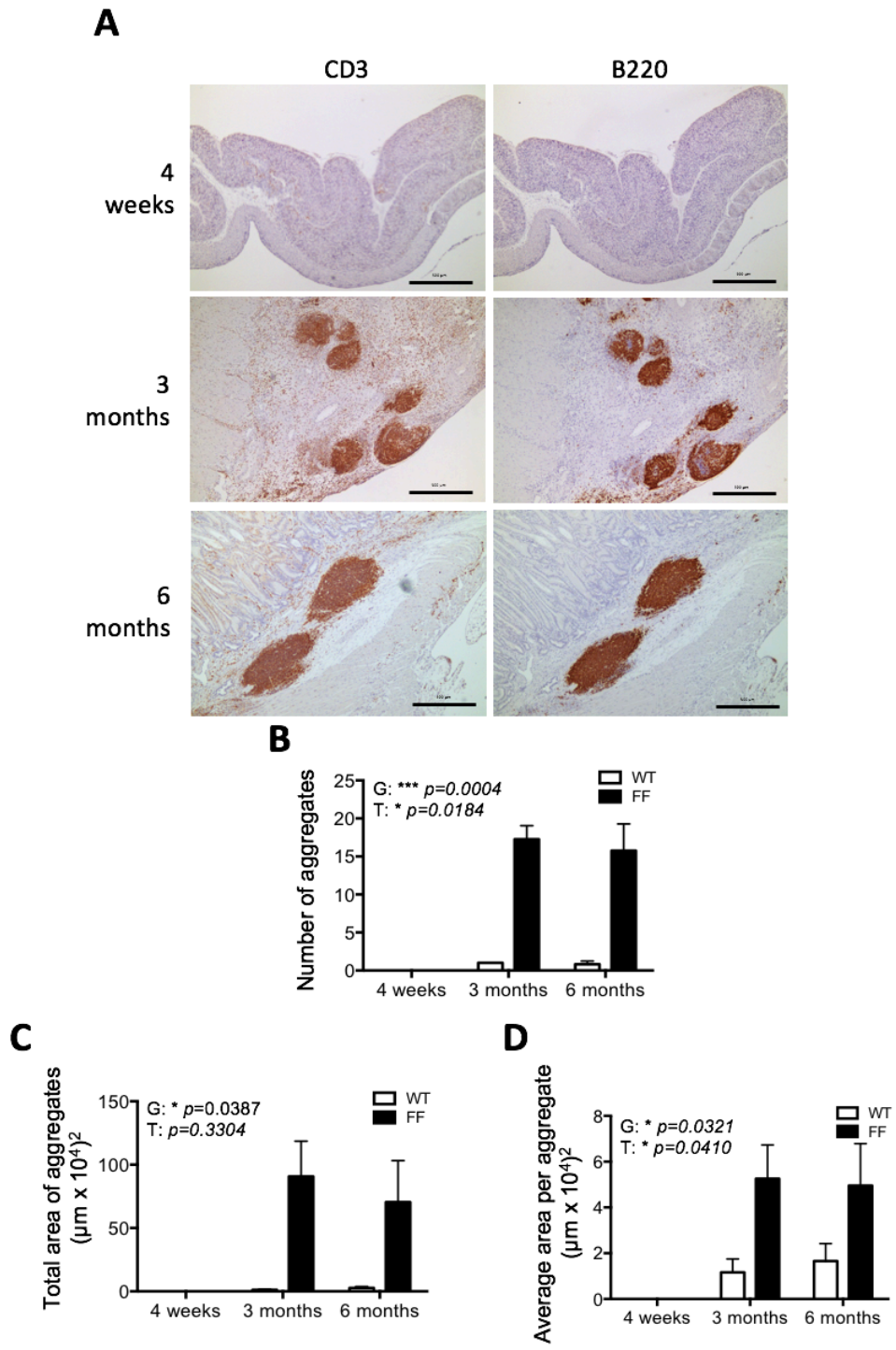

Figure 5.4 – Lymphoid neogenesis is temporally coupled to gastric tumour development. (A) Representative immunohistochemistry of CD3 and B220 in sequential sections at time points corresponding to pre (4-week-old), early (3-month-old) and advanced (6-month-old) gastric tumour development in *gp130*$^{F/F}$ mice. (B-D) Quantification, following B220 immunohistochemical detection, of the number (B), total area (C) and average area (D) of ELS in wild-type (WT) and *gp130*$^{F/F}$ (FF) mice (A-D: n = 3/group at 4 weeks, n = 3/group at 3 months, n = 6-8/group at 6 months). G; genotype –indicates a significant increase in lymphoid neogenesis in *gp130*$^{F/F}$ mice compared to WT. T; timepoint – indicates a significant change in lymphoid neogenesis across time. Graphs represent mean ± SEM. * p <0.05; *** p <0.001.

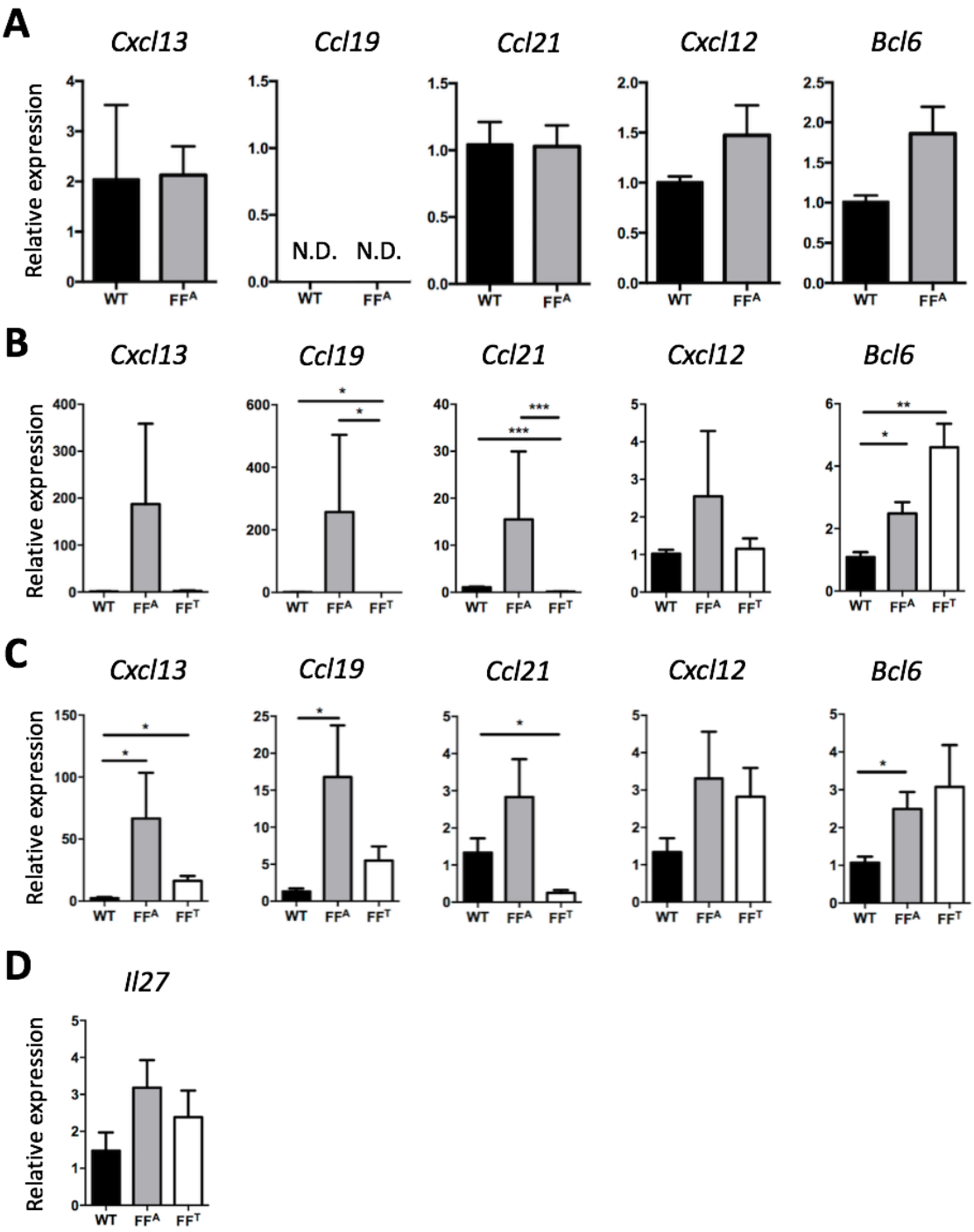

Figure 5.5 – Temporal induction of lymphoid chemokines coincides with ELS development. qPCR analysis of ELS-associated genes in the gastric antrum of *gp130*$^{+/+}$ (WT) and *gp130*$^{F/F}$ (FF^{A}) mice at 4 weeks (A), 3 months (B) and 6 months (C) of age. In *gp130*$^{F/F}$ mice with gastric cancer (3- and 6-month-old mice) gene expression was also determined in the gastric tumour tissue (FF^{T}). In 6-month-old WT and *gp130*$^{F/F}$ mice, the expression of the cytokine *Il27* (D) was also determined. (*n* = 4 per group at 4 weeks, *n* = 7 per group at 3 months, *n* = 6-7 per group at 6 months). Graphs represent mean ± SEM. * $p < 0.05$; ** $p < 0.01$; *** $p < 0.001$. (qPCR performed by Louise McLeod). The expression of all genes has been made relative to an internal housekeeping gene, *Actb*.

5.3.4 Gastric tumourigenesis and ELS development is STAT3 dependent

The activation of STAT3 is emerging as a common feature associated with ELS development. The cytokines IL-6, IL-21 and IL-22 all activate STAT3, have previously been linked with ELS development and maintenance [145, 147, 302, 303], and were highly expressed in the inflamed joints of *Il27ra*$^{-/-}$ mice with synovial ELS (see *Chapter 4*). Additionally, in *gp130*$^{F/F}$ mice, IL-11 signals through the IL-11Rα/gp130 complex to hyperactivate STAT3 causing gastric tumourigenesis [219-221]. To identify whether STAT3 activation correlated with ELS development, data from 161 intestinal-type gastric cancer patients, including 33 patients with matched non-tumour tissue was analysed from TCGA. In non-tumour tissue the expression of *SOCS3*, a STAT3 target gene, did not correlate with homeostatic chemokine levels (*Figure 5.6A*). However, in intestinal-type gastric cancer patients a positive correlation was found between *SOCS3* and *CCL19*, *CCL21* and *CXCL13* (*Figure 5.6B*). Further to this, immunohistochemical analysis identified STAT3-positive cells within lymphoid-rich aggregates in 3-month-old (*Figure 5.7A*) and 6-month-old (*Figure 5.7B*) *gp130*$^{F/F}$ mice. Notably however, STAT3 activity was not restricted to ELS and was also detected in areas of diffuse inflammatory infiltrates (*Figure 5.7C*). Together these results show that tumour-associated ELS in gastric cancer correlates with STAT3 activity.

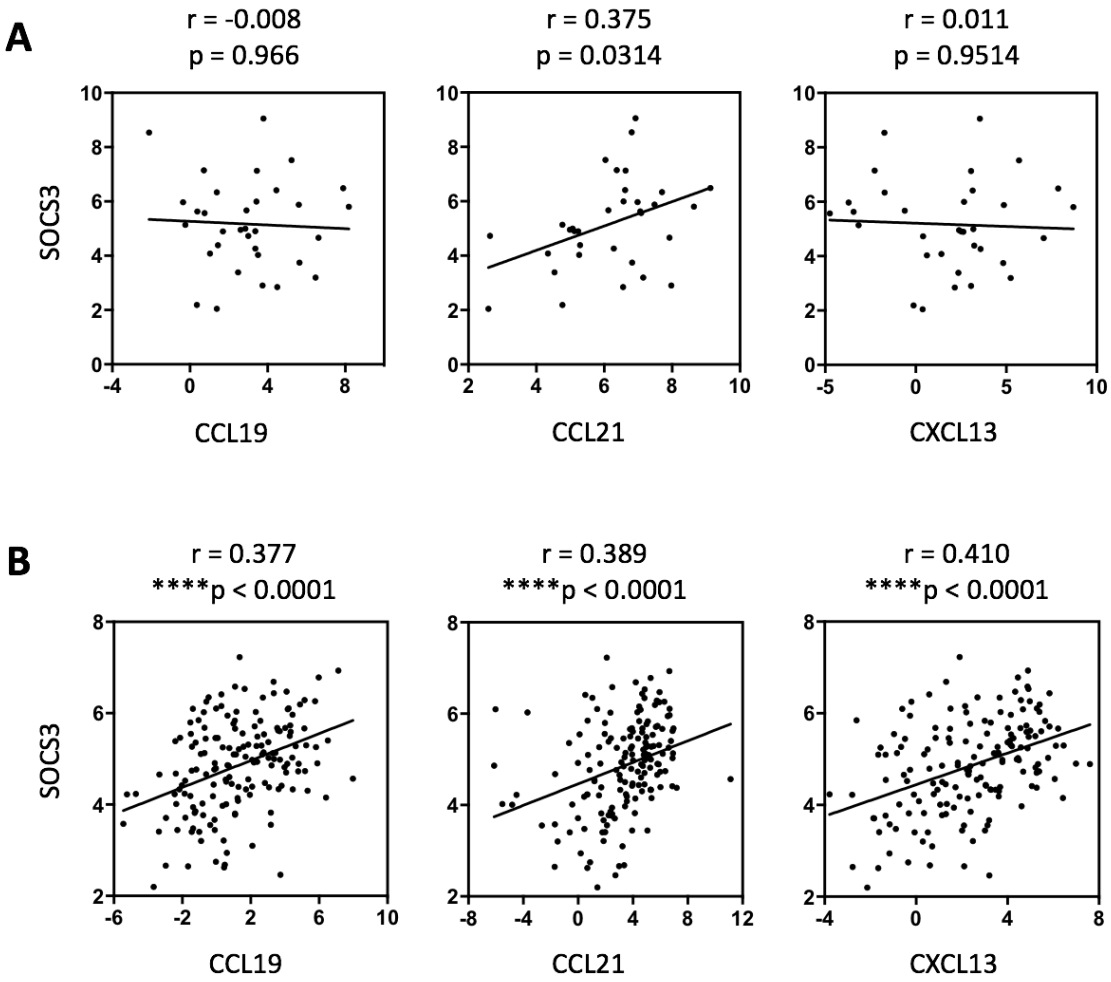

Figure 5.6 – STAT3 target gene SOCS3 correlates with lymphoid chemokine expression in human gastric cancer. Spearman rank correlation coefficients of ELS-associated genes with the STAT3 target gene SOCS3 in 33 matched non-tumour tissue (A) and 161 intestinal-type tumour tissue (B) taken from TCGA gastric cancer cohort. Data presented as log_2FPKMs.

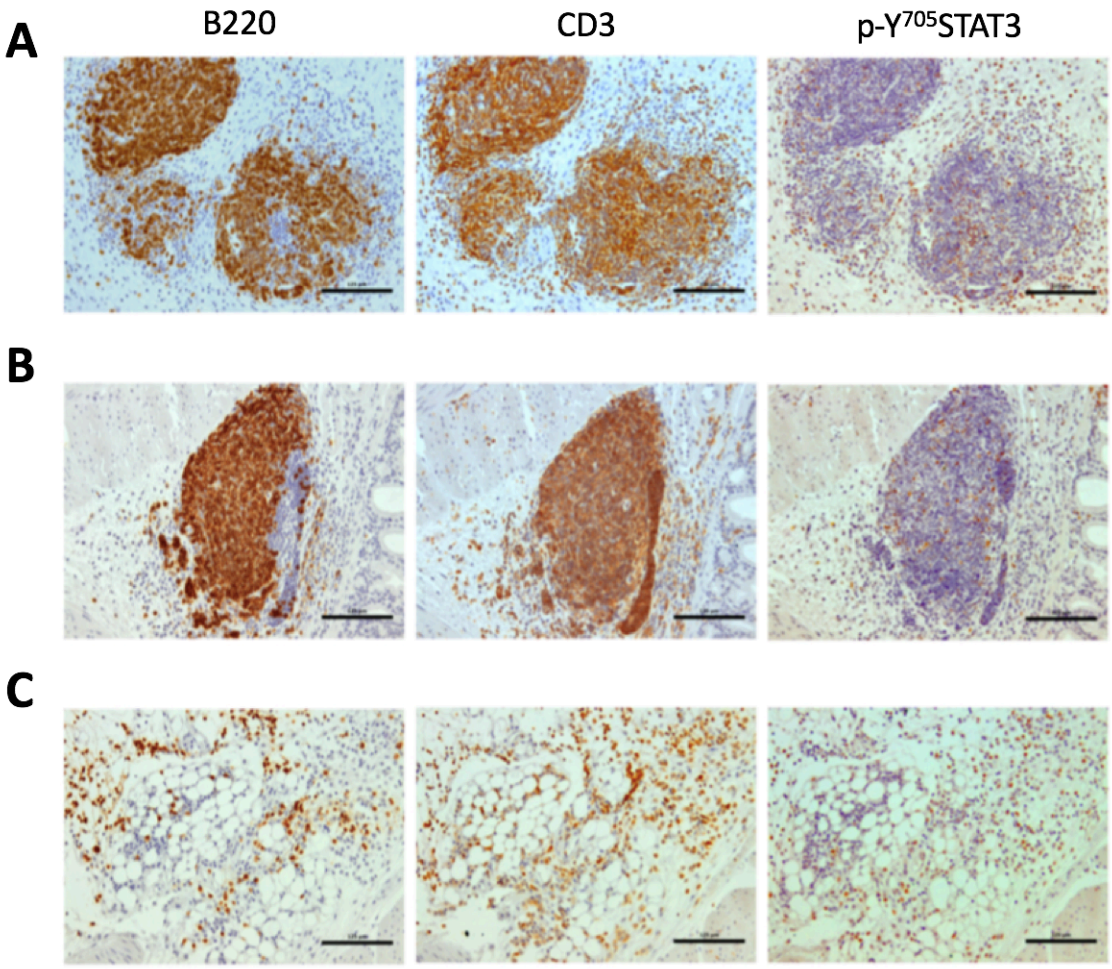

Figure 5.7 – p-Y^{705}STAT3 activity is not restricted to tumour associated ELS. Representative immunohistochemistry of CD3, B220 and p-Y^{705}STAT3 in sequential sections in 3-month-old (A) and 6-month-old (B-C) *gp130*$^{F/F}$ mice (n = 3/group). Staining shows p-Y^{705}STAT3 positive cells in lymphoid aggregates (A-B) and in surrounding diffuse areas of leukocyte infiltration (C). Scale bars: (A-C) 125 μm.

5.3.5 An ELS-chemokine gene signature is linked with advanced gastric cancer

T and B cell priming within ELS have the potential to support local anti-tumour responses [229, 236, 237]. In certain cancers, including colorectal and melanoma, gene signatures of ELS have shown prognostic value [224, 230]. To determine the clinical relevance of ELS in gastric cancer, the expression of homeostatic chemokines, *CXCL13*, *CCL19* and *CCL21*, that correlate with the development of ELS (*see Figures 5.5 and 5.6*), was investigated in intestinal-type human gastric cancer data sets from TCGA. Expression of ELS-associated chemokines was increased in patients with more advanced gastric cancer (stages ii, iii and iv) (*Figure 5.8A*), which is consistent with the temporal development of ELS observed in *gp130*$^{F/F}$ mice (*see Figure 5.4*). Additionally, compared to patients where tumour growth was confined to the submucosa (T1), increased expression of ELS genes was found in patients where the tumour had spread to the subserosal layer, serosa and nearby tissues (T2, T3 and T4 respectively) (*Figure 5.8B*). Despite an association between ELS gene expression and tumour growth, no association was observed between expression of these lymphoid chemokines and the degree of lymph node involvement (N stage) (*Figure 5.8C*) or metastasis (M stage) (*Figure 5.8D*). Similarly, no statistical significance was found between the ELS-associated genes and patient survival. Interestingly a 3-gene ELS signature based on single sample gene set enrichment of the homeostatic chemokines *CXCL13*, *CCL21* and *CCL19* also showed a similar trend [304]. Thus, an ELS gene signature was associated with advanced gastric cancer in patients but was not predictive of a favourable outcome as has been observed in some forms of cancer.

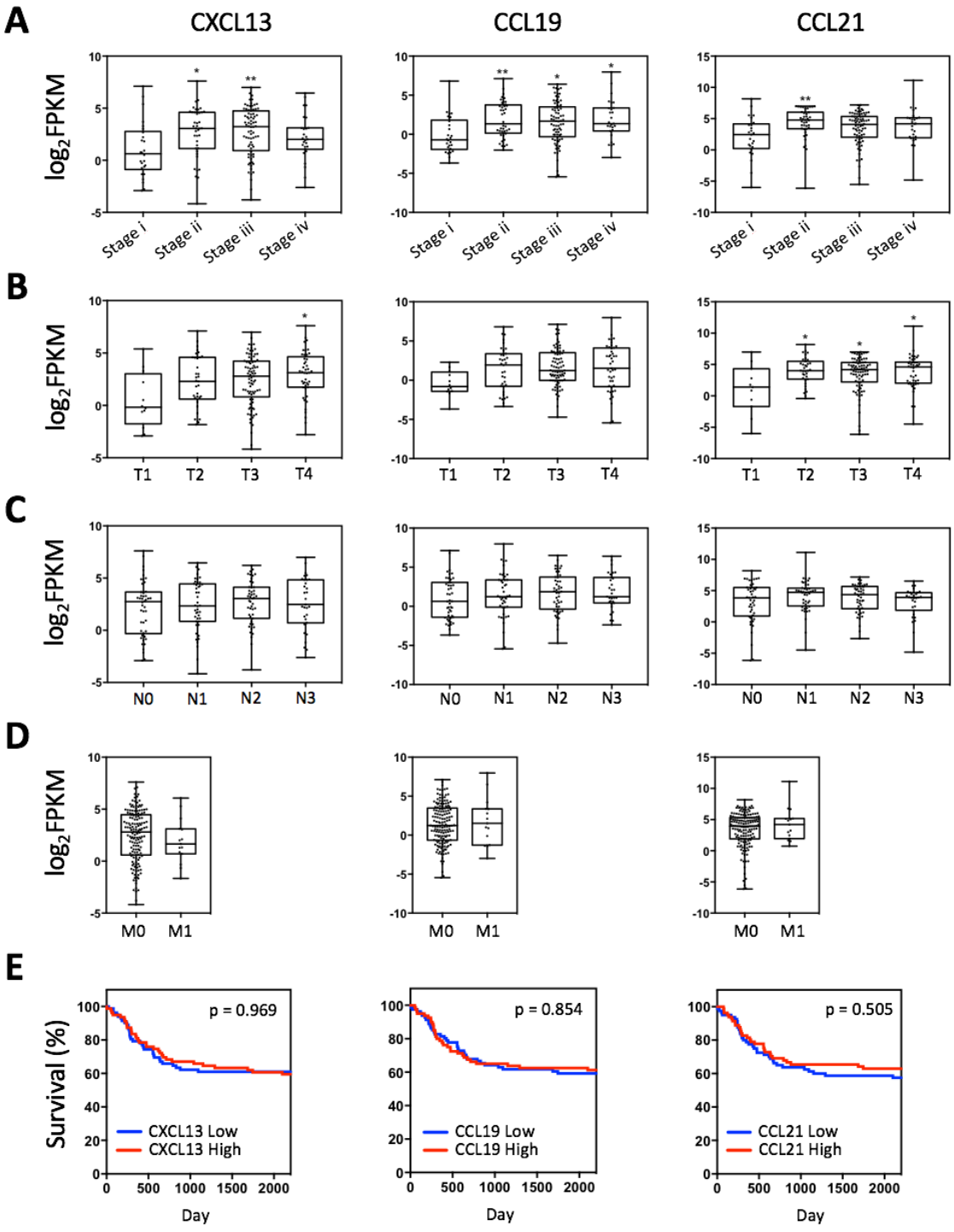

Figure 5.8 – An ELS gene signature is associated with advanced gastric cancer in patients. Analysis of ELS-associated genes with tumour stage (A), tumour growth (B), N stage (C) and M stage (D) in 174 intestinal-type gastric cancer patients from TCGA. (E) Association between homeostatic chemokine expression and patient survival ($n = 87$ per group). Data presented as log_2FPKM. * $p < 0.05$; ** $p < 0.01$.

5.3.6 A Th17 gene signature correlates with ELS development

In *Chapter 4*, a Th17 signature was found to be linked with synovial ELS development in an inflammatory arthritis model. Since hyperactivation of STAT3 was associated with ELS development in the gastric submucosa, (*see Figure 5.6 and Figure 5.7*) and that STAT3 activity is required for the differentiation of Th17 cells [20], we questioned the role of this effector T cell subset in ELS regulation. Given that the Th17-associated markers *Il17a*, *Il23* and *Rorc* have previously been shown to be elevated in response to STAT3-driven gastric tumourigenesis [249], and that gastric tumourigenesis and ELS development are tightly coupled (*see Figure 5.4A*), we investigated whether a Th17 signature is associated with ELS in clinical disease. For this, using intestinal-type human gastric cancer datasets from TCGA, Th17-associated genes were correlated against the ELS-associated genes *CXCL13*, *CCL21* and *CCL19*. Since the development of ELS in gastric cancer is observed in the submucosa and not intra-tumourally [304, 305], matched non-tumour tissue was used. The expression of the ELS-associated genes *CXCL13* and *CCL19* positively correlated with the expression of *IL17A (Figure 5.9A)*, *IL17F* (*Figure 5.9B*) and *CCR6 (Figure 5.9C)*, but little correlation was found between Th17 signature genes and *CCL21 (Figure 5.9)*. Similarly, a 3-gene ELS signature was found to positively correlate with *IL17A* levels in TCGA datasets [304]. Thus, the development of ELS in gastric cancer is associated with the expression of Th17 signature genes.

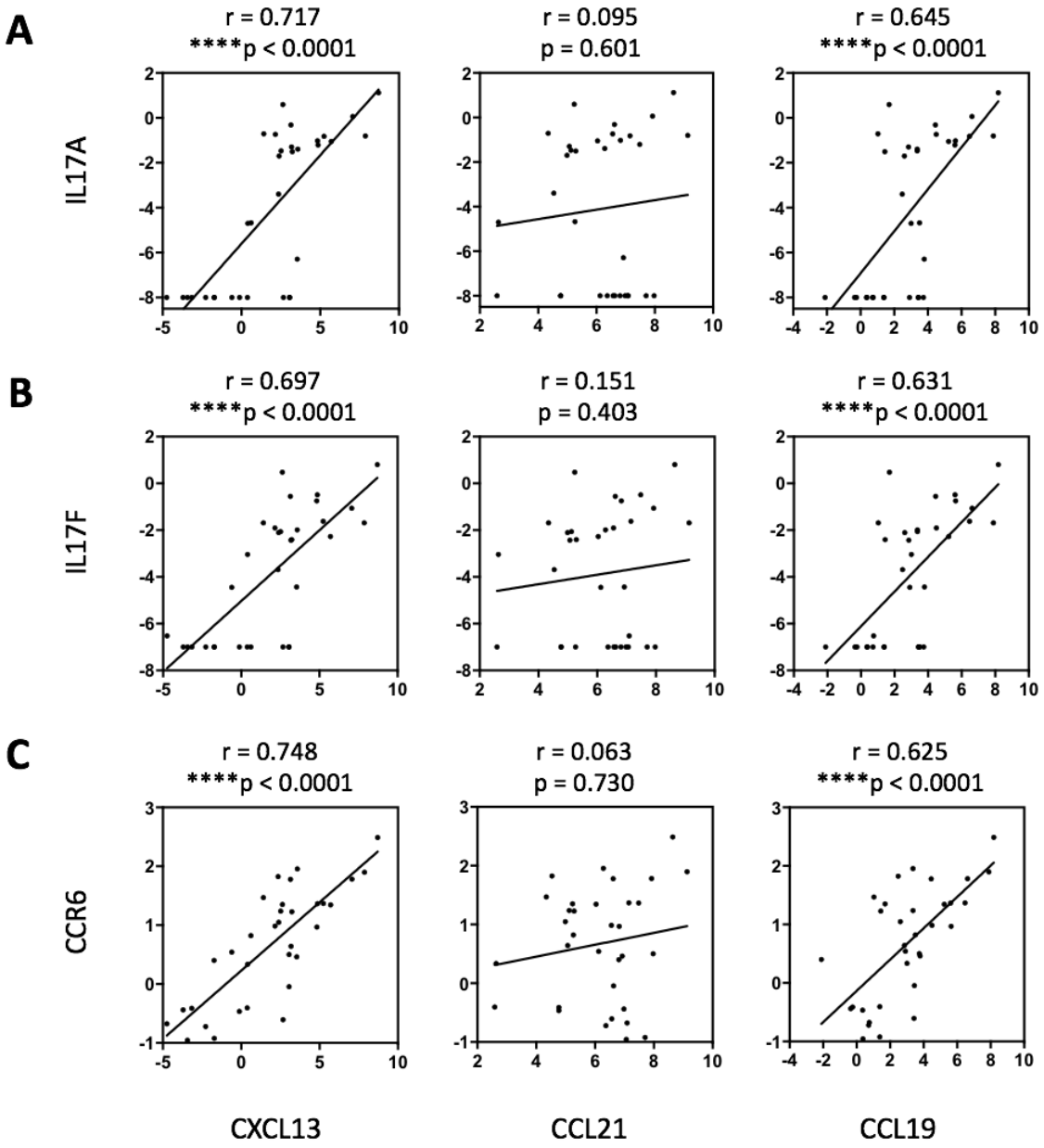

Figure 5.9 – Markers of Th17 cell effector responses correlate with lymphoid chemokine expression in human gastric cancer. Spearman rank correlation coefficients of ELS-associated chemokine expression with the signature Th17 genes, *IL17A* (A), *IL17F* (B) and *CCR6* (C) in 33 matched non-tumour tissue taken from TCGA gastric cancer cohort. Data presented as log_2FPKMs.

5.3.7 Development of submucosal lymphoid aggregates is independent of IL-17A

To determine whether IL-17A is required for ELS development, we looked for the presence of ELS by immunohistochemistry in *gp130*$^{F/F}$ mice that had been crossed with IL-17A deficient mice (*gp130*$^{F/F}$:*Il17a*$^{-/-}$; FF:*Il17*; provided by Professor Brendan Jenkins, Hudson Institute, Melbourne). In the absence of IL-17A, lymphoid aggregates still developed in the submucosa and were comprised of dense accumulations of T and B cells (*Figure 5.10A*). Although not statistically significant, we did however note that *gp130*$^{F/F}$:*Il17a*$^{-/-}$ mice appeared to develop fewer and smaller aggregates (*Figure 5.10B-D*) than those observed in *gp130*$^{F/F}$ mice. Since tumour-associated ELS development was shown to be STAT3 dependent (*see Figures 5.6 and 5.7*), *gp130*$^{F/F}$ mice were crossed with *Stat3* heterozygous mice. By removing a single *Stat3* allele, these mice have a reduced cellular pool of STAT3 available for phosphorylation [306]. As expected, this 'normalisation' of STAT3 activation in *gp130*$^{F/F}$:*Stat3*$^{+/-}$ mice prevented gastric tumourigenesis and the associated development of ELS (*Figure 5.10A-D*), further suggesting a prominent role for STAT3 signalling in ELS development.

Lymphoid aggregates in *gp130*$^{F/F}$:*Il17a*$^{-/-}$ mice were further characterised to determine whether they showed features typical of ELS. Immunohistochemical analysis identified the presence of pY^{705}-STAT3-positive cells and CXCL13-expressing cells. Also present were stromal cells expressing Pdpn, and PNAd-positive HEVs (*Figure 5.11A*). Hence lymphoid aggregates in *gp130*$^{F/F}$:*Il17a*$^{-/-}$ mice displayed characteristics consistent with the formation of ELS.

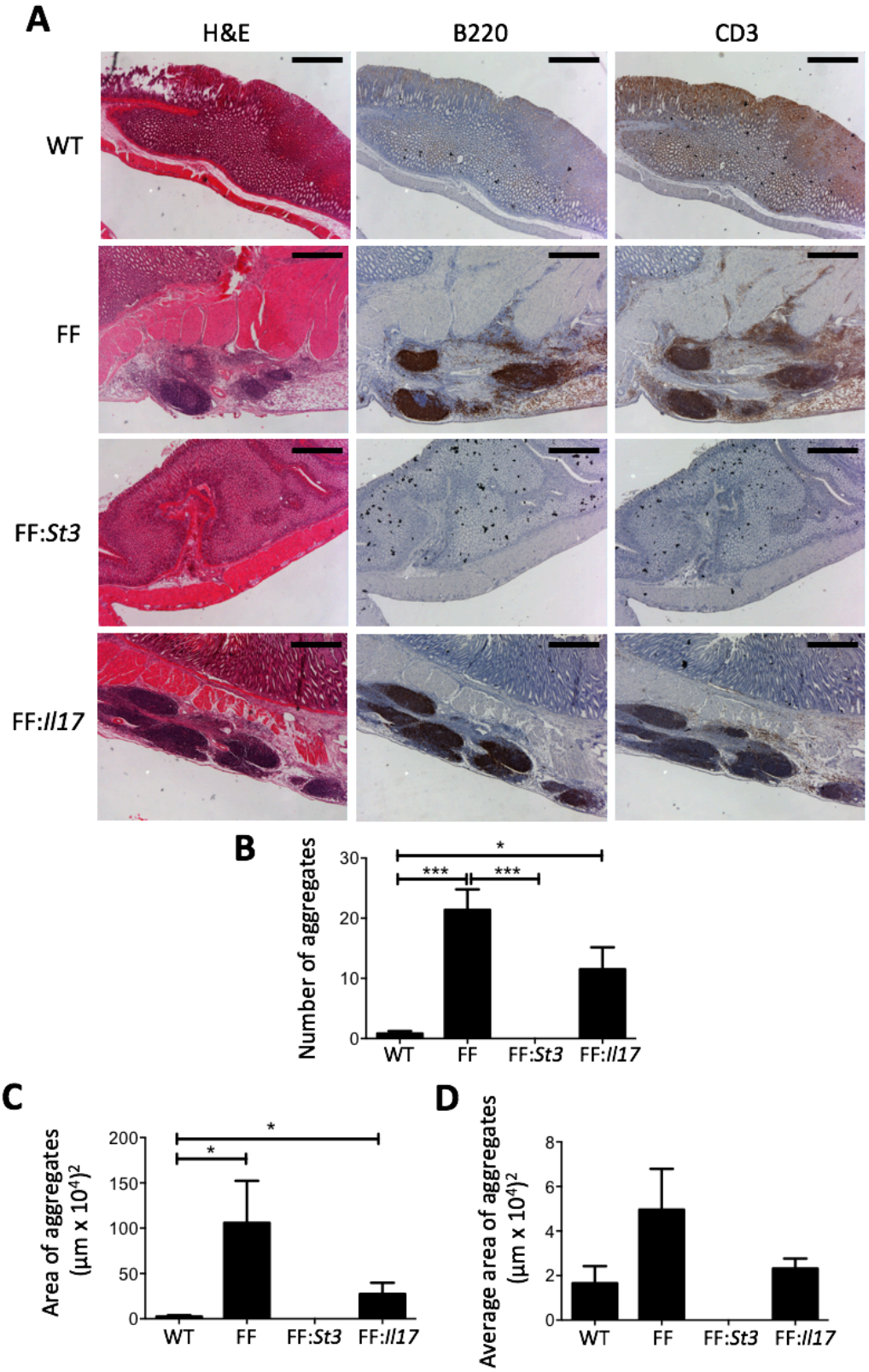

Figure 5.10 – Formation of submucosal lymphoid aggregates is STAT3 dependent but independent of IL-17A. (A) Representative H&E and immunohistochemistry of CD3 and B220 in sequential sections from WT, *gp130*$^{F/F}$ (FF), *gp130*$^{F/F}$:Stat3$^{+/-}$ (FF:*St3*) and *gp130*$^{F/F}$:Il17a$^{-/-}$ (FF:*Il17*) mice at 6 months of age. (B-D) The number (B), total area (C) and average size (D) of lymphoid aggregates were quantified in each strain (n = 6 WT, n = 5 *gp130*$^{F/F}$, n = 4 *gp130*$^{F/F}$:*Stat3*$^{+/-}$, n = 4 *gp130*$^{F/F}$:*Il17a*$^{-/-}$). Scale bars: (A) 500 µm. Graphs represent mean ± SEM. * $p < 0.05$, ** $p < 0.01$, *** $p < 0.001$.

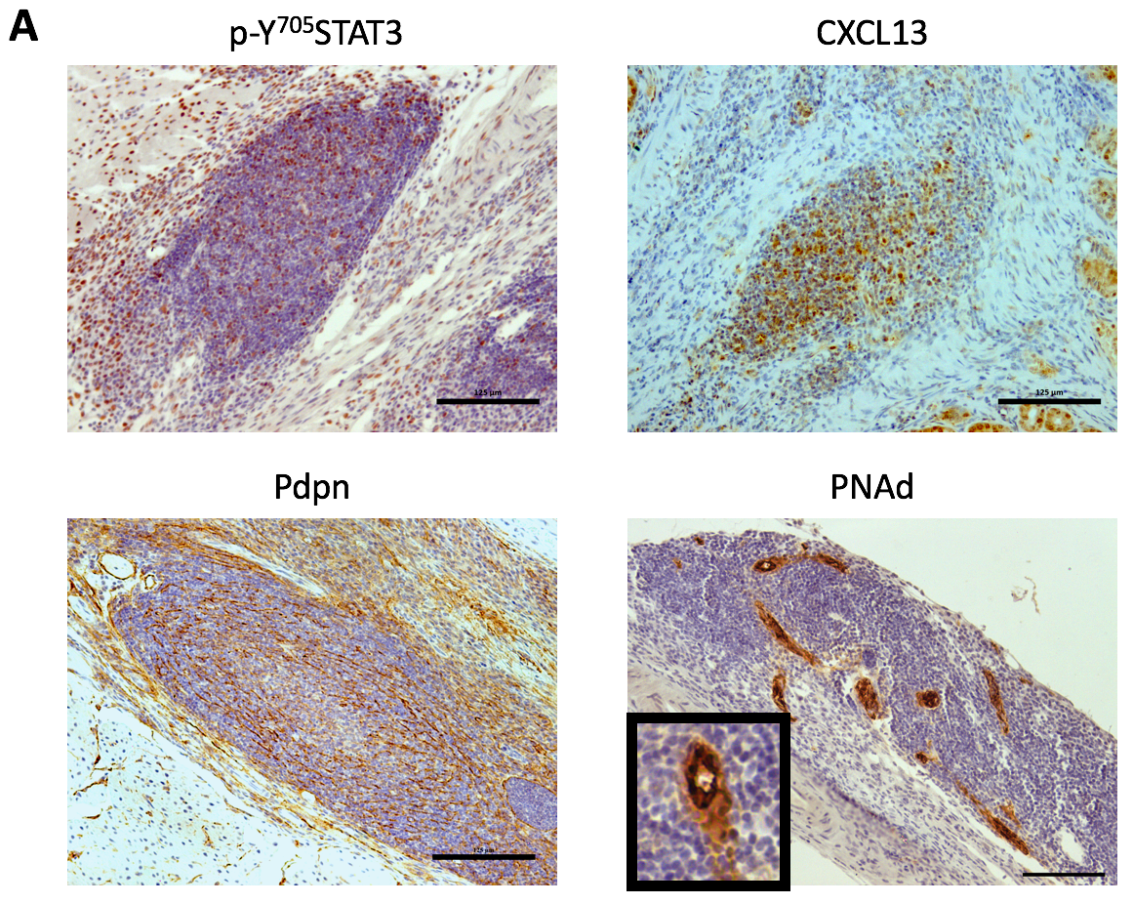

Figure 5.11 – Characterisation of tumour associated lymphoid aggregates in *gp130*$^{F/F}$:*Il17a*$^{-/-}$ mice. (A) Representative immunohistochemical staining of p-Y^{705}STAT3, CXCL13, Pdpn and PNAd^{+} HEVs (boxed area shows high power image) in *gp130*$^{F/F}$:*Il17a*$^{-/-}$ mice at 6-months of age (n = 3). Scale bars (A) 500 μm.

5.3.8 IL-17A is required for the development of functional ELS

Reactive germinal centres that mark active B cell proliferation, differentiation and maturation of the antibody response through somatic hypermutation and class-switching, are key features of functional ELS [137]. For example, ELS in non-small cell lung carcinoma were comprised of germinal centre B cells that expressed AID, the enzyme required for class-switching and somatic hypermutation of antibodies, as well as plasma cells that produced tumour-specific antibodies. These were linked with improved patient survival [233]. Similarly, ELS in the synovium of rheumatoid arthritis patients have been shown to express AID, and its expression correlates with the production of autoantibodies such as ACPA [155]. To identify whether the lymphoid aggregates in *gp130*$^{F/F}$:*Il17a*$^{-/-}$ mice represent *bona fide* functional ELS, immunohistochemistry was performed to detect CD21^{+} follicular dendritic cell networks and germinal centre B cells using peanut agglutinin. Whilst tumour-associated ELS in *gp130*$^{F/F}$ mice displayed reactive germinal centres (*Figure 5.12A*), loss of IL-17A resulted in lymphoid-rich aggregates that lacked CD21^{+} follicular dendritic cell networks and peanut agglutinin-stained germinal centres (*Figure 5.12A-C*). Thus, despite the development of submucosal lymphoid aggregates in *gp130*$^{F/F}$:*Il17a*$^{-/-}$ mice, these lack reactive germinal centres that mark mature and functional ELS.

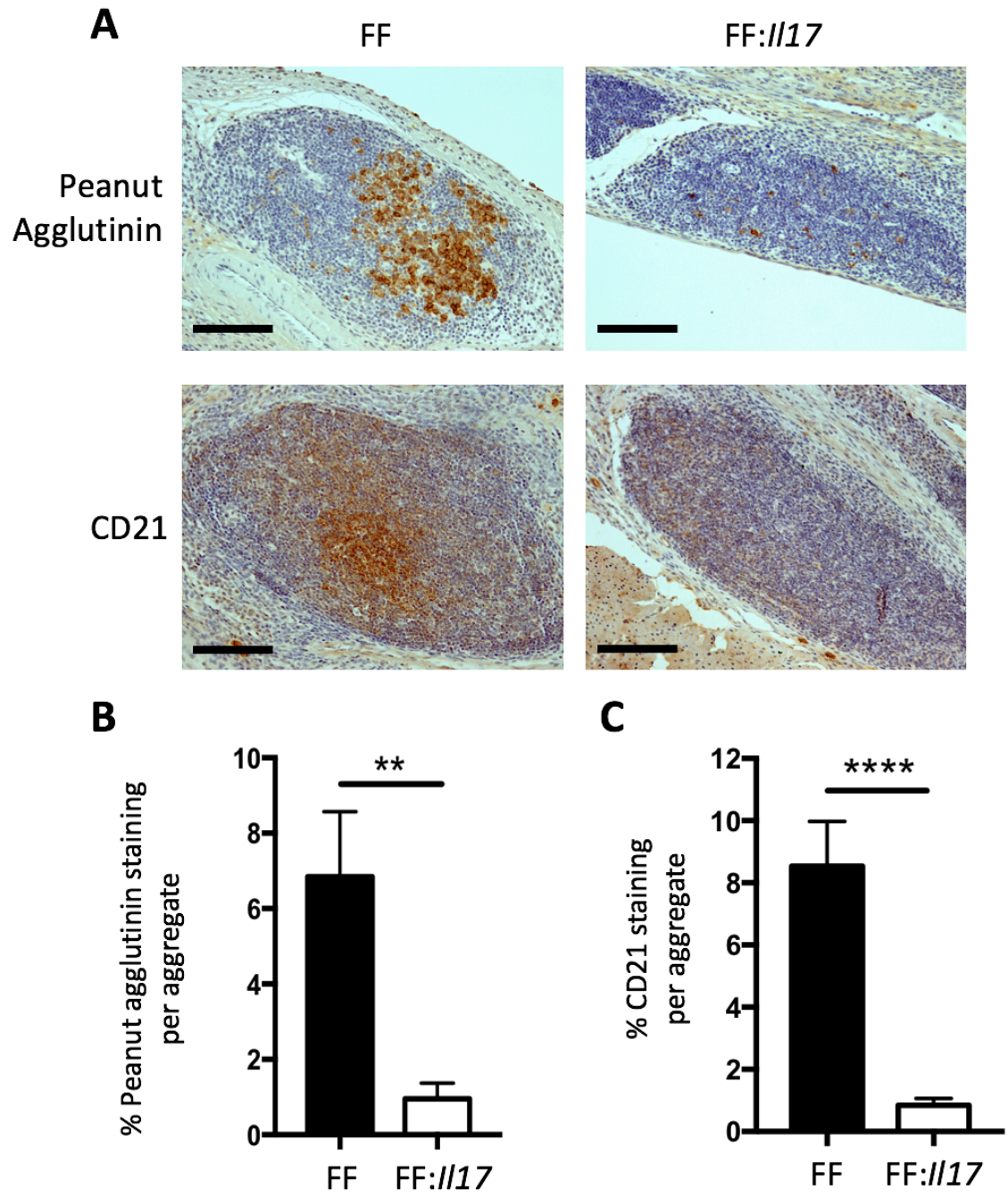

Figure 5.12 – *Il17a* is required for functional tumour-associated ELS. (A) Representative immunohistochemistry staining of peanut agglutinin and CD21 in *gp130*$^{F/F}$ (FF) and *gp130*$^{F/F}$:*Il17a*$^{-/-}$ (FF:*Il17*) mice at 6 months of age. (B-C) Quantification of peanut agglutinin (B) and CD21 (C) staining in 6-month-old *gp130*$^{F/F}$ (FF) and *gp130*$^{F/F}$:*Il17a*$^{-/-}$ (FF:*Il17*) mice (n = 3/group). Scale bars: (A) 500 μm. Graphs shown as mean ± SEM. ** p <0.01; **** p <0.0001.

5.3.9 Expression of IL-17A is not predictive of patient outcomes or stage of gastric cancer in clinical disease

Our studies above suggest that IL-17A is important for the development of functional tumour-associated ELS, which may be important in establishing local anti-tumour responses. Using TCGA datasets for intestinal-type gastric cancer, we questioned whether *IL17A* expression was associated with patient survival or the stage of the disease. Despite IL-17A being necessary for germinal centre activity in *gp130*$^{F/F}$ mice (*see Figure 5.12*), *IL17A* expression showed no correlation with the stage of gastric cancer, or the degree of lymph node involvement and metastasis (*Figure 5.13A*). Similarly, no difference in survival was found between patients with high and low expression of *IL17A* (*Figure 5.13B*). Thus, the expression of *IL17A* was not associated with clinical disease progression, nor does it have prognostic significance.

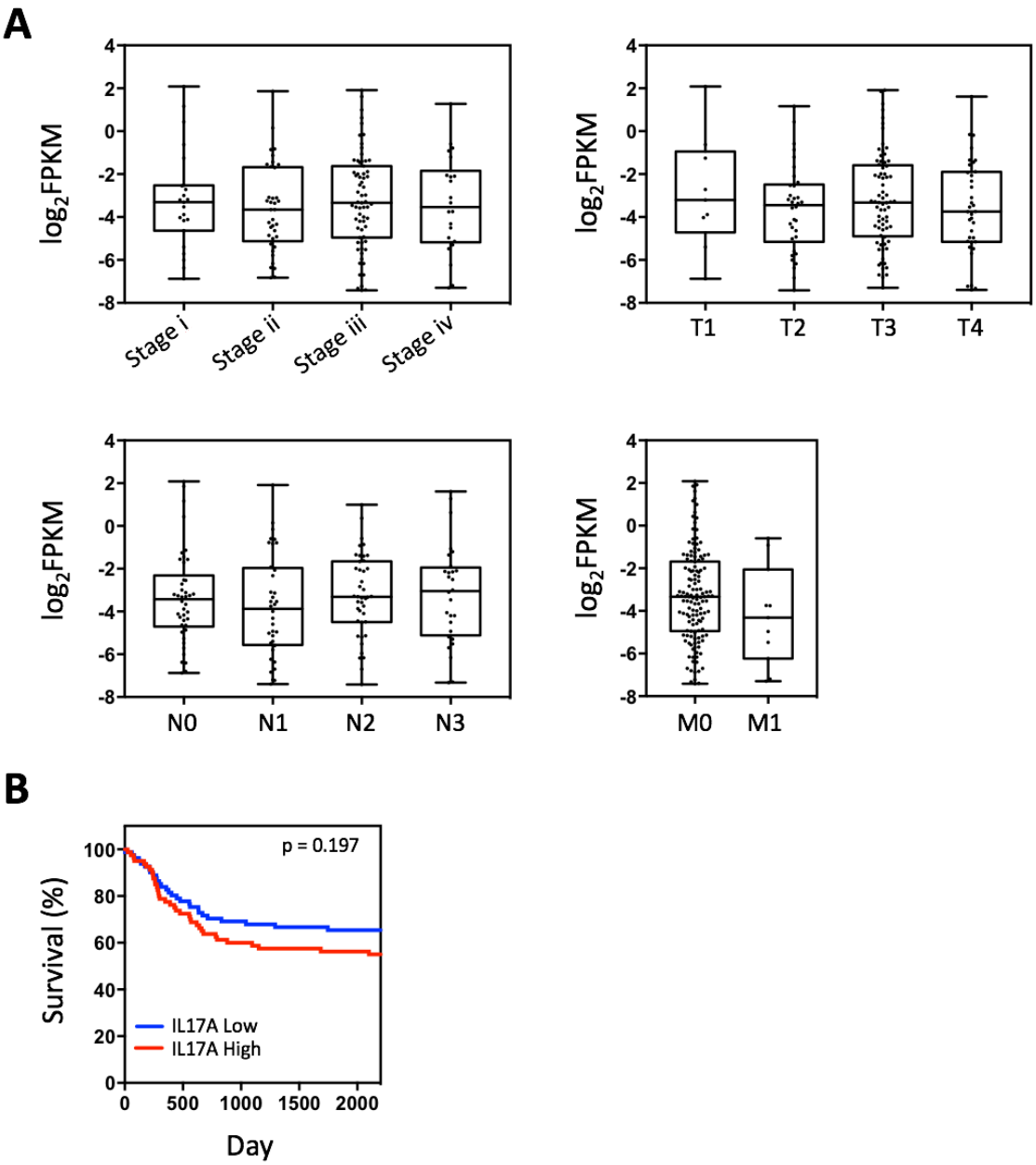

Figure 5.13 – *IL17A* expression has no prognostic significance in gastric cancer patients. (A) Evaluation of *IL17A* expression with tumour stage and indicated TNM stage in 174 intestinal-type gastric cancer patients from TCGA. (B) Association between *IL17A* gene expression and patient survival (n = 87 per group). Data presented as log_2FPKM.

5.4 Discussion

Tumour-associated ELS have recently been identified in numerous cancers. In many cases the number of ELS positively correlates with patient survival, and it has been proposed that tumour-associated ELS represent immune privileged areas that can limit cancer progression [137, 138]. Hence, there is renewed interest in understanding the immune mechanisms underlying their development in order to enhance anti-tumour immunity [238, 298, 299].

In this chapter, a clinically relevant mouse model of gastric cancer was used to show that the temporal development of gastric tumourigenesis coincided with ELS development. Through immunohistochemical analysis, these immune cell aggregates were shown to be functional ELS displaying T and B cell segregation, with peanut agglutinin- and Ki-67-positive germinal centres. In addition, the temporal development of ELS was associated with the induction of homeostatic chemokines (*Cxcl13*, *Ccl19* and *Ccl21*). Hence, tumour-associated lymphoid aggregates that develop in the gastric submucosa of *gp130*$^{F/F}$ mice display characteristics consistent with those of functional ELS.

During the course of this work another group also highlighted the presence of ELS in tumour biopsies from gastric cancer patients [305]. Here, ELS were characterised as having segregated T and B cell zones, Ki-67^{+} proliferating B cells, typically found in germinal centres, and PNAd^{+} HEVs, required for the recruitment of lymphocytes into lymphoid tissue. The histological presence of CD20^{+} immune aggregates, high tumour infiltration of T-bet^{+} Th1 cells and low infiltration of FoxP3^{+} Treg cells correlated with improved relapse-free survival [305]. Thus, the progression of gastric cancer was influenced by the presence of ELS.

Recently, in melanoma [230] and colorectal cancer [224], gene signatures of ELS were discovered as prognostic indicators of increased patient survival. In this chapter, expression of homeostatic chemokines linked with the development of ELS were increased in advanced gastric cancer patients but showed no prognostic significance. A more comprehensive evaluation of tumour-associated ELS, for example utilising RNA-seq to identify transcriptomic signatures that include markers of ELS activity, may offer an opportunity to develop more robust markers with prognostic value. In this regard, in a recent study of gastric cancer patients, a B cell metagene signature was only linked with improved survival when combined with a marker of Th1 cell activity (e.g., *TBX21* encoding Tbet) [305]. In the same study, the histological presence of tumour-associated

$CD20^+$ aggregates correlated with improved relapse-free survival [305]. This highlights the potential of using ELS as histological markers of disease progression and prognosis.

Cytokines that activate STAT3 have been linked with ELS development in multiple diseases that feature chronic inflammation. For example, IL-6 signalling through the IL-6R/gp130 complex results in STAT3 activation and the development of ELS in the lung [302]. While IL-27 can activate both STAT3 and STAT1, in adaptive immunity IL-27 is predominantly associated with the activation of STAT1 to exert anti-inflammatory outcomes [91]. For example, IL-27 through STAT1 signalling can counteract IL-6/STAT3 driven responses [91] and can suppress the development of Th17 cells [279] and ELS [146]. In *gp130*$^{F/F}$ mice, gastric tumourigenesis and submucosal ELS development in *gp130*$^{F/F}$ mice is triggered by IL-11 signalling through the IL-11Rα/gp130 complex to activate STAT3 [219-221]. Importantly, 'normalisation' of STAT3 activation in *gp130*$^{F/F}$:*Stat3*$^{+/-}$ mice prevented both gastric tumourigenesis and ELS development. Whilst phosphorylated STAT3 was detected in lymphoid aggregates, STAT3 activity was also found in areas of diffuse lymphocyte infiltration. Therefore, despite finding a correlation between the expression of ELS-associated genes and the prototypical STAT3 target gene, SOCS3, localised activation of STAT3 by immunohistochemistry remains a poor indicator of mature or active ELS.

In *Chapter 4*, studies identified a Th17 signature that was linked with the presence of synovial ELS during inflammatory arthritis. Also, in other autoimmune and infection models, effector Th17 responses have been implicated in ectopic lymphoneogenesis. In EAE, podoplanin-expressing Th17 cells and the signature cytokine IL-17 contributed to lymphoid neogenesis [143]. However, the role of Th17 cells in the development of ELS in the lungs (iBALT) appears controversial and context dependent. In response to challenge with LPS [142] and *Pseudomonas aeruginosa* [144] the development of ELS is IL-17 dependent. However, following infection with a modified vaccinia virus Ankara the development of iBALT was unaffected in the absence of IL-17 [144]. While IL-17 was also expressed within inflamed salivary glands following adenovirus challenge, another Th17-associated cytokine, IL-22, was the key mediator required for lymphoid neogenesis [145]. Consistent with the increased expression of the Th17 markers *Il17a*, *Il23* and *Rorc* observed during gastric tumourigenesis in *gp130*$^{F/F}$ mice [249], expression of *IL17A* in clinical disease also correlated with the ELS-associated genes, CXCL13 and CCL19. Despite this, the genetic ablation of IL-17A in *gp130*$^{F/F}$ mice had little impact on gastric tumourigenesis [249] or the development of submucosal lymphoid aggregates. While not

statistically significant, we noted slightly fewer and smaller lymphoid aggregates in *gp130*$^{F/F}$:*Il17a*$^{-/-}$ mice as compared to those in *gp130*$^{F/F}$ mice. We therefore questioned whether IL-17A may be important for the development of mature ELS. Consistent with this hypothesis, whilst lymphoid aggregates in *gp130*$^{F/F}$:*Il17a*$^{-/-}$ mice displayed many of the characteristics of ELS (e.g. Pdpn, Cxcl13, PNAd), they lacked follicular dendritic cell networks and the formation of germinal centres. Interestingly, despite a lack of active germinal centres in *gp130*$^{F/F}$:*Il17a*$^{-/-}$ there was no difference in tumour burden between *gp130*$^{F/F}$ and *gp130*$^{F/F}$:*Il17a*$^{-/-}$ mice [249]. Likewise, *IL17A* expression in human gastric cancer patients showed no prognostic significance. However, it could be possible that a more robust Th17 signature composed of markers identified in *Chapter 4* may have more prognostic value. Taken together, the above studies highlight a role for IL-17 and Th17 cell axis in ELS development, although this is likely to be disease and context dependent.

While ELS have been proposed as local sites for establishing anti-tumour immunity, it is also possible that ELS may contribute to persistent tissue inflammation and the associated formation of tumours. Thus, a time course was used to try and establish whether ELS developed before, or as a consequence of, gastric tumourigenesis in *gp130*$^{F/F}$ mice. However, by combining immunohistochemistry with the transcriptional evaluation of homeostatic chemokine expression we were unable to uncouple ELS development and gastric tumourigenesis. Interestingly, using a model of *Helicobacter*-induced gastritis we found that ELS could develop in the absence of gastric tumours [304]. Here, infection of WT mice with *H. felis* led to the development of submucosal ELS. This was also associated with increased expression of the homeostatic chemokines *Cxcl13* and *Ccl19*, as well as the signature Th17 cytokine, *Il17a* [304], suggesting another role for this effector T cell response in ELS development during *H. felis* infection. Therefore, it is likely that the local inflammatory response within the tissue, rather than the process of tumourigenesis, provides the cues required for ELS development.

Using TCGA datasets no association was found between gene signatures of ELS development and improved patient survival. Interestingly, in both *gp130*$^{F/F}$ mice and biopsies from gastric cancer patients, tumour-associated ELS were found extra-tumourally in the gastric submucosa rather than intra-tumourally [304, 305]. Similarly, in colorectal cancer the presence of extra-tumoural ELS correlated with advanced disease but not with a positive prognosis [307]. In contrast, the presence of intra-tumoural lymphoid aggregates in breast cancer patients was linked to improved patient survival

[227]. This raises the question as to whether the ability of ELS to improve outcomes in cancer is linked with their location. It is possible that intra-tumoural ELS are linked with improved prognosis due to their exposure to tumour antigens within the tumour stroma, which supports the development of local antigen-specific responses to tumours and enhanced anti-tumour immunity.

In summary, this chapter characterises tumour-associated lymphoid aggregates that develop in the gastric submucosa as *bona fide* ELS. These ELS featured T and B cell compartmentalisation, reactive germinal centres and their development was linked with the temporal expression of homeostatic chemokines. However, the presence of ELS did not provide prognostic benefit. Through genetic ablation of IL-17A in the *gp130*$^{F/F}$ mouse model of gastric cancer, this work identifies a novel role for IL-17A in promoting ELS activity. Thus, immunomodulation of the Th17/IL-17 axis in certain cancers may provide an opportunity to promote anti-tumour responses at tumour-associated ELS.

Chapter 6. Therapeutic targeting of the Th17 master regulator RORγt in inflammatory arthritis

6.1 Introduction

The *Rorc* gene encodes two isoforms - RORγ1 and RORγ2 (RORγt). They differ in the first 21 amino acids through alternative promoter usage. RORγ1 is ubiquitously expressed and its functions are incompletely understood [308]. RORγt however is probably best known as a transcription factor that is essential for driving the differentiation and effector function of Th17 cells [20, 309]. However, RORγt is also expressed by ILC3 populations including adult LTi cells, and IL-17-producing γδ T cells [310]. Therefore, drug targeting of RORγt is seen as a potential therapeutic approach for the treatment of diseases associated with innate and adaptive Th17-type effector responses. In this regard, the treatment of mice with RORγt inhibitors has been shown to delay the onset and severity of EAE [311] and collagen-induced arthritis [312]. To date, drug targeting of RORγt has not been tested in murine AIA, nor has this approach been explored to prevent the formation of ELS. However, the safety of targeting RORγt must be carefully considered given its important homeostatic roles. RORγt is essential for the survival and proliferation of immature $CD4^+CD8^+$ thymocytes through regulation of anti-apoptotic factors such as Bcl-xL [313, 314]. Additionally, RORγt is required for the development of LTi cells which are essential for SLO development during ontogeny [314]. It follows that *Rorc*$^{-/-}$ mice lack lymph nodes, LTi cells, have impaired Th17 cell development and also display thymic aberrations leading to metastatic T cell lymphoma and premature death [140, 309, 315].

In *Chapter 4*, a prominent Th17 signature was associated with the development of synovial ELS. Similarly, I identified altered expression of a novel regulator of Th17 effector responses, CD5L, which has been shown to regulate the formation of cholesterol metabolites that have recently been identified as natural ligands for RORγt [289, 290]. While IL-17A/IL-17RA directed antibodies have limited efficacy in clinical trials of RA, inhibitors that more broadly target the effector characteristics of this T helper cell subset may be more effective. In this context, future studies will test a small molecule inhibitor of RORγt on the development and maintenance of synovial ELS, where I hypothesise that its inhibition would impair ELS formation. In this chapter, I present my initial proof-of-concept studies evaluating a small molecule inhibitor of RORγt in WT mice during AIA.

6.2 Materials and Methods

6.2.1 RORγt inhibitor

The small molecule RORγt inhibitor was provided by Novartis. Previous studies had determined the efficacy and affinity of the inhibitor *in vitro* and during *in vivo* delayed-type hypersensitivity reactions in rats [316].

6.2.2 Inhibition of *in vitro* T cell cultures

Naïve $CD4^+$ T cells were recovered and activated under Th1, Th2 or Th17 polarising conditions as previously described in *section 2.4*. To identify the effect of RORγt inhibition on *in vitro* T cell differentiation, cultures included 1 μM RORγt inhibitor or vehicle control, DMSO. Intracellular staining for IL-17A, IFNγ and IL-4 was carried out as described in *section 2.5.2*.

6.2.3 Administration of a small molecule RORγt inhibitor during AIA

Murine AIA was induced as previously described in *section 2.2.2*. Mice were administered with either 5 mg/kg of RORγt inhibitor or vehicle control (100 mM sodium citrate buffer, pH2). Mice were treated twice a day by oral gavage starting just prior to the induction of arthritis at day 0 and continuing for 10 days. Draining lymph nodes, synovium, joint-infiltrating T cells and knee joints were recovered and processed as previously outlined in *section 2.2*.

6.3 Results

6.3.1 Inhibition of RORγt selectively prevents differentiation of Th17 cells

Previous studies with the small molecule inhibitor had confirmed its ability to target RORγt. Treatment with the inhibitor impaired Th17 differentiation in *in vitro* human $CD4^+$ T cell cultures, and reduced ear swelling in a mBSA-induced delayed-type hypersensitivity model in rats [316]. Initial experiments therefore tested the ability of the RORγt inhibitor to prevent Th17 cell differentiation in *in vitro* murine T cell cultures. Here, RORγt inhibition suppressed the differentiation of Th17 cells, but not that of IFNγ-secreting Th1 cells and IL-4-producing Th2 cells (*Figure 6.1A and B*).

6.3.2 RORγt inhibition decreases Th17 responses during AIA

To evaluate whether RORγt inhibition reduced Th17 responses *in vivo*, WT mice were treated with 5 mg/kg of RORγt inhibitor for 10 days starting just prior to arthritis induction by intra-articular injection of mBSA on day 0. Treatment significantly reduced levels of IL-17A and IL-21 in $CD4^+$ T cells isolated from draining lymph nodes (*Figure 6.2A*). To verify these findings, cells isolated from the draining lymph nodes were re-stimulated *ex vivo* with mBSA. When compared to mice treated with the vehicle control, levels of mBSA-specific IL-17A in the culture medium was significantly reduced in mice treated with the RORγt inhibitor. A similar trend was also observed for mBSA-specific IFNγ responses, although not statistically significantly (*Figure 6.2B*).

The effect of RORγt inhibition on synovial Th17 responses was then determined. Expression of *Ccr6*, a chemokine receptor expressed on Th17 cells, and the Th17-associated effector cytokine, *Il22,* were significantly reduced in the synovium of mice treated with the RORγt inhibitor compared to vehicle. For the expression of the signature Th17 effector cytokines, *Il17a* and *Il17f*, a decreasing trend was observed albeit not statistically significant at the group sizes investigated (*Figure 6.3A*). Infiltrating synovial $CD4^+$ T cells were also extracted from the inflamed synovium. Interestingly, the number of $CD4^+$ T cells from vehicle and RORγt treatment groups were comparable (*Figure 6.3B*). However, the proportion of $CD4^+$ T cells secreting IL-17A was reduced following blockade of RORγt (*Figure 6.3C and D*). Thus, the inhibitor may affect T cell differentiation rather than proliferation. Taken together, this data highlights that RORγt inhibition during AIA inhibits the Th17 effector response.

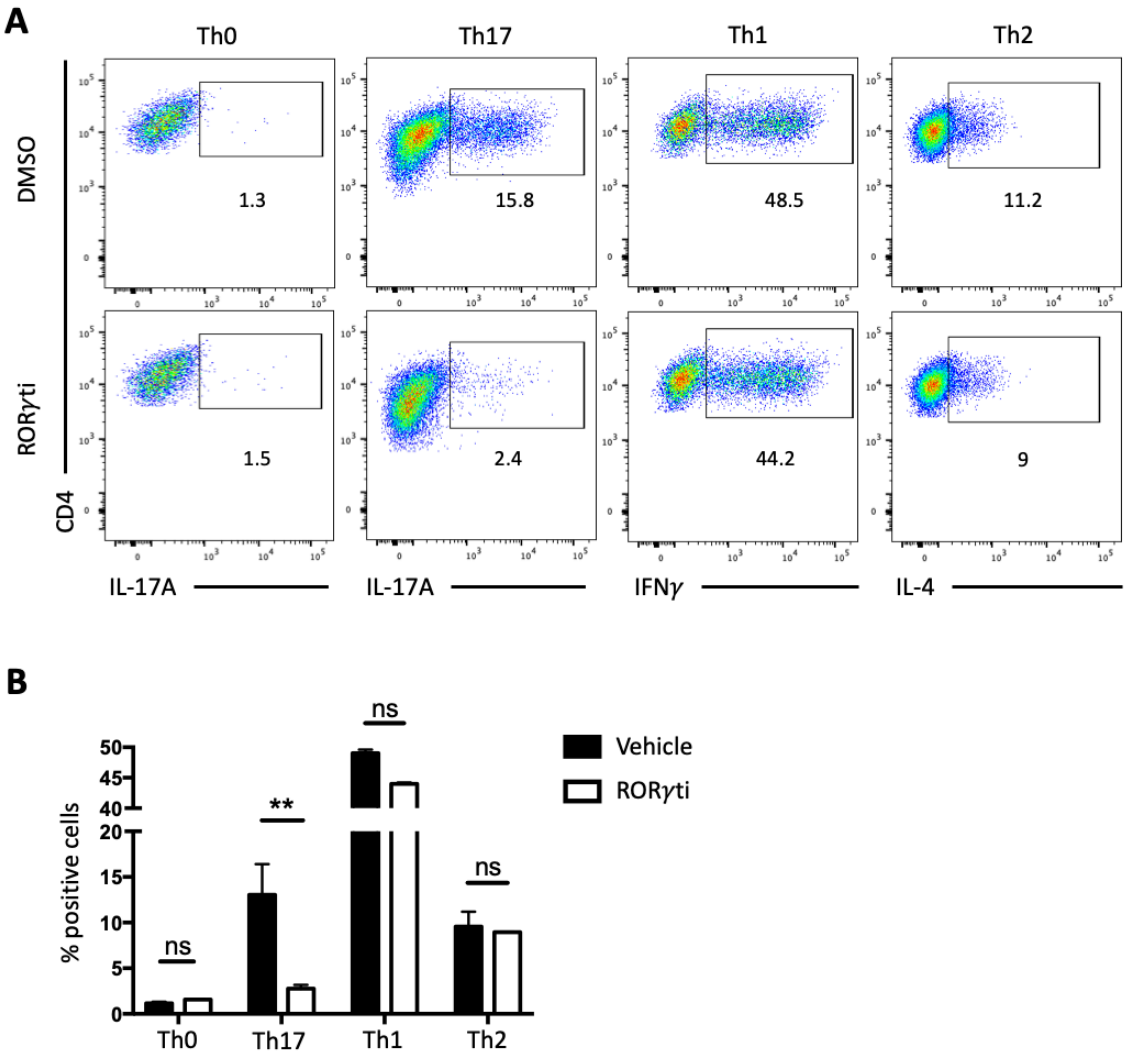

Figure 6.1 - RORγt inhibition specifically blocks Th17 cell differentiation. (A-B) Naïve CD4+ T cells cultured *in vitro* under polarizing conditions for Th17, Th1 and Th2 cells in the presence or absence of 1 μM RORγt inhibitor. (A) Representative flow cytometry plots and (B) percentage of cytokine-producing effector CD4+ T cells. (A-B) *n* = 3/group. Representative of two independent experiments. RORγti; RORγt inhibitor.

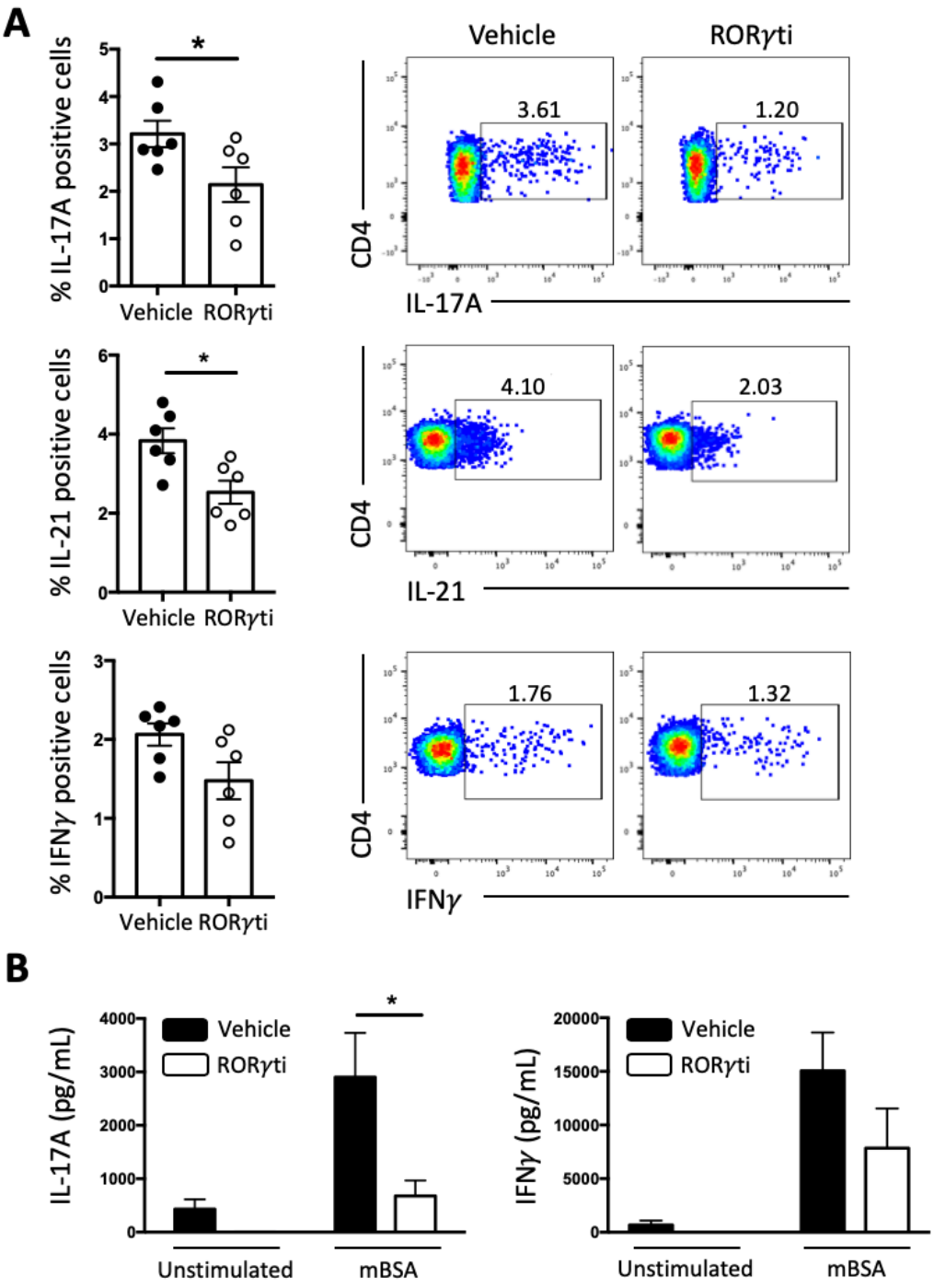

Figure 6.2 - Systemic effect of a RORγt inhibitor in AIA. (A-B) AIA was established in WT mice. Mice were treated with either vehicle (100 mM citrate buffer, pH2) or a RORγt inhibitor (5 mg/Kg) by oral gavage for 10 days, starting just prior to arthritis induction. (A) Flow cytometry of $CD4^+$ T cells in inguinal lymph nodes at day 10 of AIA. (B) Ex vivo re-stimulation of inguinal lymph nodes with 20 μg/ml mBSA for 72 hours. Levels of IL-17A and IFNγ were detected in culture supernatants by ELISA. (A-B) *n* = 6/group. RORγti; RORγt inhibitor.

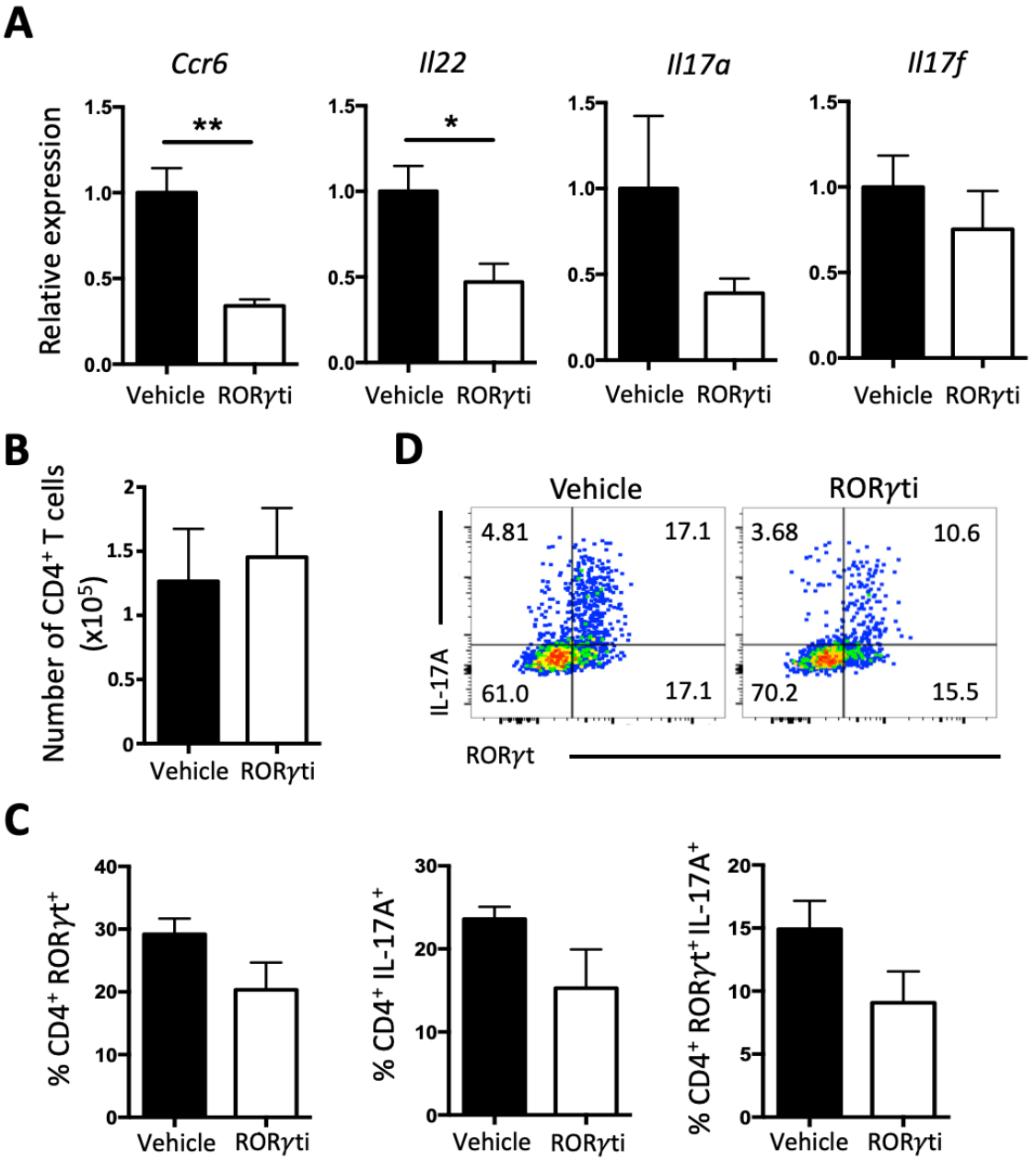

Figure 6.3 - The effect of a RORγt inhibitor on synovial T cell responses. (A-D) AIA was established in WT mice. Mice were treated with either vehicle (100 mM citrate buffer, pH2) or a RORγt inhibitor (5 mg/Kg) by oral gavage for 10 days, starting just prior to arthritis induction. (A) Relative expression of indicated genes in the synovium of vehicle and RORγt inhibitor treated mice at day 10 of AIA. (B-D) Synovium was digested in 1 mg/mL collagenase IV for 1 hour before staining for flow cytometry. (B) Number of $CD4^+$ T cells extracted from the synovium as determined by flow cytometry. The percentage (C) and representative flow cytometry plots (D) of $CD4^+RORγt^+$ cells, $CD4^+IL\text{-}17A^+$ and $CD4^+RORγt^+IL\text{-}17A^+$ cells extracted from the synovium at day 10 of AIA. (A) $n = 6$/group. (B-D) $n = 3$/group. (A) The expression of all genes has been made relative to an internal housekeeping control, *Actb*, and the expression of the vehicle set as 1. RORγti; RORγt inhibitor.

6.3.3 RORγt inhibition decreases arthritis severity

Th17 cells play a role in the pathogenesis of inflammatory arthritis. For example, IL-17A promotes expression of inflammatory cytokines (e.g. TNFα, IL-6), matrix metalloproteinases that contribute to cartilage degradation, and RANKL that is essential for the differentiation of osteoclasts and subsequent bone resorption [54, 317]. Thus, the effect of a reduced Th17 effector response, through RORγt inhibition, on the severity of arthritis was evaluated. Knee joints were scored for inflammatory infiltrate, exudate, pannus formation and cartilage and bone erosion (*Figure 6.4A and B*). In these pilot studies, treatment with the RORγt inhibitor resulted in a reduction in inflammatory infiltrate, exudate and cartilage and bone erosion. Concomitantly, there was also a reduction in the overall arthritic index (*Figure 6.4B*). However, at the group size investigated these decreases were not significant but provide rationale for a more comprehensive analysis of RORγt inhibition in AIA and particularly in the regulation of ELS in *Il27ra*$^{-/-}$ mice.

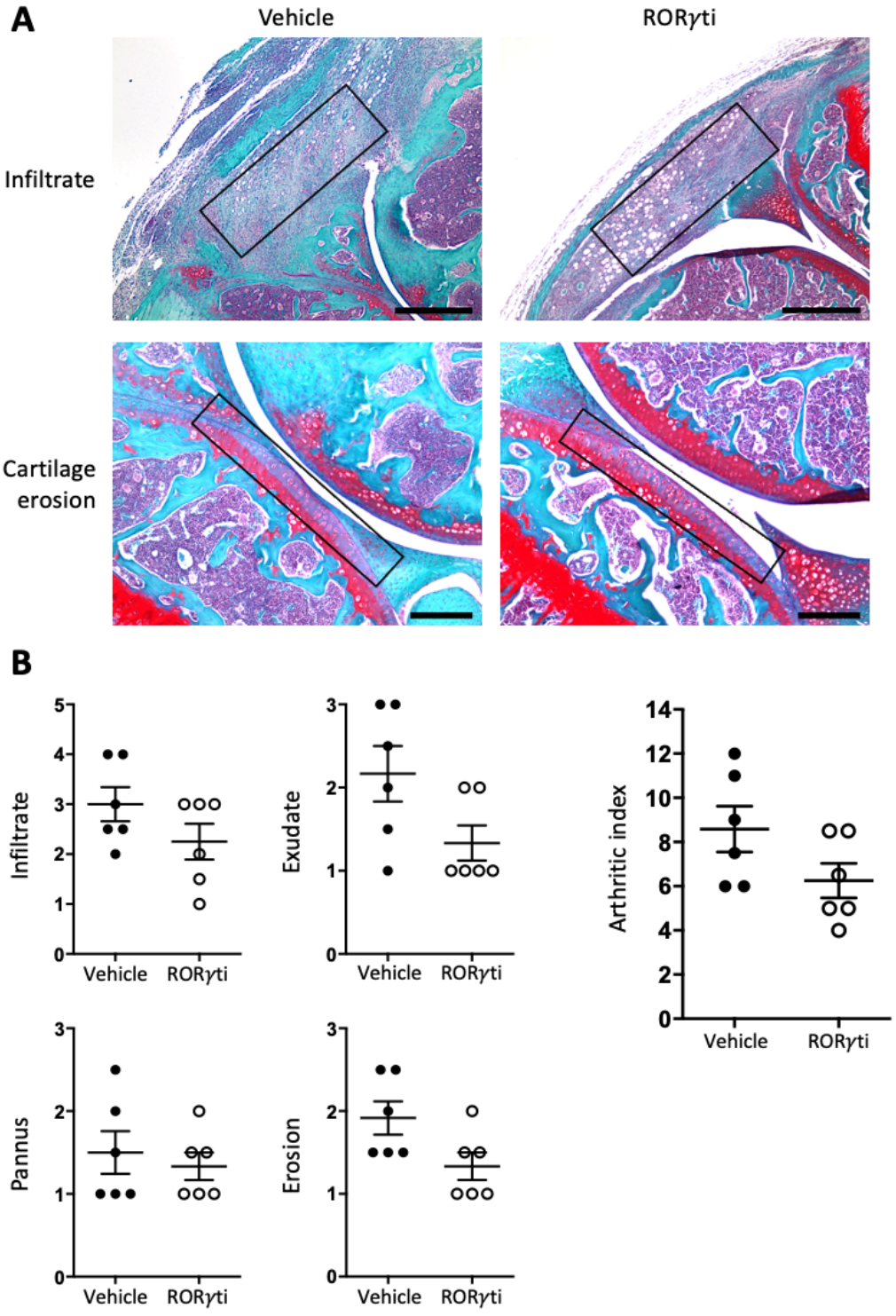

Figure 6.4 - The effect of RORγt inhibition during AIA. (A-B) AIA was established in WT mice. Mice were treated with either vehicle (100 mM citrate buffer, pH2) or a RORγt inhibitor (5 mg/Kg) by oral gavage for 10 days, starting just prior to arthritis induction. (A) Representative images of haematoxylin, fast green and safranin O staining of knee joints. Boxes highlight areas of synovial infiltrate (top) and cartilage and bone erosion (bottom), seen as the loss of safranin O staining, in vehicle and RORγt inhibitor treated mice. (B) Histopathology scoring of AIA in vehicle and RORγt inhibitor treated mice. Scale bars: (A; top) 500 μm, (A; bottom) 200 μm. (A) *n* = 6/group. (B-C) *n* = 3/group. RORγti; RORγt inhibitor.

6.4 Discussion

In this chapter, I present proof-of-concept studies using a RORγt inhibitor in WT mice during AIA. Consistent with the specific blockade of Th17 cell differentiation observed *in vitro,* treatment led to reduced expression of Th17 effector cytokines in both the draining lymph nodes and locally within the inflamed joint. This effect on Th17-associated cytokine production was associated with a reduction in arthritic index in mice treated with the RORγt inhibitor. These effects were seen in the small group sizes used and despite only starting administration just prior to arthritis induction, and thus at a point where the peripheral immune response to mBSA was established. Future experiments will determine the effect of RORγt inhibition on synovial ELS development in *Il27ra*$^{-/-}$ mice. For a comprehensive evaluation of the role of Th17 cells in the development of ELS, inhibitor dosing will be tested (i) during the priming phase of AIA in order to prevent the early formation of the Th17 cell response, and (ii) just prior to induction of local joint inflammation as performed herein. These studies will build on experiments performed in *Chapter 5* where a role for Th17/IL-17A was revealed in promoting tumour-associated ELS activity in a model of gastric cancer.

Since RORγt also controls thymocyte development and is required for LTi development and consequently SLO development, there is potential that blockade of RORγt could affect these important homeostatic functions. While short term inhibition of RORγt has been effective in the blockade of Th17-associated intestinal inflammation [318], in long term use the development of T cell lymphoma has emerged as a significant risk [316]. Here, 13-week treatment in rats was associated with thymic alterations that mirrored the phenotype observed in *Rorc* deficient mice [316]. Thus, the development of RORγt inhibitors therapeutically carries significant risk. However, the inhibitor used herein provides a useful mechanistic tool to explore the potential therapeutic effect of targeting the Th17 axis more broadly than typically explored through blockade of IL-17A and IL-17RA (e.g. secukinumab and brodalumab respectively).

Interestingly however, *Rorc*$^{-/-}$ mice still develop ELS, despite the lack of LTi cells and impairment of Th17 cell differentiation. Exposure to dextran sulphate sodium induced the formation of ELS in the colon of *Rorc*$^{-/-}$ mice [141]. Despite having defects in lymphatic vessel expansion, *Rorc*$^{-/-}$ mice developed normal ELS in a model of salivary gland inflammation with Sjögren's syndrome-like features [319]. Additionally, in response to influenza A virus infection, *Rorc*$^{-/-}$ mice developed iBALT, characterised by segregated T and B cell zones and CD21^{+} follicular dendritic cell networks [142]. However, the

development of iBALT was also found to be dependent on IL-17A production from γδ- and αβ T cells [142]. This may relate to the identification of another retinoic acid receptor related orphan receptor, RORα, that can drive the differentiation of Th17 cells [320]. Induction of EAE in *Rora* deficient mice resulted in decreased IL-17A production and severity of disease. Importantly, whilst *Rorc*$^{-/-}$ mice displayed a larger impairment in Th17 differentiation, it was only in mice with a double deficiency in RORγt and RORα that a complete abrogation of Th17 development was observed [320].

Recently, the homeostatic and pro-inflammatory roles of RORγt have been delineated. Two crucial amino acids were essential for determining the function of RORγt [321]. Mice that lacked RORγt but expressed a mutant form, lacking the two crucial amino acids, had normal thymic development but did not generate Th17 responses. In this regard, the mutant form of RORγt did not lead to the expression of genes for Th17 development (e.g. *Il17a*, *Il17f*, *Il23ra*) but did express genes required for thymic development (e.g. *Bcl2*, *Bcl2l1*). This altered mechanism of action was attributed to inhibition of ubiquitination of the mutant RORγt. Interestingly, mice expressing the mutant form of RORγt developed lymph nodes, associated with the development of LTi cells. However, they did not develop Peyer's patches [321]. This may highlight the different mechanisms required for SLO development and ELS development. Taken together, this may underline the potential to develop a therapy that exploits the inflammatory side of RORγt but not the homeostatic roles.

In summary, this chapter presents proof-of-concept studies of targeting RORγt in inflammatory arthritis. RORγt inhibition resulted in reduced levels of Th17 effector cytokines in the periphery and within the joint, and these early studies suggest a potential therapeutic effect when evaluating arthritis severity during AIA. Thus, future studies will more fully determine the effect of blocking RORγt during inflammatory arthritis, and extend to investigating the regulation of synovial ELS in *Il27ra*$^{-/-}$ mice that are associated with exacerbated Th17 responses.

Chapter 7. General Discussion

7.1 Discussion

ELS are a common feature of inflamed tissues affected by autoimmunity, infection, tissue rejection and cancer. The mechanisms controlling ELS development and activity are likely to be highly disease and context dependent; our understanding of how ELS are controlled in different inflammatory settings remain poorly defined. Research presented in this thesis investigated the major inflammatory pathways linked with synovial ELS development during experimental inflammatory arthritis. The significance of these pathways in ELS regulation were further investigated in inflammation-associated gastric cancer, where tumourigenesis and ectopic lymphoid neogenesis were temporally coupled. In summary, the data presented in this thesis propose common mechanisms that govern ELS development across inflammatory arthritis and gastric cancer.

- Through the use of transcriptomics, a prominent Th17 gene signature was associated with the development of synovial ELS in a mouse model of inflammatory arthritis.
- The characterisation of ELS in a model of STAT3-driven gastric cancer provides a novel system for the mechanistic evaluation of tumour-associated ELS.
- The genetic ablation of IL-17A in *gp130*$^{F/F}$ mice revealed an important role for IL-17A in supporting the development of active ELS.

Thus, this work provides new insights into the role of the Th17/IL-17A axis in ELS development and maintenance in models of inflammatory arthritis and gastric cancer.

7.2 Cross-disease mechanisms governing ELS

The work presented in this thesis has used mouse models of inflammatory arthritis and gastric cancer where ELS feature. Interestingly, tumour-associated ELS in *gp130*$^{F/F}$ mice were larger in size and displayed increased levels of organisation, such as T and B cell segregation, than those present in the synovium of *Il27ra*$^{-/-}$ mice. This may relate to development of ELS in *gp130*$^{F/F}$ mice at mucosal surfaces, whereas the synovium is devoid of epithelial surfaces. Consistent with this, ELS that form in the joints of patients with RA range from disorganised aggregates to highly-segregated lymphoid follicles [193]. Nonetheless, the work presented here has allowed the identification of cross-disease mechanisms that regulate ELS.

7.2.1 The Th17/IL-17A axis and ELS

In *Chapter 4*, transcriptomic profiling of the inflamed synovium identified a strong Th17 signature that was linked with the development of synovial ELS during inflammatory arthritis. Interestingly, effector Th17 responses have been linked with ELS development in other chronic inflammatory models. For example, in EAE, podoplanin-expressing Th17 cells contributed to ELS development. This was dependent on the Th17 signature cytokine, IL-17, but not IL-21 [143]. Additionally, IL-17 has been implicated in the development of iBALT. In response to challenge with LPS, iBALT development was dependent on IL-17, with *Il17ra*$^{-/-}$ mice displaying reduced expression of CXCL13 and CCL19 [142]. Interestingly, despite the requirement for IL-17, ELS still developed in *Rorc*$^{-/-}$ mice [142]. Whilst $\gamma\delta$ T cells were detected in iBALT, the majority of IL-17 secreting cells were T helper cells [142]. In this regard, my analysis of joint-infiltrating cells during AIA similarly revealed that CD4^{+} T cells were the main IL-17-producing population. In other models of iBALT development the role of IL-17 is less clear. Following infection with a modified vaccinia virus Ankara the development of iBALT was unaffected in the absence of IL-17 [144]. However, in response to challenge with *Pseudomonas aeruginosa* the development of iBALT was impaired in the absence of IL-17. Here, IL-17 was required to induce CXCL12 expression in pulmonary stromal cells [144]. In our studies, *Il17a* expression was also increased in a model of Helicobacter infection-induced gastritis that was associated with the development of ELS. Here, the presence of ELS and *Il17a* expression was associated with heightened expression of the homeostatic chemokines *Cxcl13* and *Ccl19* [304]. In *gp130*$^{F/F}$ mice, gastric tumourigenesis was similarly associated with an increase in the Th17 markers, *Il17a*, *Il23* and *Rorc* [249], and expression of *IL17A* in clinical disease correlated with the

homeostatic chemokines, *CXCL13* and *CCL19.* Despite this, the genetic ablation of IL-17A in *gp130*$^{F/F}$ mice had little impact on gastric tumourigenesis, with no difference in tumour burden between *gp130*$^{F/F}$ and *gp130*$^{F/F}$:*Il17a*$^{-/-}$ mice [249], or the development of submucosal lymphoid aggregates. These aggregates contained typical features of ELS including CXCL13-expressing cells, PNAd^{+} HEVs and podoplanin-expressing stromal cells. While not statistically significant, we noted slightly fewer and smaller lymphoid aggregates in *gp130*$^{F/F}$:*Il17a*$^{-/-}$ mice as compared to those in *gp130*$^{F/F}$ mice. We therefore questioned whether IL-17A may be important for ELS maturation. Consistent with this hypothesis, lymphoid aggregates in *gp130*$^{F/F}$:*Il17a*$^{-/-}$ mice lacked CD21^{+} follicular dendritic cell networks and germinal centres. Thus, this suggests that IL-17A is not required for the early formation of lymphoid aggregates, but promotes the maturation of functional ELS displaying germinal centre reactivity.

While IL-17A is the signature cytokine for Th17 cells, these cells can also produce IL-21 and IL-22, which have been linked with ELS development in a model of virus-induced sialadenitis with Sjögren's syndrome-like characteristics [145, 147]. Here, IL-22 induced the expression of *Cxcl13* and *Cxcl12* from stromal and epithelial cells respectively. In the absence of IL-22, lymphoid aggregates were significantly smaller and had decreased expression of *Cxcl13* and *Cxcl12* [145]. Similar to the development of iBALT and synovial ELS, both $\gamma\delta$ T cells and T helper cells contributed to IL-22 production. Initially, the majority of IL-22 expression in the salivary gland was from $\gamma\delta$ T cells, however this was later replaced by T helper cells [145]. Thus, effector cytokines often linked with Th17-type responses have been implicated in regulating ELS development and maintenance in models of autoimmunity, cancer and infection (*Figure 7.1*).

7.2.2 STAT3 regulation of ELS

Cytokines that activate STAT3 have been linked with ELS development in multiple diseases that feature chronic inflammation [145, 147, 302, 303]. For example, IL-6 signalling through the IL-6R/gp130 complex results in STAT3 activation and the development of ELS in the lung [302]. While IL-27 can activate both STAT3 and STAT1, it uniquely activates a group of STAT1 target genes to exert anti-inflammatory outcomes in adaptive immunity [93]. For example, IL-27 through STAT1 signalling can counteract IL-6/STAT3 driven responses [91] and can suppress the development of Th17 cells [279] and ELS [146, 152]. In inflammatory arthritis, STAT3 activation controls the recruitment and maintenance of activated leukocytes within the inflamed synovium and leads to increased disease severity. Here, the induction of AIA in *gp130*$^{F/F}$ mice, that display hyperactive STAT3 signalling, resulted in increased synovitis that was associated with an elevation in the number of IL-17A-secreting cells within the joint [69]. Similarly, hyperactive STAT3 signalling in *gp130*$^{Y759F/Y759F}$ mice results in the spontaneous development of arthritis [71, 322]. Using GSEA and publicly available datasets that defined STAT3-regulated genes, a robust STAT3 signature was associated with ELS-rich joint inflammation in *Il27ra*$^{-/-}$ mice. This is consistent with a previous study that linked the presence of synovial ELS with enhanced STAT3 activity [291]. In *gp130*$^{F/F}$ mice, gastric tumourigenesis and submucosal ELS development is triggered by IL-11 signalling through the IL-11Rα/gp130 complex to activate STAT3 [219-221]. Here, expression of the prototypical STAT3 target gene, *SOCS3*, also correlated with the expression of ELS-associated genes. Importantly, 'normalisation' of STAT3 activation in *gp130*$^{F/F}$:*Stat3*$^{+/-}$ mice prevented both gastric tumourigenesis and ELS development. Indeed, phosphorylated STAT3 was detected in lymphoid aggregates in *gp130*$^{F/F}$ mice, however STAT3 activity was also found in areas of diffuse lymphocyte infiltration. Similarly, in previous studies from my laboratory, significant phosphorylated-STAT3 staining was found within the joint, but not exclusively restricted to synovial ELS [146]. More recently, a study in mice showed that a haploinsufficiency of the *Ptpn2* gene was associated with the pathogenic conversion of Treg cells into Th17 cells during inflammatory arthritis, where exacerbated synovitis was also linked with heightened STAT3 activity and the development of ELS [323]. Therefore, while STAT3 activity is strongly linked with shaping a microenvironment within inflamed tissues that is conducive to ELS development, localised STAT3 activity is not specifically restricted to ELS, likely due to its broad roles in orchestrating inflammation.

7.2.3 An inhibitory role for IL-27 in ELS regulation

While studies presented within this thesis propose common mechanisms that influence ELS development, it is likely that there are disease-specific mechanisms that govern the control of ELS that are not shared. In this regard, my research in inflammatory arthritis and inflammation-associated gastric cancer potentially outline a context dependent role for IL-27 in ELS regulation. For example, ELS development in the inflamed synovium was associated with a loss of IL-27/IL-27R signalling [146]. However, the development of tumour-associated ELS in gastric cancer was not linked to a loss of *Il27* expression. Here, *Il27* expression in the gastric antrum was comparable between 6-month-old WT and *gp130*$^{F/F}$ mice. However, early expression of IL-27 may control ELS development in *gp130*$^{F/F}$ mice. As such, further investigations are required to understand the precise role of IL-27 in tumour-associated ELS formation. This would establish whether IL-27 administration can inhibit tumour-associated ELS formation, or if IL-27 blockade has potential to support the development and activity of ELS. However, divergent roles have been described for IL-27 in cancer. For example, IL-27 has been linked with promoting anti-tumour immunity through supporting $CD8^+$ and natural killer cell activity [324-327]. Paradoxically, IL-27 promotes an immunoregulatory phenotype in T cells through inducing the expression of co-inhibitory receptors (e.g. PD-1, PD-L1, TIM-3, LAG-3, TIGIT) that suppress anti-tumour immunity [115, 328]. Thus, a better appreciation of the role of IL-27 in cancer has potential to inform of its therapeutic credentials.

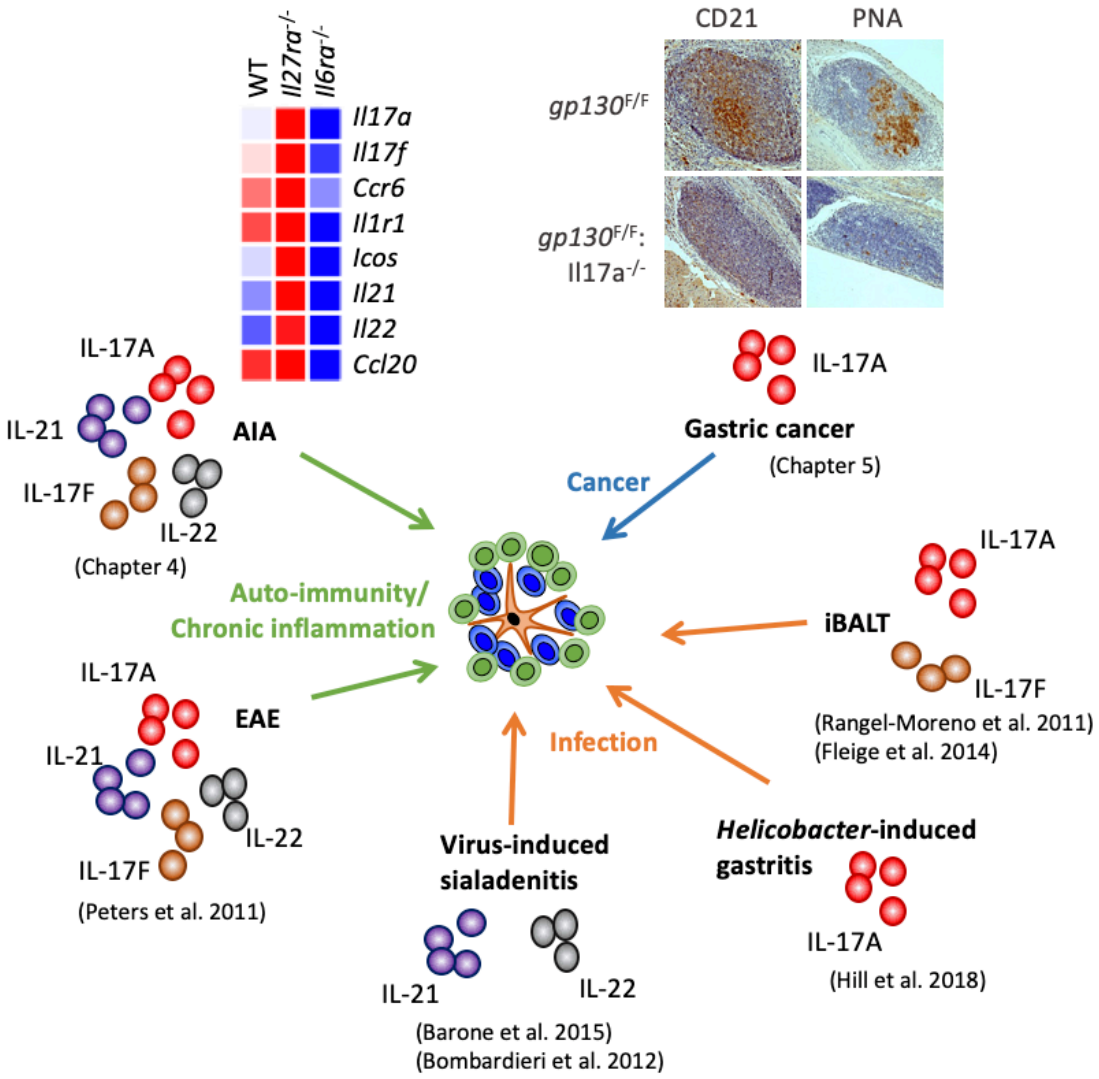

Figure 7.1 - The role of Th17 cells in ELS development, maintenance and activity. Th17 cells and effector cytokines have been implicated in ELS development, maintenance or activity in models of autoimmunity and chronic inflammation (green), infection (orange) and cancer (blue). The cytokines implicated in each inflammatory model are shown. AIA, antigen-induced arthritis; EAE, experimental autoimmune encephalomyelitis; iBALT, inducible bronchus associated lymphoid tissue.

7.3 Tumour-associated ELS and anti-tumour immunity

In *Chapter 5*, I characterised the development of tumour-associated ELS in *gp130*$^{F/F}$ mice that spontaneously develop gastric tumours. ELS were defined as having T and B cell segregation, PNAd^{+} HEVs, CD21^{+} follicular dendritic cell networks, germinal centre reactions and increased expression of homeostatic chemokines. In our study of ELS in gastric cancer, an ELS gene signature composed of *CXCL13, CCL21* and *CCL19* did not predict a favourable prognosis. However, an important question remains: *Do ELS in gastric cancer support anti-tumour immune responses?* In this context, in NSCLC, tumour-associated ELS were surrounded by CD138-positive plasma cells that secreted antibodies against tumour antigens (e.g. NY-ESO-1, TP53, LAGE-1). Furthermore, a high density of follicular B cells correlated with improved patient survival [233]. Additionally, patients with NSCLC that developed ELS had a higher number of cytotoxic IFNγ-generating CD8^{+} T cells. Interestingly, patients with a combination of high levels of CD8^{+} T cells with the presence of ELS displayed significantly improved survival compared to patients with high levels of CD8^{+} T cells in the absence of ELS [241]. Together, these studies suggest that tumour-associated ELS can play an active role in supporting anti-tumour immunity. Consistent with this, targeted delivery of the cytokine LIGHT (TNFSF14), a LTβR ligand, to tumours using a vascular targeting peptide (VTP) promoted the formation of ELS, increased tumour infiltration by T cells and improved survival. However, administration of blocking antibodies to CD8 abolished the survival benefit of LIGHT-VTP treatment [238]. Thus, these studies suggest that ELS can serve as local sites for the generation of antibodies against tumour antigens and can re-model T cell responses to enhance anti-tumour immunity.

Interestingly, *gp130*$^{F/F}$ mice that lacked expression of IL-17A developed lymphoid aggregates, but did not form germinal centres. Despite this defect in ELS activity, *gp130*$^{F/F}$:*Il17a*$^{-/-}$ mice display a similar tumour burden to *gp130*$^{F/F}$ mice [249] and expression of *IL17A* had no prognostic significance when evaluating intestinal-type gastric cancer datasets in TCGA. In this regard and as previously discussed, a more comprehensive Th17 signature may have more prognostic value (*see Chapter 5 discussion*). However, due to the reciprocal relationship between Th17 and Treg development it would be interesting to determine whether tumour-associated ELS in the gastric submucosa are enriched in Tregs that may suppress anti-tumour immunity. In this regard, a better understanding of the cellular composition and effector characteristics associated with tumour-associated ELS may provide opportunities to modulate ELS

activity through targeting defined T cell effector characteristics. In other studies of clinical gastric cancer, the presence of $CD20^+$ aggregates, a high infiltration of T-bet^+ Th1 cells and a low infiltration of $FoxP3^+$ Treg cells correlated with improved survival [305]. In patients with primary breast tumours, high numbers of $FoxP3^+$ Treg cells within ELS were associated with an increased risk of death [242]. Additionally, in a mouse model of lung adenocarcinoma, Tregs localised to tumour-associated ELS to suppress anti-tumour responses. In the same study, Treg depletion resulted in T cell proliferation within ELS and the generation of anti-tumour responses leading to tumour regression [243]. Furthermore, Treg depletion in a methylcholanthrene (MCA) carcinogen-induced fibrosarcoma mouse model resulted in HEV neogenesis and increased tumour-infiltrating T cells, resulting in a reduction in tumour growth rate [298]. The role of Tregs in regulating ELS is not restricted to cancer. For example, in a model of LPS-induced iBALT, Treg depletion resulted in increased incidence and number of iBALT [149]. Furthermore, mice deficient in CCR7 had reduced Treg cell numbers and spontaneously developed iBALT, characterised by segregated T and B cell zones and HEVs [329]. Additionally, GSEA in *Chapter 4* identified an enriched Th17 signature compared to Treg signature in synovial inflammation featuring ELS. Thus, analysis of Treg cells and T cell effector characteristics in *gp130*$^{F/F}$ mice may elucidate the role that ELS play in anti-tumour immunity in these mice.

7.4 Potential for therapeutically targeting ELS

The results presented in this thesis provide rationale for targeting the Th17/IL-17A axis in ELS-associated diseases. For example, inhibiting this pathway may be beneficial in chronic autoimmune diseases (*Figure 7.2*), whereas propagating Th17 cell responses may drive ELS function and germinal centre formation in cancer that could re-model T cell responses and promote anti-tumour immunity.

In this regard, IL-17 blockade using anti-IL-17A and anti-IL-17RA monoclonal antibodies (e.g., secukinumab and brodalumab respectively) has already been trialled in RA. For example, a phase II clinical trial of 237 patients displaying inadequate responses to methotrexate, showed that a monthly subcutaneous injection of secukinumab failed to improve clinical outcome and the study did not reach its primary endpoint - the proportion of patients achieving ACR20 versus placebo at 16 weeks [330]. Long term, 52-week studies showed that IL-17 blockade was well tolerated and gave improved ACR and DAS28 responses and decreased CRP levels. However, non-responders at 16 weeks still did not respond with longer treatment [331]. Similar results were obtained in clinical trials with brodalumab. Here, a total of 252 patients with active RA and inadequate responses to methotrexate failed to reach significant differences in ACR20 responses compared to placebo [332]. Thus, anti-IL-17A/IL-17RA therapy has already been trialled in RA with limited success. However, these trials were not conducted in patients stratified according to histological presentation of disease. In this context, results presented in *Chapter 4* highlighted an enriched Th17 signature in synovial inflammation featuring ELS. Similarly, RA patients stratified for the presence of ELS had increased levels of IL-17A compared to those without ELS [146]. Therefore, targeting of IL-17A may be more effective in ELS-positive patients.

However, other Th17 effector cytokines are also associated with ELS formation. In RA cohorts stratified for the presence of ELS, featuring T and B cell segregation and CD21L expression, the Th17 effector cytokines *IL17F*, *IL21* and *IL22* were increased in ELS-positive patients and correlated with *CD21L* expression [333]. However, no relationship was observed between the expression of *IL17A* and the presence of ELS [333]. Similarly, synovial IL-23 expression and levels of the Th17-associated chemoattractant, CCL20, were linked with the clinical presence of ELS in psoriatic arthritis [334]. This provides rationale for testing the neutralisation of other cytokines linked with the Th17 effector response in ELS-rich synovitis. In this regard, clinical trials in RA patients with guselkumab, a monoclonal antibody against the p19 subunit of IL-23, failed to reach

significant differences in ACR20 responses compared to placebo [335]. Importantly, these trials were also not conducted in patients stratified according to histological presentation of disease. As discussed above, targeting of the Th17 axis may be more beneficial in ELS-positive patients. It may also be interesting to investigate the broader inhibition of the Th17 programme in ELS-rich synovitis. For example, targeting of Th17 cells with small molecule RORγt inhibitors may prove beneficial, although a long-term safety evaluation of this approach is required given the link to potential adverse side effects, including T cell lymphoma [316].

Other inhibitors that may prove effective in targeting Th17 responses are JAK inhibitors. For example, tofacitinib, that predominantly targets JAK1 and JAK3 to disrupt JAK-STAT signalling in response to interferons, γ-chain family cytokines (e.g. IL-2, IL-7, IL-15, IL-21) and gp130 family cytokines (e.g. IL-6, IL-11). Other JAK inhibitors licensed for the treatment of RA include ruxolitinib and baracitinib that target JAK1 and JAK2 [178, 336]. The development of Th17 cells is dependent on IL-6 signalling through STAT3, and STAT3 deficiency in T cells prevents the induction of Th17 cells [20, 337]. Additionally, hyperactivation of STAT3 in *gp130*$^{F/F}$ mice results in exacerbated synovitis that was associated with an increase in the number of IL-17A-secreting cells within the joint [69]. The activation of STAT3 is also emerging as a common feature of ELS development. The cytokines, IL-6, IL-21 and IL-22, that activate STAT3 have all been linked with ELS development and maintenance in inflammatory models [145, 147, 302, 303] and in RA synovial tissue, the presence of ELS was linked to enhanced STAT3 activation [291]. Furthermore, the data presented in this thesis identified a STAT3 signature in ELS-rich synovitis and IL-11 activation of STAT3 in *gp130*$^{F/F}$ mice resulted in gastric tumourigenesis and tumour-associated ELS development. Importantly, 'normalisation' of STAT3 in *gp130*$^{F/F}$:*Stat3*$^{+/-}$ mice prevented both gastric tumourigenesis and ELS development. Thus, the use of JAK inhibitors to disrupt JAK-STAT signalling could be an attractive approach to targeting ELS. However, JAK inhibitors may also have the potential to block IL-27 signalling, thus promoting the development of ELS.

An important point to consider is that clinically patients will likely have developed ELS before treatment begins. Therefore, *is there any benefit in targeting mechanisms of ELS development?* For example, in a model of LPS-induced iBALT, *Il17a*$^{-/-}$ mice failed to develop iBALT. It follows that mice failed to develop iBALT in this model when treated with an antibody to IL-17A at the same time as the final challenge with LPS. However, when administered 1 week later, once iBALT had developed, anti-IL-17A had little effect

on iBALT [142]. In this regard, IL-17A was involved in the initiation but not the maintenance of iBALT and highlights that anti-IL-17A therapy once iBALT had developed was ineffective. However, the role of IL-17A in ELS development is likely to be disease and context dependent. For example, in *Chapter 5*, IL-17A was shown to be important for the maintenance of germinal centres in tumour-associated ELS rather than their development. Thus, targeting IL-17A may still affect the function of ELS.

Whilst IL-17A is required for the development of mature tumour-associated ELS, as evidenced by a lack of germinal centres in the lymphoid aggregates that form in *gp130*$^{F/F}$:*Il17a*$^{-/-}$ mice, other Th17 effector cytokines such as IL-21 and IL-22 have also been linked with ELS development [145, 147]. In this regard, it would be interesting to evaluate the role of other cytokines within the Th17 programme in ELS development during gastric tumourigenesis. Here, the assessment of ELS in *gp130*$^{F/F}$:*Il6*$^{-/-}$ mice may be beneficial, where the loss of IL-6 signalling is associated with reduced expression of *Il17a, Il23,* and *Rorc* in gastric tumours [249]. Interestingly *gp130*$^{F/F}$:*Il6*$^{-/-}$ mice still develop gastric tumours comparable to those in *gp130*$^{F/F}$ mice and immune cell infiltrates within the gastric submucosa [220]. However, it remains to be determined whether *bona fide* ELS featuring germinal centres can form in the absence of IL-6.

Since it is proposed that tumour-associated ELS are able to act as local sites for establishing anti-tumour immunity, propagating their activity may provide therapeutic benefit. In this context, propagating Th17 cell responses may drive ELS function and germinal centre formation promoting local anti-tumour immunity. However, the role of Th17 cells in tumourigenesis is complex [338]. For example, IL-17A can induce angiogenesis in tumour tissue and the production of IL-17 by Th17 cells in a mouse model of lung cancer promoted tumour growth [339]. In contrast, the adoptive transfer of Th17 cells reduced tumour growth in a mouse melanoma model, which was associated with the activation of CD8^{+} T cells required for anti-tumour immunity [340]. Thus, Th17 effector responses have both pro- and anti-tumour effects. Therefore, given the inhibitory role of IL-27 on ELS development in arthritis [146], blockade of IL-27 may offer an interesting opportunity to promote ELS development in cancer.

Additionally, enhancing the development of tumour-associated ELS may also offer therapeutic opportunities in cancer. For example, administration of LIGHT-VTP to tumours resulted in intra-tumoural ELS formation, enhanced T cell tumour infiltration and improved survival [238]. In addition, in a lung cancer transplantation model that was unresponsive to checkpoint inhibitor therapy with anti-CTLA4 and anti-PD-1, treatment

with LIGHT-VTP in combination with checkpoint inhibitor therapy resulted in prolonged survival [238]. Thus, ELS immunomodulation may represent attractive therapeutic targets in autoimmunity and cancer.

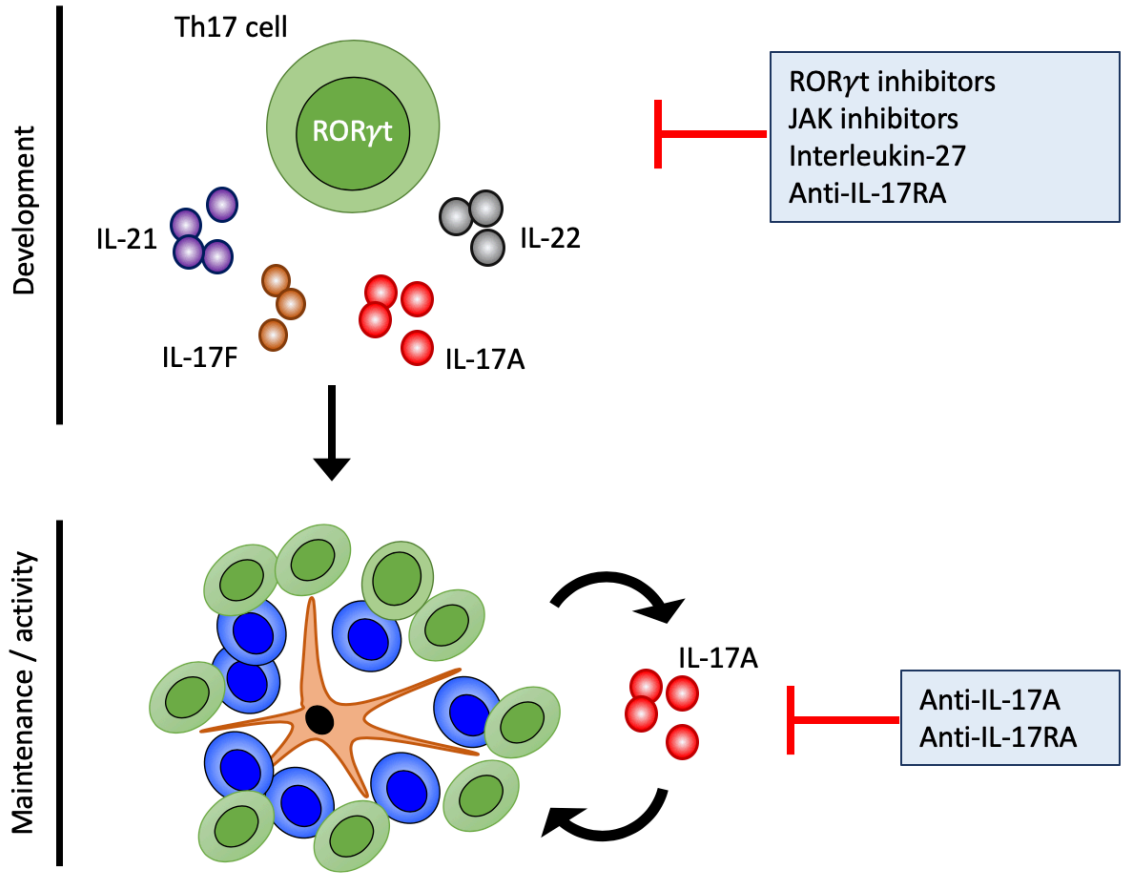

Figure 7.2 - Mechanisms for targeting Th17 cell involvement in ELS development, maintenance or activity in autoimmunity. Th17 cells and their effector cytokines are implicated in ELS development, maintenance and activity. Potential inhibition of Th17 cells could be through targeting RORγt, the master transcriptional regulator of Th17 cells, the use of JAK inhibitors, that disrupt the JAK-STAT signalling pathway or administration of interleukin-27. The targeting of IL-17A, may disrupt the development of ELS or germinal centre function. Blockade of IL-17 receptor (IL-17RA) will inhibit both IL-17A and IL-17F and therefore may have broader action.

7.5 Future perspectives

7.5.1 Th17 cell plasticity and ELS

Th17 effector cells are highly susceptible to functional plasticity. As previously discussed, Th17 cells can adopt Th1-like characteristics that have been shown to contribute to disease severity in EAE, as well as a Tfh-like phenotype that supports germinal centre B cells in Peyer's patches (*see Chapter 4 discussion*). Indeed, polyfunctional ex-Th17 cells (also called nonclassical Th1 cells) that no longer secrete IL-17 but produce other proinflammatory cytokines have now been isolated from the synovium of RA patients [295]. Furthermore, GSEA identified a pathogenic Th17 phenotype in ELS-rich synovitis. Given that IFNγ-secreting Th1 cells produced *Cxcl13*, it would be interesting to identify whether pathogenic Th17 cells, that adopt Th1-like characteristics (e.g., *Tbx21*) also produce CXCL13 contributing to ELS development. Whilst these examples highlight the plasticity of Th17 cells in driving inflammation, Th17 cells have also been shown to adopt anti-inflammatory phenotypes [283]. Using IL-17A fate reporter mice, Th17 cells in the intestine were found to adopt a T regulatory type 1 (Tr1)-like phenotype and secrete IL-10. Furthermore, the adoptive transfer of Tr1-like exTh17 cells prevented the development of colitis in a Th17 cell mediated colitis model [283]. Thus, understanding the mechanisms of Th17 plasticity may allow their immunomodulation into anti-inflammatory phenotypes to provide therapeutic benefit.

7.5.2 ELS composition and single-cell RNA-seq

As discussed in *section 7.3*, a better understanding of the cellular composition and effector characteristics associated with ELS may provide opportunities to modulate their activity through targeting defined T cell effector characteristics. While a whole-tissue RNA-seq approach was taken here, advances in sequencing technologies such as single-cell RNA-seq could provide more information regarding ELS composition and regulation. In this regard, single-cell transcriptome profiling of synovial tissue has been used to identify cellular subpopulations present in RA [341]. Thus, single-cell RNA-seq could allow analysis of the cellular composition of ELS as well as the effector characteristics of those cells that reside within ELS. In this regard, use of single-cell RNA-seq to compare ELS across different diseases has the potential of identifying differences in the composition and effector characteristics linked with ELS in autoimmunity and cancer.

7.5.3 Identifying the antigen required to promote ELS

The work presented here has focussed on the modulation of inflammation with regards to ELS development. However, other groups are investigating the antigen required to promote ELS. In this regard, studies of tumour-associated ELS have identified CD138-positive plasma cells that secreted antibodies against tumour antigens (e.g. NY-ESO-1, TP53, LAGE-1) [233]. Additionally, single cell cloning and the generation of recombinant antibodies from synovial B cells recovered from ELS^+ RA patients has uncovered autoantibody specificity to citrullinated histones, mainly H2A and H2B as well as citrullinated vimentin, fibrinogen and calreticulin [342, 343]. Therefore, while targeting inflammatory pathways associated with ELS development is an attractive approach being investigated for the modulation of ELS, knowing more about how antigens shape the inflammatory response and the development of ELS is similarly important. Key questions that remain unanswered include: *do ELS persist when antigen is present, but then resolve when the antigen is cleared?* In this regard, mBSA antigen-induced arthritis and many other inflammatory models featuring ELS are resolving models, where the regression of ELS coincides with the resolution of inflammation.

7.5.4 Immunometabolism and ELS

Whilst there is currently a limited understanding in how immunometabolism regulates ELS, it is an emerging area of interest. As previously discussed, expression of *SLC5A12*, a co-transporter for lactate expressed on $CD4^+$ T cells correlated with synovial tissue T cell score and the presence of ELS [288, 344] (*see Chapter 4 discussion*). In my RNA-seq dataset, *Cd5l*, which is a novel regulator of cholesterol and fatty acid metabolism that alters RORγt activity and Th17 pathogenicity [278], was differentially regulated in ELS-rich synovitis. Recently, studies have also linked N-myristoyltransferase (NMT) activity with altering Th17 responses in arthritis through regulating AMP kinase activity [345]. Here, T cells from RA patients had decreased levels of NMT compared to healthy controls. Interestingly, overexpression of NMT in RA T cells reduced expression of *RORC* and *IL17A* [345]. Thus, modulation of metabolic pathways has the potential to effect Th17 responses and ELS activity.

Chapter 8. Appendix

8.1 Isotype controls

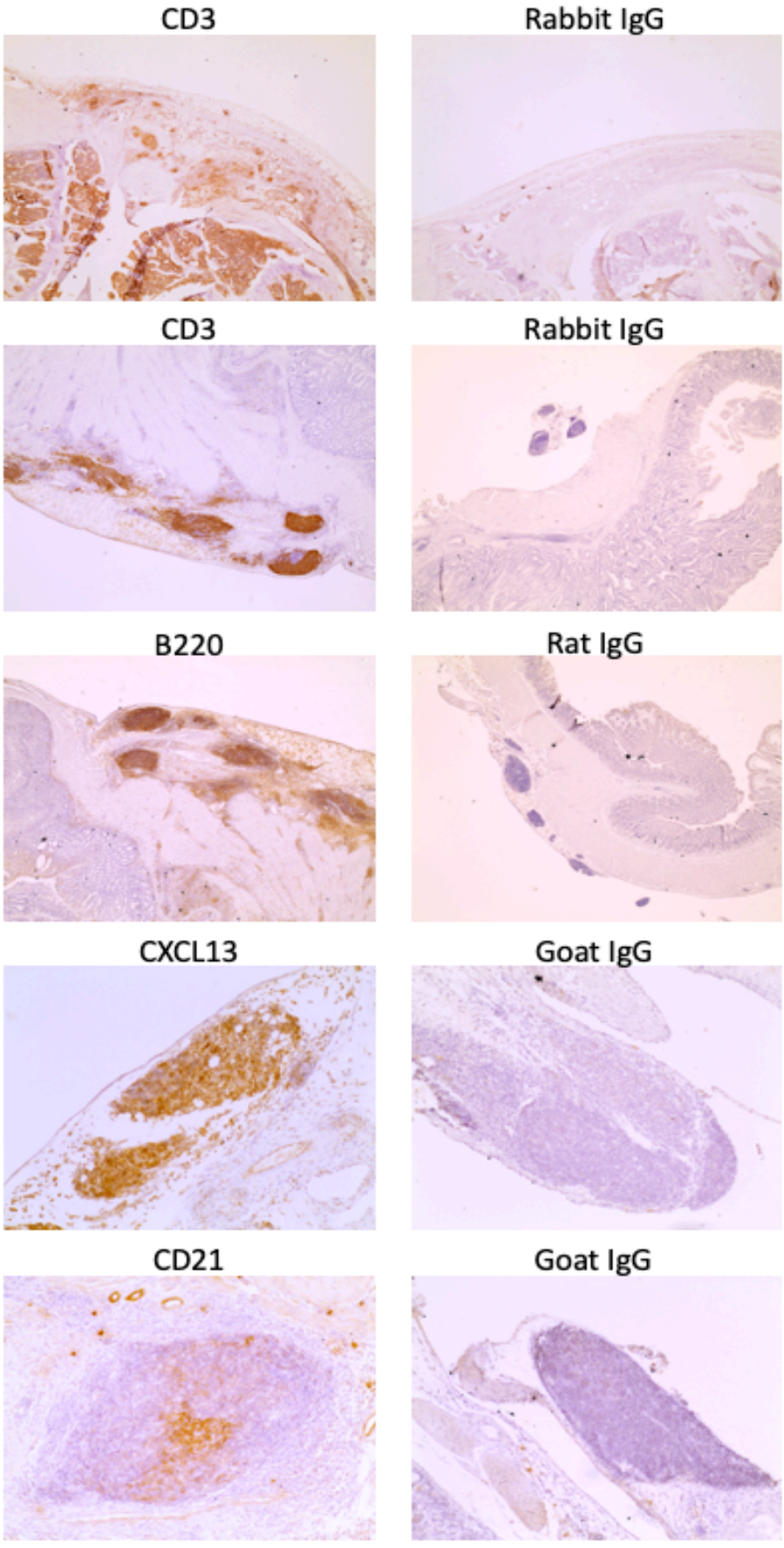

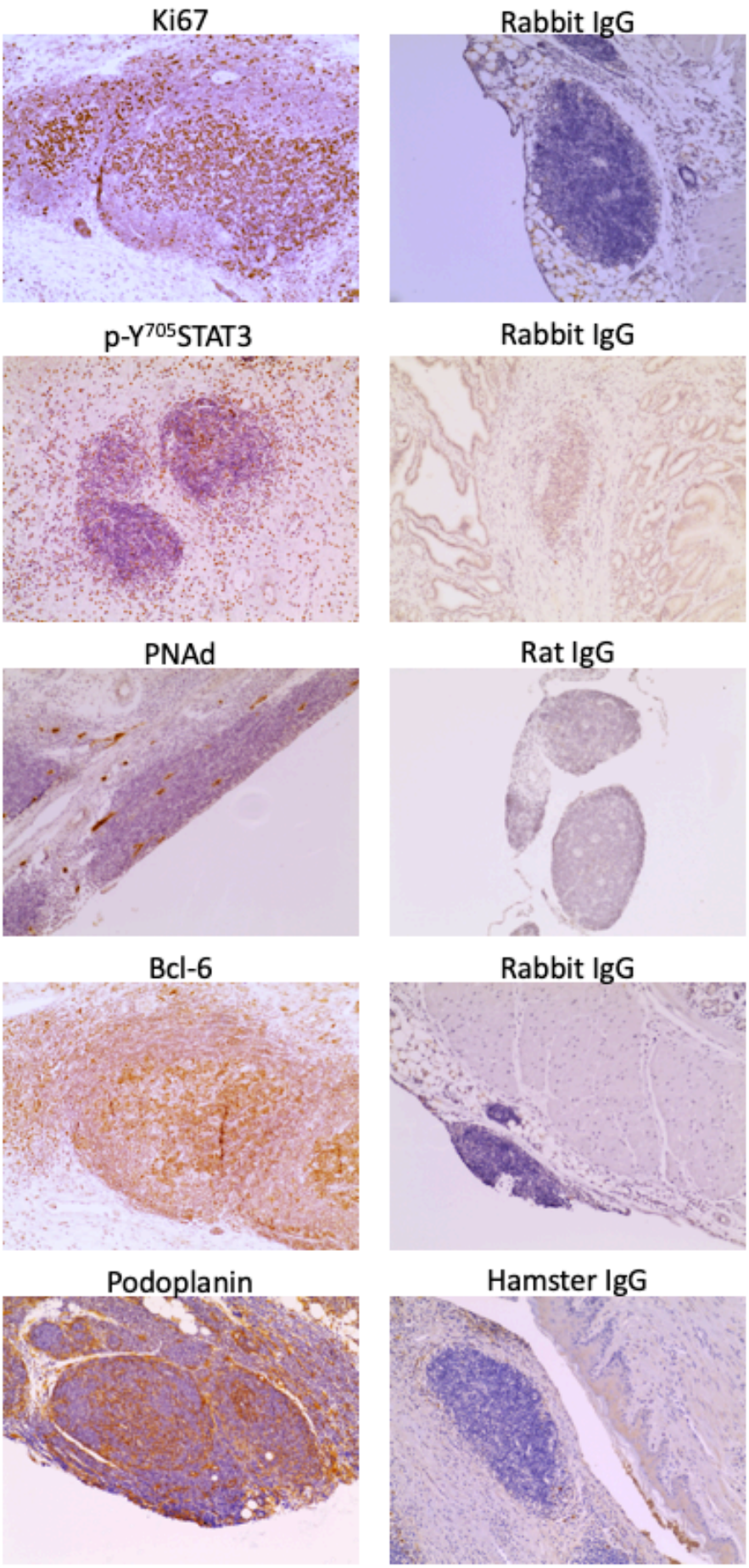
Ki67
Rabbit IgG
p-Y705STAT3
Rabbit IgG
PNAd
Rat IgG
Bcl-6
Rabbit IgG
Podoplanin
Hamster IgG

1. Medzhitov, R., *Origin and physiological roles of inflammation.* Nature, 2008. **454**(7203): p. 428-35.
2. Chaplin, D.D., *Overview of the immune response.* J Allergy Clin Immunol, 2010. **125**(2 Suppl 2): p. S3-23.
3. Janeway, C.A. and R. Medzhitov, *Innate immune recognition.* Annu Rev Immunol, 2002. **20**: p. 197-216.
4. Guo, H., J.B. Callaway, and J.P. Ting, *Inflammasomes: mechanism of action, role in disease, and therapeutics.* Nat Med, 2015. **21**(7): p. 677-87.
5. Iwasaki, A. and R. Medzhitov, *Control of adaptive immunity by the innate immune system.* Nat Immunol, 2015. **16**(4): p. 343-53.
6. Davis, M.M., et al., *A murine T cell receptor gene complex: isolation, structure and rearrangement.* Immunol Rev, 1984. **81**: p. 235-58.
7. Oettinger, M.A., et al., *RAG-1 and RAG-2, adjacent genes that synergistically activate V(D)J recombination.* Science, 1990. **248**(4962): p. 1517-23.
8. Tonegawa, S., *Reiteration frequency of immunoglobulin light chain genes: further evidence for somatic generation of antibody diversity.* Proc Natl Acad Sci U S A, 1976. **73**(1): p. 203-7.
9. Flajnik, M.F. and M. Kasahara, *Origin and evolution of the adaptive immune system: genetic events and selective pressures.* Nat Rev Genet, 2010. **11**(1): p. 47-59.
10. Bretscher, P. and M. Cohn, *A theory of self-nonself discrimination.* Science, 1970. **169**(3950): p. 1042-9.
11. June, C.H., et al., *T-cell proliferation involving the CD28 pathway is associated with cyclosporine-resistant interleukin 2 gene expression.* Mol Cell Biol, 1987. **7**(12): p. 4472-81.
12. Greenwald, R.J., G.J. Freeman, and A.H. Sharpe, *The B7 family revisited.* Annu Rev Immunol, 2005. **23**: p. 515-48.
13. Hsieh, C.S., et al., *Development of TH1 CD4+ T cells through IL-12 produced by Listeria-induced macrophages.* Science, 1993. **260**(5107): p. 547-9.
14. Swain, S.L., et al., *IL-4 directs the development of Th2-like helper effectors.* J Immunol, 1990. **145**(11): p. 3796-806.
15. Veldhoen, M., et al., *TGFbeta in the context of an inflammatory cytokine milieu supports de novo differentiation of IL-17-producing T cells.* Immunity, 2006. **24**(2): p. 179-89.
16. Stritesky, G.L., N. Yeh, and M.H. Kaplan, *IL-23 promotes maintenance but not commitment to the Th17 lineage.* J Immunol, 2008. **181**(9): p. 5948-55.
17. Starnes, T., et al., *Cutting edge: IL-17F, a novel cytokine selectively expressed in activated T cells and monocytes, regulates angiogenesis and endothelial cell cytokine production.* J Immunol, 2001. **167**(8): p. 4137-40.
18. Ferretti, S., et al., *IL-17, produced by lymphocytes and neutrophils, is necessary for lipopolysaccharide-induced airway neutrophilia: IL-15 as a possible trigger.* J Immunol, 2003. **170**(4): p. 2106-12.
19. Lockhart, E., A.M. Green, and J.L. Flynn, *IL-17 production is dominated by gammadelta T cells rather than CD4 T cells during Mycobacterium tuberculosis infection.* J Immunol, 2006. **177**(7): p. 4662-9.
20. Korn, T., et al., *IL-17 and Th17 Cells.* Annu Rev Immunol, 2009. **27**: p. 485-517.

21. Yao, Z., et al., *Herpesvirus Saimiri encodes a new cytokine, IL-17, which binds to a novel cytokine receptor.* Immunity, 1995. **3**(6): p. 811-21.
22. Ishigame, H., et al., *Differential roles of interleukin-17A and -17F in host defense against mucoepithelial bacterial infection and allergic responses.* Immunity, 2009. **30**(1): p. 108-19.
23. Zhu, J., H. Yamane, and W.E. Paul, *Differentiation of effector CD4 T cell populations (*).* Annu Rev Immunol, 2010. **28**: p. 445-89.
24. Chen, W., et al., *Conversion of peripheral CD4+CD25- naive T cells to CD4+CD25+ regulatory T cells by TGF-beta induction of transcription factor Foxp3.* J Exp Med, 2003. **198**(12): p. 1875-86.
25. Park, S.R., *Activation-induced Cytidine Deaminase in B Cell Immunity and Cancers.* Immune Netw, 2012. **12**(6): p. 230-9.
26. Muramatsu, M., et al., *Class switch recombination and hypermutation require activation-induced cytidine deaminase (AID), a potential RNA editing enzyme.* Cell, 2000. **102**(5): p. 553-63.
27. Hoffman, W., F.G. Lakkis, and G. Chalasani, *B Cells, Antibodies, and More.* Clin J Am Soc Nephrol, 2016. **11**(1): p. 137-54.
28. Serhan, C.N. and J. Savill, *Resolution of inflammation: the beginning programs the end.* Nat Immunol, 2005. **6**(12): p. 1191-7.
29. Takano, T., et al., *Neutrophil-mediated changes in vascular permeability are inhibited by topical application of aspirin-triggered 15-epi-lipoxin A4 and novel lipoxin B4 stable analogues.* J Clin Invest, 1998. **101**(4): p. 819-26.
30. Maddox, J.F. and C.N. Serhan, *Lipoxin A4 and B4 are potent stimuli for human monocyte migration and adhesion: selective inactivation by dehydrogenation and reduction.* J Exp Med, 1996. **183**(1): p. 137-46.
31. Godson, C., et al., *Cutting edge: lipoxins rapidly stimulate nonphlogistic phagocytosis of apoptotic neutrophils by monocyte-derived macrophages.* J Immunol, 2000. **164**(4): p. 1663-7.
32. Huynh, M.L., V.A. Fadok, and P.M. Henson, *Phosphatidylserine-dependent ingestion of apoptotic cells promotes TGF-beta1 secretion and the resolution of inflammation.* J Clin Invest, 2002. **109**(1): p. 41-50.
33. Schett, G. and M.F. Neurath, *Resolution of chronic inflammatory disease: universal and tissue-specific concepts.* Nat Commun, 2018. **9**(1): p. 3261.
34. McInnes, I.B. and G. Schett, *The pathogenesis of rheumatoid arthritis.* N Engl J Med, 2011. **365**(23): p. 2205-19.
35. Aggarwal, B.B., *Signalling pathways of the TNF superfamily: a double-edged sword.* Nat Rev Immunol, 2003. **3**(9): p. 745-56.
36. Hunter, C.A. and S.A. Jones, *IL-6 as a keystone cytokine in health and disease.* Nat Immunol, 2015. **16**(5): p. 448-57.
37. Santarlasci, V., et al., *IL-1 and T Helper Immune Responses.* Front Immunol, 2013. **4**: p. 182.
38. Couper, K.N., D.G. Blount, and E.M. Riley, *IL-10: the master regulator of immunity to infection.* J Immunol, 2008. **180**(9): p. 5771-7.
39. Griffith, J.W., C.L. Sokol, and A.D. Luster, *Chemokines and chemokine receptors: positioning cells for host defense and immunity.* Annu Rev Immunol, 2014. **32**: p. 659-702.

40. Zlotnik, A. and O. Yoshie, *Chemokines: a new classification system and their role in immunity.* Immunity, 2000. **12**(2): p. 121-7.
41. Murphy, P.M., et al., *International union of pharmacology. XXII. Nomenclature for chemokine receptors.* Pharmacol Rev, 2000. **52**(1): p. 145-76.
42. Moser, B., et al., *Chemokines: multiple levels of leukocyte migration control.* Trends Immunol, 2004. **25**(2): p. 75-84.
43. Constantin, G., et al., *Chemokines trigger immediate beta2 integrin affinity and mobility changes: differential regulation and roles in lymphocyte arrest under flow.* Immunity, 2000. **13**(6): p. 759-69.
44. Sarmiento, J., et al., *Diverging mechanisms of activation of chemokine receptors revealed by novel chemokine agonists.* PLoS One, 2011. **6**(12): p. e27967.
45. Baggiolini, M., *Chemokines in pathology and medicine.* J Intern Med, 2001. **250**(2): p. 91-104.
46. Cyster, J.G., *Chemokines, sphingosine-1-phosphate, and cell migration in secondary lymphoid organs.* Annu Rev Immunol, 2005. **23**: p. 127-59.
47. Jones, G.W., et al., *IL-27: a double agent in the IL-6 family.* Clin Exp Immunol, 2018.
48. Yasukawa, K., et al., *Structure and expression of human B cell stimulatory factor-2 (BSF-2/IL-6) gene.* EMBO J, 1987. **6**(10): p. 2939-45.
49. Hirano, T., et al., *Complementary DNA for a novel human interleukin (BSF-2) that induces B lymphocytes to produce immunoglobulin.* Nature, 1986. **324**(6092): p. 73-6.
50. Woloski, B.M. and G.M. Fuller, *Identification and partial characterization of hepatocyte-stimulating factor from leukemia cell lines: comparison with interleukin 1.* Proc Natl Acad Sci U S A, 1985. **82**(5): p. 1443-7.
51. Klimpel, G.R., *Soluble factor(s) from LPS-activated macrophages induce cytotoxic T cell differentiation from alloantigen-primed spleen cells.* J Immunol, 1980. **125**(3): p. 1243-9.
52. Yoshizaki, K., et al., *Isolation and characterization of B cell differentiation factor (BCDF) secreted from a human B lymphoblastoid cell line.* J Immunol, 1984. **132**(6): p. 2948-54.
53. Andus, T., et al., *Recombinant human B cell stimulatory factor 2 (BSF-2/IFN-beta 2) regulates beta-fibrinogen and albumin mRNA levels in Fao-9 cells.* FEBS Lett, 1987. **221**(1): p. 18-22.
54. McInnes, I.B. and G. Schett, *Cytokines in the pathogenesis of rheumatoid arthritis.* Nat Rev Immunol, 2007. **7**(6): p. 429-42.
55. Bethin, K.E., S.K. Vogt, and L.J. Muglia, *Interleukin-6 is an essential, corticotropin-releasing hormone-independent stimulator of the adrenal axis during immune system activation.* Proc Natl Acad Sci U S A, 2000. **97**(16): p. 9317-22.
56. Hodes, G.E., et al., *Individual differences in the peripheral immune system promote resilience versus susceptibility to social stress.* Proc Natl Acad Sci U S A, 2014. **111**(45): p. 16136-41.
57. Rohleder, N., M. Aringer, and M. Boentert, *Role of interleukin-6 in stress, sleep, and fatigue.* Ann N Y Acad Sci, 2012. **1261**: p. 88-96.

58. Kraakman, M.J., et al., *Blocking IL-6 trans-signaling prevents high-fat diet-induced adipose tissue macrophage recruitment but does not improve insulin resistance.* Cell Metab, 2015. **21**(3): p. 403-16.
59. Scheller, J. and S. Rose-John, *Interleukin-6 and its receptor: from bench to bedside.* Med Microbiol Immunol, 2006. **195**(4): p. 173-83.
60. Rose-John, S., et al., *Interleukin-6 biology is coordinated by membrane-bound and soluble receptors: role in inflammation and cancer.* J Leukoc Biol, 2006. **80**(2): p. 227-36.
61. Twohig, J.P., et al., *Activation of naïve CD4.* Nat Immunol, 2019. **20**(4): p. 458-470.
62. Matthews, V., et al., *Cellular cholesterol depletion triggers shedding of the human interleukin-6 receptor by ADAM10 and ADAM17 (TACE).* J Biol Chem, 2003. **278**(40): p. 38829-39.
63. Jones, G.W., et al., *Loss of CD4+ T cell IL-6R expression during inflammation underlines a role for IL-6 trans signaling in the local maintenance of Th17 cells.* J Immunol, 2010. **184**(4): p. 2130-9.
64. Jones, S.A., *Directing transition from innate to acquired immunity: defining a role for IL-6.* J Immunol, 2005. **175**(6): p. 3463-8.
65. Campbell, I.L., et al., *Trans-signaling is a dominant mechanism for the pathogenic actions of interleukin-6 in the brain.* J Neurosci, 2014. **34**(7): p. 2503-13.
66. Tanaka, T., M. Narazaki, and T. Kishimoto, *IL-6 in inflammation, immunity, and disease.* Cold Spring Harb Perspect Biol, 2014. **6**(10): p. a016295.
67. Taniguchi, K., et al., *A gp130-Src-YAP module links inflammation to epithelial regeneration.* Nature, 2015. **519**(7541): p. 57-62.
68. Rawlings, J.S., K.M. Rosler, and D.A. Harrison, *The JAK/STAT signaling pathway.* J Cell Sci, 2004. **117**(Pt 8): p. 1281-3.
69. Nowell, M.A., et al., *Therapeutic targeting of IL-6 trans signaling counteracts STAT3 control of experimental inflammatory arthritis.* J Immunol, 2009. **182**(1): p. 613-22.
70. Jones, G.W., et al., *Exacerbated inflammatory arthritis in response to hyperactive gp130 signalling is independent of IL-17A.* Ann Rheum Dis, 2013. **72**(10): p. 1738-42.
71. Atsumi, T., et al., *A point mutation of Tyr-759 in interleukin 6 family cytokine receptor subunit gp130 causes autoimmune arthritis.* J Exp Med, 2002. **196**(7): p. 979-90.
72. Jenkins, B.J., et al., *Pathologic consequences of STAT3 hyperactivation by IL-6 and IL-11 during hematopoiesis and lymphopoiesis.* Blood, 2007. **109**(6): p. 2380-8.
73. McLoughlin, R.M., et al., *Interplay between IFN-gamma and IL-6 signaling governs neutrophil trafficking and apoptosis during acute inflammation.* J Clin Invest, 2003. **112**(4): p. 598-607.
74. Onogawa, T., *Local delivery of soluble interleukin-6 receptors to improve the outcome of alpha-toxin producing Staphylococcus aureus infection in mice.* Immunobiology, 2005. **209**(9): p. 651-60.

75. Hurst, S.M., et al., *Il-6 and its soluble receptor orchestrate a temporal switch in the pattern of leukocyte recruitment seen during acute inflammation.* Immunity, 2001. **14**(6): p. 705-14.
76. Nagabhushanam, V., et al., *Innate inhibition of adaptive immunity: Mycobacterium tuberculosis-induced IL-6 inhibits macrophage responses to IFN-gamma.* J Immunol, 2003. **171**(9): p. 4750-7.
77. Silver, J.S., et al., *IL-6 mediates the susceptibility of glycoprotein 130 hypermorphs to Toxoplasma gondii.* J Immunol, 2011. **187**(1): p. 350-60.
78. Harker, J.A., et al., *Late interleukin-6 escalates T follicular helper cell responses and controls a chronic viral infection.* Science, 2011. **334**(6057): p. 825-9.
79. Nurieva, R.I., et al., *Generation of T follicular helper cells is mediated by interleukin-21 but independent of T helper 1, 2, or 17 cell lineages.* Immunity, 2008. **29**(1): p. 138-49.
80. Dienz, O., et al., *The induction of antibody production by IL-6 is indirectly mediated by IL-21 produced by CD4+ T cells.* J Exp Med, 2009. **206**(1): p. 69-78.
81. Diehl, S. and M. Rincón, *The two faces of IL-6 on Th1/Th2 differentiation.* Mol Immunol, 2002. **39**(9): p. 531-6.
82. Harrington, L.E., et al., *Interleukin 17-producing CD4+ effector T cells develop via a lineage distinct from the T helper type 1 and 2 lineages.* Nat Immunol, 2005. **6**(11): p. 1123-32.
83. Zhou, L., et al., *IL-6 programs T(H)-17 cell differentiation by promoting sequential engagement of the IL-21 and IL-23 pathways.* Nat Immunol, 2007. **8**(9): p. 967-74.
84. Acosta-Rodriguez, E.V., et al., *Interleukins 1beta and 6 but not transforming growth factor-beta are essential for the differentiation of interleukin 17-producing human T helper cells.* Nat Immunol, 2007. **8**(9): p. 942-9.
85. O'Connor, R.A., et al., *Foxp3$^+$ Treg cells in the inflamed CNS are insensitive to IL-6-driven IL-17 production.* Eur J Immunol, 2012. **42**(5): p. 1174-9.
86. Korn, T., et al., *IL-6 controls Th17 immunity in vivo by inhibiting the conversion of conventional T cells into Foxp3+ regulatory T cells.* Proc Natl Acad Sci U S A, 2008. **105**(47): p. 18460-5.
87. Komatsu, N., et al., *Pathogenic conversion of Foxp3+ T cells into TH17 cells in autoimmune arthritis.* Nat Med, 2014. **20**(1): p. 62-8.
88. Ohshima, S., et al., *Interleukin 6 plays a key role in the development of antigen-induced arthritis.* Proc Natl Acad Sci U S A, 1998. **95**(14): p. 8222-6.
89. Alonzi, T., et al., *Interleukin 6 is required for the development of collagen-induced arthritis.* J Exp Med, 1998. **187**(4): p. 461-8.
90. Eugster, H.P., et al., *IL-6-deficient mice resist myelin oligodendrocyte glycoprotein-induced autoimmune encephalomyelitis.* Eur J Immunol, 1998. **28**(7): p. 2178-87.
91. Yoshida, H. and C.A. Hunter, *The immunobiology of interleukin-27.* Annu Rev Immunol, 2015. **33**: p. 417-43.
92. Kimura, D., et al., *Interleukin-27-Producing CD4(+) T Cells Regulate Protective Immunity during Malaria Parasite Infection.* Immunity, 2016. **44**(3): p. 672-682.
93. Hirahara, K., et al., *Asymmetric Action of STAT Transcription Factors Drives Transcriptional Outputs and Cytokine Specificity.* Immunity, 2015. **42**(5): p. 877-89.

94. Pflanz, S., et al., *IL-27, a heterodimeric cytokine composed of EBI3 and p28 protein, induces proliferation of naive CD4+ T cells.* Immunity, 2002. **16**(6): p. 779-90.
95. Chen, Q., et al., *Development of Th1-type immune responses requires the type I cytokine receptor TCCR.* Nature, 2000. **407**(6806): p. 916-20.
96. Yoshida, H., et al., *WSX-1 is required for the initiation of Th1 responses and resistance to L. major infection.* Immunity, 2001. **15**(4): p. 569-78.
97. Takeda, A., et al., *Cutting edge: role of IL-27/WSX-1 signaling for induction of T-bet through activation of STAT1 during initial Th1 commitment.* J Immunol, 2003. **170**(10): p. 4886-90.
98. Lucas, S., et al., *IL-27 regulates IL-12 responsiveness of naive CD4+ T cells through Stat1-dependent and -independent mechanisms.* Proc Natl Acad Sci U S A, 2003. **100**(25): p. 15047-52.
99. Kim, G., et al., *A novel role for IL-27 in mediating the survival of activated mouse CD4 T lymphocytes.* J Immunol, 2013. **190**(4): p. 1510-8.
100. Villarino, A., et al., *The IL-27R (WSX-1) is required to suppress T cell hyperactivity during infection.* Immunity, 2003. **19**(5): p. 645-55.
101. Villarino, A.V., et al., *IL-27 limits IL-2 production during Th1 differentiation.* J Immunol, 2006. **176**(1): p. 237-47.
102. Hall, A.O., et al., *The cytokines interleukin 27 and interferon-gamma promote distinct Treg cell populations required to limit infection-induced pathology.* Immunity, 2012. **37**(3): p. 511-23.
103. Stumhofer, J.S., et al., *Interleukins 27 and 6 induce STAT3-mediated T cell production of interleukin 10.* Nat Immunol, 2007. **8**(12): p. 1363-71.
104. Young, A., et al., *Cutting edge: suppression of GM-CSF expression in murine and human T cells by IL-27.* J Immunol, 2012. **189**(5): p. 2079-83.
105. Stumhofer, J.S., et al., *Interleukin 27 negatively regulates the development of interleukin 17-producing T helper cells during chronic inflammation of the central nervous system.* Nat Immunol, 2006. **7**(9): p. 937-945.
106. Awasthi, A., et al., *A dominant function for interleukin 27 in generating interleukin 10-producing anti-inflammatory T cells.* Nat Immunol, 2007. **8**(12): p. 1380-9.
107. Fitzgerald, D.C., et al., *Suppression of autoimmune inflammation of the central nervous system by interleukin 10 secreted by interleukin 27-stimulated T cells.* Nat Immunol, 2007. **8**(12): p. 1372-9.
108. Diveu, C., et al., *IL-27 blocks RORc expression to inhibit lineage commitment of Th17 cells.* J Immunol, 2009. **182**(9): p. 5748-56.
109. Villarino, A.V., et al., *IL-27R deficiency delays the onset of colitis and protects from helminth-induced pathology in a model of chronic IBD.* Int Immunol, 2008. **20**(6): p. 739-52.
110. Bancroft, A.J., et al., *WSX-1: a key role in induction of chronic intestinal nematode infection.* J Immunol, 2004. **172**(12): p. 7635-41.
111. Artis, D., et al., *The IL-27 receptor (WSX-1) is an inhibitor of innate and adaptive elements of type 2 immunity.* J Immunol, 2004. **173**(9): p. 5626-34.
112. Clement, M., et al., *Cytomegalovirus-Specific IL-10-Producing CD4+ T Cells Are Governed by Type-I IFN-Induced IL-27 and Promote Virus Persistence.* PLoS Pathog, 2016. **12**(12): p. e1006050.

113. Patin, E.C., et al., *IL-27 Induced by Select Candida spp. via TLR7/NOD2 Signaling and IFN-β Production Inhibits Fungal Clearance.* J Immunol, 2016. **197**(1): p. 208-21.
114. Moon, S.J., et al., *In vivo action of IL-27: reciprocal regulation of Th17 and Treg cells in collagen-induced arthritis.* Exp Mol Med, 2013. **45**: p. e46.
115. Hirahara, K., et al., *Interleukin-27 priming of T cells controls IL-17 production in trans via induction of the ligand PD-L1.* Immunity, 2012. **36**(6): p. 1017-30.
116. Randall, T.D., D.M. Carragher, and J. Rangel-Moreno, *Development of secondary lymphoid organs.* Annu Rev Immunol, 2008. **26**: p. 627-50.
117. Boehm, T., N. Iwanami, and I. Hess, *Evolution of the immune system in the lower vertebrates.* Annu Rev Genomics Hum Genet, 2012. **13**: p. 127-49.
118. Pitzalis, C., et al., *Ectopic lymphoid-like structures in infection, cancer and autoimmunity.* Nat Rev Immunol, 2014. **14**(7): p. 447-462.
119. Mebius, R.E., P. Rennert, and I.L. Weissman, *Developing lymph nodes collect CD4+CD3- LTbeta+ cells that can differentiate to APC, NK cells, and follicular cells but not T or B cells.* Immunity, 1997. **7**(4): p. 493-504.
120. van de Pavert, S.A., et al., *Chemokine CXCL13 is essential for lymph node initiation and is induced by retinoic acid and neuronal stimulation.* Nat Immunol, 2009. **10**(11): p. 1193-9.
121. van de Pavert, S.A., et al., *Maternal retinoids control type 3 innate lymphoid cells and set the offspring immunity.* Nature, 2014. **508**(7494): p. 123-7.
122. Yoshida, H., et al., *Different cytokines induce surface lymphotoxin-alphabeta on IL-7 receptor-alpha cells that differentially engender lymph nodes and Peyer's patches.* Immunity, 2002. **17**(6): p. 823-33.
123. Cupedo, T., et al., *Presumptive lymph node organizers are differentially represented in developing mesenteric and peripheral nodes.* J Immunol, 2004. **173**(5): p. 2968-75.
124. Luther, S.A., K.M. Ansel, and J.G. Cyster, *Overlapping roles of CXCL13, interleukin 7 receptor alpha, and CCR7 ligands in lymph node development.* J Exp Med, 2003. **197**(9): p. 1191-8.
125. Dejardin, E., et al., *The lymphotoxin-beta receptor induces different patterns of gene expression via two NF-kappaB pathways.* Immunity, 2002. **17**(4): p. 525-35.
126. Ansel, K.M., et al., *A chemokine-driven positive feedback loop organizes lymphoid follicles.* Nature, 2000. **406**(6793): p. 309-14.
127. Hashi, H., et al., *Compartmentalization of Peyer's patch anlagen before lymphocyte entry.* J Immunol, 2001. **166**(6): p. 3702-9.
128. Mebius, R.E., et al., *A developmental switch in lymphocyte homing receptor and endothelial vascular addressin expression regulates lymphocyte homing and permits CD4+ CD3- cells to colonize lymph nodes.* Proc Natl Acad Sci U S A, 1996. **93**(20): p. 11019-24.
129. Rosen, S.D., *Ligands for L-selectin: homing, inflammation, and beyond.* Annu Rev Immunol, 2004. **22**: p. 129-56.
130. Luther, S.A., et al., *Coexpression of the chemokines ELC and SLC by T zone stromal cells and deletion of the ELC gene in the plt/plt mouse.* Proc Natl Acad Sci U S A, 2000. **97**(23): p. 12694-9.

131. Link, A., et al., *Fibroblastic reticular cells in lymph nodes regulate the homeostasis of naive T cells.* Nat Immunol, 2007. **8**(11): p. 1255-65.
132. Brown, F.D. and S.J. Turley, *Fibroblastic reticular cells: organization and regulation of the T lymphocyte life cycle.* J Immunol, 2015. **194**(4): p. 1389-94.
133. Barone, F., et al., *Stromal Fibroblasts in Tertiary Lymphoid Structures: A Novel Target in Chronic Inflammation.* Front Immunol, 2016. **7**: p. 477.
134. Buckley, C.D., et al., *Stromal cells in chronic inflammation and tertiary lymphoid organ formation.* Annu Rev Immunol, 2015. **33**: p. 715-45.
135. Mionnet, C., et al., *Identification of a new stromal cell type involved in the regulation of inflamed B cell follicles.* PLoS Biol, 2013. **11**(10): p. e1001672.
136. Rodda, L.B., et al., *Single-Cell RNA Sequencing of Lymph Node Stromal Cells Reveals Niche-Associated Heterogeneity.* Immunity, 2018. **48**(5): p. 1014-1028.e6.
137. Dieu-Nosjean, M.C., et al., *Tertiary lymphoid structures in cancer and beyond.* Trends Immunol, 2014. **35**(11): p. 571-80.
138. Jones, G.W., D.G. Hill, and S.A. Jones, *Understanding Immune Cells in Tertiary Lymphoid Organ Development: It Is All Starting to Come Together.* Front Immunol, 2016. **7**: p. 401.
139. Chen, S.C., et al., *Ectopic expression of the murine chemokines CCL21a and CCL21b induces the formation of lymph node-like structures in pancreas, but not skin, of transgenic mice.* J Immunol, 2002. **168**(3): p. 1001-8.
140. Cherrier, M., S. Sawa, and G. Eberl, *Notch, Id2, and RORγt sequentially orchestrate the fetal development of lymphoid tissue inducer cells.* J Exp Med, 2012. **209**(4): p. 729-40.
141. Lochner, M., et al., *Microbiota-induced tertiary lymphoid tissues aggravate inflammatory disease in the absence of RORgamma t and LTi cells.* J Exp Med, 2011. **208**(1): p. 125-34.
142. Rangel-Moreno, J., et al., *The development of inducible bronchus-associated lymphoid tissue depends on IL-17.* Nat Immunol, 2011. **12**(7): p. 639-46.
143. Peters, A., et al., *Th17 Cells Induce Ectopic Lymphoid Follicles in Central Nervous System Tissue Inflammation.* Immunity. **35**(6): p. 986-996.
144. Fleige, H., et al., *IL-17-induced CXCL12 recruits B cells and induces follicle formation in BALT in the absence of differentiated FDCs.* J Exp Med, 2014. **211**(4): p. 643-51.
145. Barone, F., et al., *IL-22 regulates lymphoid chemokine production and assembly of tertiary lymphoid organs.* Proc Natl Acad Sci U S A, 2015.
146. Jones, G.W., et al., *Interleukin-27 inhibits ectopic lymphoid-like structure development in early inflammatory arthritis.* J Exp Med, 2015. **212**(11): p. 1793-802.
147. Bombardieri, M., et al., *Inducible tertiary lymphoid structures, autoimmunity, and exocrine dysfunction in a novel model of salivary gland inflammation in C57BL/6 mice.* J Immunol, 2012. **189**(7): p. 3767-76.
148. Kielczewski, J.L., et al., *Tertiary Lymphoid Tissue Forms in Retinas of Mice with Spontaneous Autoimmune Uveitis and Has Consequences on Visual Function.* J Immunol, 2016. **196**(3): p. 1013-25.
149. Foo, S.Y., et al., *Regulatory T cells prevent inducible BALT formation by dampening neutrophilic inflammation.* J Immunol, 2015. **194**(9): p. 4567-76.

150. Schmutz, S., et al., *Cutting edge: IL-7 regulates the peripheral pool of adult ROR gamma+ lymphoid tissue inducer cells.* J Immunol, 2009. **183**(4): p. 2217-21.
151. Meier, D., et al., *Ectopic lymphoid-organ development occurs through interleukin 7-mediated enhanced survival of lymphoid-tissue-inducer cells.* Immunity, 2007. **26**(5): p. 643-54.
152. Lee, B.H., et al., *Gene therapy using IL-27 ameliorates Sjögren's syndrome-like autoimmune exocrinopathy.* Arthritis Res Ther, 2012. **14**(4): p. R172.
153. Kim, K.W., et al., *Up-regulation of stromal cell-derived factor 1 (CXCL12) production in rheumatoid synovial fibroblasts through interactions with T lymphocytes: role of interleukin-17 and CD40L-CD40 interaction.* Arthritis Rheum, 2007. **56**(4): p. 1076-86.
154. Rangel-Moreno, J., et al., *Pulmonary expression of CXC chemokine ligand 13, CC chemokine ligand 19, and CC chemokine ligand 21 is essential for local immunity to influenza.* Proc Natl Acad Sci U S A, 2007. **104**(25): p. 10577-82.
155. Humby, F., et al., *Ectopic lymphoid structures support ongoing production of class-switched autoantibodies in rheumatoid synovium.* PLoS Med, 2009. **6**(1): p. e1.
156. Bombardieri, M., et al., *A BAFF/APRIL-dependent TLR3-stimulated pathway enhances the capacity of rheumatoid synovial fibroblasts to induce AID expression and Ig class-switching in B cells.* Ann Rheum Dis, 2011. **70**(10): p. 1857-65.
157. Grewal, J.S., et al., *Salivary glands act as mucosal inductive sites via the formation of ectopic germinal centers after site-restricted MCMV infection.* FASEB J, 2011. **25**(5): p. 1680-96.
158. Nacionales, D.C., et al., *B cell proliferation, somatic hypermutation, class switch recombination, and autoantibody production in ectopic lymphoid tissue in murine lupus.* J Immunol, 2009. **182**(7): p. 4226-36.
159. Croia, C., et al., *Implication of Epstein-Barr virus infection in disease-specific autoreactive B cell activation in ectopic lymphoid structures of Sjögren's syndrome.* Arthritis Rheumatol, 2014. **66**(9): p. 2545-57.
160. GeurtsvanKessel, C.H., et al., *Dendritic cells are crucial for maintenance of tertiary lymphoid structures in the lung of influenza virus-infected mice.* J Exp Med, 2009. **206**(11): p. 2339-49.
161. Moyron-Quiroz, J.E., et al., *Role of inducible bronchus associated lymphoid tissue (iBALT) in respiratory immunity.* Nat Med, 2004. **10**(9): p. 927-34.
162. Smolen, J.S., D. Aletaha, and I.B. McInnes, *Rheumatoid arthritis.* Lancet, 2016. **388**(10055): p. 2023-2038.
163. Kitas, G.D. and S.E. Gabriel, *Cardiovascular disease in rheumatoid arthritis: state of the art and future perspectives.* Ann Rheum Dis, 2011. **70**(1): p. 8-14.
164. Nurmohamed, M.T., M. Heslinga, and G.D. Kitas, *Cardiovascular comorbidity in rheumatic diseases.* Nat Rev Rheumatol, 2015. **11**(12): p. 693-704.
165. van der Helm-van Mil, A.H., J.Z. Wesoly, and T.W. Huizinga, *Understanding the genetic contribution to rheumatoid arthritis.* Curr Opin Rheumatol, 2005. **17**(3): p. 299-304.
166. Begovich, A.B., et al., *A missense single-nucleotide polymorphism in a gene encoding a protein tyrosine phosphatase (PTPN22) is associated with rheumatoid arthritis.* Am J Hum Genet, 2004. **75**(2): p. 330-7.

167. Stahl, E.A., et al., *Genome-wide association study meta-analysis identifies seven new rheumatoid arthritis risk loci.* Nat Genet, 2010. **42**(6): p. 508-14.
168. Fishman, D., et al., *The effect of novel polymorphisms in the interleukin-6 (IL-6) gene on IL-6 transcription and plasma IL-6 levels, and an association with systemic-onset juvenile chronic arthritis.* J Clin Invest, 1998. **102**(7): p. 1369-76.
169. Paradowska-Gorycka, A., et al., *Association of single nucleotide polymorphisms in the IL27 gene with rheumatoid arthritis.* Scand J Immunol, 2014. **80**(4): p. 298-305.
170. van Gaalen, F.A., et al., *Association between HLA class II genes and autoantibodies to cyclic citrullinated peptides (CCPs) influences the severity of rheumatoid arthritis.* Arthritis Rheum, 2004. **50**(7): p. 2113-21.
171. Aletaha, D., F. Alasti, and J.S. Smolen, *Rheumatoid factor, not antibodies against citrullinated proteins, is associated with baseline disease activity in rheumatoid arthritis clinical trials.* Arthritis Res Ther, 2015. **17**: p. 229.
172. Gonzalez, A., et al., *Mortality trends in rheumatoid arthritis: the role of rheumatoid factor.* J Rheumatol, 2008. **35**(6): p. 1009-14.
173. Nielen, M.M., et al., *Specific autoantibodies precede the symptoms of rheumatoid arthritis: a study of serial measurements in blood donors.* Arthritis Rheum, 2004. **50**(2): p. 380-6.
174. Orr, C., et al., *Synovial tissue research: a state-of-the-art review.* Nat Rev Rheumatol, 2017. **13**(8): p. 463-475.
175. *https://www.nice.org.uk/guidance/ng100*. 2018.
176. Fransen, J. and P.L. van Riel, *The Disease Activity Score and the EULAR response criteria.* Clin Exp Rheumatol, 2005. **23**(5 Suppl 39): p. S93-9.
177. Felson, D.T., et al., *The American College of Rheumatology preliminary core set of disease activity measures for rheumatoid arthritis clinical trials. The Committee on Outcome Measures in Rheumatoid Arthritis Clinical Trials.* Arthritis Rheum, 1993. **36**(6): p. 729-40.
178. Choy, E.H., A.F. Kavanaugh, and S.A. Jones, *The problem of choice: current biologic agents and future prospects in RA.* Nat Rev Rheumatol, 2013. **9**(3): p. 154-63.
179. Raza, K., *The Michael Mason prize: early rheumatoid arthritis--the window narrows.* Rheumatology (Oxford), 2010. **49**(3): p. 406-10.
180. Gerlag, D.M., et al., *Effects of B-cell directed therapy on the preclinical stage of rheumatoid arthritis: the PRAIRI study.* Ann Rheum Dis, 2019. **78**(2): p. 179-185.
181. Singh, J.A., et al., *2012 update of the 2008 American College of Rheumatology recommendations for the use of disease-modifying antirheumatic drugs and biologic agents in the treatment of rheumatoid arthritis.* Arthritis Care Res (Hoboken), 2012. **64**(5): p. 625-39.
182. Smolen, J.S., et al., *EULAR recommendations for the management of rheumatoid arthritis with synthetic and biological disease-modifying antirheumatic drugs.* Ann Rheum Dis, 2010. **69**(6): p. 964-75.
183. De Stefano, R., et al., *Comparison of combination therapies in the treatment of rheumatoid arthritis: leflunomide-anti-TNF-alpha versus methotrexate-anti-TNF-alpha.* Clin Rheumatol, 2010. **29**(5): p. 517-24.

184. Lipsky, P.E., et al., *Infliximab and methotrexate in the treatment of rheumatoid arthritis. Anti-Tumor Necrosis Factor Trial in Rheumatoid Arthritis with Concomitant Therapy Study Group.* N Engl J Med, 2000. **343**(22): p. 1594-602.
185. Weinblatt, M.E., et al., *A trial of etanercept, a recombinant tumor necrosis factor receptor:Fc fusion protein, in patients with rheumatoid arthritis receiving methotrexate.* N Engl J Med, 1999. **340**(4): p. 253-9.
186. Weinblatt, M.E., et al., *Adalimumab, a fully human anti-tumor necrosis factor alpha monoclonal antibody, for the treatment of rheumatoid arthritis in patients taking concomitant methotrexate: the ARMADA trial.* Arthritis Rheum, 2003. **48**(1): p. 35-45.
187. Smolen, J.S., et al., *Golimumab in patients with active rheumatoid arthritis after treatment with tumour necrosis factor alpha inhibitors (GO-AFTER study): a multicentre, randomised, double-blind, placebo-controlled, phase III trial.* Lancet, 2009. **374**(9685): p. 210-21.
188. Cohen, S.B., et al., *Rituximab for rheumatoid arthritis refractory to anti-tumor necrosis factor therapy: Results of a multicenter, randomized, double-blind, placebo-controlled, phase III trial evaluating primary efficacy and safety at twenty-four weeks.* Arthritis Rheum, 2006. **54**(9): p. 2793-806.
189. Genovese, M.C., et al., *Abatacept for rheumatoid arthritis refractory to tumor necrosis factor alpha inhibition.* N Engl J Med, 2005. **353**(11): p. 1114-23.
190. Emery, P., et al., *IL-6 receptor inhibition with tocilizumab improves treatment outcomes in patients with rheumatoid arthritis refractory to anti-tumour necrosis factor biologicals: results from a 24-week multicentre randomised placebo-controlled trial.* Ann Rheum Dis, 2008. **67**(11): p. 1516-23.
191. Scott, L.J., *Tocilizumab: A Review in Rheumatoid Arthritis.* Drugs, 2017. **77**(17): p. 1865-1879.
192. Edwards, J.C., M.J. Leandro, and G. Cambridge, *B lymphocyte depletion in rheumatoid arthritis: targeting of CD20.* Curr Dir Autoimmun, 2005. **8**: p. 175-92.
193. Pitzalis, C., S. Kelly, and F. Humby, *New learnings on the pathophysiology of RA from synovial biopsies.* Curr Opin Rheumatol, 2013. **25**(3): p. 334-44.
194. Klimiuk, P.A., et al., *Tissue cytokine patterns distinguish variants of rheumatoid synovitis.* Am J Pathol, 1997. **151**(5): p. 1311-9.
195. Dennis, G., Jr., et al., *Synovial phenotypes in rheumatoid arthritis correlate with response to biologic therapeutics.* Arthritis Res Ther, 2014. **16**(2): p. R90.
196. Kavanaugh, A., et al., *Assessment of rituximab's immunomodulatory synovial effects (ARISE trial). 1: clinical and synovial biomarker results.* Annals of the rheumatic diseases, 2008. **67**(3): p. 402-408.
197. Cañete, J.D., et al., *Clinical significance of synovial lymphoid neogenesis and its reversal after anti-tumour necrosis factor α therapy in rheumatoid arthritis.* Annals of the Rheumatic Diseases, 2009. **68**(5): p. 751-756.
198. Hirano, T., et al., *Excessive production of interleukin 6/B cell stimulatory factor-2 in rheumatoid arthritis.* Eur J Immunol, 1988. **18**(11): p. 1797-801.
199. Nowell, M.A., et al., *Soluble IL-6 receptor governs IL-6 activity in experimental arthritis: blockade of arthritis severity by soluble glycoprotein 130.* J Immunol, 2003. **171**(6): p. 3202-9.

200. Niedbala, W., et al., *Interleukin 27 attenuates collagen-induced arthritis.* Annals of the rheumatic diseases, 2008. **67**(10): p. 1474-9.
201. Pickens, S.R., et al., *Local expression of interleukin-27 ameliorates collagen-induced arthritis.* Arthritis Rheum, 2011. **63**(8): p. 2289-98.
202. Bugatti, S., et al., *High expression levels of the B cell chemoattractant CXCL13 in rheumatoid synovium are a marker of severe disease.* Rheumatology (Oxford), 2014. **53**(10): p. 1886-95.
203. Lanfant-Weybel, K., et al., *Synovium CD20 expression is a potential new predictor of bone erosion progression in very-early arthritis treated by sequential DMARDs monotherapy -- a pilot study from the VErA cohort.* Joint Bone Spine, 2012. **79**(6): p. 574-80.
204. Rosengren, S., et al., *Elevated autoantibody content in rheumatoid arthritis synovia with lymphoid aggregates and the effect of rituximab.* Arthritis Res Ther, 2008. **10**(5): p. R105.
205. Thurlings, R.M., et al., *Synovial lymphoid neogenesis does not define a specific clinical rheumatoid arthritis phenotype.* Arthritis Rheum, 2008. **58**(6): p. 1582-9.
206. Klimiuk, P.A., et al., *Circulating tumour necrosis factor alpha and soluble tumour necrosis factor receptors in patients with different patterns of rheumatoid synovitis.* Ann Rheum Dis, 2003. **62**(5): p. 472-5.
207. Klaasen, R., et al., *The relationship between synovial lymphocyte aggregates and the clinical response to infliximab in rheumatoid arthritis: a prospective study.* Arthritis Rheum, 2009. **60**(11): p. 3217-24.
208. Cragg, M.S., et al., *The biology of CD20 and its potential as a target for mAb therapy.* Curr Dir Autoimmun, 2005. **8**: p. 140-74.
209. Vos, K., et al., *Early effects of rituximab on the synovial cell infiltrate in patients with rheumatoid arthritis.* Arthritis Rheum, 2007. **56**(3): p. 772-8.
210. Rosengren, S., et al., *CXCL13: a novel biomarker of B-cell return following rituximab treatment and synovitis in patients with rheumatoid arthritis.* Rheumatology (Oxford), 2011. **50**(3): p. 603-10.
211. Van Cutsem, E., et al., *Gastric cancer.* Lancet, 2016. **388**(10060): p. 2654-2664.
212. Fox, J.G. and T.C. Wang, *Inflammation, atrophy, and gastric cancer.* J Clin Invest, 2007. **117**(1): p. 60-9.
213. LAUREN, P., *THE TWO HISTOLOGICAL MAIN TYPES OF GASTRIC CARCINOMA: DIFFUSE AND SO-CALLED INTESTINAL-TYPE CARCINOMA. AN ATTEMPT AT A HISTO-CLINICAL CLASSIFICATION.* Acta Pathol Microbiol Scand, 1965. **64**: p. 31-49.
214. Hussain, S.P. and C.C. Harris, *Inflammation and cancer: an ancient link with novel potentials.* Int J Cancer, 2007. **121**(11): p. 2373-80.
215. Marusawa, H. and B.J. Jenkins, *Inflammation and gastrointestinal cancer: an overview.* Cancer Lett, 2014. **345**(2): p. 153-6.
216. Bromberg, J.F., et al., *Stat3 as an oncogene.* Cell, 1999. **98**(3): p. 295-303.
217. Yakata, Y., et al., *Expression of p-STAT3 in human gastric carcinoma: significant correlation in tumour invasion and prognosis.* Int J Oncol, 2007. **30**(2): p. 437-42.
218. Ellmark, P., et al., *Identification of protein expression signatures associated with Helicobacter pylori infection and gastric adenocarcinoma using recombinant antibody microarrays.* Mol Cell Proteomics, 2006. **5**(9): p. 1638-46.

219. Tebbutt, N.C., et al., *Reciprocal regulation of gastrointestinal homeostasis by SHP2 and STAT-mediated trefoil gene activation in gp130 mutant mice.* Nat Med, 2002. **8**(10): p. 1089-97.
220. Ernst, M., et al., *STAT3 and STAT1 mediate IL-11-dependent and inflammation-associated gastric tumorigenesis in gp130 receptor mutant mice.* J Clin Invest, 2008. **118**(5): p. 1727-38.
221. Jenkins, B.J., et al., *Hyperactivation of Stat3 in gp130 mutant mice promotes gastric hyperproliferation and desensitizes TGF-beta signaling.* Nat Med, 2005. **11**(8): p. 845-52.
222. Tye, H., et al., *STAT3-driven upregulation of TLR2 promotes gastric tumorigenesis independent of tumor inflammation.* Cancer Cell, 2012. **22**(4): p. 466-78.
223. Bergomas, F., et al., *Tertiary intratumor lymphoid tissue in colo-rectal cancer.* Cancers (Basel), 2011. **4**(1): p. 1-10.
224. Coppola, D., et al., *Unique ectopic lymph node-like structures present in human primary colorectal carcinoma are identified by immune gene array profiling.* Am J Pathol, 2011. **179**(1): p. 37-45.
225. Suzuki, A., et al., *Mature dendritic cells make clusters with T cells in the invasive margin of colorectal carcinoma.* J Pathol, 2002. **196**(1): p. 37-43.
226. Martinet, L., et al., *Human solid tumors contain high endothelial venules: association with T- and B-lymphocyte infiltration and favorable prognosis in breast cancer.* Cancer Res, 2011. **71**(17): p. 5678-87.
227. Martinet, L., et al., *High endothelial venule blood vessels for tumor-infiltrating lymphocytes are associated with lymphotoxin β-producing dendritic cells in human breast cancer.* J Immunol, 2013. **191**(4): p. 2001-8.
228. Cipponi, A., et al., *Neogenesis of lymphoid structures and antibody responses occur in human melanoma metastases.* Cancer Res, 2012. **72**(16): p. 3997-4007.
229. Martinet, L., et al., *High endothelial venules (HEVs) in human melanoma lesions: Major gateways for tumor-infiltrating lymphocytes.* Oncoimmunology, 2012. **1**(6): p. 829-839.
230. Messina, J.L., et al., *12-Chemokine gene signature identifies lymph node-like structures in melanoma: potential for patient selection for immunotherapy?* Sci Rep, 2012. **2**: p. 765.
231. Nielsen, J.S., et al., *CD20+ tumor-infiltrating lymphocytes have an atypical CD27- memory phenotype and together with CD8+ T cells promote favorable prognosis in ovarian cancer.* Clin Cancer Res, 2012. **18**(12): p. 3281-92.
232. Dieu-Nosjean, M.C., et al., *Long-term survival for patients with non-small-cell lung cancer with intratumoral lymphoid structures.* J Clin Oncol, 2008. **26**(27): p. 4410-7.
233. Germain, C., et al., *Presence of B cells in tertiary lymphoid structures is associated with a protective immunity in patients with lung cancer.* Am J Respir Crit Care Med, 2014. **189**(7): p. 832-44.
234. de Chaisemartin, L., et al., *Characterization of chemokines and adhesion molecules associated with T cell presence in tertiary lymphoid structures in human lung cancer.* Cancer Res, 2011. **71**(20): p. 6391-9.

235. Remark, R., et al., *Characteristics and clinical impacts of the immune environments in colorectal and renal cell carcinoma lung metastases: influence of tumor origin.* Clin Cancer Res, 2013. **19**(15): p. 4079-91.
236. Schrama, D., et al., *Targeting of lymphotoxin-alpha to the tumor elicits an efficient immune response associated with induction of peripheral lymphoid-like tissue.* Immunity, 2001. **14**(2): p. 111-21.
237. Schrama, D., et al., *Immunological tumor destruction in a murine melanoma model by targeted LTalpha independent of secondary lymphoid tissue.* Cancer Immunol Immunother, 2008. **57**(1): p. 85-95.
238. Johansson-Percival, A., et al., *De novo induction of intratumoral lymphoid structures and vessel normalization enhances immunotherapy in resistant tumors.* Nat Immunol, 2017. **18**(11): p. 1207-1217.
239. Di Caro, G., et al., *Occurrence of tertiary lymphoid tissue is associated with T-cell infiltration and predicts better prognosis in early-stage colorectal cancers.* Clin Cancer Res, 2014. **20**(8): p. 2147-58.
240. Väyrynen, J.P., et al., *Characteristics and significance of colorectal cancer associated lymphoid reaction.* Int J Cancer, 2014. **134**(9): p. 2126-35.
241. Goc, J., et al., *Dendritic cells in tumor-associated tertiary lymphoid structures signal a Th1 cytotoxic immune contexture and license the positive prognostic value of infiltrating CD8+ T cells.* Cancer Res, 2014. **74**(3): p. 705-15.
242. Gobert, M., et al., *Regulatory T cells recruited through CCL22/CCR4 are selectively activated in lymphoid infiltrates surrounding primary breast tumors and lead to an adverse clinical outcome.* Cancer Res, 2009. **69**(5): p. 2000-9.
243. Joshi, N.S., et al., *Regulatory T Cells in Tumor-Associated Tertiary Lymphoid Structures Suppress Anti-tumor T Cell Responses.* Immunity, 2015. **43**(3): p. 579-90.
244. Finkin, S., et al., *Ectopic lymphoid structures function as microniches for tumor progenitor cells in hepatocellular carcinoma.* Nat Immunol, 2015. **16**(12): p. 1235-44.
245. Hawkins, P., et al., *Applying refinement to the use of mice and rats in rheumatoid arthritis research.* Inflammopharmacology, 2015. **23**(4): p. 131-50.
246. Jones, G.W., et al., *In Vivo Models for Inflammatory Arthritis.* Methods Mol Biol, 2018. **1725**: p. 101-118.
247. van den Berg, W.B., L.A. Joosten, and P.L. van Lent, *Murine antigen-induced arthritis.* Methods Mol Med, 2007. **136**: p. 243-53.
248. Hyc, A., et al., *Preparation of rat synovial membrane for studies of cytokine secretion.* Folia Histochem Cytobiol, 2007. **45**(1): p. 57-60.
249. Kennedy, C.L., et al., *The molecular pathogenesis of STAT3-driven gastric tumourigenesis in mice is independent of IL-17.* J Pathol, 2011. **225**(2): p. 255-64.
250. Suto, A., et al., *Development and characterization of IL-21-producing CD4+ T cells.* J Exp Med, 2008. **205**(6): p. 1369-79.
251. Faul, F., et al., *G*Power 3: a flexible statistical power analysis program for the social, behavioral, and biomedical sciences.* Behav Res Methods, 2007. **39**(2): p. 175-91.
252. Charan, J. and N.D. Kantharia, *How to calculate sample size in animal studies?* J Pharmacol Pharmacother, 2013. **4**(4): p. 303-6.

253. Metzker, M.L., *Sequencing technologies - the next generation.* Nat Rev Genet, 2010. **11**(1): p. 31-46.
254. Wang, Z., M. Gerstein, and M. Snyder, *RNA-Seq: a revolutionary tool for transcriptomics.* Nat Rev Genet, 2009. **10**(1): p. 57-63.
255. Ozsolak, F. and P.M. Milos, *RNA sequencing: advances, challenges and opportunities.* Nat Rev Genet, 2011. **12**(2): p. 87-98.
256. Takagi, N., et al., *Blockage of interleukin-6 receptor ameliorates joint disease in murine collagen-induced arthritis.* Arthritis Rheum, 1998. **41**(12): p. 2117-21.
257. ; Available from: https://www.encodeproject.org/documents/cede0cbe-d324-4ce7-ace4-f0c3eddf5972/@@download/attachment/ENCODE%20Best%20Practices%20for%20RNA_v2.pdf.
258. Sayols, S., D. Scherzinger, and H. Klein, *dupRadar: a Bioconductor package for the assessment of PCR artifacts in RNA-Seq data.* BMC Bioinformatics, 2016. **17**(1): p. 428.
259. Gallego Romero, I., et al., *RNA-seq: impact of RNA degradation on transcript quantification.* BMC Biol, 2014. **12**: p. 42.
260. Parekh, S., et al., *The impact of amplification on differential expression analyses by RNA-seq.* Sci Rep, 2016. **6**: p. 25533.
261. McFarland-Mancini, M.M., et al., *Differences in wound healing in mice with deficiency of IL-6 versus IL-6 receptor.* J Immunol, 2010. **184**(12): p. 7219-28.
262. Sommer, J., et al., *Interleukin-6, but not the interleukin-6 receptor plays a role in recovery from dextran sodium sulfate-induced colitis.* Int J Mol Med, 2014. **34**(3): p. 651-60.
263. Garbers, C., et al., *An interleukin-6 receptor-dependent molecular switch mediates signal transduction of the IL-27 cytokine subunit p28 (IL-30) via a gp130 protein receptor homodimer.* J Biol Chem, 2013. **288**(6): p. 4346-54.
264. Schuster, B., et al., *Signaling of human ciliary neurotrophic factor (CNTF) revisited. The interleukin-6 receptor can serve as an alpha-receptor for CTNF.* J Biol Chem, 2003. **278**(11): p. 9528-35.
265. Crabé, S., et al., *The IL-27 p28 subunit binds cytokine-like factor 1 to form a cytokine regulating NK and T cell activities requiring IL-6R for signaling.* J Immunol, 2009. **183**(12): p. 7692-702.
266. Conesa, A., et al., *A survey of best practices for RNA-seq data analysis.* Genome Biol, 2016. **17**: p. 13.
267. Tarazona, S., et al., *Differential expression in RNA-seq: a matter of depth.* Genome Res, 2011. **21**(12): p. 2213-23.
268. Griffith, M., et al., *Informatics for RNA Sequencing: A Web Resource for Analysis on the Cloud.* PLoS Comput Biol, 2015. **11**(8): p. e1004393.
269. Williams, A.G., et al., *RNA-seq Data: Challenges in and Recommendations for Experimental Design and Analysis.* Curr Protoc Hum Genet, 2014. **83**: p. 11.13.1-20.
270. Rousseeuw, P., *Silhouettes: a graphical aid to the interpretation and validation of cluster analysis*. 1987, Journal of Computational and Applied Mathematics. p. 53-65.

271. Tibshirani, R., G. Walther, and T. Hastie, *Estimating the number of clusters in a data set via the gap statistic*. 2001, Journal of the Royal Statistical Society. p. 411-423.
272. Lee, Y., et al., *Induction and molecular signature of pathogenic TH17 cells.* Nat Immunol, 2012. **13**(10): p. 991-9.
273. Roychoudhuri, R., et al., *BACH2 represses effector programs to stabilize T(reg)-mediated immune homeostasis.* Nature, 2013. **498**(7455): p. 506-10.
274. Yeremenko, N., et al., *Tumor necrosis factor and interleukin-6 differentially regulate Dkk-1 in the inflamed arthritic joint.* Arthritis Rheumatol, 2015. **67**(8): p. 2071-5.
275. Wang, X., et al., *Overexpression of human matrix metalloproteinase-12 enhances the development of inflammatory arthritis in transgenic rabbits.* Am J Pathol, 2004. **165**(4): p. 1375-83.
276. Kim, K.E., et al., *Downregulation of erythroid differentiation regulator 1 (Erdr1) plays a critical role in psoriasis pathogenesis.* Exp Dermatol, 2016. **25**(7): p. 570-2.
277. Kim, K.E., et al., *Therapeutic effect of erythroid differentiation regulator 1 (Erdr1) on collagen-induced arthritis in DBA/1J mouse.* Oncotarget, 2016. **7**(47): p. 76354-76361.
278. Wang, C., et al., *CD5L/AIM Regulates Lipid Biosynthesis and Restrains Th17 Cell Pathogenicity.* Cell, 2015. **163**(6): p. 1413-27.
279. Stumhofer, J.S., et al., *Interleukin 27 negatively regulates the development of interleukin 17-producing T helper cells during chronic inflammation of the central nervous system.* Nat Immunol, 2006. **7**(9): p. 937-45.
280. Yoshida, H., et al., *WSX-1 Is Required for the Initiation of Th1 Responses and Resistance to L. major Infection.* Immunity, 2001. **15**(4): p. 569-578.
281. Fielding, C.A., et al., *Interleukin-6 signaling drives fibrosis in unresolved inflammation.* Immunity, 2014. **40**(1): p. 40-50.
282. Ciofani, M., et al., *A validated regulatory network for Th17 cell specification.* Cell, 2012. **151**(2): p. 289-303.
283. Gagliani, N., et al., *Th17 cells transdifferentiate into regulatory T cells during resolution of inflammation.* Nature, 2015. **523**(7559): p. 221-5.
284. Langrish, C.L., et al., *IL-23 drives a pathogenic T cell population that induces autoimmune inflammation.* J Exp Med, 2005. **201**(2): p. 233-40.
285. Mayer, A., et al., *Antigen presenting cell-derived IL-6 restricts Th2-cell differentiation.* Eur J Immunol, 2014. **44**(11): p. 3252-62.
286. Chang, X. and C. Wei, *Glycolysis and rheumatoid arthritis.* Int J Rheum Dis, 2011. **14**(3): p. 217-22.
287. Zhou, J., et al., *Exploration of the serum metabolite signature in patients with rheumatoid arthritis using gas chromatography-mass spectrometry.* J Pharm Biomed Anal, 2016. **127**: p. 60-7.
288. Haas, R., et al., *Lactate Regulates Metabolic and Pro-inflammatory Circuits in Control of T Cell Migration and Effector Functions.* PLoS Biol, 2015. **13**(7): p. e1002202.
289. Jin, L., et al., *Structural basis for hydroxycholesterols as natural ligands of orphan nuclear receptor RORgamma.* Mol Endocrinol, 2010. **24**(5): p. 923-9.

290. Soroosh, P., et al., *Oxysterols are agonist ligands of RORγt and drive Th17 cell differentiation.* Proc Natl Acad Sci U S A, 2014. **111**(33): p. 12163-8.
291. Timmer, T.C., et al., *Inflammation and ectopic lymphoid structures in rheumatoid arthritis synovial tissues dissected by genomics technology: identification of the interleukin-7 signaling pathway in tissues with lymphoid neogenesis.* Arthritis Rheum, 2007. **56**(8): p. 2492-502.
292. Hirota, K., et al., *Fate mapping of IL-17-producing T cells in inflammatory responses.* Nat Immunol, 2011. **12**(3): p. 255-63.
293. Harbour, S.N., et al., *Th17 cells give rise to Th1 cells that are required for the pathogenesis of colitis.* Proc Natl Acad Sci U S A, 2015. **112**(22): p. 7061-6.
294. Hirota, K., et al., *Plasticity of Th17 cells in Peyer's patches is responsible for the induction of T cell-dependent IgA responses.* Nat Immunol, 2013. **14**(4): p. 372-9.
295. Basdeo, S.A., et al., *Ex-Th17 (Nonclassical Th1) Cells Are Functionally Distinct from Classical Th1 and Th17 Cells and Are Not Constrained by Regulatory T Cells.* J Immunol, 2017. **198**(6): p. 2249-2259.
296. Kobayashi, S., et al., *TGF-β induces the differentiation of human CXCL13-producing CD4(+) T cells.* Eur J Immunol, 2016. **46**(2): p. 360-71.
297. Yoshitomi, H., et al., *Human Sox4 facilitates the development of CXCL13-producing helper T cells in inflammatory environments.* Nat Commun, 2018. **9**(1): p. 3762.
298. Hindley, J.P., et al., *T-cell trafficking facilitated by high endothelial venules is required for tumor control after regulatory T-cell depletion.* Cancer Res, 2012. **72**(21): p. 5473-82.
299. Yu, P., et al., *Priming of naive T cells inside tumors leads to eradication of established tumors.* Nat Immunol, 2004. **5**(2): p. 141-9.
300. Judd, L.M., et al., *Gastric cancer development in mice lacking the SHP2 binding site on the IL-6 family co-receptor gp130.* Gastroenterology, 2004. **126**(1): p. 196-207.
301. Bénézech, C., et al., *CLEC-2 is required for development and maintenance of lymph nodes.* Blood, 2014. **123**(20): p. 3200-7.
302. Goya, S., et al., *Sustained interleukin-6 signalling leads to the development of lymphoid organ-like structures in the lung.* J Pathol, 2003. **200**(1): p. 82-7.
303. Deteix, C., et al., *Intragraft Th17 infiltrate promotes lymphoid neogenesis and hastens clinical chronic rejection.* J Immunol, 2010. **184**(9): p. 5344-51.
304. Hill, D.G., et al., *Hyperactive gp130/STAT3-driven gastric tumourigenesis promotes submucosal tertiary lymphoid structure development.* Int J Cancer, 2018. **143**(1): p. 167-178.
305. Hennequin, A., et al., *Tumor infiltration by Tbet+ effector T cells and CD20+ B cells is associated with survival in gastric cancer patients.* Oncoimmunology, 2016. **5**(2): p. e1054598.
306. Jenkins, B.J., et al., *The threshold of gp130-dependent STAT3 signaling is critical for normal regulation of hematopoiesis.* Blood, 2005. **105**(9): p. 3512-20.
307. Bento, D.C., et al., *High endothelial venules are rare in colorectal cancers but accumulate in extra-tumoral areas with disease progression.* Oncoimmunology, 2015. **4**(3): p. e974374.

308. Jetten, A.M., *Retinoid-related orphan receptors (RORs): critical roles in development, immunity, circadian rhythm, and cellular metabolism.* Nucl Recept Signal, 2009. **7**: p. e003.
309. Ivanov, I.I., et al., *The orphan nuclear receptor RORgammat directs the differentiation program of proinflammatory IL-17+ T helper cells.* Cell, 2006. **126**(6): p. 1121-33.
310. Jones, G.W. and S.A. Jones, *Ectopic lymphoid follicles: inducible centres for generating antigen-specific immune responses within tissues.* Immunology, 2015.
311. Xiao, S., et al., *Small-molecule RORγt antagonists inhibit T helper 17 cell transcriptional network by divergent mechanisms.* Immunity, 2014. **40**(4): p. 477-89.
312. Chang, M.R., et al., *Pharmacologic repression of retinoic acid receptor-related orphan nuclear receptor γ is therapeutic in the collagen-induced arthritis experimental model.* Arthritis Rheumatol, 2014. **66**(3): p. 579-88.
313. Sun, Z., et al., *Requirement for RORgamma in thymocyte survival and lymphoid organ development.* Science, 2000. **288**(5475): p. 2369-73.
314. Eberl, G., et al., *An essential function for the nuclear receptor RORgamma(t) in the generation of fetal lymphoid tissue inducer cells.* Nat Immunol, 2004. **5**(1): p. 64-73.
315. Liljevald, M., et al., *Retinoid-related orphan receptor γ (RORγ) adult induced knockout mice develop lymphoblastic lymphoma.* Autoimmun Rev, 2016. **15**(11): p. 1062-1070.
316. Guntermann, C., et al., *Retinoic-acid-orphan-receptor-C inhibition suppresses Th17 cells and induces thymic aberrations.* JCI Insight, 2017. **2**(5): p. e91127.
317. Miossec, P. and J.K. Kolls, *Targeting IL-17 and TH17 cells in chronic inflammation.* Nat Rev Drug Discov, 2012. **11**(10): p. 763-76.
318. Withers, D.R., et al., *Transient inhibition of ROR-γt therapeutically limits intestinal inflammation by reducing TH17 cells and preserving group 3 innate lymphoid cells.* Nat Med, 2016. **22**(3): p. 319-23.
319. Nayar, S., et al., *Bimodal Expansion of the Lymphatic Vessels Is Regulated by the Sequential Expression of IL-7 and Lymphotoxin α1β2 in Newly Formed Tertiary Lymphoid Structures.* J Immunol, 2016. **197**(5): p. 1957-67.
320. Yang, X.O., et al., *T helper 17 lineage differentiation is programmed by orphan nuclear receptors ROR alpha and ROR gamma.* Immunity, 2008. **28**(1): p. 29-39.
321. He, Z., et al., *A two-amino-acid substitution in the transcription factor RORγt disrupts its function in T.* Nat Immunol, 2017. **18**(10): p. 1128-1138.
322. Ogura, H., et al., *Interleukin-17 promotes autoimmunity by triggering a positive-feedback loop via interleukin-6 induction.* Immunity, 2008. **29**(4): p. 628-36.
323. Svensson, M.N., et al., *Reduced expression of phosphatase PTPN2 promotes pathogenic conversion of Tregs in autoimmunity.* J Clin Invest, 2019. **129**(3): p. 1193-1210.
324. Chiyo, M., et al., *Expression of IL-27 in murine carcinoma cells produces antitumor effects and induces protective immunity in inoculated host animals.* Int J Cancer, 2005. **115**(3): p. 437-42.
325. Hisada, M., et al., *Potent antitumor activity of interleukin-27.* Cancer Res, 2004. **64**(3): p. 1152-6.

326. Salcedo, R., et al., *IL-27 mediates complete regression of orthotopic primary and metastatic murine neuroblastoma tumors: role for CD8+ T cells.* J Immunol, 2004. **173**(12): p. 7170-82.
327. Salcedo, R., et al., *Immunologic and therapeutic synergy of IL-27 and IL-2: enhancement of T cell sensitization, tumor-specific CTL reactivity and complete regression of disseminated neuroblastoma metastases in the liver and bone marrow.* J Immunol, 2009. **182**(7): p. 4328-38.
328. Chihara, N., et al., *Induction and transcriptional regulation of the co-inhibitory gene module in T cells.* Nature, 2018. **558**(7710): p. 454-459.
329. Kocks, J.R., et al., *Regulatory T cells interfere with the development of bronchus-associated lymphoid tissue.* J Exp Med, 2007. **204**(4): p. 723-34.
330. Genovese, M.C., et al., *Efficacy and safety of secukinumab in patients with rheumatoid arthritis: a phase II, dose-finding, double-blind, randomised, placebo controlled study.* Ann Rheum Dis, 2013. **72**(6): p. 863-9.
331. Genovese, M.C., et al., *One-year efficacy and safety results of secukinumab in patients with rheumatoid arthritis: phase II, dose-finding, double-blind, randomized, placebo-controlled study.* J Rheumatol, 2014. **41**(3): p. 414-21.
332. Pavelka, K., et al., *A study to evaluate the safety, tolerability, and efficacy of brodalumab in subjects with rheumatoid arthritis and an inadequate response to methotrexate.* J Rheumatol, 2015. **42**(6): p. 912-9.
333. Cañete, J.D., et al., *Ectopic lymphoid neogenesis is strongly associated with activation of the IL-23 pathway in rheumatoid synovitis.* Arthritis Res Ther, 2015. **17**: p. 173.
334. Celis, R., et al., *Synovial cytokine expression in psoriatic arthritis and associations with lymphoid neogenesis and clinical features.* Arthritis Res Ther, 2012. **14**(2): p. R93.
335. Smolen, J.S., et al., *A randomised phase II study evaluating the efficacy and safety of subcutaneously administered ustekinumab and guselkumab in patients with active rheumatoid arthritis despite treatment with methotrexate.* Ann Rheum Dis, 2017. **76**(5): p. 831-839.
336. Schwartz, D.M., et al., *JAK inhibition as a therapeutic strategy for immune and inflammatory diseases.* Nat Rev Drug Discov, 2017. **17**(1): p. 78.
337. Yang, X.O., et al., *STAT3 regulates cytokine-mediated generation of inflammatory helper T cells.* J Biol Chem, 2007. **282**(13): p. 9358-63.
338. Bailey, S.R., et al., *Th17 cells in cancer: the ultimate identity crisis.* Front Immunol, 2014. **5**: p. 276.
339. Chang, S.H., et al., *T helper 17 cells play a critical pathogenic role in lung cancer.* Proc Natl Acad Sci U S A, 2014. **111**(15): p. 5664-9.
340. Martin-Orozco, N., et al., *T helper 17 cells promote cytotoxic T cell activation in tumor immunity.* Immunity, 2009. **31**(5): p. 787-98.
341. Stephenson, W., et al., *Single-cell RNA-seq of rheumatoid arthritis synovial tissue using low-cost microfluidic instrumentation.* Nat Commun, 2018. **9**(1): p. 791.
342. Corsiero, E., et al., *Single cell cloning and recombinant monoclonal antibodies generation from RA synovial B cells reveal frequent targeting of citrullinated histones of NETs.* Ann Rheum Dis, 2016. **75**(10): p. 1866-75.

343. Corsiero, E., et al., *Characterization of a Synovial B Cell-Derived Recombinant Monoclonal Antibody Targeting Stromal Calreticulin in the Rheumatoid Joints.* J Immunol, 2018. **201**(5): p. 1373-1381.
344. Pucino, V., et al., *Lactate at the crossroads of metabolism, inflammation, and autoimmunity.* Eur J Immunol, 2017. **47**(1): p. 14-21.
345. Wen, Z., et al., *N-myristoyltransferase deficiency impairs activation of kinase AMPK and promotes synovial tissue inflammation.* Nat Immunol, 2019. **20**(3): p. 313-325.